AD-A083 933 NEW MEXICO UNIV ALBUQUERQUE DEPT OF MECHANICAL ENGI--ETC F/G 11/1
THE WAVY MECHANICAL FACE SEAL - THEORETICAL AND EXPERIMENTAL RE--ETC(U)
JAN 80 A O LEBECK, L A YOUNG N00014-76-C-0071
UNCLASSIFIED ME-105(80)ONR-414-1 NL

1 OF 3
AD
AD A083933

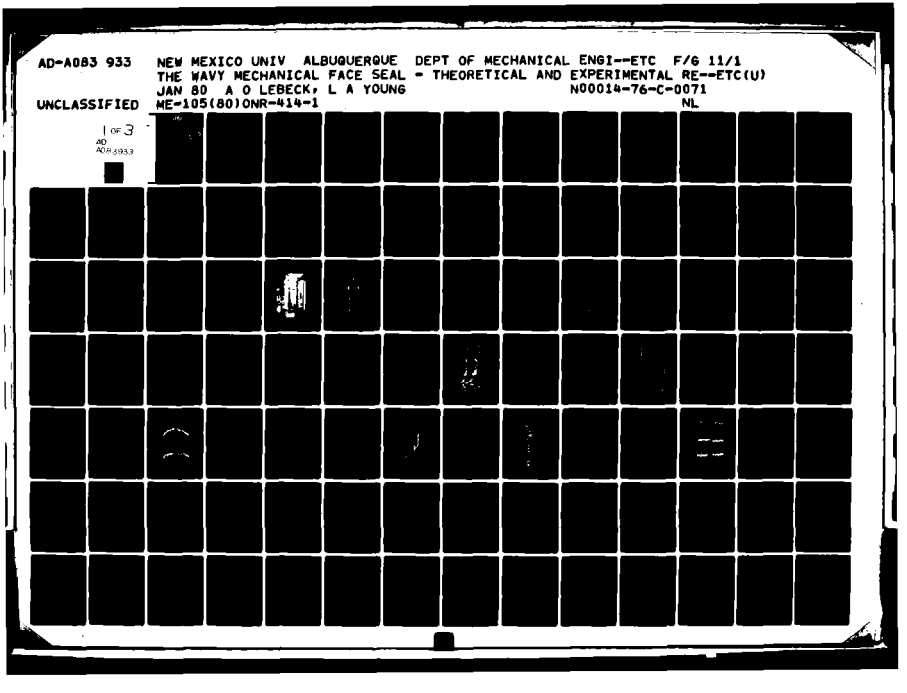

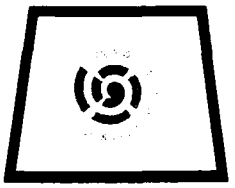

THE UNIVERSITY OF NEW MEXICO
COLLEGE OF ENGINEERING

BUREAU OF ENGINEERING RESEARCH

THE WAVY MECHANICAL FACE SEAL
THEORETICAL AND EXPERIMENTAL RESULTS

BY

A. O. LEBECK

AND

L. A. YOUNG

SUMMARY REPORT ME-105(80)ONR-414-1

JANUARY 1980

Prepared for the Office of Naval Research under
Contract Number ONR-N-00014-76-C-0071.

THE WAVY MECHANICAL FACE SEAL

THEORETICAL AND EXPERIMENTAL RESULTS

by

A. O. Lebeck
Associate Professor of Mechanical Engineering

and

L. A. Young
Research Assistant

The University of New Mexico
Department of Mechanical Engineering
and
Bureau of Engineering Research
Albuquerque, New Mexico 87131

Summary Report ME-105(80)ONR-414-1

January 1980

Prepared for the Office of Naval
Research under Contract Number
ONR-N-00014-76-C-0071

SECURITY CLASSIFICATION OF THIS PAGE (When Data Entered)

REPORT DOCUMENTATION PAGE

READ INSTRUCTIONS BEFORE COMPLETING FORM

1. REPORT NUMBER

2. GOVT ACCESSION NO. AD-A083 933

3. RECIPIENT'S CATALOG NUMBER

4. TITLE (and Subtitle)
THE WAVY MECHANICAL FACE SEAL - THEORETICAL AND EXPERIMENTAL RESULTS.

5. TYPE OF REPORT & PERIOD COVERED
Summary Report
Dec. 1, 1978-Nov. 30, 1979

6. PERFORMING ORG. REPORT NUMBER
ME-105(80)ONR-414-1

7. AUTHOR(s)
A. O. Lebeck
L. A. Young

8. CONTRACT OR GRANT NUMBER(s)
ONR-N-00014-76-C-0071

9. PERFORMING ORGANIZATION NAME AND ADDRESS
The University of New Mexico
Albuquerque, New Mexico 87131

10. PROGRAM ELEMENT, PROJECT, TASK AREA & WORK UNIT NUMBERS

11. CONTROLLING OFFICE NAME AND ADDRESS
Director, Power Program
Department of the Navy - Office of Naval Research
Arlington, VA 22217

12. REPORT DATE
January 1980

13. NUMBER OF PAGES
205

14. MONITORING AGENCY NAME & ADDRESS (if different from Controlling Office)

15. SECURITY CLASS. (of this report)
Unclassified

15a. DECLASSIFICATION/DOWNGRADING SCHEDULE

16. DISTRIBUTION STATEMENT (of this Report)

Approved for public release; distribution unlimited

17. DISTRIBUTION STATEMENT (of the abstract entered in Block 20, if different from Report)

18. SUPPLEMENTARY NOTES

19. KEY WORDS (Continue on reverse side if necessary and identify by block number)
Mechanical Seals, Seals, Face Seals, Lubrication, Wear, Friction

20. ABSTRACT (Continue on reverse side if necessary and identify by block number)

In this report the results of theoretical and experimental investigations on the effects of waviness on mechanical face seal performance are presented. In previous work it was shown how waviness imposed on a seal face leads to reduced friction and wear while creating only a small leakage in a water seal. It was also shown that the waviness must be moved slowly around the seal ring in order that the effect of waviness remain indefinitely.

(continued on reverse)

DD FORM 1 JAN 73 1473 EDITION OF 1 NOV 65 IS OBSOLETE

SECURITY CLASSIFICATION OF THIS PAGE (When Data Entered)

(continued from obverse)

A test apparatus for measuring the effects of waviness is described. A computer based system is used to record the data and monitor the test. A test procedure is outlined.

Results from wavy seal experiments show that waviness reduces seal wear compared to a flat face seal a factor of four to forty and reduces torque a factor of four. Long term tests show that by moving the wave the effect remains indefinitely. As the amount of waviness is increased, friction torque decreases and leakage increases. Wear profiles show that the seal faces have a tilt in addition to waviness. This alters the pressure distribution significantly when compared to the radially parallel wavy faces analyzed previously. Tests using a converging radially tapered seal show that the taper wears away with time.

A theory is developed for predicting thermoelastic instability in seal rings. Results show that ring deflection has a predominant influence at low numbers of waves. Experimental results are needed to verify the theory.

The hydrodynamic theory previously developed for wavy face seals is completely revised and presented as a more comprehensive theory. This was necessary because of the tilt variation on the seal faces. Using this theory it is shown that certain combinations of waviness and tilt lead to minimum torque and minimum leakage. This optimum design has faces which are either radially converging or parallel with contact all around the seal to provide low leakage. These results point the way to even better seal designs than the experimental seal.

Using the model a comparison between theory and experiment was made. The theoretical solution requires that a complete deflection analysis and simultaneous solution be made. Agreement between experiment and theory is good for both torque and leakage. Agreement of theory with measured deflection is excellent.

In conclusion, the report shows both theoretically and experimentally how waviness can be used to great advantage in a water seal to reduce friction and wear.

APPLICATION OF RESEARCH TO THE NEEDS OF THE U.S. NAVY

Mechanical face seals are used in numerous applications in Naval machinery. These applications range from propeller shaft seals to boiler feed pump seals. In such equipment the mechanical seal plays a vital role. When such seals fail, repair is costly both in terms of lost time and direct costs, so any improvement in seal life and reliability would be of significant benefit.

As more advanced equipment is designed, it is sometimes difficult to achieve desired performance in more severe service environments with the present state of the art of seal design. Thus, an improvement in seal technology would serve this important application.

The immediate objective of the research herein is to further the understanding of mechanical face seal lubrication phenomena. The ultimate objective is to develop the capability of designing contacting face seals having a longer life, greater reliability, and for extreme environments. Thus, the objectives of this research are compatible with mechanical face seal needs for Naval machinery.

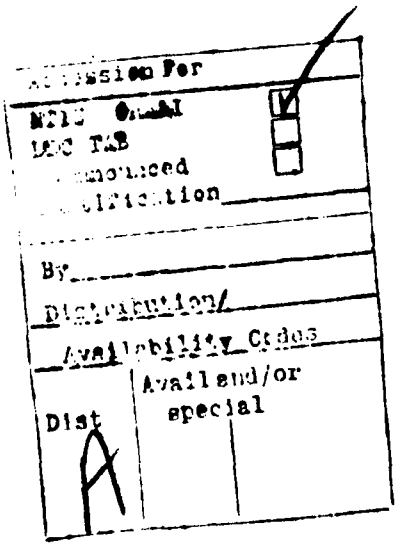

TABLE OF CONTENTS

TABLE OF CONTENTS (continued)

LIST OF FIGURES

LIST OF FIGURES (continued)

LIST OF TABLES

List of Symbols

a	Area - m^2
a, b	Temperature solution coefficients - 1/m
$A = \frac{EJ_x}{GJ_\theta}$	Stiffness ratio - dimensionless
b_f	Fraction of seal face subject to fluid pressure
b_m	Fraction of seal face subject to mechanical pressure
$B = \frac{r_o^2 - r_b^2}{r_o^2 - r_i^2}$	Balance ratio for an outside pressurized seal
c	One-half maximum roughness height - m
d	Diameter of gas pressure hole - m
e	Distance between gas pressure hole center and centroid - m
E	Youngs modulus - N/m^2
$E(\ )$	Expectancy operator
f_1, f_2, f_3	Deflection functions - dimensionless
$f(h)$	Roughness distribution function
F	Fraction of load supported by fluid pressure
F_f	Friction force due to fluid friction
F_m	Friction force due to mechanical friction
$\bar{F} = \frac{Fc}{r_o^3 \omega\eta}$	Dimensionless friction force
G	Shear modulus - N/m^2
h	Nominal film thickness or ring thickness - m
$\bar{h} = \frac{h}{c}$	Dimensionless film thickness

h_{a_n}, h_{b_n}	nth cos and sin harmonics of film thickness
h_a, h_b	h_{a_n} and h_{b_n} for n = 3
h_{ma}, h_{ga}, h_{pa}, h_{mb}, h_{gb}, h_{pb}	Third harmonic components for waviness due to face pressure moment, gas pressure, and face pressure
h_o	Mean film thickness - m
H	Total film thickness - m
$\bar{H} = \frac{H}{c}$	Dimensionless total film thickness
H_∞	Convection heat transfer coefficient - W/m^2K
$J_x = \int_A \frac{y^2}{1 - x/r_c} dA$	Stiffness constant about x axis for ring cross section - m^4
$J_y = \int_A \frac{x^2}{1 - x/r_c} dA$	Stiffness constant about the y axis for ring cross section - m^4
$J_{xy} = \int_A \frac{xy}{1 - x/r_c} dA$	Stiffness constant - m^4
J_θ	Torsional stiffness constant for ring cross section - m^4
k	Diffusivity - m^2/s
K	Thermal conductivity - W/mK
$\bar{K} = \frac{J_x c^3 E}{r_o^4 r_c^3 \omega_n}$	Dimensionless ring stiffness
l	Length of the ring - m
m_x, m_y, m_θ	Distributed moment loads on seal ring - N·m/m
$m_{\theta g}$, $m_{\theta ga_n}$, $m_{\theta gb_n}$	Distributed moment and harmonic components due to gas pressure
$m_{\theta p}$, $m_{\theta pa_n}$, $m_{\theta pb_n}$	Distributed moment and harmonic components due to face pressure

$m_{\theta ga}$, $m_{\theta gb}$	As above for n = 3
$m_{\theta pa}$, $m_{\theta pb}$	As above for n = 3
M_θ, M_x	Moments about the θ and x axis within the ring - Nm
n	Number of the harmonic or number of waves around seal face
p	Fluid pressure - N/m^2
p_g, p_{gas}	Gas pressure causing waviness - N/m^2
p_{H_2O}	Sealed water pressure - N/m^2
$\bar{p} = \frac{pc^2}{r_o^2 \omega\eta}$	Dimensionless fluid pressure
p_i	Seal inside pressure - N/m^2
p_m	Pressure at asperity contact--equals yield or ultimate compressive strength - N/m^2
$\bar{p}_m = \frac{p_m c^2}{r_o^2 \omega\eta}$	Dimensionless contact pressure
p_o	Seal outside pressure - N/m^2
p_s	Shear strength of asperities - N/m^2
$\bar{p}_s = \frac{p_s c^2}{r_o^2 \omega\eta}$	Dimensionless shear strength
p_{sp}	Spring pressure on face
P( )	Probability
p_x, p_y, p_θ	Distributed pressure loads on seal ring - N/m
p_y, p_{ya_n}, p_{yb_n}	Distributed pressure and harmonic components due to face pressure

q	Heat flow per unit area - W/m^2
q_r, q_θ	Flow in two-dimensional model - m^2/s
$\bar{q} = \frac{q}{r_o^2 \omega c}$	Dimensionless unit flow
Q	total leakage for the seal - m^3/s
$\bar{Q} = \frac{Q}{r_o^2 \omega c}$	Dimensionless leakage
r	Radial coordinate
r,θ	Seal coordinates
$\bar{r} = \frac{r}{r_o}$	Dimensionless radial coordinate
r_b	Seal balance radius - m
r_c	Radius to centroid of seal ring - m
r_f	Friction radius - m
r_i	Inside radius of seal - m
r_o	Outside radius of seal - m
R	Mean radius of seal - m
t	Time - s
T	Temperature or temperature amplitude - K
T_H/T_S	Face temperature ratio
Tq	Seal friction torque - N·m
U_c	Thermal contact conductance across face - W/m^2K
v	Ring equation face displacement - m
v, v_{a_n}, v_{b_n}	Ring centroidal deflection and harmonics - m

$w(r)$	Seal wear as a function of radius - m
W	Load support - N
$\bar{W} = \frac{Wc^2}{r_o^4 \omega \eta}$	Dimensionless load support
$\bar{W}^* = \pi(1-\bar{r}_i^2) \times [\bar{p}_o B + \bar{p}_i(1-B)]$	Required load support
x, y, z	Rectangular coordinates
x, y, θ	Ring coordinates
Z	Constant as defined
α	Coefficient of thermal expansion - 1/K
β	Angular speed of temperature wave relative to moving ring - 1/s
γ	Angle of tilt of seal ring
δ	Random portion of film thickness - m
δ_p	Pressure caused face displacement - m
δ_T	Temperature caused face displacement - m
Δ	A factor to provide a bound on viscous friction or change of
$\bar{\Delta} = \frac{c}{\bar{p}_s r_o}$	Dimensionless Δ
η	Phase shift angle between temperature waves of two faces or viscosity - $N \cdot s/m^2$
θ	Angular coordinate
μ	Friction coefficient
σ	Standard deviation of combined roughness - m
τ	Shear stress - N/m^2

ϕ	Angular speed of temperature wave relative to fixed ring - 1/s or rotation of seal ring about its centroid
ϕ_{a_n}, ϕ_{b_n}	nth cos and sin harmonics of face tilt or rotation
ϕ_a, ϕ_b	ϕ_{a_n} and ϕ_{b_n} for n = 3
ϕ_{ma}, ϕ_{ga}, ϕ_{pa}, ϕ_{mb}, ϕ_{gb}, ϕ_{pb}	Third harmonic tilt components due to face pressure moment, gas pressure, and face pressure, respectively
$\bar{\phi} = \phi \frac{r_o}{c}$	Adjusted face rotation
ω	Angular speed of ring H relative to ring S
-	All symbols with a bar are dimensionless as defined

Subscripts:

S	Fixed ring
H	Rotating ring
M	Middle surface

Chapter 1

Introduction

Mechanical Face Seals

In applications where a rotating shaft must pass from one fluid region to another, contacting mechanical face seals* play the essential role of minimizing the transfer of fluid between the regions. Applications of face seals range from water pump seals to process pump seals to propeller shaft seals.

The performance and reliability of contacting mechanical face seals are of great importance for any type of equipment where minimal leakage, high reliability, and long life are necessary. Even for equipment where these factors are not so critical, seal failures and short seal life lead to high operating cost due to down time and maintenance cost.

Even though mechanical face seal technology has been steadily improving over the past several decades, further improvement in the state of the art of seal design would be most beneficial. Although seals having an acceptable life and reliability can be designed for many applications, further improvement in seal life and reliability would result in significant cost savings to the user. Also, there are numerous mechanical face seal applications where seal loading, reliability, life, and leakage requirements are difficult to achieve within the present state of the art. Examples of such applications are seals for pumps for nuclear power plants and seals for large diameter submarine propeller shafts. Additionally, the friction losses in face seals represent a significant fraction of energy consumed for pumping purposes. Within the present state of the art of seal design, it is very difficult to design a low leakage seal that

*The class of low leakage face seals where there is definite contact and wear of the faces as opposed to hydrostatic or hydrodynamic where a definite clearance is maintained.

also has a low friction loss.

The main barrier to the advancement of the state of the art is that the mechanics of seal operation are not well enough understood to be able to reasonably anticipate seal performance as a function of design parameters. There are no well established fundamental theoretical bases that can be used to indicate the type of seal design that will give improved performance. Improvements that have been made have been brought about largely by trial and error combined with elementary sealing theories.

In order to be able to predict the performance of contacting face seals as a function of design parameters, it is essential that the lubrication mechanisms between the faces be well understood. At present it is known that hydrodynamic or hydrostatic lubrication plays some role in providing load support for oil seals as well as water seals. But, the precise nature of this lubrication is not known. Several theories have been put forth. However, these theories have not been verified for contacting face seals, and it is not possible as yet to use these theories for the design of contacting face seals.

In this work, the results from further research into hydrodynamic and hydrostatic lubrication mechanisms in face seals is reported. Much has been learned about these mechanisms. Based upon experimental work there is a strong promise that effective use of hydrodynamic and hydrostatic mechanisms can be made to dramatically improve face seal performance.

Seal Lubrication

The mechanical face seal consists basically of two annular rings which rotate relative to each other and which are pressed together by spring and fluid pressures (see Figure 1-1). The surfaces that rub together are generally manufactured as flat as possible initially so as to minimize leakage. The effective gap between the faces is ideally quite small (order of 1 μm) so that leakage flow across the faces will be quite small. The difficulty in designing a mechanical seal is in maintaining the gap at a very low value while at the same time providing

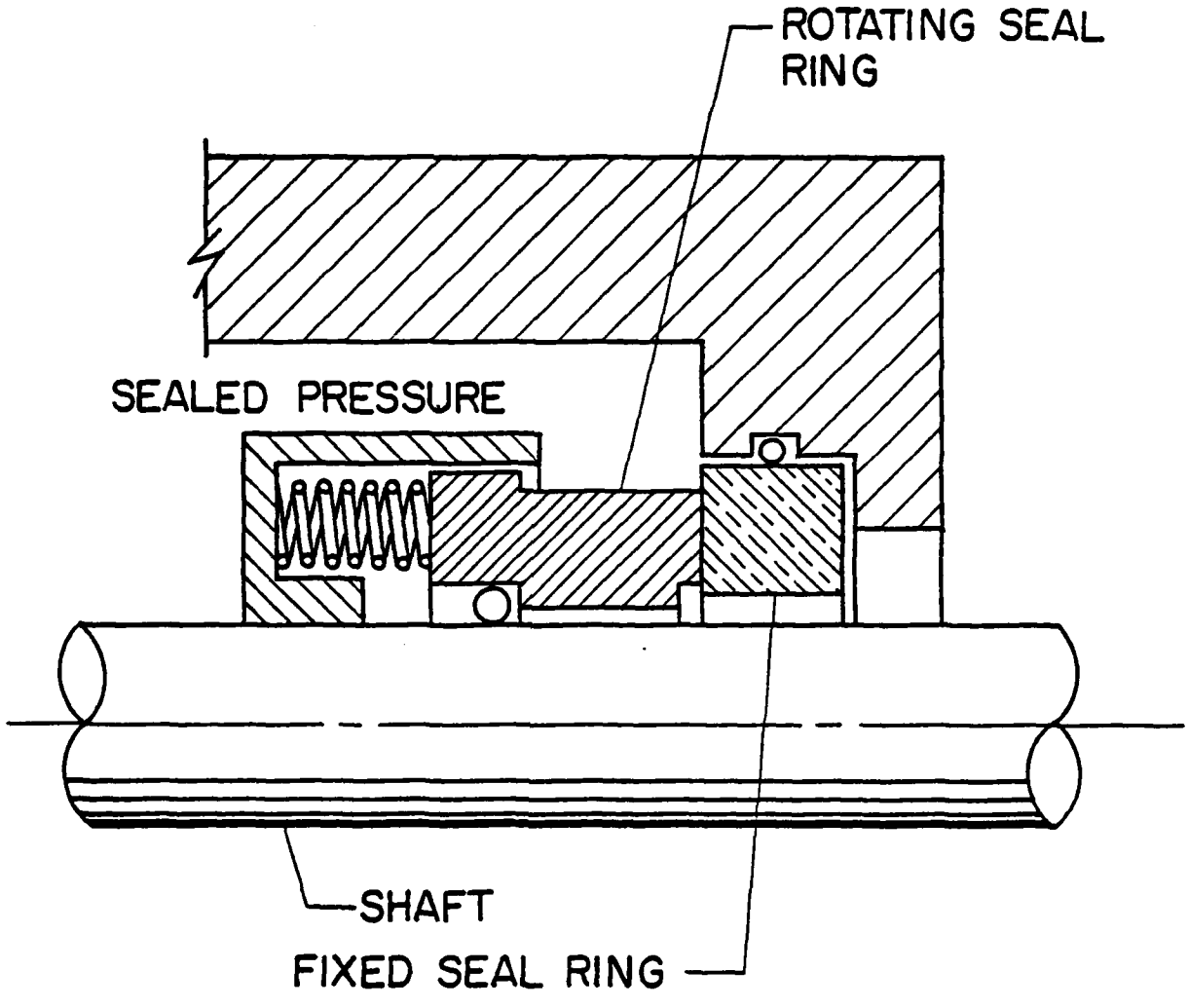

Figure 1-1. Mechanical Face Seal.

a definite lubricant film between the faces.

The load that must be supported at the faces of a mechanical seal is due primarily to loading caused by the sealed pressure. The unit face load can be expressed as some fraction B of the sealed pressure where B can be made greater or less than unity by geometry selection. The load support at the faces is derived from fluid pressure and mechanical pressure. If the fluid pressure at the faces is large enough to support all of the load, then there will be no contact and no adhesive wear.* If none of the load is supported by fluid pressure, the load must be carried by mechanical contact and the wear rate will be large.

In practice, seals often operate at one of two extremes. At one extreme, a large gap will be created by hydrostatic or hydrodynamic pressure, all of the load will be supported by fluid pressure, and the seal will leak a large amount. At the opposite extreme, the gap will close completely and leakage will be very low. Only a small fraction of the load will be carried by fluid pressure, and wear and heat generation will increase.

Based on the above, it can be concluded that an effective seal should operate between these two extremes--having both adequate fluid pressure load support and low leakage. The seal should operate so that it just touches to minimize leakage but such that the load is carried by fluid pressure, not mechanical pressure. To do this requires that any fluid pressure generation mechanism used to provide load support to the seal must be very carefully controlled. At present, in commercial contacting face seals this lubrication is left primarily to chance, and often such seals operate at one of the extremes mentioned. Quite commonly such seals will operate in the low leakage condition where wear progresses at a definite rate. Such seals are quite satisfactory for many applications. However, when pressure or speed requirements are increased, then this mode of operation may lead to rapid failure through wear or heat checking.

*There may still be abrasive wear even if the surfaces do not touch.

In order to be able to design into the seal the proper balance between fluid pressure load support and leakage, the origin of lubrication mechanisms must first be fully understood. A considerable amount of research has been accomplished in this area over the years. Various theories have emerged and have been described in a previous annual report [1].* These theories fall roughly into two categories, hydrostatic and hydrodynamic. In this research program, attention has been directed toward studying the effects of waviness as a source of hydrodynamic and hydrostatic pressure in face seals. Particular attention has been focused on hydrodynamic effects in relation to roughness and low viscosity applications where some touching is expected. Waviness was selected among the various hydrodynamic theories because it is controllable in seals and a better understanding could lead to improved seal designs.

Sources of waviness in seals have been described in detail previously [1]. Waviness may be produced accidentally as an uncontrolled variable or intentionally in a precisely controlled manner. A wavy seal ring is shown in Figures 1-2 and 1-3.

Wavy Face Seal

The concept of waviness is that where the film thickness varies in some fashion circumferentially around the seal. Generally speaking, film thickness may vary radially as well as tangentially.

$$h = h(r,\theta) \ . \tag{1-1}$$

In the present work interest is focused upon film thickness shapes of the following functional form

$$h = h_0 + f_1(r) \cos n\theta + f_2(r) \sin n\theta \ . \tag{1-2}$$

At any particular radius r the film shape is periodic with n waves around the seal and is therefore wavy. However, film shape can also vary in some general manner with r.

*Numbers in brackets refer to List of References at the end of report.

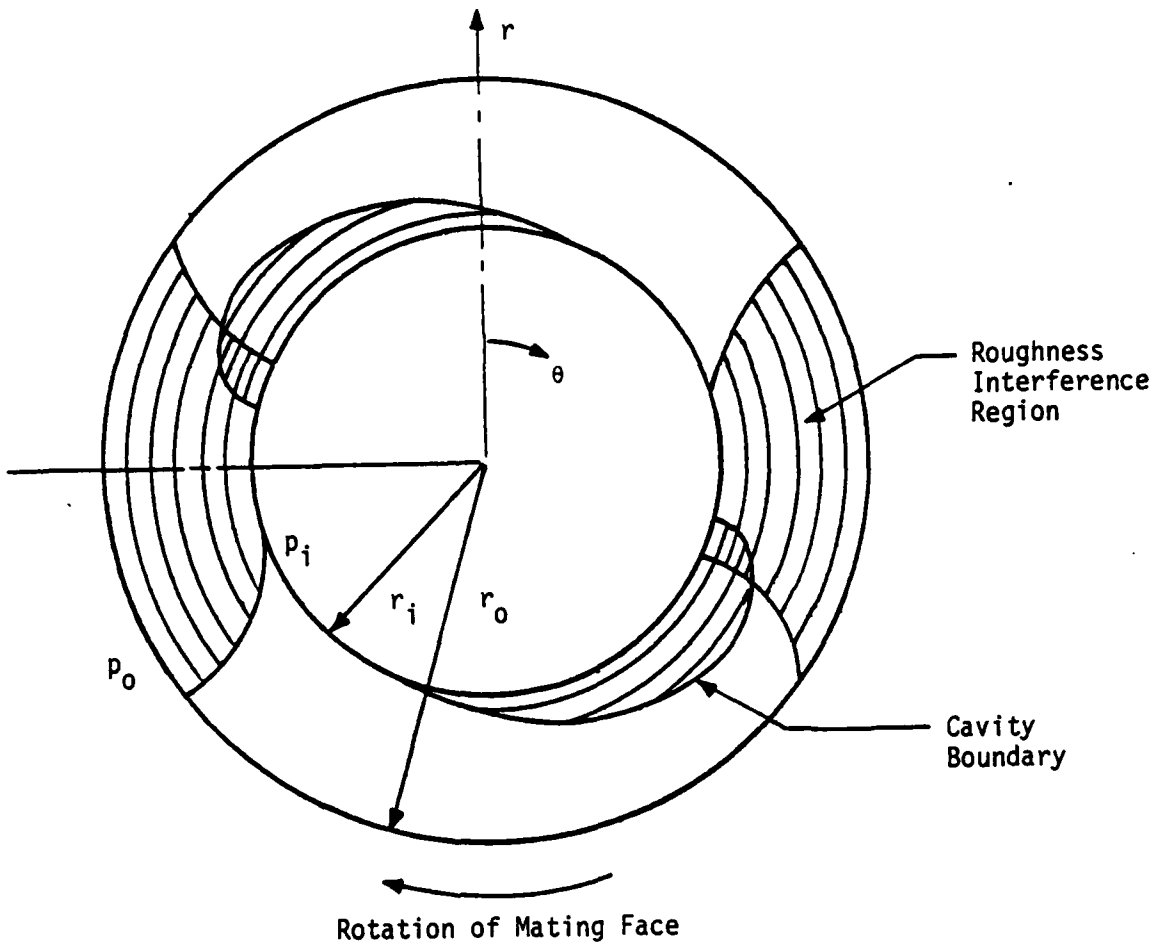

Figure 1-2. Wavy Seal Geometry.

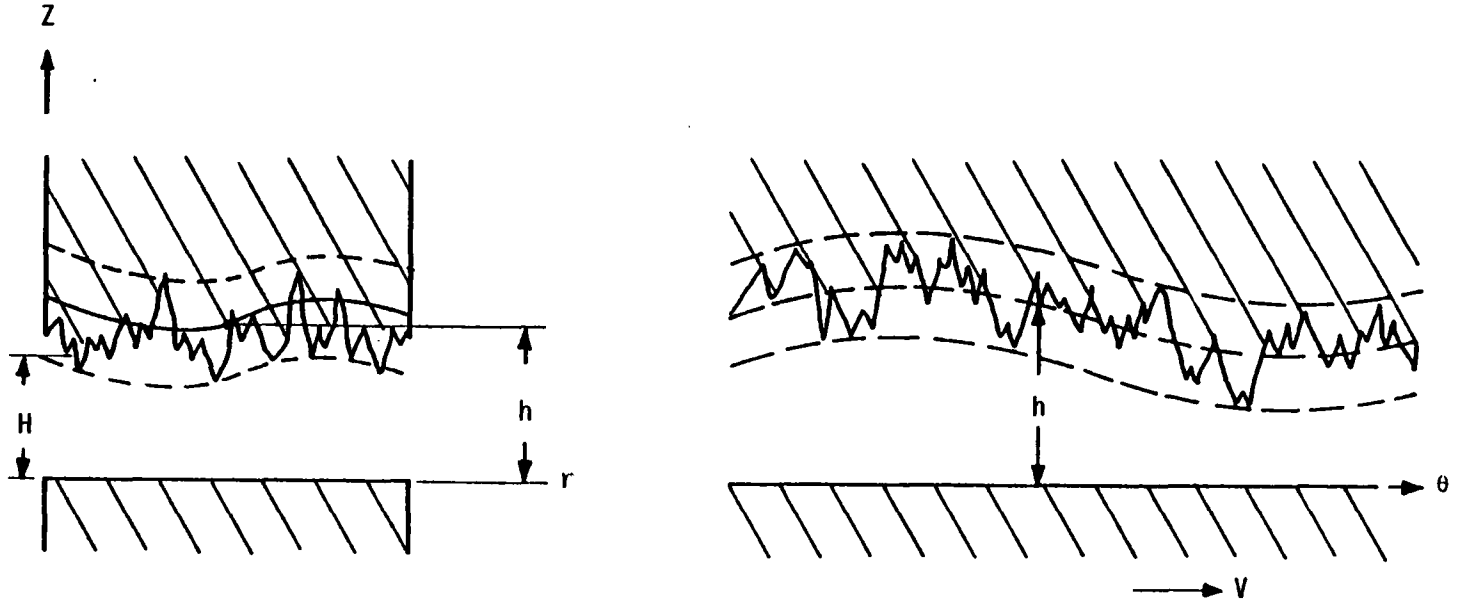

Figure 1-3. Seal Roughness and Radial Profile

If $f_1(r)$ = const and $f_2(r)$ = const, then the faces are always radially parallel. This component of film thickness variation is commonly termed waviness. If the $f_i(r) \neq$ const, then the faces are not in general radially parallel. The $f_i(r)$ are referred to as tilt. Thus, the film thickness shapes of interest are combinations of waviness and tilt. Since at any radius the film thickness is wavy, the combination of waviness and tilt defined above will also be called a wavy film shape.

The reason for choosing film shapes as described by equation (1-2) as a subject for study is that these shapes can conveniently be generated by planned mechanical distortions in a seal ring, and the shapes also include common modes of unplanned distortion found in operating seals. For example, generally seals undergo a uniform tilt due to pressure and thermal deformation. When rings are loaded by any non-axisymmetric load they become wavy as described by equation (1-2).

Now, for the sake of illustration, assume a seal has a wavy film thickness shape given by equation (1-2) where n = 2. Assume a ring is pressed against a perfectly flat, moving, mating ring. For n = 2 there will generally be 2 or 4 regions where film thickness is smallest (only 2 are shown) and where contact can be expected to occur (see Figures 1-2 and 1-3). In general, a fluid pressure distribution develops according to the Reynolds equation. Both hydrostatic and hydrodynamic components are included. Angular rotation of the mating face causes pressure to build up in the converging regions as the minimum film thickness region is approached. In diverging regions, cavitation will occur as the pressure attempts to become negative. For an outside pressurized seal the cavity may appear as shown in Figure 1-2 depending upon the $f_i(r)$. The fluid will flow in streamers across the cavity and a full film will again develop at the downstream cavity boundary.

The problem to be solved is to determine the fluid and mechanical pressure distribution for the given configuration. Given the pressure distribution, then load support and leakage can be calculated, and the effect of various parameters can be studied. Given this tool, then waviness shapes which provide improved performance can be found.

During the first portion of this research program only radially parallel face waviness was considered. Much effort was spent in developing solution methods and studying predicted results.

As background, the pressure distribution for wavy parallel faces has been solved by various methods by Findlay [2], Pape [3], and Stanghan-Batch and Iny [4] for perfectly smooth faces. These results show that even a small waviness produces sufficient load support for complete liftoff. However, heavily loaded or low viscosity seals do not operate with full fluid pressure load support and complete separation. A definite wear results. Surfaces of such seals contact during operation, and pressure distribution is affected by interactions with surface roughness (see Figure 1-3). Seals of this type operate in a mixed friction regime. Fluid pressure load support due to waviness may provide a significant fraction of the load support, but asperity contact must provide the balance.

As a starting point for this research program, these important effects were included in a wavy seal lubrication model. In the first annual report for this project, reference [5], this more general problem was solved using a one-dimensional theory. In the second annual report, [1], the much more complex two-dimensional solution to the above problem was solved. The effects of waviness, roughness, asperity contact, wear, cavitation, and elastic deflection were included in this model. Using this model, predictions were made for the relative wear rate, friction, and leakage as a function of roughness, waviness, speed, size, pressure, viscosity, and material.

A number of conclusions were reached based on these first two annual reports:

1) The effects of roughness on hydrodynamic lubrication are not completely understood. Certain fundamental questions remain concerning the roughness model used.

2) As to the potential of utilizing hydrodynamic effects caused by parallel face waviness to advantage by design, the results show that wear rate and friction can be greatly reduced while

maintaining leakage at acceptable levels.

3) While a comparison of predicted results to experimental results given in the literature is generally good, data contained in the literature are incomplete, so more complete experimental data are needed for comparison.

4) In low viscosity or heavily loaded applications where some touching is expected to occur, waviness will wear away with time and any benefit derived will be lost.

5) Based upon data for some commercial seals and using the model, it was determined that there was insufficient accidentally caused waviness to produce significant hydrodynamic effects in water. One cannot generalize to say that such effects do not occur in commercial seals. However, the model is provided so that the question can be answered on a case by case basis.

Item 1) was treated extensively in the third annual report [6]. Even after this analysis certain fundamental questions remain concerning how to deal with roughness in lubrication problems. A contribution to the literature on the subject was made [7]. This thorough analysis led to conclusions allowing certain simplifying assumptions discussed in Chapter 3 of this report.

Item 2) was also treated extensively in the third annual report [6]. A methodology for the design of a wavy face seal was developed and applied. Theoretical results showed large reduction in friction and wear rate compared to conventional designs whereas leakage could be controlled.

Concerning item 3), the second and third annual reports [1,6] describe a test apparatus designed to test the wavy seal theory. This apparatus has been in operation for more than one year, and many tests have been conducted. These test results are reported in Chapter 2 and compared to theory in Chapter 4 of this report.

As will be discussed, the test results do verify predicted behavior. However, early in the test program it was observed that film

thickness was not of the radially parallel face type, but consisted of combined waviness and tilt as previously described. This necessitated modification of the waviness model to include this more generalized type of film thickness. These results are reported in Chapter 4 of this report.

Concerning item 4) above, a solution to this problem was first proposed in the first annual report [5]. It was proposed to move the waviness slowly around the seal so that whatever wear occurred would be uniformly distributed. Then the shape of the wave would be preserved and tests using a constant wave could be made. The concept is illustrated in Figure 1-4. This concept was incorporated into the test apparatus and is described in detail in references [1] and [6].

In summary, in this report experimental results using waviness are presented, the waviness theory is modified to accommodate certain unanticipated film thickness shape characteristics, and theory and experiment are compared. A related development, that of the role of thermoelastic instability in face seals, is also included in Chapter 3.

Distorted Ring Under Zero Pressure

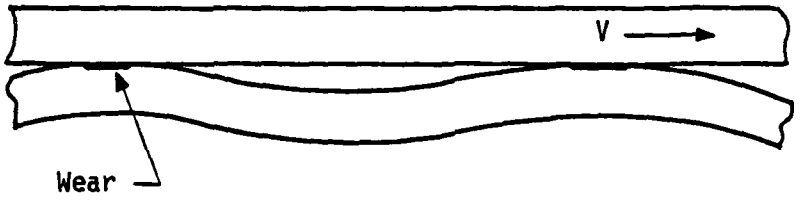

Distorted Ring Under Pressure

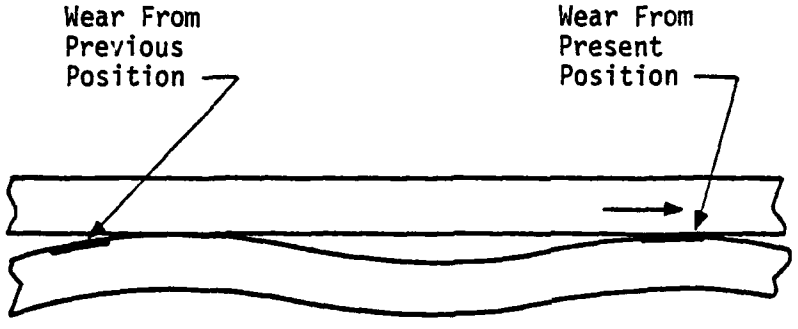

Distorted Ring Under Pressure
After Wave Has Moved

Figure 1-4. Moving Waviness Concept.

Chapter 2

Experimental Results

Test Apparatus

In order to test the various theories of seal lubrication developed in this research program, a mechanical seal test apparatus was designed and fabricated. The details of the design are included in the previous summary report [6]. The important features of the apparatus plus changes and additions since the previous report will be discussed here.

The design of the test apparatus satisfies several criteria. A wide range of speed and sealed pressure is available in order to verify modeled behavior over a wide range of conditions. Certain otherwise uncontrolled variables such as shaft runout, seal waviness, and seal radial taper are very carefully controlled. For testing the lubrication model of interest, a controllable waviness can be applied to the seal faces, and in order to reduce the effects of wear, this waviness is moved circumferentially with respect to the primary ring. Leakage from the seal is measured. Torque is measured in a manner such that the seal torque is measured independently of bearing torque or torque arising from a second seal used in a tandem arrangement. Many of the distortions commonly found in commercial seals are minimized.

The specifications are as follows:

Configuration:	Horizontal shaft, single seal with torque measured on the seal housing. Rotating secondary seal ring.
Size:	Accepts up to 92 mm (3.63 in.) nominal shaft size seal. 102 mm (4 in.) nominal seal face diameter.
Speed:	500 to 4000 RPM. 3 to 21 m/s (9 to 70 ft/s) for a 102 mm (4 in.) seal.
Pressure:	0 to 6.9 MPa (0 to 1000 psi) continuous. Vessel is rated at 13.8 MPa (2000 psi).

Bearings:	Five ABEC-7 bearings on precision spindle. Bearings are rated at a maximum of 53000 N (12000 lb) thrust at 4000 RPM (corresponds to a 102 mm (4 in.) seal at 6.9 MPa (1000 psi).
Motor:	3700 W (5 Hp) variable speed drive (belt type).
Fluid:	Materials are selected for seawater service.
Balance:	Balance ratio of 1.0 (lower values can be used).
Seal Rings:	Zero moment design. Designed to minimize the effects of pressure caused radial taper.
Waviness:	Seal waviness is controlled by variable ring distortion. It can be moved relative to the primary ring.
Temperature:	Can be controlled at any given temperature above 38°C (100°F).
Quantities Measured:	Speed, pressure, temperature, waviness, torque, and leakage.

Figure 2-1 shows the general layout of the test apparatus. The bolted vessel on the right-hand end contains the pressurized seal. Immediately to the left is the waviness drive plate and the cage-like torque sensing element. The entire test vessel is supported cantilever style by the torque sensing element. Further to the left is the bearing housing which is attached to the frame. The variable speed motor drive is located to the left of the bearing housing.

On the level below the test vessel in Figure 2-1 is located all of the auxiliary equipment. To the left end is the oil supply system including a tank, pump, filter, and cooler. On the right end is the high pressure water circulation pump and heat exchanger.

Figure 2-2 shows the essential features of the seal test apparatus in detail. The shaft turns on five precision angular contact bearings designed to operate under the large thrust load. Cooling water is circulated through the test chamber through openings not shown. The torque sensing element acts as the support for the vessel. The pressure vessel is designed to be readily taken apart by removal

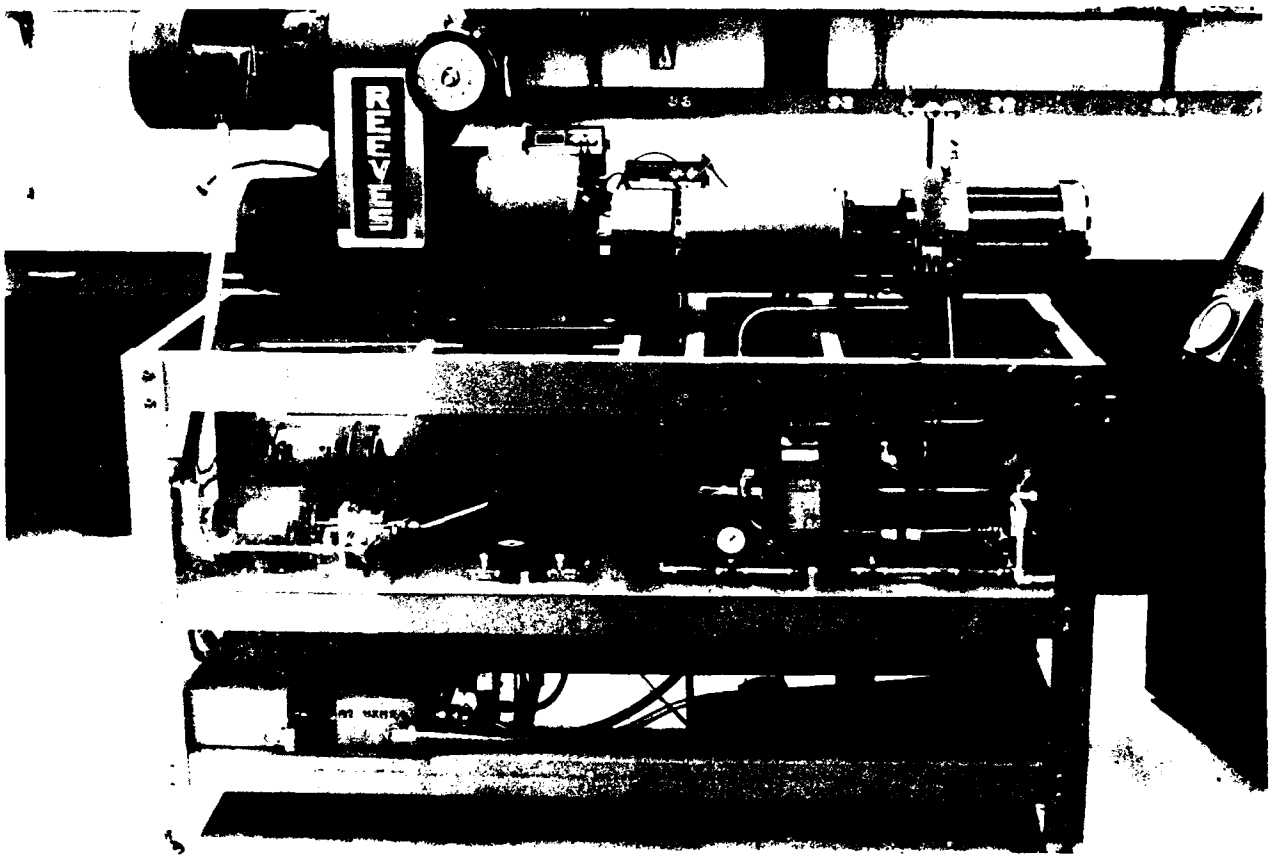

Figure 2-1. Mechanical Face Seal Test Apparatus.

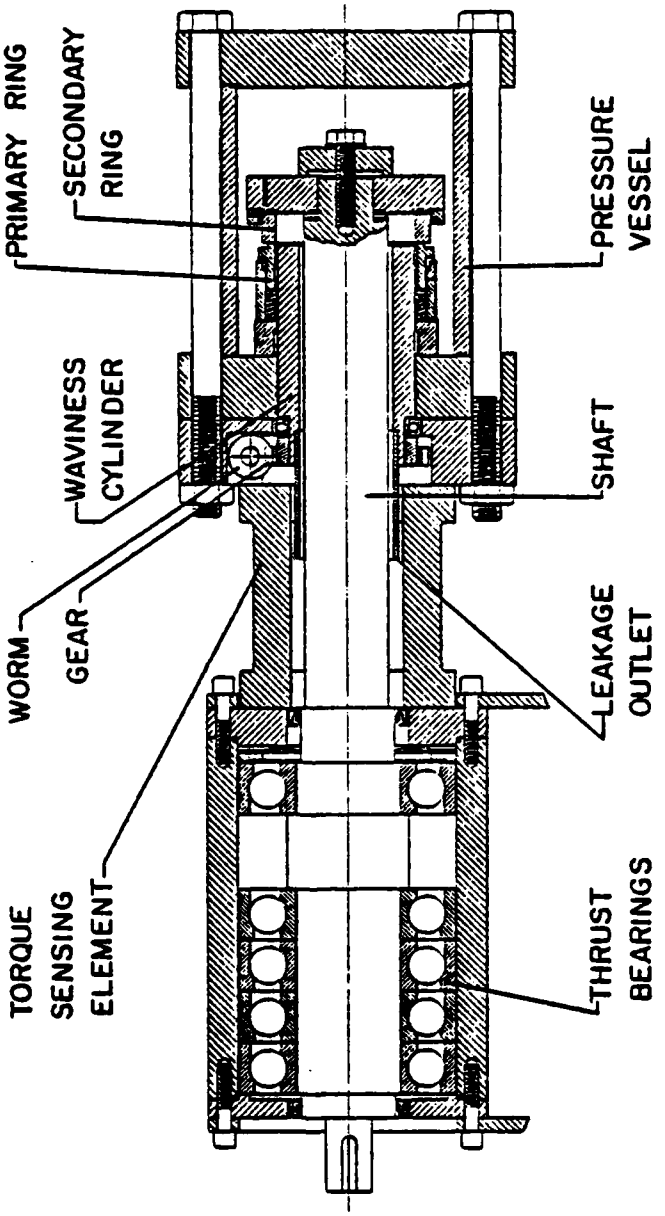

Figure 2-2. Section View.

of bolts. The secondary ring support rotor is removed by removing the capscrew. To minimize axial runout at the seal face, the end of the shaft is ground true with the bearings. The rotor is ground both where it mates with the shaft and the secondary seal ring. The two secondary seal ring faces are ground parallel.

The primary ring is made of Pure Carbon P658RC. The unusual proportions of the ring result from adjusting the geometry so that sealed pressure causes no rotation about a circumferential axis. The primary ring is driven by lugs which engage two notches. Two as opposed to a greater number of notches were used because this arrangement gives the primary ring maximum freedom to float radially to align itself. Second harmonic waviness is minimized by driving the ring through the centroid of its cross section. Any remaining second harmonic waviness produced by drive forces will be more easily flattened than the third harmonic waviness built into the ring, so it is not considered important. The secondary seal is located at the left end on the inside diameter. The balance ratio for the design shown is 1.0. Springs to the left of the seal provide a preload of about 0.2 MPa (30 psi).

The secondary seal ring is fabricated from tungsten carbide. This ring is also of a zero pressure moment design. An unusual feature of the particular design is that the mechanical force at the right-hand side of the seal has been reduced to nearly zero by placing the O-ring seal on the right-hand face as opposed to the outside diameter. It is useful to minimize the axial force to reduce coning effects caused by friction at the load bearing point in conjunction with radial deformation due to pressure and temperature. The secondary seal ring is held in place by spring clips (not shown) which engage notches in the ring.

Figures 2-2 and 2-3 show how the moving wave concept was implemented in the seal test apparatus. The drive ring is designed so that the primary ring can float and align itself but cannot rotate about the shaft axis. The primary ring thus takes its alignment from the face of the rotating secondary ring. The waviness drive cylinder is driven by a worm at low speed (one revolution per 9.47 h). The waviness drive cylinder seals into the housing with two O-rings designed so that gas

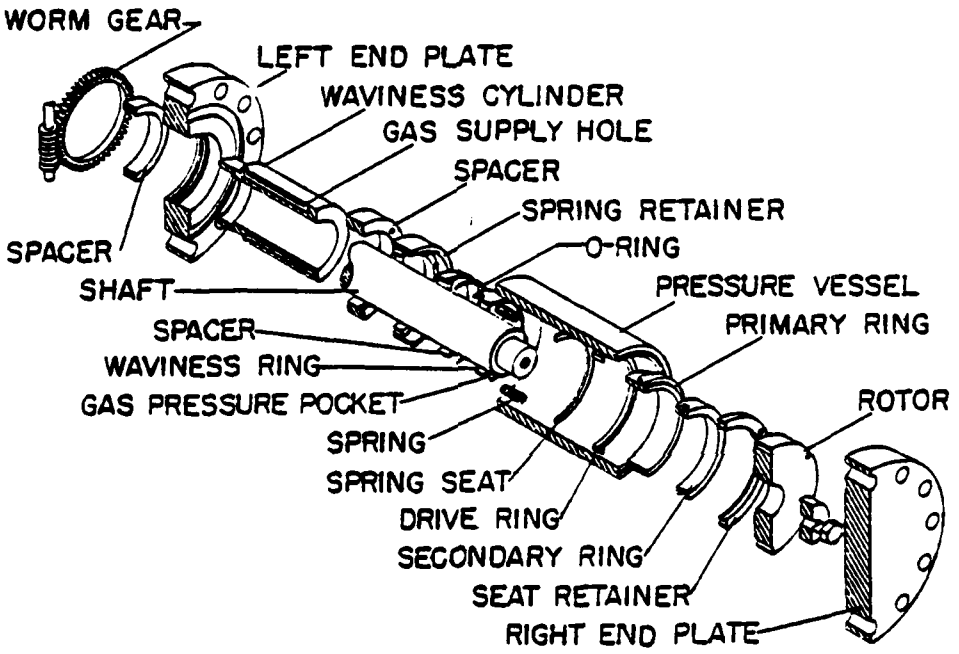

Figure 2-3. Exploded View.

pressure can be supplied through the end plate and into the waviness cylinder. Each of the six holes on the waviness drive cylinder is connected to this gas pressure. When the primary ring is positioned over these six holes and sealed off by six O-rings, then the primary ring becomes subjected to six small regions of gas pressure on its inside. These forces produce moments about the centroid of the ring. The staggered location causes alternating moments of opposite sign. Face waviness and an alternating face taper are produced by these moments. As the waviness cylinder is turned by the worm and gear, the waviness pattern moves relative to the seal primary ring.

The torque sensing element is shown in Figures 2-1 and 2-2. The axial load that must be carried by this member is large, 53000 N at 6.9 MPa (12000 lbs at 1000 psi) whereas the torque to be measured is quite small (down to a few N•m (in.-lb)). The axial load is carried by ten 3 x 25 x 102 mm (0.120 x 1 x 4 in.) long elements. These elements have a very high axial stiffness and strength but low torsional stiffness. The torsional load is sensed by two beams which have a low axial stiffness. The axial and torsional loads are in effect isolated so that torque can be measured independent of axial load. Strain gages are mounted on the two beams. Test results verify the design behavior. There is no measurable influence of pressure on torque at least up to 300 psi where the test was performed.

The torque sensing element is sensitive to temperature. A temperature increase of the bearing housing causes a torque shift of 0.109 $(T_{housing} - T_{reference})$ in.lb/°F. This effect is repeatable and has been corrected in the data reduction.

Waviness Drive

Since the previous report was written several additions have been made to the system. The first addition is the waviness drive. Figure 2-4 shows a motor driven gear arrangement which connects to the shaft of the worm which drives the waviness cylinder. The apparatus shown normally drives the waviness cylinder at one rotation per 9.47 h for the purpose of providing a slowly moving wave for testing the effects

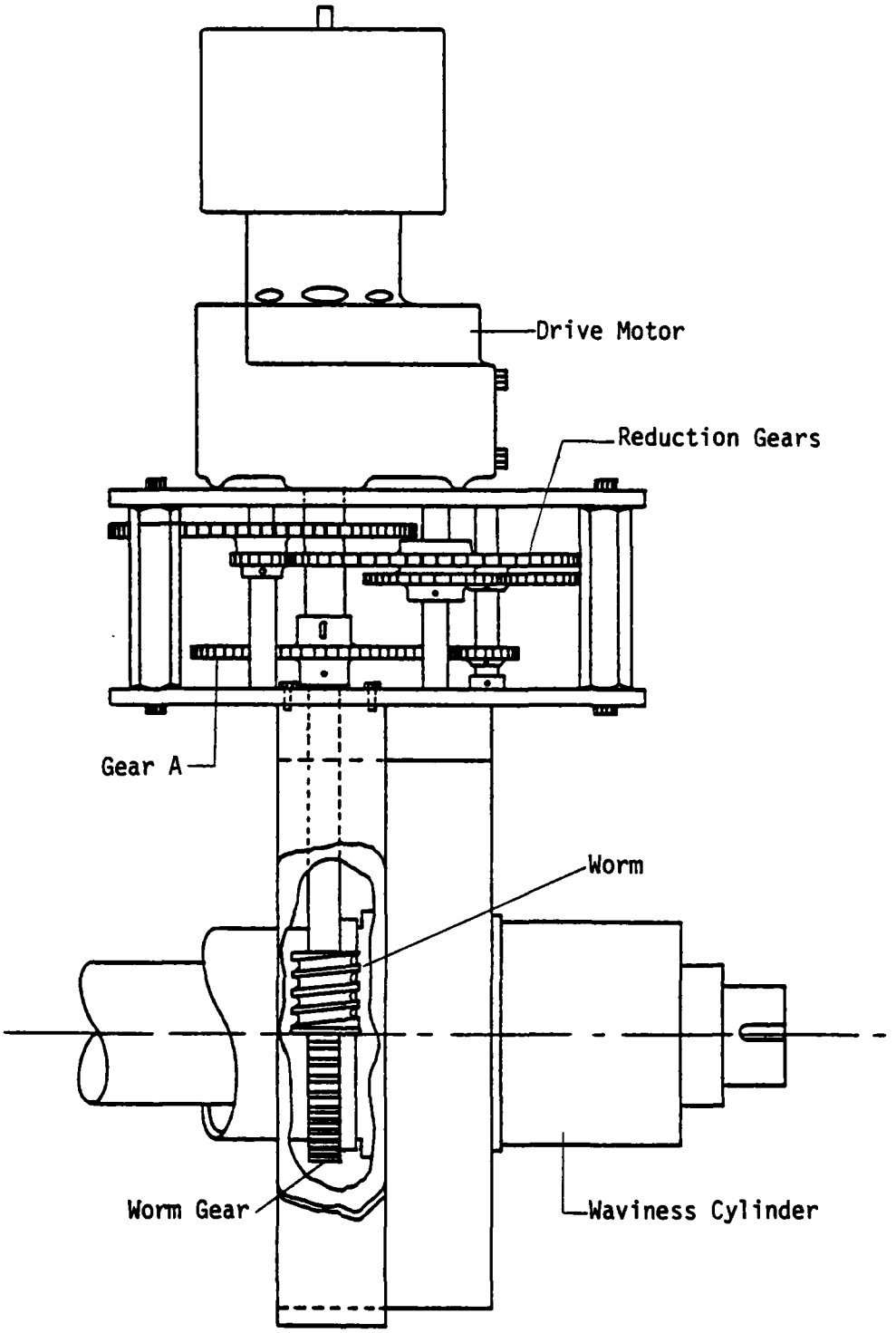

Figure 2-4. Waviness Drive.

of waviness. By sliding gear A, shown in the figure, the motor can be connected directly to the worm so that the waviness cylinder speed is about 1/2 RPM. This higher speed arrangement is used for setup and calibration purposes.

Leakage Measuring Device

A second addition to the test apparatus is a leakage measuring device. For early tests (up through test number 37), leakage was measured using a graduated cylinder and clock. This had the disadvantage that a continuous measurement of leakage rate was not available. Also, certain inconsistencies occurred because the leakage could not be averaged over a sufficiently long period of time in order to average out leakage fluctuations (described later).

To electronically record leakage on a continuous basis presents some problem when leakage rate may vary over an extremely wide range, say from a fraction of a cm^3/min to 100 cm^3/min. Since a computer is part of the system, the approach used is to measure the time required for a given small quantity of flow and compute the average flow rate. This has been accomplished using the tipping device shown in Figure 2-5. The device tips alternately after about 2.0 cm^3 of flow. Each time tipping occurs, a photodiode with associated circuitry closes a relay which in turn closes a second relay. The computer is then informed of this event and the time is noted. By noting the time for each tip, the leakage rate is calculated after each tip and recorded and plotted.

The device shown in Figure 2-5 is fabricated of thin sheet brass and the tipping bucket is supported by jeweled bearings to minimize friction and wear. Calibration tests show the device is consistent and reliable. At high leakage rates (100 ml/m) some error is introduced by the time response of the bucket. However, most of the leakage rates measured are well below this rate so that no significant error is introduced.

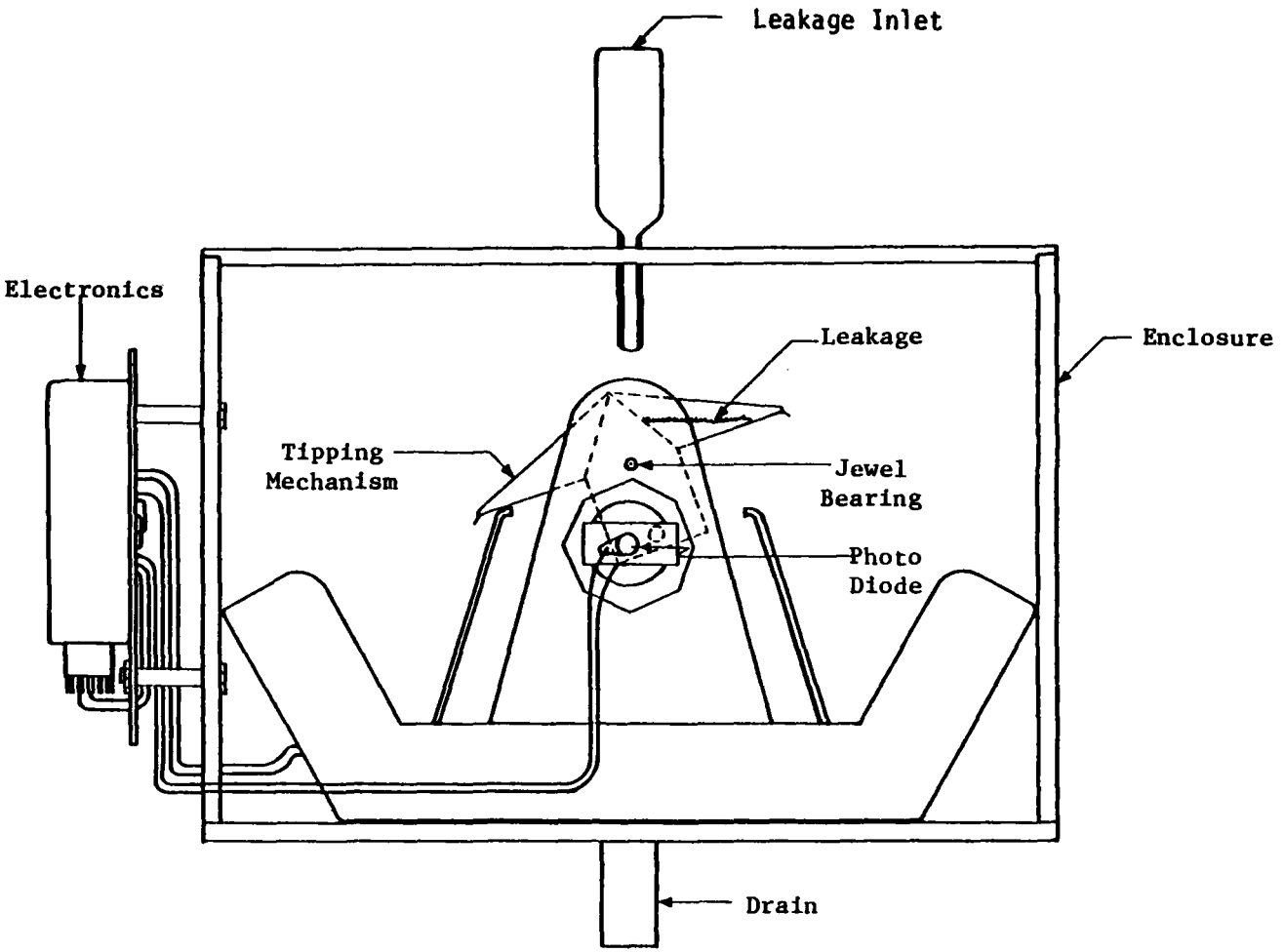

Figure 2-5. Leakage Measuring Device.

Computer Control and Data Acquisition

During August 1979 all of the data gathering, storing, display, and control functions were taken over by computer. The components of the original control system were retained as a back up and so that the apparatus can still be operated independently of the computer as is needed.

The computer based system will now be described in some detail. The basic system used is illustrated in Figure 2-6. The computer can read voltage, etc. through the plug in cards in the 6940 or can output signals through the 6940 by other cards such as the relay card shown. In addition, the computer controls the plotter and its own internal printer and tape drive. All logic is stored in the computer. The control-data acquisition system uses the program listing which is shown in Appendix A. The functions of the program are as follows:

Pressure - An analog pressure signal is supplied by a BLH pressure transducer to the low level A/D converter card. This signal is read approximately one time per second. If pressure is below the pressure set point, a relay in the relay output card is activated for 50 ms which in turn activates a second relay having an approximate one second latch time. This second relay controls the air valve to the high pressure pump. Air is turned on for approximately one second allowing the pressure pump to make one stroke. Using this system, pressure can be controlled to within about 5 psi of a set point. If pressure becomes greater than 120 percent of the set point or less than 70 percent of the set point, this indicates a malfunction and the apparatus is shut down.

Torque - An analog signal is supplied by the torque transducer described in the previous annual report [6]. This signal is read by the low level A/D card approximately 12 times per minute. The signal is corrected for a torque shift caused by bearing housing temperature, and the proper calibration constant is applied to give direct torque readings. The 12 points are averaged and the average is plotted and recorded on tape along with the time.

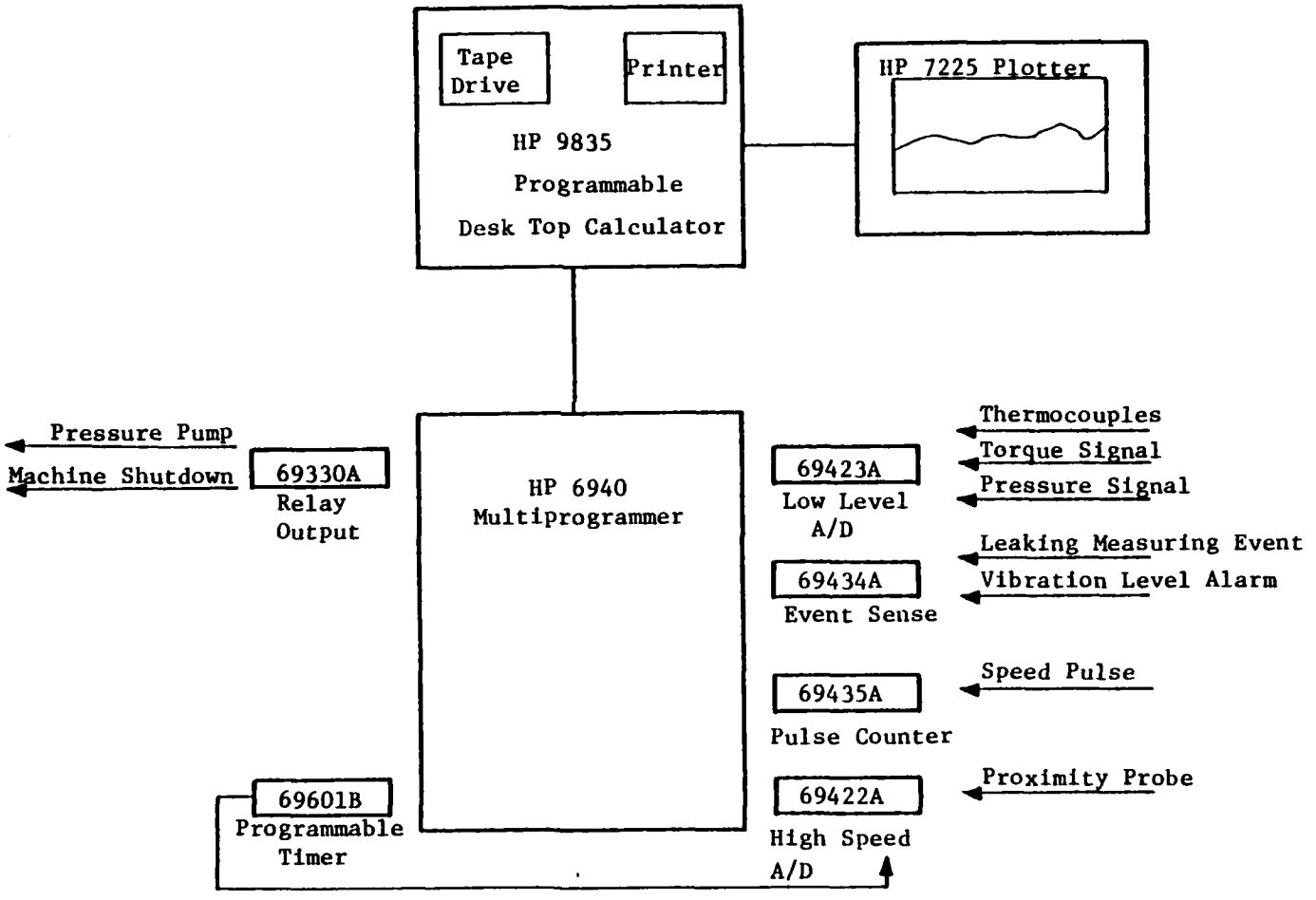

Figure 2-6. Computer System.

Calibration of the torque transducer to obtain a calibration constant is accomplished by a subroutine contained in the control program. Torque transducer voltage output is read for zero applied torque and a given applied torque, and a calibration constant is established.

Zero level of the torque signal is also established using the control program at the beginning and end of each test. The zero level of torque is determined by hand cranking the drive both clockwise and counterclockwise, taking a number of readings in each direction, and establishing the voltage level output that corresponds to zero torque level.

Face Temperature - The low level A/D card has a built-in thermocouple reference. The face temperature thermocouple is read 12 times per minute, converted to temperature, averaged, plotted, and stored on tape. If face temperature goes above a set point, the apparatus is shut down.

Leakage - Each time the leakage measuring device tips, the time of this event is recorded. At approximately one minute intervals, the number of tips and the time between the first and last tip is determined. The leakage rate is calculated, stored on tape, and plotted. If there have been no tips within the one minute interval, then this fact is noted on tape and no point is plotted. When an interval is encountered during which a tip has occurred, leak rate is determined by the total elapsed time between tips even though these may be more than one minute apart, and the leakage rate is computed, plotted, and recorded on tape.

Bearing Housing Temperature - This temperature is read using the low level A/D card each time torque is read for the purpose of correcting torque. If housing temperature exceeds a certain level, then the apparatus is shut down. The 12 readings taken within one minute are averaged and recorded on tape every ten minutes.

Oil Temperature - This temperature is read one time per minute using the low level A/D card. Temperature is compared to a limit.

The apparatus is shut down if temperature goes above this limit. This temperature is recorded on tape approximately every ten minutes.

Water Temperature - The procedure for water temperature is the same as for oil temperature. Water temperature control is handled by the Honeywell controller described previously [6].

Vibration Level - Vibration level is monitored continuously by a vibration analyzer. The signal is compared to a set point using an electronic comparator circuit. When vibration level exceeds a certain level, a relay is closed. On manual operation, closing of the relay shuts down the test apparatus. Under computer control, each time the relay closes, the computer is signaled through the event sense card. If this occurs more than five times and for a period greater than ten seconds, the test apparatus is shut down.

Plotting - Torque, face temperature, and leakage rate are plotted as functions of time at one minute intervals throughout the test. An example of such a plot is shown in Figure 2-7. This provides a visual indication of the test results as the test proceeds. Data stored on the tape can be replotted after a test is completed.

Proximity Probe - The proximity probe for measuring the change in gap at the face of the seal (described later) is read using the high speed A/D card. This provides a large number of readings over a short period of time.

Surface Analyzer - The high speed A/D card in conjunction with the programmable timer is used to read a roughness signal for the surface analyzer. The timer pulses the A/D card at a high rate of speed so that 5 to 10000 points can be quickly input into the computer for further analysis. The computer roughness analysis is described in detail later.

The program performs its various functions above by being in an infinite loop. There are several possible loops and modified loops built into the program to perform various tasks at different times. To change from one loop to another, certain keys are defined to shift control. To illustrate some of the features of the program, the key

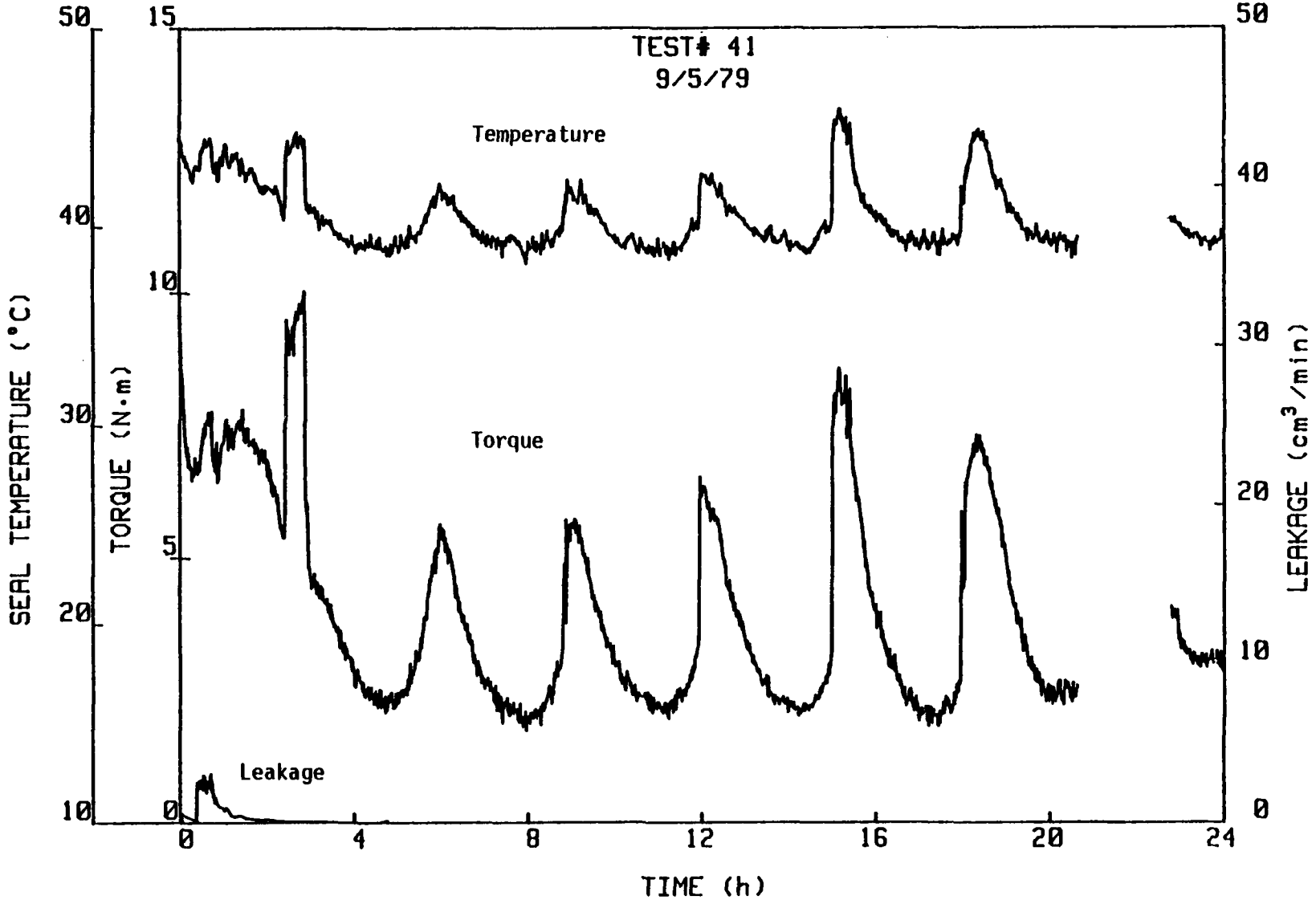

Figure 2-7. Sample Plot.

definitions are given in Table 2-1.

Operation of the test apparatus using the computer control is greatly simplified compared to using chart recorders, etc. The data is corrected and converted automatically to the proper units. Having all output on the same graph with a greatly compressed time scale is quite helpful in interpreting the results. There is also considerable flexibility for changing the type of data collected. Control and safety features are easily programmed in.

Problems that have arisen in the system have been related to computer hardware. The original input/output ROM in the computer had a logic error which caused the computer to hang up at random. The time clock had a malfunction which caused it to reset to zero at random. One loose connector caused a computer hangup. Since these problems have been corrected, operation has been reliable and several tests have been run using the computer system.

Test Program

Using the apparatus described, 45 different test runs have been made to date. The time duration for these tests ranges from a few hours to several hundred hours. The types of tests run are as follows:

Flat face:	Seal faces lapped flat and run
Waviness:	Continuously moving waviness of differing amounts
Wear:	A test of long duration to provide measurable wear
Pressure:	Pressure is varied from standard conditions
Speed:	Speed is varied from standard conditions
Proximity Probe:	Proximity probe is used to measure face displacement

Standard or base case test conditions have been established as follows:

Table 2-1

Key Definitions

Key	Function
K0	"Shut Down" - This subprogram trips main control relay out and shuts down the apparatus. Program shifts to idle where "CONTROL PROGRAM READY" is displayed. Program can be shifted back to the "start" mode.
K1	"Run" - Data is taken. Time is set at zero. "Run" can be used any time during a test. "Run" will restart the data at time = 0 and previous data will be erased. Subsequent shifts to "start" and "Conrun" do not shift time axis and previous data are retained.
K2	"Start" - When "CONTROL PROGRAM READY" then "start" can be executed. This closes the main control relay so the machine can be started up. Pressure is controlled.
K3	"Axis" - To draw and set up axes any time. "Axis" subprogram runs in the "start" mode so that pressure is controlled so that test may continue. "Axis" goes to "start" after axes have been plotted. To continue test use "Conrun." Data which were taken beyond the previous time axis will be plotted first before current data are plotted. Program will automatically do this after an "axis" and "conrun" are used. Data can be stored for only five hours beyond the plotter limit. Going beyond this will cause the program to exceed dimensional limits.
K4	"Rezero" - The torque can be rezeroed at any time. Temperature correction is shifted accordingly. Machine is placed in "CONTROL PROGRAM READY" mode after rezeroing. Test can be started over by using "start" and run, or it can be continued by using "start" and "conrun."
K5	"Conrun" - Continues running after a "start" interrupt. Program takes data from where it left off. Missing data are represented by a gap.
K6	"Testend" - Gives value of current file and stops taking data. Program goes into "start" mode. Finds torque, temperature, and leakage averages. Use "shutdown" to stop machine.

p_{H_2O} = 3.45 MPa (500 psi)

RPM = 1800

Albuquerque tap water

38°C (100°F) seal temperature environment

Seal rings were prepared as follows:

Secondary rotating ring: WC, lapped and polished, 0.03 to 0.08 μm (1 to 3 μin.) CLA, radial taper $<100.10^{-6}$

Primary stationary floating ring: P658RC carbon, as lapped, 0.51 μm (20 μin.) CLA, radial taper $<50.10^{-6}$

The above specifications on seal rings were held for most of the tests. However, in some cases where previous wear was small, WC rings were used for more than one test without relapping. New (as manufactured) carbon rings had a lower surface roughness than quoted above for those prepared on our own lapping machine. Also, the radial taper on carbon rings prepared in our own lab was generally (but not always) less than 20.10^{-6}. Radial taper on some of the as manufactured rings was larger than this.

Seal roughness (CLA) was measured in a radial and tangential direction both before and after each test. Radial taper was measured before and after each test. For measuring carbon ring wear, the nose height of the seal was measured relative to the shoulder using the surface analyzer and a gage pin. For later tests, the carbon was oven dried after test to minimize distortion due to water absorption. In later tests, surface roughness statistics were determined using the surface analyzer in conjunction with the computer.

The installation procedure for the seal faces was to wipe each face with solvent, dry the faces, and then wet each surface with water before they were mated.

Appendix B contains tabulated results for all tests. Appendix C contains performance curves for those tests conducted since the computer system has been installed. The detailed results for each type of test

will now be presented and discussed.

Flat Face

Figure 2-8 shows typical temperature and torque versus time performance curves for a flat faced seal. There was no measurable leakage in this test so it does not appear on the graph. The gap in the curves was caused by a data collection malfunction; the seal itself ran continuously. The torque curve is characteristic of a flat faced test; there is a wide unpredictable variation in torque level. Occasionally, the torque will increase abruptly. Face temperature follows torque as expected.

Upon disassembly, surface analyzer traces of the carbon show a divergent coning of about $1300 \cdot 10^{-6}$ (see data in Appendix B). This indicates that during operation thermal coning caused the seal faces to form a convergent taper. After operation under this condition, the faces wear flat such that when cooled they appear to be divergent.

Figure 2-8 shows that initial torque is relatively low and gradually increases with time. This behavior agrees with the theory presented in reference [8] which suggests that during initial operation, thermal coning produces a convergent film shape and reduces friction. As the face wears flat, the friction increases.

Table 2-2 shows results for five flat faced tests ($p_{gas} = 0$). No measurable leakage is shown for any of the tests. Average friction torque (for the final hours of the test) varied widely from 7.7 to 13.7 N·m. Although the gradual increase in flat faced seal torque can be explained as mentioned, the sudden changes in the torque curves are more difficult to explain. It is possible that sudden increases are caused by the faces drying out, i.e., the fluid becomes sealed off at the outside diameter. Dry carbon has a much higher friction coefficient than wet carbon. After the temperature increases, sufficient convergent coning occurs such that fluid reenters the gap and friction is reduced.

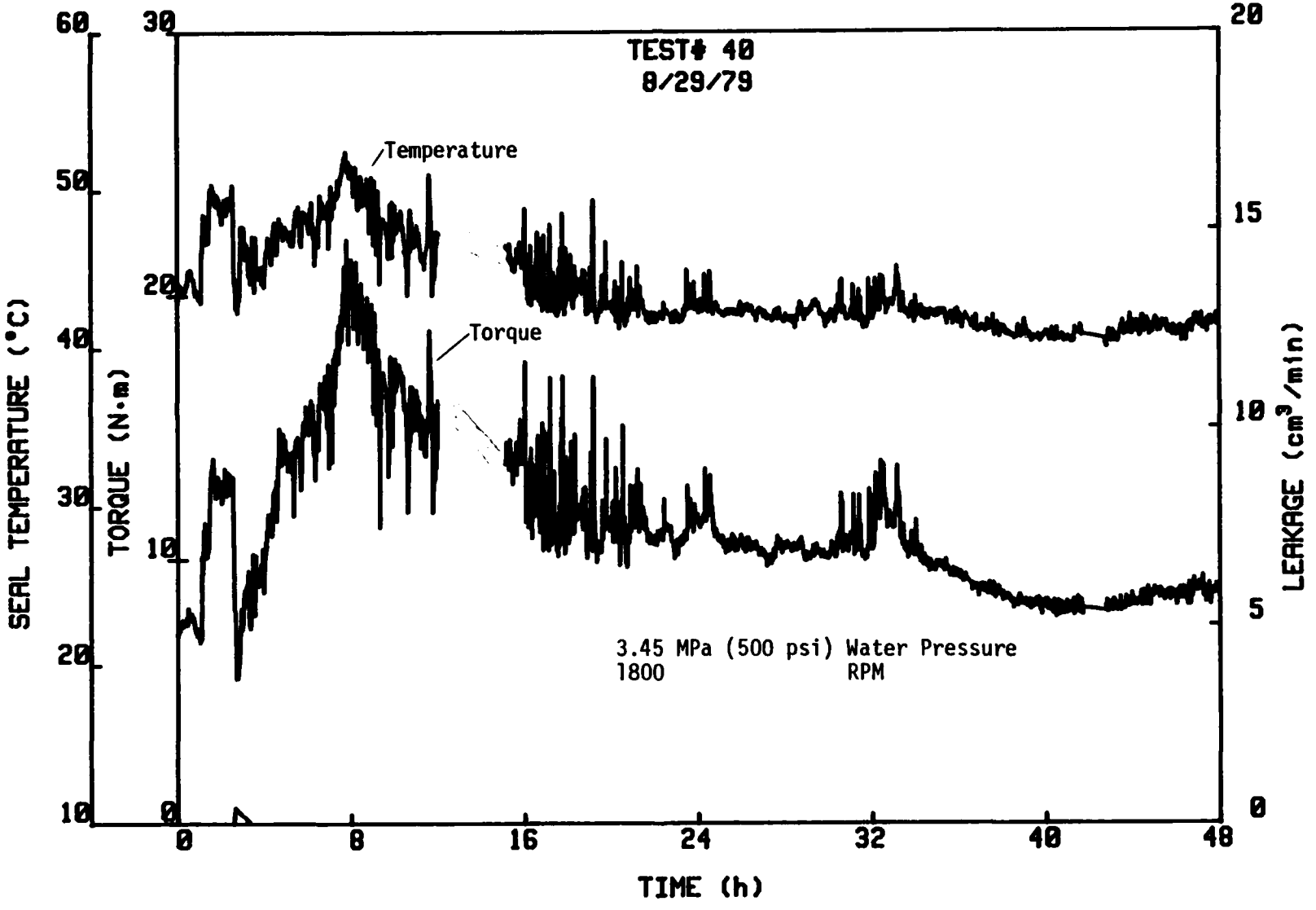

Figure 2-8. Typical Flat Face Performance Curve.

Table 2-2

Flat Face and Waviness Tests

(Test durations greater than 10 hrs)

p_{H_2O} = 3.45 MPa 1800 RPM

p_{gas} (MPa)	Test No.	Test Duration (h)	Average Face Temperature (C)	Average Torque (N·m)	Average Leakage (cm^3/min)
0	5	19	44.4	7.7	0.0
0	13	24	46.1	12.3	0.0
0	22	100	48.9	13.7	0.0
0	35	100	43.9	8.4	0.0
0	40	111	42.8	9.2	0.0
3.45	41	102	41.1	4.6	0.0
4.14	29	25	42.8	5.1	0.0
4.76	23	100	40.6	2.0	0.3
4.83	27	21	40.0	2.9	0.7
4.83	36	100	40.0	2.4	1.4
5.03	12	24	41.1	2.3	0.6
6.90	21	100	40.0	1.5	1.1
6.90	25	43	40.0	2.5	0.6
6.90	32	18	40.0	3.1	0.7
6.90	34	100	39.4	1.4	1.4
6.90	38	42	39.4	2.0	2.5
6.90	39	100	39.4	1.6	3.2
7.07	10	24	40.0	2.9	1.2
8.27	44	73	38.3	2.1	8.2
8.52	11	23	40.0	2.3	5.2

Waviness

Figure 2-9 shows a typical test result for a wavy seal. At the start of the test the torque is high and then levels off to a lower cyclic value. The initial high torque is caused by the fact that it takes several hours for the carbon face to assume its equilibrium shape. Once this occurs, then the torque cycle becomes constant with increasing time.

Like torque, leakage stabilizes at some constant cyclic value. The period of the leakage cycle is 1.58 h. This corresponds to 1/6 of the time for one revolution of the waviness cylinder (9.47 h). The torque and leakage variations are being caused by a superposition of the third harmonic waviness over a second harmonic waviness which is being produced by the two drive forces. Thus, the significance of the cyclic behavior is that operation can be influenced by unwanted deflections, and that such deflections must be controlled. Otherwise, the extremes of the cycle could represent unacceptable operating conditions. In the case shown, the extremes are not large. Additional waviness test curves are shown in Appendix C.

The greatest difference between the flat face and wavy test results is that the torque and temperature of the wavy seal are much lower than for the flat face seal. In Table 2-2 the results of a number of waviness tests at different gas pressures are shown. The data are averages over the last 9.47 h of the test. The effect of waviness on torque is large. Torque values are reduced to one fourth of those values for the flat face.

For leakage, the trend is as expected with leakage increasing from unmeasurable quantities in the case of the flat face to several mℓ/min at the higher gas pressures. The scatter in results is greater than for torque. One reason for this is that some of the earlier leakage measurements were made using a clock and graduated cylinder before the computerized apparatus was completed. It is likely that this approach introduced some error because there was no way to average over a complete leakage cycle as shown in Figure 2-9. In addition, since leakage is related to film thickness cubed, very small differences in operating

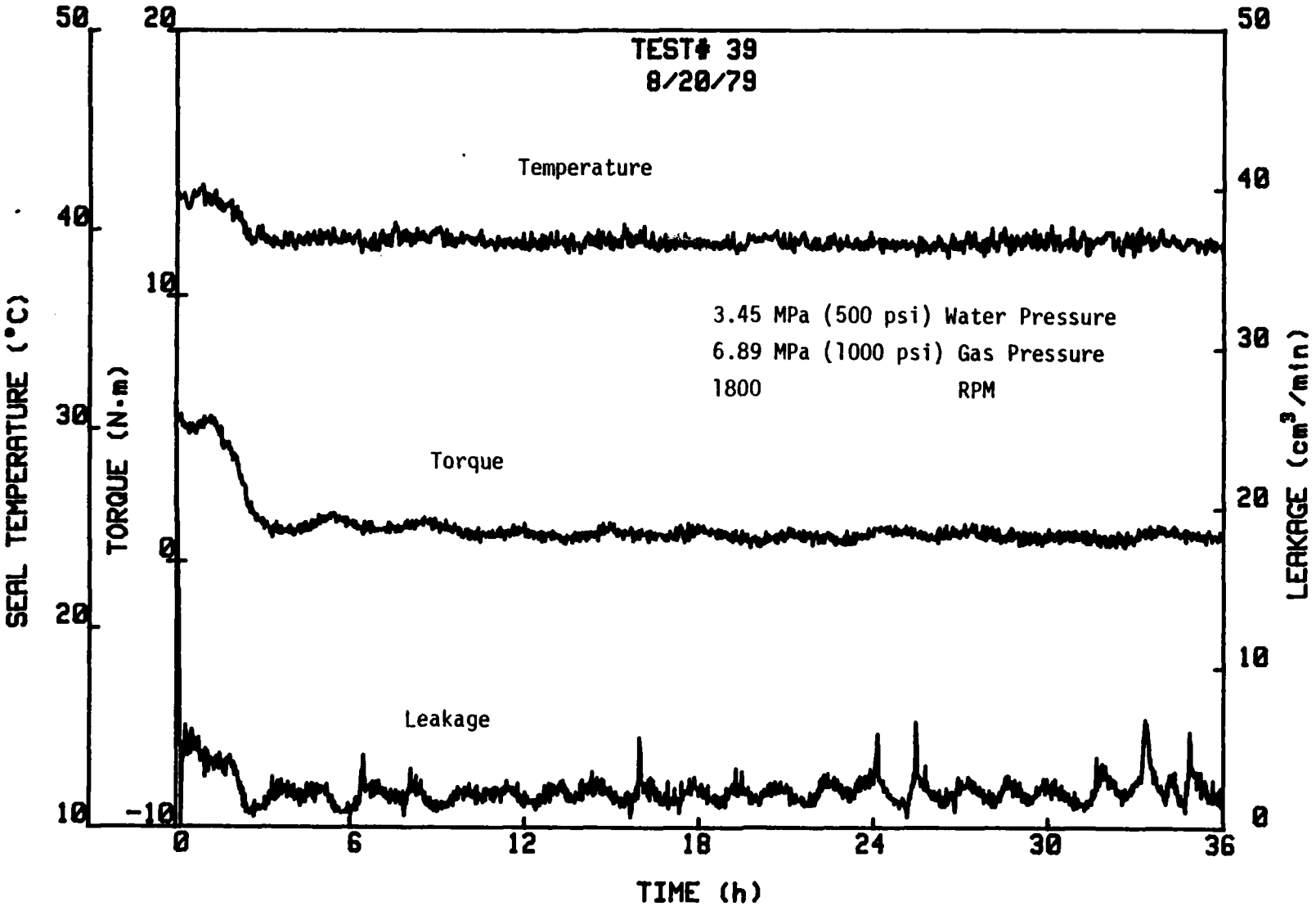

Figure 2-9. Typical Waviness Performance Curves.

equilibrium film thickness lead to large variations in leakage.

Wear

Table 2-3 shows the results of several 100 h wear tests. Torque, leakage, and temperature values fit in with the trends previously described. Wear results require some explanation. First, looking at the flat face results, tests 35 and 40 give comparable results whereas test 22 shows a very high wear. Comparing torque and temperature of 35 and 40 to 22 shows that test 22 operated at a significantly higher temperature and torque. Thus, a different type of equilibrium was established such that wear was much larger.

Several of the tests show a negative wear. The significance of this is that wear was less than the distortion in the 3 mm (0.125 in.) nose of the carbon caused by water absorption and thermal effects. This result occurred in spite of careful drying procedures. Wear measurements on a given seal are repeatable so that this was not the source of error. It is known that strains of the order of 0.001 can be introduced in carbon by water absorption. For the 3 mm nose height, this would correspond to a dimensional change of 3 μm (125 μin.). Thus, for now it is concluded that the actual wear magnitude for the cases giving a negative reading are of the same order as the nose distortion or 3 μm (125 μin.). Based on Table 2-3, the wear rate for p_{gas} = 6.9 MPa wavy cases are from four to forty times lower than the flat face test.

To help in narrowing this range, a series of 500 h duration tests are being run to attempt to establish a more repeatable wear rate, particularly for the waviness cases.

Radial Taper

In order to test the validity of the hydrostatic theory of Reference [8] which considers hydrostatic pressure, load sharing, and thermal coning, three tests (24, 42, 43) were run where a converging radial taper was lapped into the seal before the test.

To create the radial taper, the device shown in Figure 2-10 was inserted into the back of the seal, pressurized, and the seal lapped

Table 2-3

Wear Test Results

Speed = 1800 RPM
Cooling Water Temperature = 38°C (100°F)
Outside Seal Radius = 53.00 mm (2.088 in.)
Balance Ratio = 1.00

Water Pressure = 3.45 MPa (500 psi)
Test Duration = 100 h
Inside Seal Radius = 48.3 mm (1.900 in.)

Test No.	Gas Pressure MPa (psi)	Calculated Waviness Amplitude μm (μin.)	Torque* N·m (in.-lb)	Leakage* ml/min	Face Temperature °C (°F)	Average Wear Carbon μm (μin.)
22	0 (0)	0 (0)	13.7 (121)	0.0	50 (122)	122 (4800)
35	0 (0)	0 (0)	8.4 (74)	0.0	44 (111)	12 (456)
40	0 (0)	0 (0)	9.8 (87)	0.0	43 (109)	16 (641)
23	4.76 (690)	6.2 (245)	1.9 (17)	0.3	40 (104)	22 (860)
36	4.81 (700)	6.3 (249)	2.4 (21)	1.4	40 (104)	-1.3 (-52)
21	6.89 (1000)	9.0 (356)	1.5 (13)	1.0	40 (104)	2.5 (98)
34	6.89 (1000)	9.0 (356)	1.3 (12)	1.4	39 (103)	-1.1 (-45)
39	6.89 (1000)	9.0 (356)	1.6 (14)	3.2	39 (103)	-1.1 (-42)

*Averaged over last two hours of test.

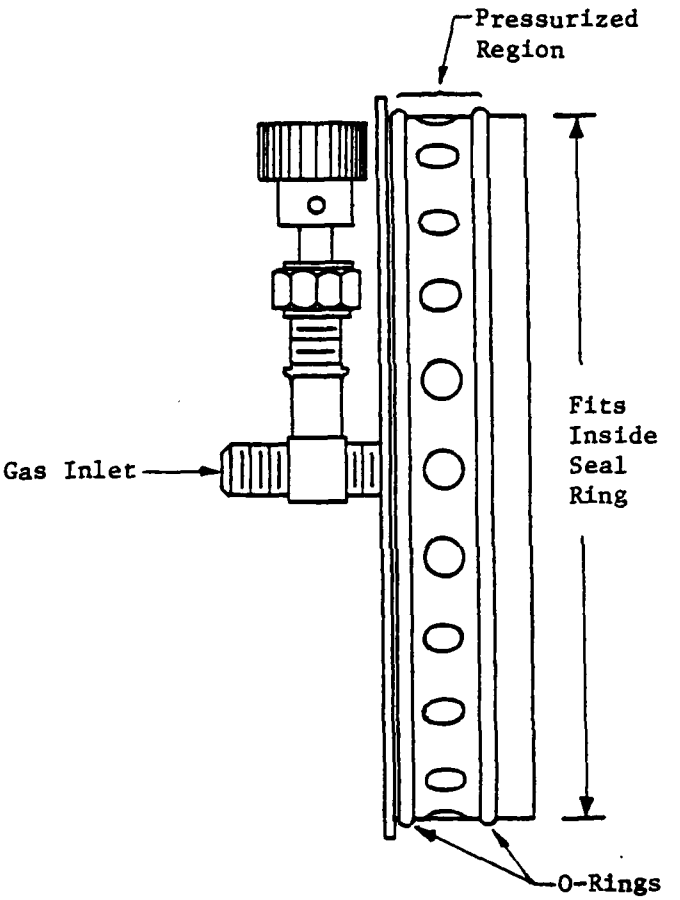

Figure 2-10. Radial Taper Device.

flat. The device is designed to create a uniform moment about the ring centroid causing the faces to diverge. After lapping and releasing the pressure, a converging taper results. Taper is proportional to the pressure applied.

Table 2-4 shows the results from three radial taper tests and one flat faced test for comparison. Torque in the radial taper cases is less than one half of that in the flat faced case. Thus, the converging radial taper produces a larger component of hydrostatic lifting force than in the flat faced case. Test number 43 shows that torque is insensitive to the amount of taper. However, it can be shown for a balance ratio of 1.0; this result can be expected in this range of large radial tapers.

Figure C-5 (test 42) of Appendix C shows a gradual decrease in torque with time as wear progresses across the face of the seal. Also, there is some leakage initially which gradually diminishes to unmeasurable values with time. The torque and temperature are quite steady compared to a flat faced test except for an occasional excursion such as at 184 and 264 h for test 42 (Figure C-5).

Figure 2-11 shows a comparison of the original taper to the worn taper after the test. It is clear that a certain fraction of the seal face has worn flat. This causes a change in operating performance with time. Table 2-4 shows that a greater fraction of the seal is worn flat for a longer duration test. This result suggests that after a long period of operation the taper would wear off completely and the seal would continue operation performing like a flat faced seal. A comparison of these results to theory will be made in a later report.

Pressure

Table 2-5 shows the effects of varying sealed pressure for a wavy seal. At the lowest test pressure, leakage is large in comparison. This occurs because the wave is not flattened out as much as at higher sealed pressures. At the highest pressure, torque is significantly larger than at the lower sealed pressures. This indicates that a significant fraction of the face load is being carried by mechanical

Table 2-4

Radial Taper Test Results
p_{H_2O} = 3.45 MPa, 1800 RPM

Test Type	Test No.	Test Duration (h)	Avg* Face Temp (°C)	Avg* Torque (N·m)	Avg* Leakage (cm^3/min)	Initial Taper	Fraction of Face Flattened by Wear
Flat Face	35	100	43.9	8.4	0.0	0	-
Radial Taper	24	116	41.4	3.9	0.0	$1060 \cdot 10^{-6}$	0.33
Radial Taper	42	335	39.8	2.5	0.0	$1110 \cdot 10^{-6}$	0.49
Radial Taper	43	165	39.4	3.0	0.0	$2430 \cdot 10^{-6}$	0.29

*Average over last nine hours of test.

Radial Profile (.001 filter)
Test #42 (Initial Trace)

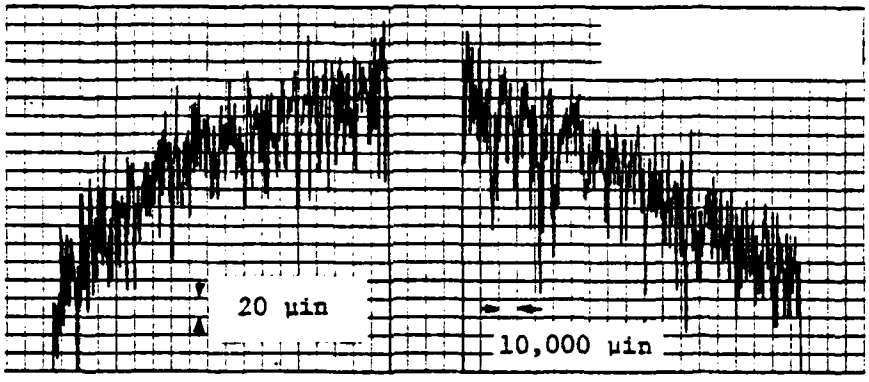

Radial Profile (.001 filter)
Test #42 (Final Trace)

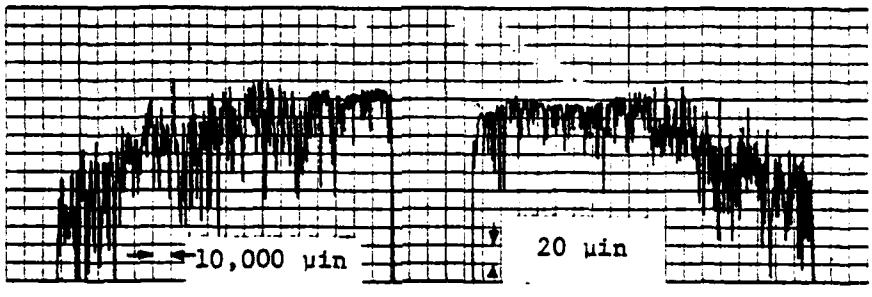

Figure 2-11. Radial Taper Profile, Before and After Test.

Table 2-5

Sealed Pressure Effects - Wavy Seal

$p_{gas} \cong 6.9$ MPa 1800 RPM

Test Number	p_{H_2O} MPa	Test Duration h	Average Face Temperature °C	Average Torque N•m	Average Leakage cm^3/min
9	1.73	25	40	2.2	11.0
21	3.45	100	40	1.5	1.1
34	3.45	100	39	1.4	1.4
39	3.45	100	39	1.6	3.2
17	5.18	32	41	5.5	2.3

contact. However, this torque is about one half of that of the flat faced seal. Results for test number 18 in Appendix B shows that by increasing the gas pressure, the friction torque can be reduced to one half of that for case 17 above while leakage increases to 6 cm^3/min. In general, this behavior is as expected. Some modifications of the results in Table 2-5 would be expected if the test duration were made the same for all tests.

Speed

Table 2-6 shows two sets of results where sealed pressure and waviness pressure are held constant while speed is varied, one set of data at a higher waviness pressure than the other. A comparison is made somewhat difficult because the test durations are different, however, certain observations can be made. Considering the results for p_{gas} = 6.9 MPa, torque increases with increasing speed. Leakage appears to increase, although this is not definite.

The trend in torque values is exactly opposite to what we would expect assuming hydrodynamic mechanisms are operative. Hydrodynamic theory predicts a reduced torque at higher speed, at least over some range of speeds [1]. The explanation for this apparent contradiction in behavior is complex and is taken up in detail in Chapter 3.

The data for p_{gas} = 4.8 to 5.5 MPa show no particular trend one way or the other. It is thought that the low speed results particularly may be influenced measurably compared to the others by the seal not being worn in at its particular operating conditions. Although large time tests are needed to refine the data, it is not expected that the above noted trend would change.

Proximity Probe

Figure 2-12 shows the installation of a Kaman Science KD-2300-.5SU displacement measuring probe. The probe operates based on impedance variations caused by eddy currents induced in a conductive target. A change in displacement of the carbon, to which the probe is bonded, relative to the WC face, produces a change in DC output of the probe driver. This signal variation was read using the high speed A/D card

Table 2-6

Speed Effects - Wavy Seal

p_{H_2O} = 3.45 MPa

Test Number	Speed	p_{gas} MPa	Duration h	Average Face Temp. °C	Average Torque N·m	Average Leakage cm^3/min
26	500	6.9	4	40	1.6	0.3
33	900	6.9	20	40	1.8	0.2
34	1800	6.9	100	39	1.4	1.4
39	1800	6.9	100	39	1.6	3.2
21	1800	6.9	100	40	1.5	1.1
30	2700	6.9	46	41	3.2	4.5
31	3600	6.9	6	43	5.0	1.8
28	900	4.8	5	40	3.4	0.4
36	1800	4.8	100	40	2.4	1.4
19	2700	5.5	24	40	2.9	0.9

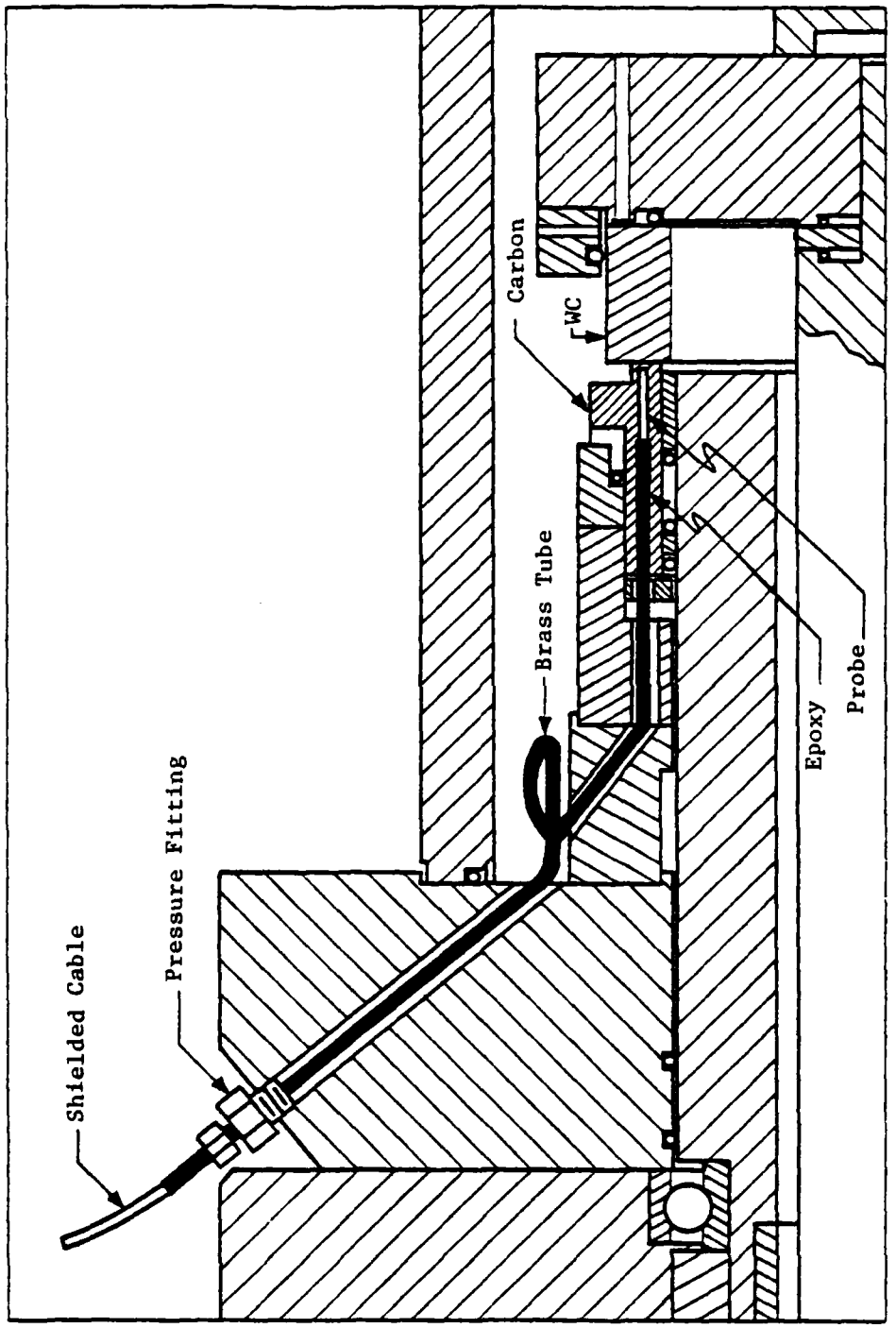

Figure 2-12. Proximity Probe Installation.

described previously. Sensitivity of the probe was found to be 1.4 volts/mm so that a 1 μm displacement change caused a 1.4 mv change in signal.

Although the WC used in these experiments is slightly magnetic, it was found that Kaman's probe KD-2300-.5SUM for magnetic materials would not operate. The probe referenced above for non-magnetic materials operated successfully.

To operate satisfactorily the probe and its cable must be protected from water. To do this, the probe was epoxied into the carbon and a 3.2 mm OD brass tube was epoxied at the rear of the seal and sealed at the vessel housing. This provided a completely water tight passage for the probe cable. The objective of the experiments was to measure the relative change in displacement between the carbon and the WC that occurs as the waviness cylinder is rotated. Such data can be used to verify deflection theory which is an essential part of modeling the seal behavior. No attempt was made to establish a zero displacement reading or to measure actual film thickness. Only relative displacements were obtained.

The procedure used was to drive the waviness cylinder at its high speed, about two minutes per revolution. A switch was connected to the drive system so as to trigger the computer when exactly one turn of the waviness cylinder was completed. Voltage output at equal time steps was read and stored in computer memory. About 500 voltage readings were taken per turn of the waviness cylinder. Figure 2-13 shows a typical output signal for one turn of the waviness cylinder. There is a considerable amount of noise on the signal. A Fourier analysis of the signal filters out the noise and shows that the signal has predominant third and sixth harmonic components as expected. Table 2-7 shows the Fourier analysis results of all of the various proximity probe tests.

Tests were run with the seal under spring load only and under water pressure and spring load combined and at various gas pressures. Results show that the waviness is repeatable and that water pressure causes considerable flattening of the wave. The tests were performed

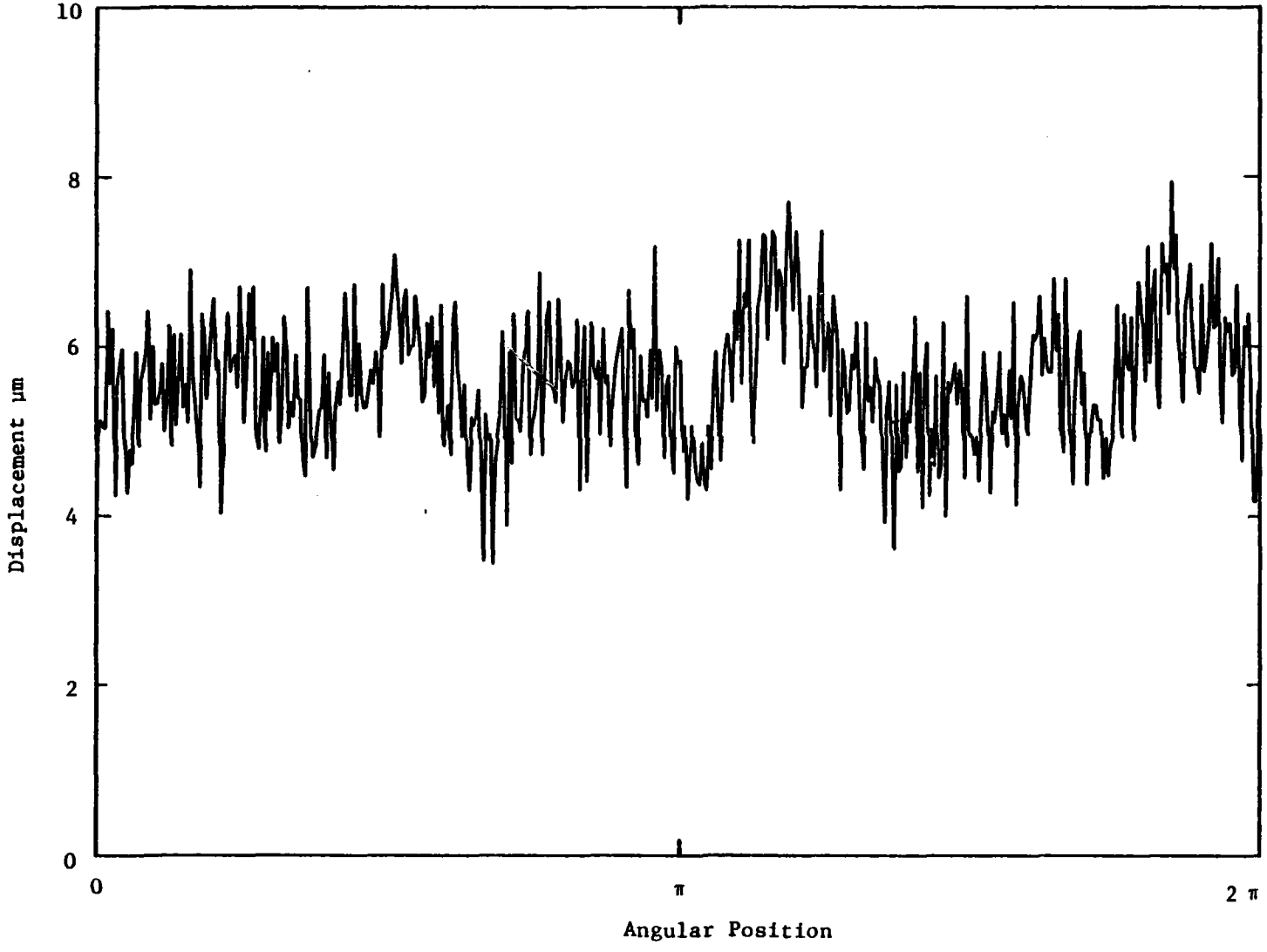

Figure 2-13. Output From Proximity Probe.

Table 2-7

Proximity Probe Results (Static)

P_{H_2O} (MPa)	P_{gas} (MPa)	→ trials h_3 (μm)							h_3 (Average) (μm)	→ trials h_6 (μm)							h_6 (Average) (μm)
0	3.45	1.39	1.75	1.64	1.64	1.61	1.85	1.86	1.73	0.06	0.04	0.15	0.03	0.09	0.19	0.17	0.11
0	6.90	4.97	4.87	4.76	5.12	5.29	5.40	5.55	5.14	0.49	0.68	0.55	0.68	0.99	0.93	0.85	0.74
3.45	3.45	0.15	0.20	0.10	--	--	--	--	0.15	0.05	0.10	0.05	--	--	--	--	0.06
3.45	4.83	0.21	0.13	--	--	--	--	--	0.17	0.05	0.11	--	--	--	--	--	0.08
3.45	6.90	0.32	0.31	0.32	--	--	--	--	0.32	0.42	0.41	0.40	--	--	--	--	0.41

on an unworn carbon ring. A comparison of these results to theory is made in Chapter 3.

The original plan was to measure waviness and particularly the change in waviness during an operating waviness test. This was not done however because of a bearing seizure of the waviness cylinder caused by the higher speed operation of the waviness cylinder. The repair of this failure required that the proximity probe be destroyed. These tests may be performed at a later time after the proximity probe is replaced.

Wear Profile

After each wear test a wear profile of the carbon surface was made using the surface analyzer. Three such profiles are shown in Figure 2-14. These profiles are for p_{H2O} = 3.45 MPa, p_{gas} = 6.9 MPa, 1800 RPM, 100 h tests. The significant feature of all three wear profiles is that both the inside and outside corners of the seal face are worn tapered. The approximate amount of taper is shown in the figure. The tapering on the third case is not nearly as pronounced as in the first two cases. There is no apparent explanation for this. It should be noted that wear and taper of the WC mating face was insignificant relative to the taper shown.

The significance of the tapering on both corners is that the seal face must rock or tilt from a converging configuration to a diverging configuration as the waviness cylinder passes by. Thus, from these results and the proximity probe results, it is concluded that the waviness producing device creates waviness as well as an alternating tilt around the seal. The faces do not remain radially parallel as was assumed in the hydrodynamic theory contained in Reference [1]. A full explanation of this type of deformation is contained in Chapter 3.

Surface Roughness

Surface roughness was measured before and after each test. These data are shown in Appendix B. After a test the roughness of the carbon ranges from 0.2 to 0.5 μm CLA. The WC is generally around 0.05 μm CLA.

.001 filter
Test #21

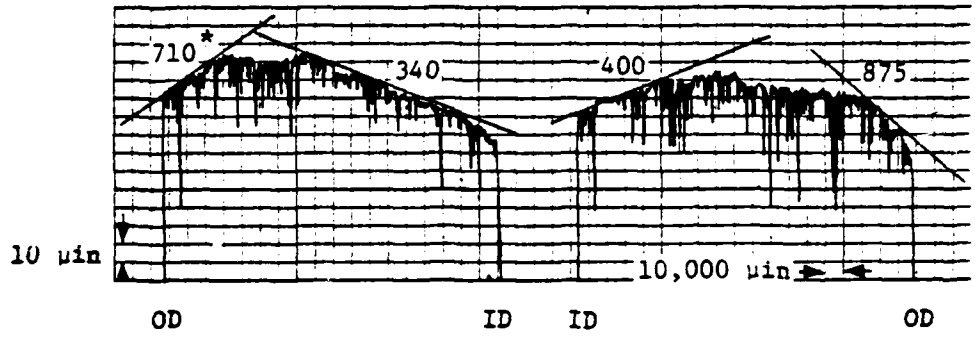

.0003 filter
Test #34

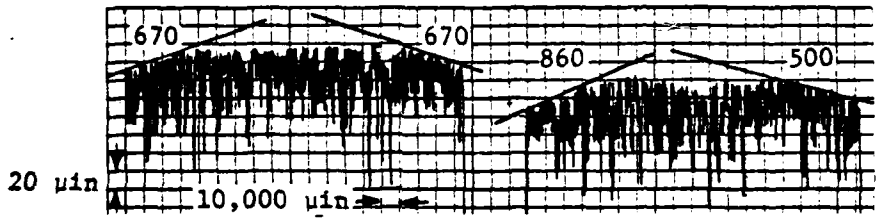

.0003 filter
Test #39

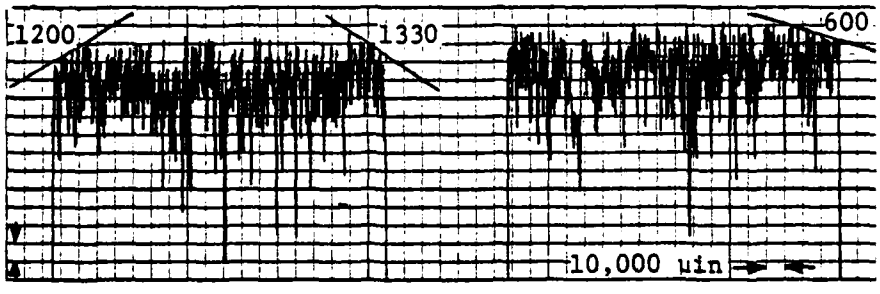

*Slope in µm/m

Figure 2-14. Carbon Surface Radial Profiles for Three 6.9 MPa 100h Waviness Tests.

After studying the roughness values, no particular pattern or relationship with other variables seem apparent. However, after more data has been accumulated, a closer examination is needed.

Since the time the computer was installed in the system, it has been possible to perform a statistical analysis on data obtained in the surface roughness analysis. To do this the surface analyzer output is connected directly to the high speed A/D card described previously. As the surface analyzer makes its trace across the surface, several thousand ordinate values are read and stored into the computer. A computer program has been written to take these points and calculate CLA, standard deviation, skewness, Kurtosis, a histogram, and an autocorrelation function. These data provide much more information about the surface than is provided by the CLA reading given by the surface analyzer.

Examples of the output data are given in Figures 2-15 and 2-16 for the carbon ring of test number 41. The histogram is characteristic of a surface having a series of valleys with peaks being chopped off, typical of carbon. The negative skewness characterizes the shape of the histogram shown. The autocorrelation function shown in Figure 2-15 decays toward zero showing that the roughness has no periodicity, which is expected. Characteristic asperity size is taken at $R(x) = 0.5$ which corresponds to 9.5 μm.

Table 2-8 shows a summary of results from several statistical analyses of the type described. Test 40 was a flat face, whereas test 41 was a p_{gas} = 3.45 MPa waviness test. Comparing test 40 at 0° to test 41 at 0° shows no significant difference in the surface statistics. This suggests that the wear processes may be similar, even though seal performance was greatly different.

The carbon ring from test number 41 was analyzed at three different angular locations to see if there would be any difference in surface characteristics dependent upon where within one wave the sample was taken. Again, there appears to be no significant difference. Thus, once the carbon is worn in, surface statistics do not greatly change as a function of whether or not contact has been recent or not.

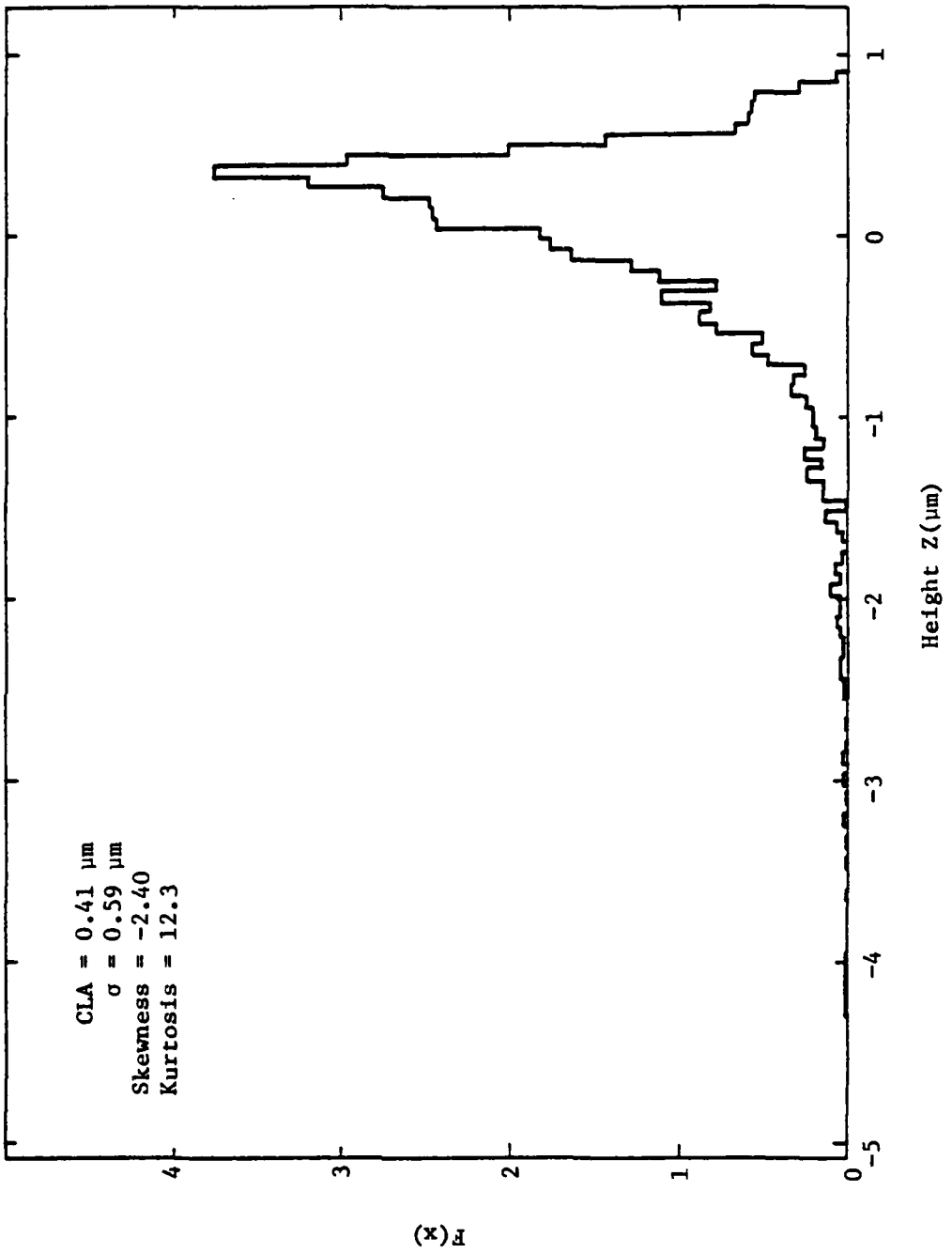

Figure 2-15. Roughness Distribution - Test 41.

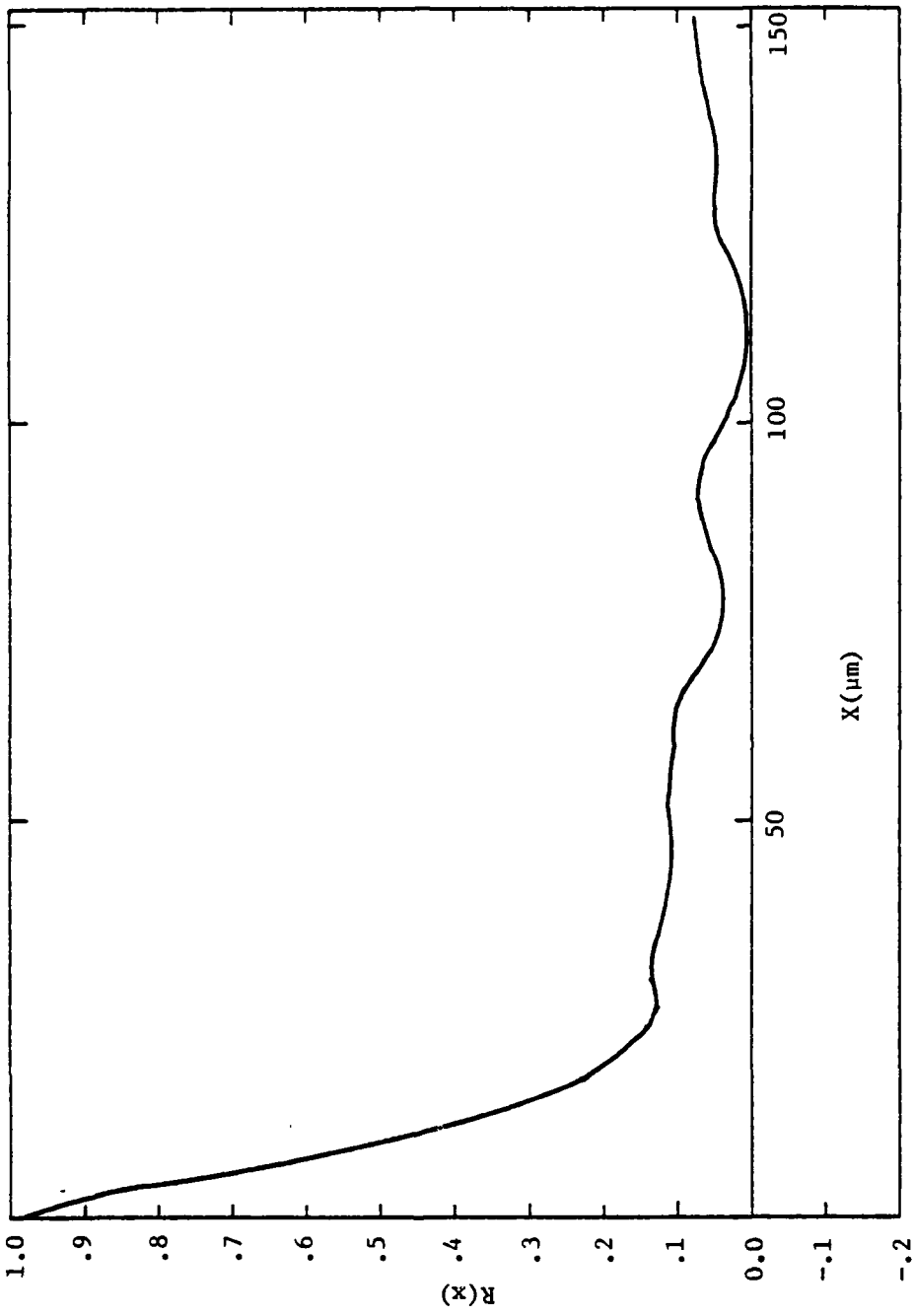

Figure 2-16. Autocorrelation Function - Test 41.

Table 2-8

Carbon Surface Statistics

Test No. Location	σ (μm)		Skewness		$\ell_{0.5}$ (μm)	
	Radial	Tangential	Radial	Tangential	Radial	Tangential
40 0°	0.56	0.47	-2.95	-2.48	13.4	9.9
41 0°	0.59	0.45	-2.40	-2.49	9.5	10.2
41 40°	0.60	0.43	-1.94	-2.68	9.1	7.4
41 80°	0.76	0.59	-2.56	-2.86	12.0	10.2
Avg	0.63	0.49				

One significant feature can be noted from Table 2-8. In all cases, the standard deviation is lower when measured in the tangential direction than when measured in the radial direction. This may be caused by characteristic tangential grooving of the carbon surface. However, the roughness in both directions is similar so that the seal surface can be considered as isotropic for analysis purposes.

At the present time, only a limited number of seal statistical analyses such as above have been made. As more data becomes available, it is expected that these data will be useful in comparing surfaces generated by wear in different types of sealing environments.

Chapter 3

Thermoelastic Instability in Face Seals

As a part of an overall interest in understanding mechanical seal fundamentals, some effort has been spent in attempting to better understand the role of thermoelastic instability in face seals. Interest in this phenomenon is heightened given the opportunity to do testing using the experimental seal test apparatus described previously.

Thermoelastic instability in a face seal occurs when unbounded circumferential pressure and temperature variations occur in an otherwise parallel face contact. Previous investigators have shown [9,10,11] that for a given material pair and geometry, there is a certain critical speed of sliding above which such pressure and temperature variations grow. This is called the threshold of instability or critical speed. Below this critical speed, such variations will diminish with time.

Given this basic knowledge, the theory of thermoelastic instability has been applied to various mechanical configurations in an attempt to accurately predict critical speed, and predictions have been compared to experimental results. Mechanical face seals represent one application where the prediction of thermoelastic instability is of great interest to designers.

Netzel [12] has reported evidence of patch contact on the hard faces of two high speed anhydrous ammonia seals and one water seal. Existing theory [9] based on an insulator sliding on a conducting body shows that the critical speed in these applications is much lower than reality. Theory [9] based on two conducting bodies gives critical sliding speeds higher than those observed.

In order to more accurately predict critical speeds in mechanical seals, a modified theory of thermoelastic instability for mechanical face seals is developed herein. The effects of ring deflection and heat transfer between the rings, heretofore neglected, are included. It is shown that at lower numbers of waves, ring deflection predominates

and completely changes the character of the instability relationships. Thermal contact resistance between the faces acts to decrease the critical sliding speed. A similar approach was taken in reference [13]. However, certain assumptions made concerning heat transfer led to results which are inconsistent with those of Burton [9]. In this paper, these assumptions are avoided, and the results are consistent with those of Burton.

Theory

Figure 3-1 shows the basic mechanical face seal configuration. As one ring rotates relative to the other, sliding occurs at the sealing interface. The faces are loaded against each other by spring and fluid pressures. Both seal rings are assumed to be of thickness h and mean radius R.

Figure 3-2 shows the faces of the seals developed. Ring H is rotating at angular speed ω and ring S is fixed. It is assumed that there exists a sinusoidal temperature disturbance on face S moving relative to face S at angular speed ϕ. It is also assumed that a different sinusoidal temperature disturbance occurs on face H also moving at speed ϕ. There are n periods or waves around the seal, and the condition $n \geq 2$ must be satisfied for the ring geometry.

Relative to the fixed ring, the temperature variations are assumed as follows

$$T_S(\theta,t) = T_S \sin n(\theta - \phi t) , \tag{3-1}$$

$$T_H(\theta,t) = T_H \sin n(\theta - \phi t + \eta) , \tag{3-2}$$

where the angle η allows for a phase shift between the two temperature waves. Relative to the rotating ring, $T_H(\theta,t)$ becomes

$$T_H(\theta,t) = T_H \sin(\theta + \beta t + \eta) , \tag{3-3}$$

where

$$\phi + \beta = \omega . \tag{3-4}$$

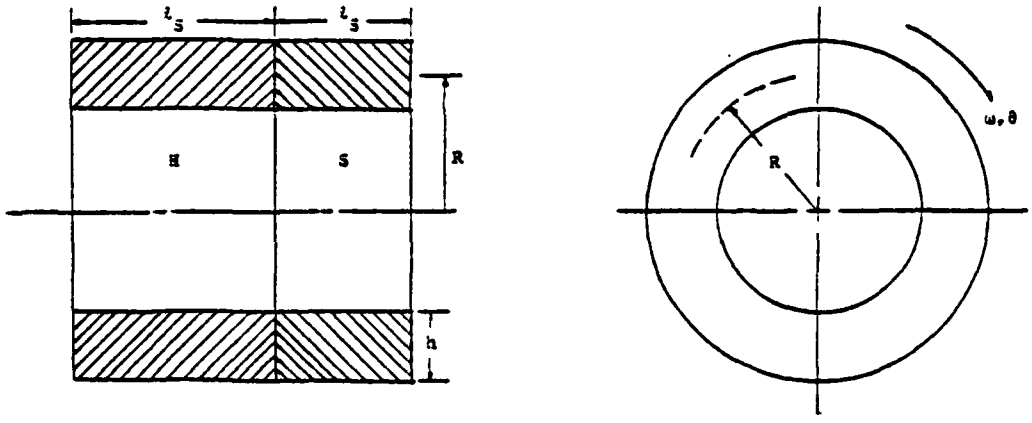

Figure 3-1. Mechanical Face Seal.

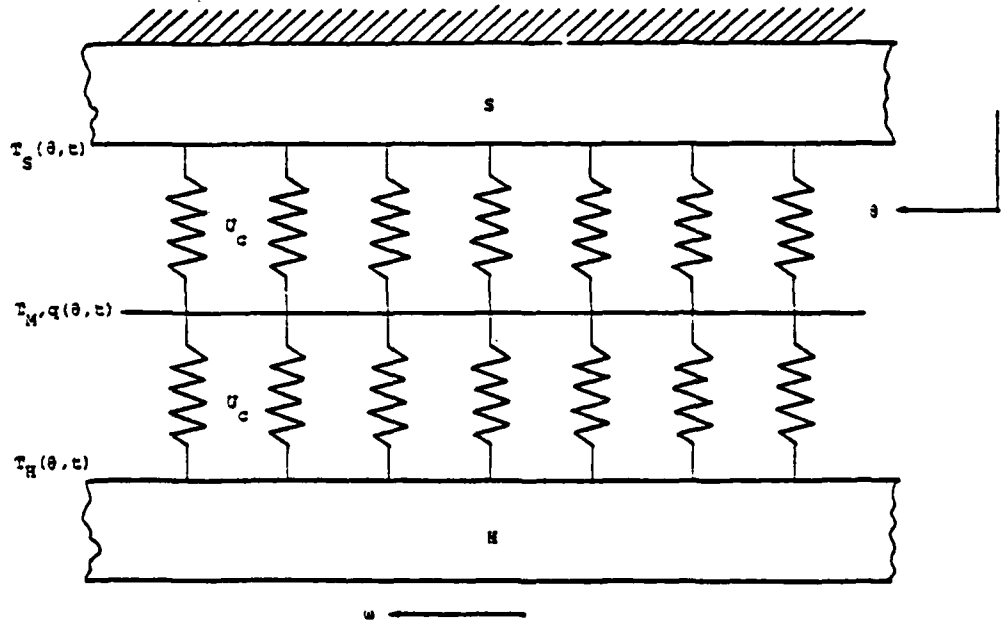

Figure 3-2. Seal Rings.

Given the sinusoidal temperature distribution at the face, the temperature distribution within the ring can be found. With reference to Figure 3-3, it is assumed that the ring is thin such that radial temperature variations can be neglected. It is also assumed that there is heat transfer to surrounding fluid media as shown. Thus, the governing equation for heat transfer becomes

$$\frac{\partial^2 T}{\partial y^2} + \frac{\partial^2 T}{\partial \theta^2}\frac{1}{R^2} - (T - T_\infty)\frac{H_\infty}{Kh} = \frac{\partial T}{\partial t}\frac{1}{k} . \tag{3-5}$$

Given the form of the face temperature, equation (3-1) or (3-3), the exact solution for the above equation for a finite length seal ring is difficult to find, so the solution for a semiinfinite body is used where

$$\frac{\partial T}{\partial y} \to 0 \quad \text{as } y \to \infty . \tag{3-6}$$

Similar to that given by Burton [1], the solution for body S becomes

$$T_S(\theta,t,y) = T_S e^{-b_S y_S} \sin n(\theta - \phi t + a_S y_S) , \tag{3-7}$$

where

$$a_S = + \left(\frac{- Z_S + \sqrt{Z_S^2 + \left(\frac{n\phi}{k_S}\right)^2}}{2n^2} \right)^{1/2} , \tag{3-8}$$

$$b_S = + \left(\frac{+ Z_S + \sqrt{Z_S^2 + \left(\frac{n\phi}{k_S}\right)^2}}{2} \right)^{1/2} , \tag{3-9}$$

$$Z_S = \frac{n^2}{R^2} + \frac{H_\infty}{K_S h} . \tag{3-10}$$

It has been found that $e^{-b_S \ell_S} \ll 1$ for most values of b_S encountered in this investigation. That is, the temperature disturbance is very shallow. However, for n = 2 or 3, in some cases $b_S \ell_S$ is as small as unity, so some error is introduced. Nevertheless, the temperature distribution given by equation (3-7) for a semiinfinite thin plate will be considered as a reasonable first approximation for a finite length thin plate or cylinder.

The signs on the square roots in equations (3-8) and (3-9) were selected to give real roots with the proper phase shift for the assumed direction of ϕ.

For body H, the solution for equation (3-5) gives

$$T_H(\phi,t,y) = T_H e^{-b_H y_H} \sin n(\theta - \phi t + \eta + a_H y_H) \tag{3-11}$$

relative to the fixed reference.

$$a_H = -\left(\frac{-Z_H + \sqrt{Z_H^2 + \left(\frac{n\beta}{k_H}\right)^2}}{2n^2}\right)^{1/2}, \tag{3-12}$$

$$b_H = +\left(\frac{Z_H + \sqrt{Z_H^2 + \left(\frac{n\beta}{k_H}\right)^2}}{2}\right)^{1/2}, \tag{3-13}$$

$$Z_H = \frac{n^2}{R^2} + \frac{H_\infty}{K_H h}. \tag{3-14}$$

Heat transfer per unit area into the faces is given by

$$q = -K \left.\frac{\partial T}{\partial y}\right|_{y=0}, \tag{3-15}$$

or

$$q_S = -K_S T_S[- b_S \sin n(\theta - \phi t) + n a_S \cos n(\theta - \phi t)] , \quad (3\text{-}16)$$

$$q_H = -K_H T_H[- b_H \sin n(\theta - \phi t + \eta) + n a_H \cos n(\theta - \phi t + \eta)] \quad (3\text{-}17)$$

both relative to the fixed reference.

As shown in Figure 3-2, it is assumed that heat is transferred between the seal faces by conduction. This conduction represents thermal contact resistance. It is also assumed that all of the heat generated by friction occurs midway between the faces and is conducted to the two faces through the thermal contact resistance U_c.

Calling the temperature at the midway point T_M, then

$$(T_M - T_S)U_c = q_S , \quad (3\text{-}18)$$

$$(T_M - T_H)U_c = q_H . \quad (3\text{-}19)$$

Eliminating T_M,

$$(T_H - T_S)U_c = q_S - q_H . \quad (3\text{-}20)$$

Upon substituting for T_S, T_H, q_S, and q_H from equations (3-1), (3-2), (3-16), and (3-17) and separating the sine and cosine terms, the following expressions are obtained

$$(K_H b_H + U_c)T_H \cos n\eta + K_H T_H n a_H \sin n\eta - T_S(K_S b_S + U_c) = 0 , \quad (3\text{-}21)$$

$$- K_H T_H n a_H \cos n\eta + (K_H b_H + U_c)T_H \sin n\eta + K_S T_S n a_S = 0 . \quad (3\text{-}22)$$

From these expressions,

$$\tan n\eta = \frac{(U_c + K_S b_S)K_H n a_H - (U_c + K_H b_H)K_S n a_S}{(U_c + K_S b_S)(U_c + K_H b_H) + K_H K_S n^2 a_H a_S} , \quad (3\text{-}23)$$

$$\frac{T_H}{T_S} = \frac{U_c + K_S b_S}{(U_c + K_H b_H)\cos n\eta + K_H n a_H \sin n\eta} . \tag{3-24}$$

Thus, given the material properties and speeds ϕ and β and using equations (3-8), (3-9), (3-12), and (3-13) to solve for a_S, b_S, a_H and b_H, then the phase shift η and the temperature ratio can be determined.

The total heat generated at the interface must be transferred into the faces. Friction heat at the interface is proportional to the interface pressure p and the sliding speed. Thus an energy balance gives

$$p\mu R(\phi + \beta) = q_H + q_S . \tag{3-25}$$

Equation (3-25) provides an expression for p in terms of T_S and T_H.

Considering now the thermal deflection that occurs due to the temperature distribution in the rings, it will be assumed that for low harmonic numbers n ring deflection theory is applicable whereas for high harmonic numbers n, semiinfinite plate theory is applicable. It should be noted that at all harmonic numbers the semiinfinite plate theory gives larger thermal deflections than the ring theory.

Using ring theory presented in reference [14], and with reference to Figure 3-4 for ring S, it can be shown that

$$M_x = \frac{E_S J_{xS}}{R}\left(\gamma - \frac{v''}{R}\right) - E_S \alpha_S \int_A Ty \, da , \tag{3-26}$$

$$M_\theta = \frac{G_S J_{\theta S}}{R}\left(\gamma' - \frac{v'}{R}\right) \tag{3-27}$$

and

$$M_x'' + M_\theta' = 0 , \tag{3-28}$$

$$M_\theta' - M_x = 0 , \tag{3-29}$$

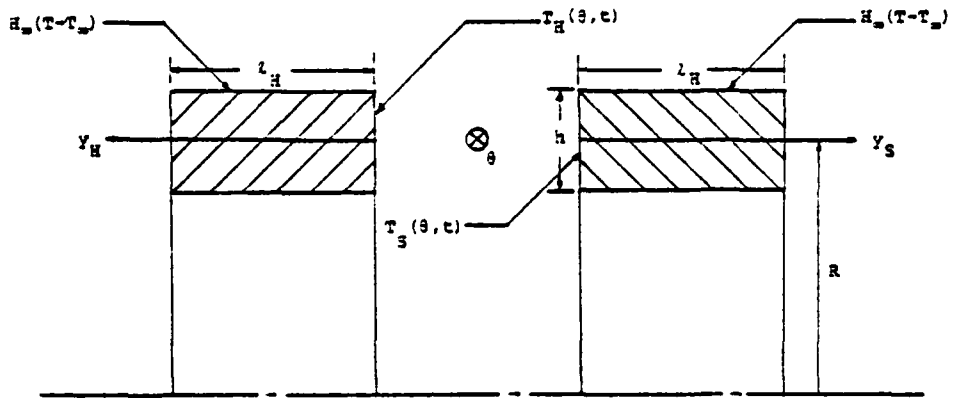

Figure 3-3. Seal Cross Section.

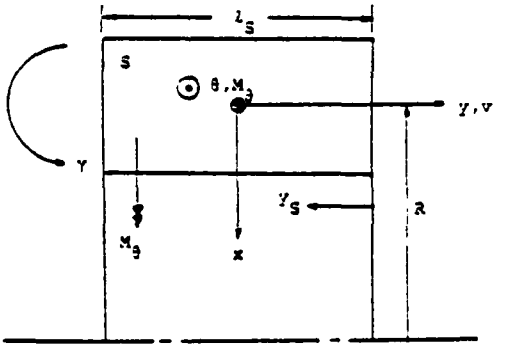

Figure 3-4. Geometry for Ring Deflection.

where the primes denote derivatives with respect to θ, and v and γ represent the face displacement and rotation, respectively. Using equation (3-7) for the temperature distribution in the ring, equations (3-26), (3-27), (3-28) and (3-29) can be solved simultaneously to give the displacement v which represents the thermal deflection δ_{TS}.

$$\delta_{TS} = R\alpha_S T_S[f_{1S}(n) \sin n(\theta - \phi t) + f_{2S}(n) \cos n(\theta - \phi t)] , \quad (3\text{-}30)$$

where

$$f_{1S}(n) = \frac{Rh}{J_{xS}(n^2 - 1)} \left\{ \frac{\left(\frac{\ell_S}{2} - y_S\right) e^{-b_S y_S}}{b_S^2 + n^2 a_S^2} (- b_S \cos na_S y_S + na_S \sin na_S y_S) \right.$$

$$\left. + \frac{e^{-b_S y_S}}{\left(b_S^2 + n^2 a_S^2\right)^2} \left[\left(b_S^2 - n^2 a_S^2\right) \cos na_S y_S - 2na_S b_S \sin na_S y_S \right] \right\}_0^{\ell_S} , \quad (3\text{-}31)$$

$$f_{2S}(n) = \frac{Rh}{J_{xS}(n^2 - 1)} \left\{ \frac{\left(\frac{\ell_S}{2} - y_S\right) e^{-b_S y_S}}{b_S^2 + n^2 a_S^2} (- b_S \sin na_S y_S - na_S \cos na_S y_S) \right.$$

$$\left. + \frac{e^{-b_S y_S}}{\left(b_S^2 + n^2 a_S^2\right)^2} \left[\left(b_S^2 - n^2 a_S^2\right) \sin na_S y_S + 2na_S b_S \cos na_S y_S \right] \right\}_0^{\ell_S} . \quad (3\text{-}32)$$

For body H,

$$\delta_{TH} = R\alpha_H T_H[f_{1H}(n) \sin n(\theta - \phi t + \eta) + f_{2H}(n) \cos n(\theta - \phi t + \eta)] , \quad (3\text{-}33)$$

where the expressions for f_{1H} and f_{2H} are the same as equations (3-31) and (3-32) except for the subscripts.

For the semiinfinite plate assumption, based on the work of Burton [9] it can be shown that

$$f_{1S}(n) = \frac{2k_S a_S}{R\phi} , \tag{3-34}$$

$$f_{2S}(n) = \frac{2k_S}{nR\phi} \left(b_S - \frac{n}{R}\right) , \tag{3-35}$$

$$f_{1H}(n) = - \frac{2k_H a_H}{R\beta} , \tag{3-36}$$

$$f_{2H}(n) = - \frac{2k_H}{nR\beta} \left(b_H - \frac{n}{R}\right) . \tag{3-37}$$

For elastic deflection it is again assumed for small n that ring theory applies and for large n semiinfinite plate theory applies. Based upon previous work [13] and assuming that face pressure is sinusoidal, elastic deflection is given by

$$\delta_{PS} = \frac{pR}{E_S} f_{3S}(n) , \tag{3-38}$$

$$\delta_{PH} = \frac{pR}{E_H} f_{3H}(n) , \tag{3-39}$$

where for ring theory

$$f_{3S}(n) = \frac{R^3 h}{J_{xS}} \frac{n^2 + \frac{E_S J_{xS}}{G_S J_{\theta S}}}{n^2 (n^2 - 1)^2} \tag{3-40}$$

and for the semiinfinite plate

$$f_{3S}(n) = \frac{2}{n} . \tag{3-41}$$

f_{3H} is obtained by changing the subscripts in equations (3-40) and (3-41).

In order for the rings to maintain contact, the sum of the thermal and elastic deflections must be zero (assuming no wear).

$$0 = \delta_{TH} + \delta_{TS} - \delta_{PH} - \delta_{PS} \cdot \tag{3-42}$$

Equations (3-30), (3-33), (3-38) and (3-39) are substituted into equation (3-42). Pressure p is eliminated using equations (3-25), (3-16) and (3-17). Then for the resulting equations to be valid in general, the coefficients of the sin $n(\theta - \phi t)$ and cos $n(\theta - \phi t)$ terms must vanish independently. This gives

$$\mu(\phi + \beta)R\left[\alpha_S f_{1S}(n) + \frac{T_H}{T_S}\alpha_H f_{1H}(n)\cos n\eta - \frac{T_H}{T_S}\alpha_H f_{2H}(n)\sin n\eta\right]$$

$$= \left[K_S b_S + \frac{T_H}{T_S}K_H b_H \cos n\eta + \frac{T_H}{T_S}K_H n a_H \sin n\eta\right] x \left[\frac{f_{3H}(n)}{E_H} + \frac{f_{3S}(n)}{E_S}\right], \tag{3-43}$$

$$\mu(\phi + \beta)R\left[\alpha_S f_{2S}(n) + \frac{T_H}{T_S}\alpha_H f_{1H}(n)\sin n\eta + \frac{T_H}{T_S}\alpha_H f_{2H}(n)\cos n\eta\right]$$

$$= \left[-K_S n a_S + \frac{T_H}{T_S}K_H b_H \sin n\eta - \frac{T_H}{T_S}K_H n a_H \cos n\eta\right] x \left[\frac{f_{3H}(n)}{E_H} + \frac{f_{3S}(n)}{E_S}\right], \tag{3-44}$$

where $\frac{T_H}{T_S}$ and η are given by equations (3-23) and (3-24).

Equations (3-43) and (3-44) represent two equations in two unknowns ϕ and β. Since only the ratio T_H/T_S appears, T_H and T_S can take any arbitrary value. Thus, solutions to these equations represent critical speeds where the system is on the threshold of instability. Numerical methods are required for a solution.

To provide a check on the above equations, the semiinfinite body assumption was used and $U_c \to \infty$ and $H_\infty = 0$. These conditions make the above equations conform precisely to those of Burton [9]. Using the

above equations, solutions were carried out for graphite running against cast iron as in Burton's [9] Table III. The results from the above equations agreed with those of Burton.

Results

Netzel [12] found evidence of hot spots in three different high speed seals using a combination of carbon versus tungsten carbide. The data and observations are given in Table 3-1.

Table 3-1. Hot Spot Observations

Fluid	Pressure (psi)	Speed (RPM)	Shaft Size (in.)	No. of Spots
Anhydrous Ammonia	600	7200	4-1/2	3
Anhydrous Ammonia	850	3600	4	2
Water	600	7200	4-1/2	5-6

In view of these observations it is useful to perform stability evaluations on a seal having similar materials and a comparable size. With S representing the carbon and H the tungsten carbide, the base case data chosen follow:

$$
\begin{aligned}
k_S &= 3.5 \times 10^{-6}\ m^2/s & k_H &= 2.8 \times 10^{-5}\ m^2/s \\
K_S &= 5.0\ W/mK & K_H &= 70.0\ W/mK \\
E_S &= 2.0 \times 10^{10}\ N/m^2 & E_H &= 5.0 \times 10^{11}\ N/m^2 \\
G_S &= 0.83 \times 10^{10}\ N/m^2 & G_H &= 2.1 \times 10^{11}\ N/m^2 \\
\alpha_S &= 5.0 \times 10^{-6}/K & \alpha_H &= 5.0 \times 10^{-6}/K \\
\ell_S &= 0.02\ m & \ell_H &= 0.02\ m \\
J_{xS} &= 3.3 \times 10^{-9}\ m^4 & J_{xH} &= 3.3 \times 10^{-9}\ m^4 \\
J_{\theta S} &= 6.9 \times 10^{-10}\ m^4 & J_{\theta S} &= 6.9 \times 10^{-10}\ m^4
\end{aligned}
\qquad (3\text{-}45)
$$

Data common to both seal rings are

$$R = 0.05 \text{ m}$$

$$\mu = 0.2$$

$$h = 0.005 \text{ m} \qquad (3\text{-}46)$$

$$H_\infty = 0$$

$$U_c = 1.0 \times 10^4 \text{ W/m}^2\text{K}$$

The value of contact resistance represents a case where a 0.38 μm (15 μin.) RMS roughness carbon is sliding on perfectly smooth tungsten carbide with the contact voids filled with ammonia gas as calculated by formulas developed by Fenech and Rohsenow [15].

To provide some frame of reference for the model proposed, it will be compared to the other models mentioned previously. Burton's model based on a conductor sliding on an insulator [9] will be termed model I. Burton's model which considers two conducting semiinfinite plates with $U_c = \infty$ [9] will be termed model II. The present model will be termed model IIIR and model IIIS based on ring theory and semiinfinite plate theory, respectively.

The predictions for each of the models using the base case data are shown plotted in Figure 3-5. The results from model I would suggest that nearly all seals would be unstable, a result which is contrary to fact. This model cannot be applied to this particular problem. Model II considers the effect of a second conducting body. This result shows that the second body, even through it may be a poor conductor (which is the case here with carbon), greatly increases the critical speed. This model also shows that the lowest harmonics could be expected to occur first as speed is increased. For a ring the lowest number that can occur is two, so model II predicts a critical sliding speed of 500/s.

Model IIIR shows a quite different behavior. It shows that the critical speed increases rapidly as n decreases. This is caused by ring deflection. As the number n decreases, the relative stiffness

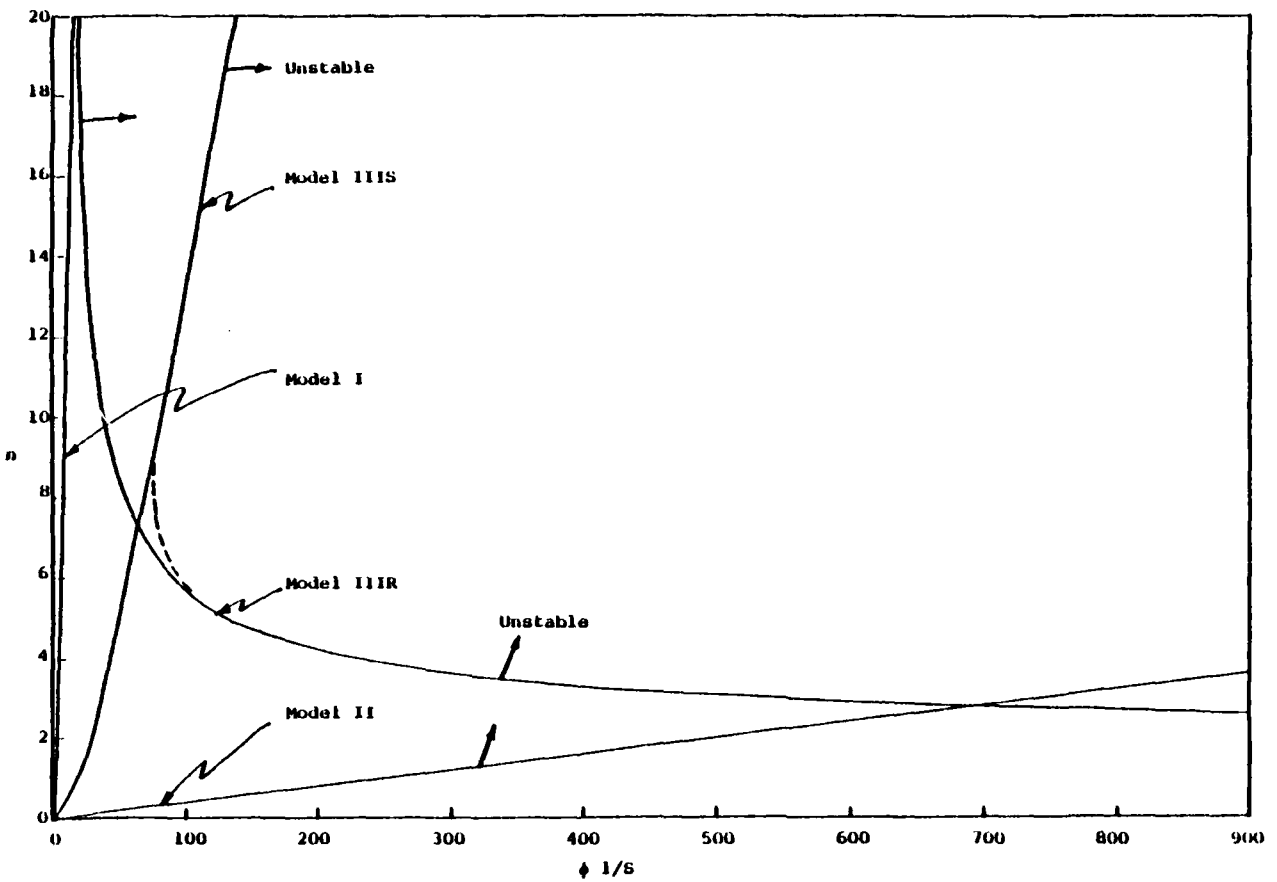

Figure 3-5. Comparison of Models.

of the ring decreases dramatically compared to the edge stiffness of a semiinfinite plate. On the other hand, model IIIR shows that the critical speed becomes quite low as n increases. This occurs because the ring stiffness becomes extremely high at large n.

Model IIIS is basically the same as model II except that thermal contact resistance between the faces is considered. The result shows that contact resistance lowers the critical speed. The shape of the curve for model IIIS is otherwise the same as model II.

Now, following the original assumptions concerning the validity of the ring and semiinfinite plate deflection models, it can be argued that there should be a transition between curves IIIR and IIIS as suggested by the dashed curve in Figure 3-5. The precise nature of this transition curve is not known, however, it can be argued that if the thermal and elastic deflection of both the ring and plate models are added together, a first approximation for the entire curve will be obtained. This can be rationalized by noting that at low n the ring deflection will dominate and the effect of the semiinfinite plate deflection will be small in comparison and vice versa at high n. The result is shown in Figure 3-6. Model IIISR represents the combination of the two models.

The result of this combination is a curve having a nose which determines the lowest critical speed. For the base case results, this speed is about 60/s at n = 6-7. The shape of this curve suggests that as speed increases there will suddenly occur an instability with n as prescribed by the curve. A further increase in speed would cause n to either increase or decrease depending on which way the curve is followed.

For the experimental data, the curve suggests that either n equal 2 or 3 or that n be very large (beyond the range of the curve).

The effect of thermal contact resistance is also shown on Figure 3-6. Contact resistance was reduced a factor of 100 to simulate the effect of having a liquid between the faces, and the curves were recalculated. For this case the first critical speed moves up to 500/s. At the operating speed of the water seal described previously, 7200 RPM,

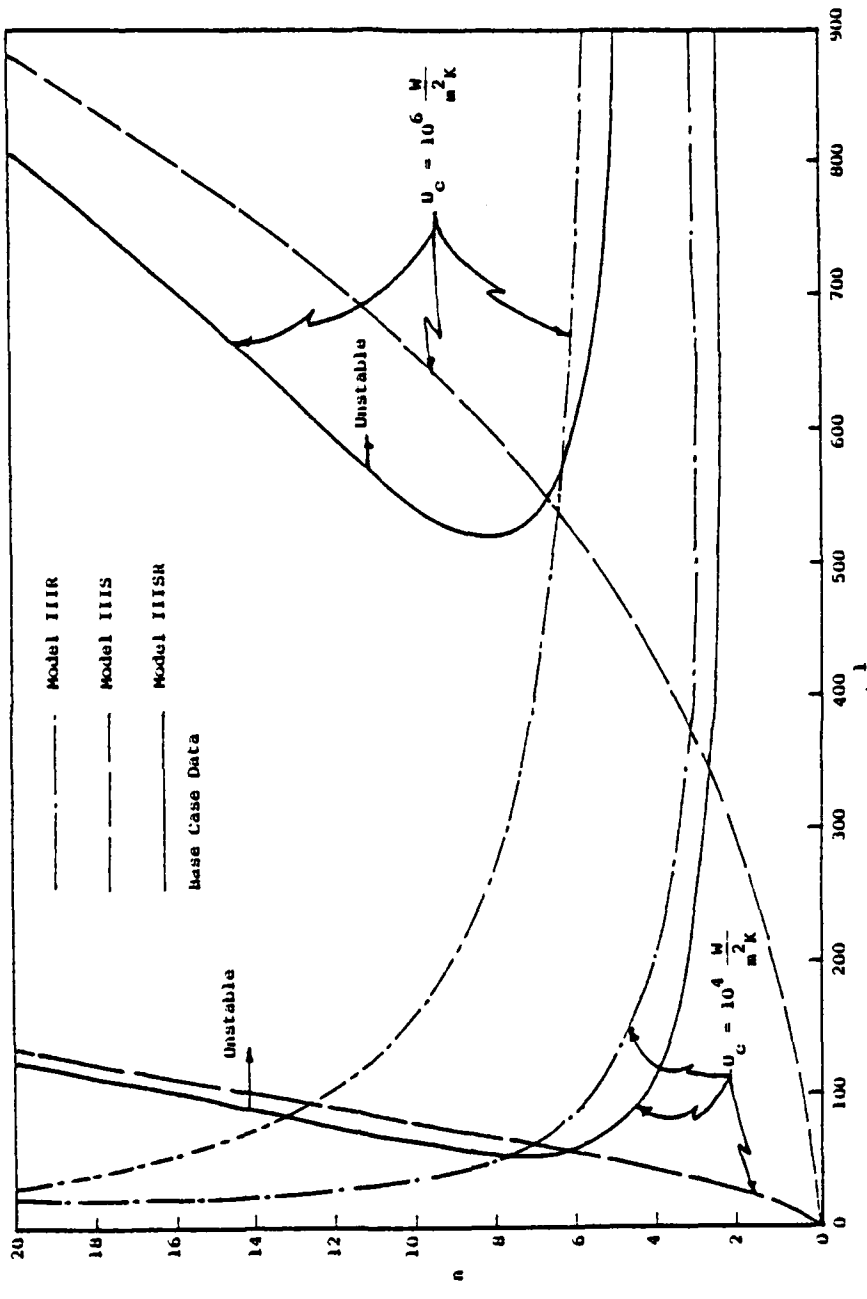

Figure 3-6. Model III.

the curve predicts values of n of 5 or 6 or again very high (16 to 18).

The model provides for convection losses through H_∞. The effect of convection losses is to reduce the amplitude of the thermal deflection. The results presented so far were for $H_\infty = 0$. Introducing $H_\infty = 1000\ W/m^2K$ into the model causes $\phi_c \to \infty$. This result suggests that convection cooling could be very important in reducing or eliminating thermoelastic instability in seal rings, however, further studies are needed to understand this effect.

Chapter 4

Wavy Seal Analysis

Wavy Seal Theory

As will be shown later in this chapter, the modeling of the experimental seal described herein requires a more comprehensive model than that developed for hydrodynamic lubrication in previous reports and papers [5,1,6,16,17]. The primary difference between the behavior of the actual seal and the ideal seal assumed in the previous analysis is that in the actual seal there is a tilt superimposed over the waviness. In the previous analysis it was assumed that the seal faces alway remain radially parallel in spite of waviness (except for some of the results contained in Chapter 3 of reference [1]). As was shown by these results, tilt of the faces greatly changes the hydrodynamic effect in the seal. Hydrostatic effects may become much more significant than hydrodynamic effects. Thus, in this more comprehensive model, certain features have been added to account for a completely arbitrary film shape and wear.

The development of this more comprehensive model to the level of sophistication of the previous model [1] is quite difficult, so certain approximations are made. First, a simplified approach to evaluating the effects of surface roughness is taken. Second, because the cavity shape becomes more complex, approximate cavity boundary conditions are used to simplify the solution. The model will now be described in detail.

Reynolds Equation for Rough Surfaces

The Reynolds equation predicts the pressure distribution for an arbitrary film shape. Both hydrostatic and hydrodynamic effects are accounted for. In previous reports [5,1,6] considerable attention was given to how the Reynolds equations should be modified to account for surface roughness. A contribution to the literature on the subject was made [7]. Certain discrepancies between the Patir-Cheng theory [18]

and the Teale and Lebeck interpretation of their theory were found [7]. By including the effects of side leakage, it was found that flow resistance decreased compared to the Patir-Cheng results. Recently, Tonder [19] also computed distinctly different results than found by Patir and Cheng. Even though they disagree, both theories show that the surface roughness correction used in previous wavy seal model [1], as originally introduced by Christensen [20] and Tonder [21], provides too little flow resistance. Thus, before making calculations based on a new seal model, some resolution of these issues is needed.

To provide some insight into this issue, the flow factors as computed by Patir and Cheng [18] and Tonder [19] are compared. For one-sided roughness with the smooth surface moving (which simulates the carbon versus hard face roughness combination quite well) and an $h/\sigma = 2$ or $\overline{h} = h/c = 0.67$ the shear flow factors calculated are 0.7 and 0.8 (compared to 1.0 for smooth surfaces) from the Patir-Cheng [18] and Tonder [19] results, respectively. Pressure flow factors are 0.75 and 1.2 (compared to 1.0 for smooth surfaces), respectively. While the shear flow factors agree to some extent, the pressure flow factors show opposite trends.

Given this irreconciliable difference in theory in conjunction with the necessity to produce a useful though approximate seal model, it was decided that it would be best to avoid choosing either of these models until the basic issues are resolved. It was decided to completely neglect the effects of surface roughness on the Reynolds equation. This choice has the advantage that when the above issue is resolved, then the results can be recomputed based upon correction due to roughness as opposed to being recomputed because the roughness model chosen was incorrect. The former is much preferred.

One can in fact neglect surface roughness effects on seal lubrication while introducing only a small error. Experience shows that in a wavy or tapered seal, the film thickness is as low as $\overline{h} = 0.67$ for only a small fraction of the face area. For most of the seal, $\overline{h} > 1$, where no significant surface roughness effects occur. Thus, any error introduced occurs in only a small fraction of the seal face. The error

introduced is not large to begin with since at $\bar{h} = 0.67$, typically a lower limit for a seal, $\phi_x = 0.75$ or 1.25, a 25 percent error.

Seal Model

Even though the effect of roughness on the Reynolds equation is to be neglected, computation of mechanical load support and friction require the use of surface roughness concept. Thus, surface roughness is shown in Figure 4-1, along with seal geometry. h is the nominal film thickness at a point r,θ and in general in a function of r and θ. h is defined to the mean level of the rough surface. It is assumed that the roughness is distributed over a range -c to +c and that the distribution is polynomial.

$$f(h) = \frac{35}{32c^7} (c^2 - h^2)^3 \quad . \tag{4-1}$$

Total film thickness is given by

$$H = h + \delta \quad , \tag{4-2}$$

where δ represents the random part of the film thickness.

Based upon the assumption that roughness effects are neglected, the Reynolds equation is

$$\frac{1}{\bar{r}} \frac{\partial}{\partial \theta} \left(\frac{\partial \bar{p}}{\partial \theta} \bar{h}^3 \right) + \frac{\partial}{\partial \bar{r}} \left(\bar{r} \frac{\partial \bar{p}}{\partial \bar{r}} \bar{h}^3 \right) = 6\bar{r} \frac{\partial \bar{h}}{\partial \theta} \quad . \tag{4-3}$$

Flow is given by

$$\bar{q}_\theta = - \frac{\bar{h}^3}{12\bar{r}} \frac{\partial \bar{p}}{\partial \theta} + \frac{\bar{r}\bar{h}}{2} \quad , \tag{4-4}$$

$$\bar{q}_r = - \frac{\bar{h}^3}{12} \frac{\partial \bar{p}}{\partial \bar{r}} \quad , \tag{4-5}$$

where h represents the nominal film thickness as defined above. Symbols are nondimensionalized as shown in the list of symbols. Because of the definition of h, it is possible for h to become negative. When

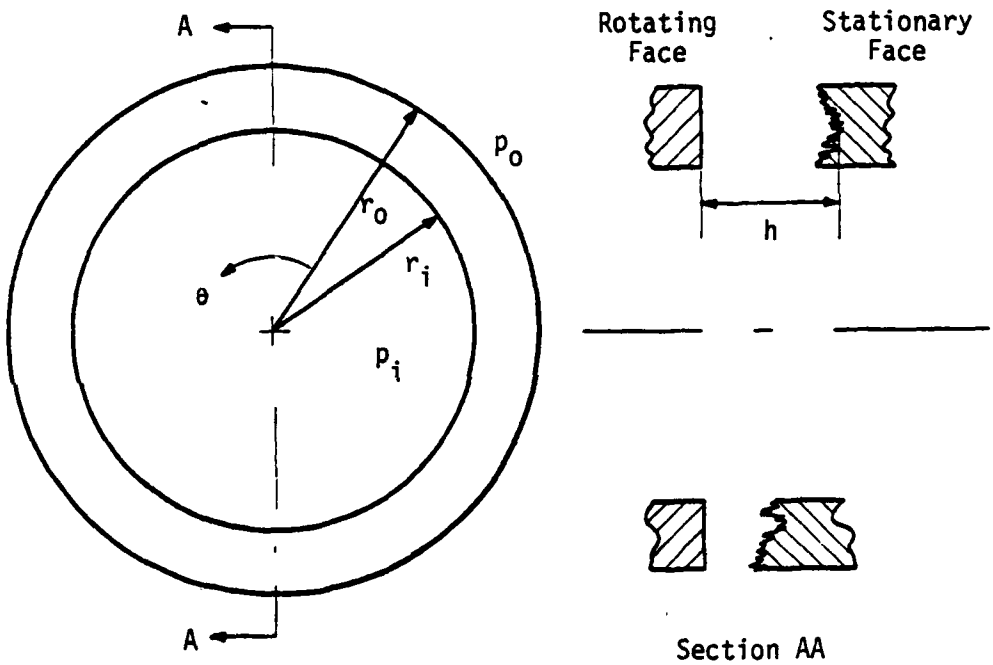

Figure 4-1. Seal face Geometry and Surface Roughness.

this occurs, h is set equal to zero.

Boundary conditions are

$$p(r_i) = p_i \ , \tag{4-6}$$

$$p(r_o) = p_o \ . \tag{4-7}$$

In the previous model [1], cavitation was accounted for by an exact procedure which provided flow continuity across the cavity. A unique numerical technique was developed for the solution. For the present case the cavity boundary condition is treated by first solving for the complete pressure distribution disregarding cavitation and negative pressures. Then, all pressures less than the cavity pressure are set equal to the cavity pressure. This procedure, equivalent to the half Sommerfeld condition in journal bearings, introduces some error into the load support and leakage calculations. However, because of the complications of multiple and arbitrarily shaped cavities introduced in this more general problem and because of the greater numerical effort required to obtain deflection solutions, the simplification was found necessary at least for the computation of the preliminary results presented here.

Equation (4-3) is solved numerically by over relaxation methods as before [1]. Care must be taken in setting up the equation so that film thickness slope discontinuities do not introduce large errors.

Load support is calculated as before [1] and consists of the fluid pressure component plus the mechanical component

$$\bar{W} = \int_0^{2\pi} \int_{\bar{r}_i}^{\bar{r}_o} [\bar{p}_m b_m + \bar{p} b_f] \, \bar{r} \, d\bar{r} \, d\theta \ , \tag{4-8}$$

where

$$b_m = P(H > h) \ , \tag{4-9}$$

the probability that contact occurs or the fraction of asperity area in contact. For the polynomial distribution

$$b_m = \int_h^c f(h)\, dh = 1 - \frac{1}{32}\left[16 + 35\bar{h} - 35\bar{h}^3 + 21\bar{h}^5 - 5\bar{h}^7\right] , \quad (4\text{-}10)$$

$$b_f = 1 - b_m , \quad (4\text{-}11)$$

which is the fraction of area subjected to fluid pressure. For practical purposes,

$$b_f \cong 1.0 . \quad (4\text{-}12)$$

p_m is the compressive strength of the asperities as before [1].

The applied load is given by

$$\bar{W}^* = \pi\left(1 - \bar{r}_i^2\right)\left[\bar{p}_o B + \bar{p}_i(1 - B) + \bar{p}_{sp}\right] \quad (4\text{-}13)$$

and for equilibrium, the film thickness must be adjusted so that

$$\bar{W}^* = \bar{W} . \quad (4\text{-}14)$$

Leakage is given by

$$\bar{Q}_i = \int_0^{2\pi} -\frac{\bar{h}^3}{12}\frac{\partial \bar{p}}{\partial \bar{r}}\bigg|_{\bar{r}_i} \bar{r}_i\, d\theta , \quad (4\text{-}15)$$

or

$$\bar{Q}_o = \int_0^{2\pi} -\frac{\bar{h}^3}{12}\frac{\partial \bar{p}}{\partial \bar{r}}\bigg|_{\bar{r}_o} \bar{r}_o\, d\theta . \quad (4\text{-}16)$$

When cavitation occurs and negative pressures are set equal to the cavitation pressure as described, some discrepany between $\bar{Q}_i$ and $\bar{Q}_o$ is expected.

Friction is calculated as before [1]. Shear stress for the fluid

is given by

$$\tau = \eta r\omega E\left(\frac{1}{H}\right) + \frac{1}{2r}\frac{\partial p}{\partial \theta} E(h) \ . \tag{4-17}$$

Assuming a friction radius r_f where

$$r_f = \frac{2(r_o^3 - r_i^3)}{3(r_o^2 - r_i^2)} \ . \tag{4-18}$$

Then the total fluid friction force due to the fluid is

$$\bar{F}_f = \frac{1}{\bar{r}_f}\int_0^{2\pi}\int_{\bar{r}_i}^{\bar{r}_o}\left[\bar{r}\ E\left(\frac{1}{\bar{H}}\right) + \frac{1}{2\bar{r}}\frac{\partial \bar{p}}{\partial \theta} E(\bar{H})\right]\bar{r}^2\ d\bar{r}\ d\theta \ . \tag{4-19}$$

$E(\frac{1}{H})$ was given previously and represents the expected value of one over the fluid film thickness. $E(\bar{H})$, the expected value of the film thickness, is taken as $\bar{h}$ in accordance with the present approximation. In the cavity region $\frac{\partial \bar{p}}{\partial \theta} = 0$, and the first term in the above integral is multiplied by the ratio of the film thickness at the beginning of the cavity to the current film thickness to account for the fraction of the full film.

The factor

$$\bar{\Delta} = \frac{1}{\bar{p}_s}\frac{c}{r_o} \tag{4-20}$$

is used as before [1] to limit the viscous shear stress to the mechanical shear strength and is used in the integration for $E\left(\frac{1}{\bar{H}}\right)$.

Friction due to mechanical contact is given by

$$\tau = p_s b_m \ , \tag{4-21}$$

$$\bar{F}_m = \frac{r_o}{c}\frac{1}{\bar{r}_f}\int_0^{2\pi}\int_{\bar{r}_i}^{\bar{r}_o}\bar{p}_s b_m \bar{r}^2\ d\bar{r}\ d\theta \ , \tag{4-22}$$

where p_s is the mechanical shear strength and b_m again is the fraction of area in mechanical contact.

Total friction is given by the sum of the above two terms, and coefficient of friction is thus,

$$\mu = \frac{F_f + F_m}{W} = \frac{\bar{F}_f + \bar{F}_m}{\bar{W}} \frac{c}{r_o} . \tag{4-23}$$

As shown in previous work [1] the average wear rate of the soft face is proportional to

$$\text{wear} \approx (1 - F) , \tag{4-24}$$

where F represents the fraction of the load carried by fluid pressure. F is computed using equation (4-8) with the mechanical load support term omitted.

Film Thickness Shape

As will be shown later, the film thickness function consists of some portion due to wear and some portion due to net deflection. Deflection creates changes in film thickness by displacement of the centroid of the ring plus rotation of the ring about its centroidal axis. It is assumed that deflection occurs only in the soft (low modulus) face. Figure 4-2 shows these two components of deflection. Coordinate system x-y is fixed in space a constant distance C from the nondeflecting ring. The ring centroid deflects in the y direction and in the ϕ direction about the centroidal axis. For small angles ϕ, one can show that

$$h = \text{const} - v + (r - r_c)\,\phi . \tag{4-25}$$

In general, the ring deflections v and ϕ can be represented as a Fourier series. The v term can be written in terms of an equivalent h term. Thus,

AD-A083 933 NEW MEXICO UNIV ALBUQUERQUE DEPT OF MECHANICAL ENGI--ETC F/G 11/1
THE WAVY MECHANICAL FACE SEAL - THEORETICAL AND EXPERIMENTAL RE--ETC(U)
JAN 80 A O LEBECK, L A YOUNG N00014-76-C-0071
UNCLASSIFIED ME-105(80)ONR-414-1 NL

2 OF 3
AD
A083933

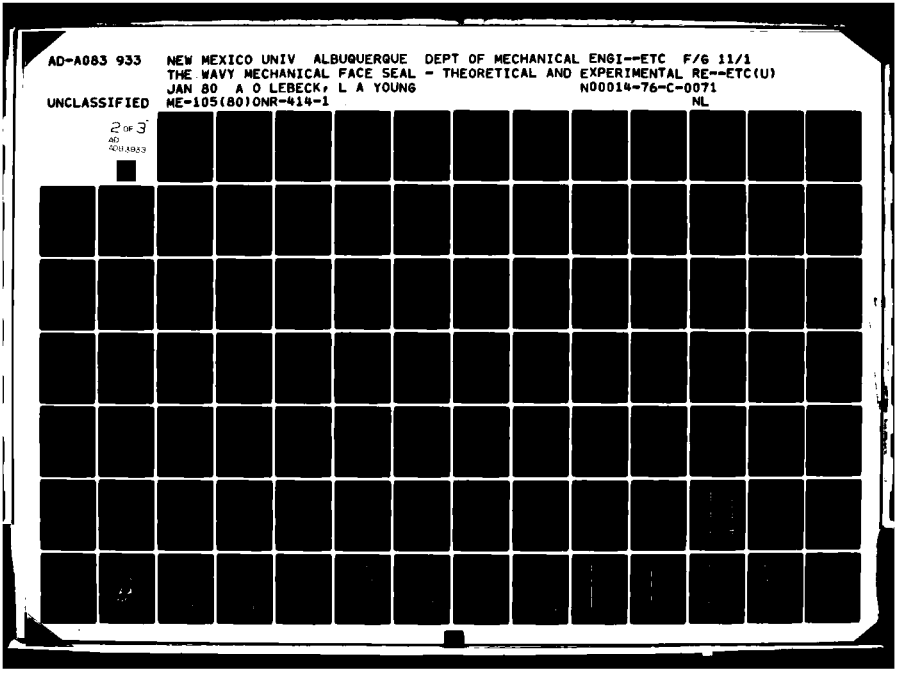

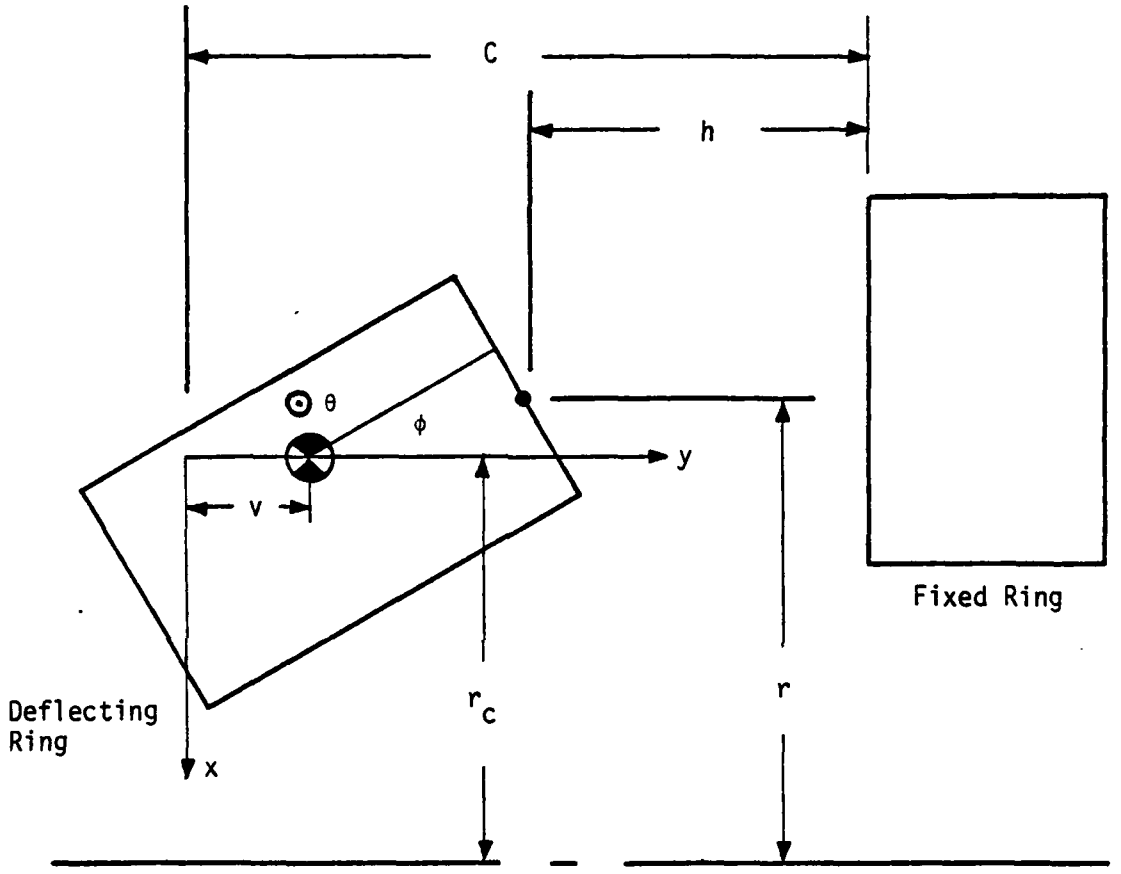

Figure 4-2. Ring Deflection in Relation to Film Thickness.

$$h = h_o + w(r) + \sum_{n=1}^{\infty} (h_{a_n} \cos n\theta + h_{b_n} \sin n\theta)$$

$$+ (r - r_c) \sum_{n=1}^{\infty} (\phi_{a_n} \cos n\theta + \phi_{b_n} \sin n\theta) \ . \qquad (4\text{-}26)$$

The term h_o is the minimum value of h.* In general load support W increases with decreasing h_o. Therefore, h_o is determined by the condition

$$W(h_o) = W^* \ , \qquad (4\text{-}27)$$

where $W(h_o)$ and W^* are given by equations (4-8) and (4-13), respectively.

w(r) represents the wear term. For a seal with a moving waviness or an axisymmetric seal, wear becomes a function of r only. For the moving waviness seal the wear simply becomes uniformly distributed in the θ direction.

Assuming h_{a_n}, h_{b_n}, ϕ_{a_n} and ϕ_{b_n} are known, w(r) can be easily found for the fully worn in condition by

$$w(r) = -\min\left[\sum_{n=1}^{\infty} (h_{a_n} \cos n\theta + h_{b_n} \sin n\theta)\right.$$

$$\left. + (r - r_c) \sum_{n=1}^{\infty} (\phi_{a_n} \cos n\theta + \phi_{b_n} \sin n\theta)\right] \ . \qquad (4\text{-}28)$$

This condition requires that at all values of r, the seal will be just touching at some angle θ. This condition is necessary for uniform wear of the seal ring which is the condition reached after the wave has moved around the seal a number of times. Partial wear conditions (where only a fraction of the width of the face has worn) can also be determined as shown later.

The deflection terms h_{a_n}, h_{b_n}, ϕ_{a_n} and ϕ_{b_n} arise from all loads imposed on the ring r. These loads include deliberately applied loads such as waviness pressure and face loads generated by the face pressure

*w(r) is adjusted to make this true.

distribution. Before considering complications of deflection, the solution to the previous seal model equations will be given for an arbitrary set of h_{a_n}, h_{b_n}, ϕ_{a_n}, ϕ_{b_n} to see how seal lubrication and leakage behave for this general type of deflection. For this purpose, it will be assumed that all significant disturbances h_{a_n}, h_{b_n}, ϕ_{a_n}, ϕ_{b_n} are of the third harmonic. The three will be dropped to shorten the subscript. Thus,

$$h = h_o + w(r) + (h_a + (r - r_c)\,\phi_a)\cos 3\theta + (h_b + (r - r_c)\,\phi_b)\sin 3\theta \; . \qquad (4\text{-}29)$$

Solution

For a given h_a, h_b, ϕ_a, ϕ_b, material properties, roughness, sealed pressure, balance ratio, etc. the general method of solution is as follows:

1) Calculate w(r) using equation (4-28)
2) Assume a value for h_o
3) Solve Reynolds equation (4-3) for the given boundary conditions using over relaxation
4) Set all negative pressures equal to zero
5) Calculate load support using equation (4-8)
6) Compare W to W* and adjust h_o using a secant root finding technique. Return to step 3) and repeat until W = W*
7) Calculate friction and leakage

To demonstrate the solution, a base case common to the test conditions of Chapter 2 has been established as follows:

$p_i = 0$

$p_o = 3.45$ MPa (500 psi)

$p_m = 262$ MPa (38000 psi)

$p_s = 0.1\, p_m$

$p_{sp} = 0.207$ MPa (30 psi)

(continued on following page)

$$c = 0.51\ \mu m\ (0.14\ \mu m\ CLA)\ (20\ \mu in.)\ (5.4\ \mu in.\ CLA)$$

$$B = 1.0$$

$$\eta = 6.83 \cdot 10^{-4}\ Pa \cdot s, H_2O \text{ at } 38°C\ (100°F)\ (0.99 \cdot 10^{-7}\ lb \cdot s/in.^2)$$

$$RPM = 1800\ (188.5/s)$$

$$r_i = 48.26\ mm\ (1.900\ in.)$$

$$r_o = 53.04\ mm\ (2.088\ in.)$$

$$r_c = 52.83\ mm\ (2.080\ in.) \qquad (4\text{-}30)$$

Corresponding nondimensional constants are:

$$\bar{p}_o = 2.46 \cdot 10^{-3}$$

$$\bar{p}_m = 1.87 \cdot 10^{-1}$$

$$\bar{p}_s = 1.87 \cdot 10^{-2}$$

$$\bar{p}_{sp} = 1.48 \cdot 10^{-4} \qquad (4\text{-}31)$$

$$r_o/c = 1.044 \cdot 10^{5}$$

$$\bar{r}_i = 0.9100$$

$$\bar{r}_c = 0.9962$$

The waviness selected for this example is

$$\bar{h}_a = 5.0 \qquad \bar{h}_b = 0.0$$

$$\bar{\phi}_a = 42.43 \qquad \bar{\phi}_b = 42.43 \qquad (4\text{-}32)$$

where

$$\bar{\phi} = \phi \frac{r_o}{c} . \qquad (4\text{-}33)$$

Using the solution method outlined with a 20 x 20 grid, the pressure distribution is shown in Figure 4-3. Note the presence of the odd-shaped cavity (denoted by zero pressure) and the nonsymmetric pressure distribution. This cavity shape is much different than that

	r_i									$\bar{p} \times 10^5$									r_o
$\theta = 0$	0.	24.	46.	68.	89.	108.	125.	142.	156.	170.	182.	193.	202.	211.	219.	225.	231.	237.	242.	246.
	0.	25.	50.	73.	95.	114.	132.	149.	163.	176.	188.	198.	207.	215.	222.	228.	233.	238.	242.	246.
	0.	25.	49.	73.	95.	116.	134.	150.	165.	178.	189.	199.	208.	216.	223.	228.	234.	238.	242.	246.
	0.	9.	26.	47.	69.	91.	112.	131.	149.	164.	178.	190.	200.	210.	218.	225.	231.	236.	241.	246.
	0.	0.	0.	0.	0.	0.	20.	52.	83.	109.	132.	152.	170.	185.	199.	210.	222.	231.	239.	246.
	0.	0.	0.	0.	0.	0.	0.	0.	0.	0.	4.	49.	88.	120.	146.	168.	192.	213.	231.	246.
	0.	0.	0.	0.	0.	0.	0.	0.	0.	0.	0.	0.	0.	0.	34.	80.	128.	171.	211.	246.
	0.	127.	183.	129.	0.	0.	0.	0.	0.	0.	0.	0.	0.	0.	0.	0.	0.	77.	166.	246.
	0.	120.	255.	407.	557.	665.	705.	635.	419.	108.	0.	0.	0.	0.	0.	0.	0.	0.	17.	246.
	0.	62.	137.	231.	346.	478.	631.	813.	1011.	1192.	1330.	1399.	1358.	1107.	942.	669.	420.	237.	167.	246.
	0.	32.	71.	119.	177.	247.	330.	434.	558.	699.	856.	1031.	1220.	1396.	1522.	1577.	1534.	1341.	921.	246.
	0.	17.	37.	61.	89.	122.	159.	203.	253.	308.	367.	430.	496.	557.	605.	633.	631.	583.	463.	246.
	0.	10.	22.	36.	52.	69.	89.	110.	134.	159.	185.	211.	238.	262.	282.	297.	303.	299.	202.	246.
	0.	8.	17.	28.	40.	52.	66.	81.	97.	114.	132.	150.	168.	185.	201.	215.	227.	237.	243.	246.
	0.	8.	18.	28.	39.	51.	64.	78.	93.	108.	124.	139.	155.	171.	186.	200.	213.	225.	236.	246.
	0.	10.	21.	32.	45.	50.	72.	86.	101.	116.	131.	146.	160.	175.	189.	201.	214.	225.	236.	246.
	0.	12.	25.	39.	53.	68.	83.	98.	113.	128.	143.	157.	171.	184.	196.	208.	218.	228.	237.	246.
	0.	15.	31.	47.	63.	80.	96.	112.	127.	142.	156.	169.	182.	194.	204.	214.	223.	231.	239.	246.
	0.	19.	37.	56.	75.	92.	109.	126.	141.	155.	169.	181.	192.	202.	212.	220.	227.	234.	240.	246.
$\theta = 120$	0.	24.	46.	68.	89.	108.	125.	142.	156.	170.	182.	193.	202.	211.	219.	225.	231.	237.	242.	246.

$\bar{h}_a = 5.0$ $\bar{h}_b = 0.0$ $\bar{\phi}_a = 42.43$ $\bar{\phi}_b = 42.43$

Figure 4-3. Pressure Distribution for Base Case.

obtained for radially parallel faces [1]. The arbitrary nature of the cavity shapes produced by combined waviness and tilt necessitates the use of the approximate cavity boundary conditions discussed previously.

Based on equation (4-28) the wear was calculated. The film thickness is shown plotted in Figure 4-4 at four different angular positions. At $\theta = 0$, the film shape is convergent but maintains a gap at r_i. At 30° the film shape is convergent but touches at r_i. At 60° the film shape is divergent and touches at r_o; whereas at 90° the film shape is divergent and does not touch at r_o. The face is worn into a curved shape. From the results shown in Figures 4-3 and 4-4, it is apparent that combined waviness and tilt may in general lead to nonsymmetric pressure distributions, curved wear surfaces, and film shapes which vary dramatically with θ.

The computed results for the base case are

$$\begin{aligned} \mu &= 0.026 \\ Q &= 37.0 \text{ ml/min} \\ T_q &= 7.3 \text{ N·m} \\ \% &= 77.9 \\ \bar{h}_o &= 0.577 \end{aligned} \tag{4-34}$$

While torque is about one-half of that of a comparable flat faced seal, leakage is quite large. Leakage is large because of the gaps shown in Figure 4-4. For a flat faced seal % = 49. Thus, average wear rate for the above seal would be expected to be $(1 - 0.78)/(1 - 0.49) = 0.43$ or 43% of that of the flat faced seal according to equation (4-24). Hydrodynamic action is clearly present as is indicated by the cavitation region shown in Figure 4-3. Hydrodynamic action in the base case is also clearly shown by comparing to a solution for the above base case when the speed was set to 0.18 RPM. For 0.18 RPM, the results are

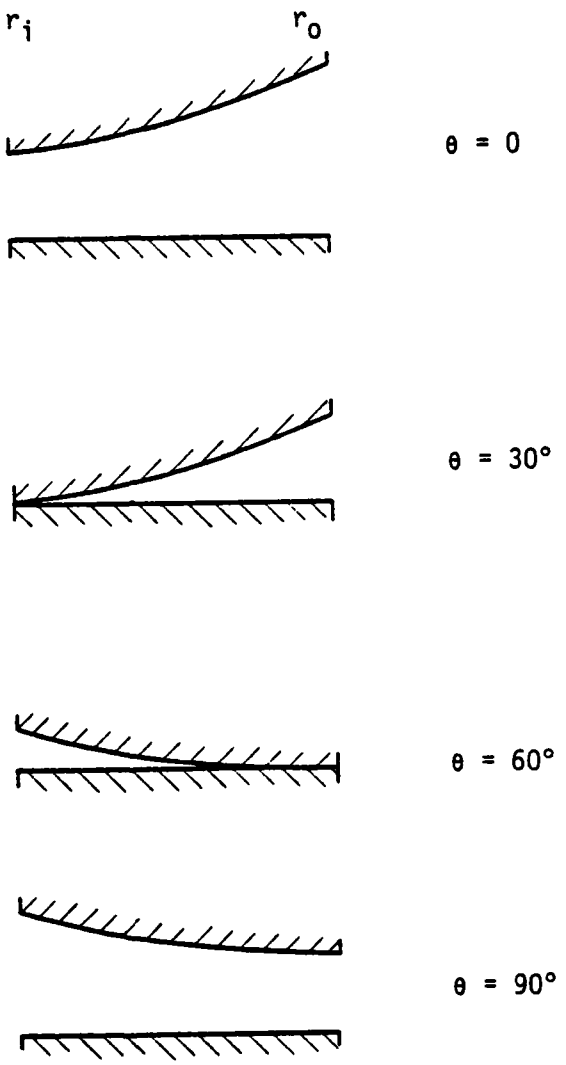

$\overline{h}_a = 5 \quad \overline{h}_b = 0 \quad \overline{\phi}_a = 42.4 \quad \overline{\phi}_b = 42.4$

Figure 4-4. Worn Film Shape for Base Case at Four Angular Positions.

$$\mu = 0.047$$
$$Q = 31.2 \text{ ml/min}$$
$$T_q = 13.3 \text{ N m} \qquad (4\text{-}35)$$
$$\% = 52.8$$

The friction torque is much larger and the % is much lower indicating that the fraction of load supported by fluid pressure in this static case is much smaller than in the dynamic case.

General Studies

To evaluate the potential wear and friction reduction using combined parallel face waviness and tilt, several parameter studies were made. First, Figure 4-5 shows leakage and torque as functions of $\bar{\phi}_a$ for a fixed $\bar{h}_a$. Note that both $\bar{h}_b$ and $\bar{\phi}_b$ are zero so that the wave and the tilt are in phase. Considering first the 0 RPM or static case, it is clear that a certain tilt combined with the given waviness produces a minimum value of torque. Leakage values are quite large until this critical value is reached, after which they remain quite small. At 1800 RPM the general behavior is similar except that torque values are much lower than for the static case, and leakage values are slightly higher. A comparison of the 0 and 1800 RPM friction curves clearly indicates that hydrodynamic effects are occurring and increasing the fraction of fluid pressure load support.

The curve also shows for the 1800 RPM case that operation at what will be called the optimum tilt (the minimum point on the torque curve) provides much better seal performance than for parallel face waviness where $\bar{\phi}_a = 0$. Leakage is much lower and torque is somewhat lower. This result points out a method whereby hydrodynamic effects may be used to great advantage while leakage remains controlled at low levels.

Considering the optimum point, a detailed study shows that this occurs when

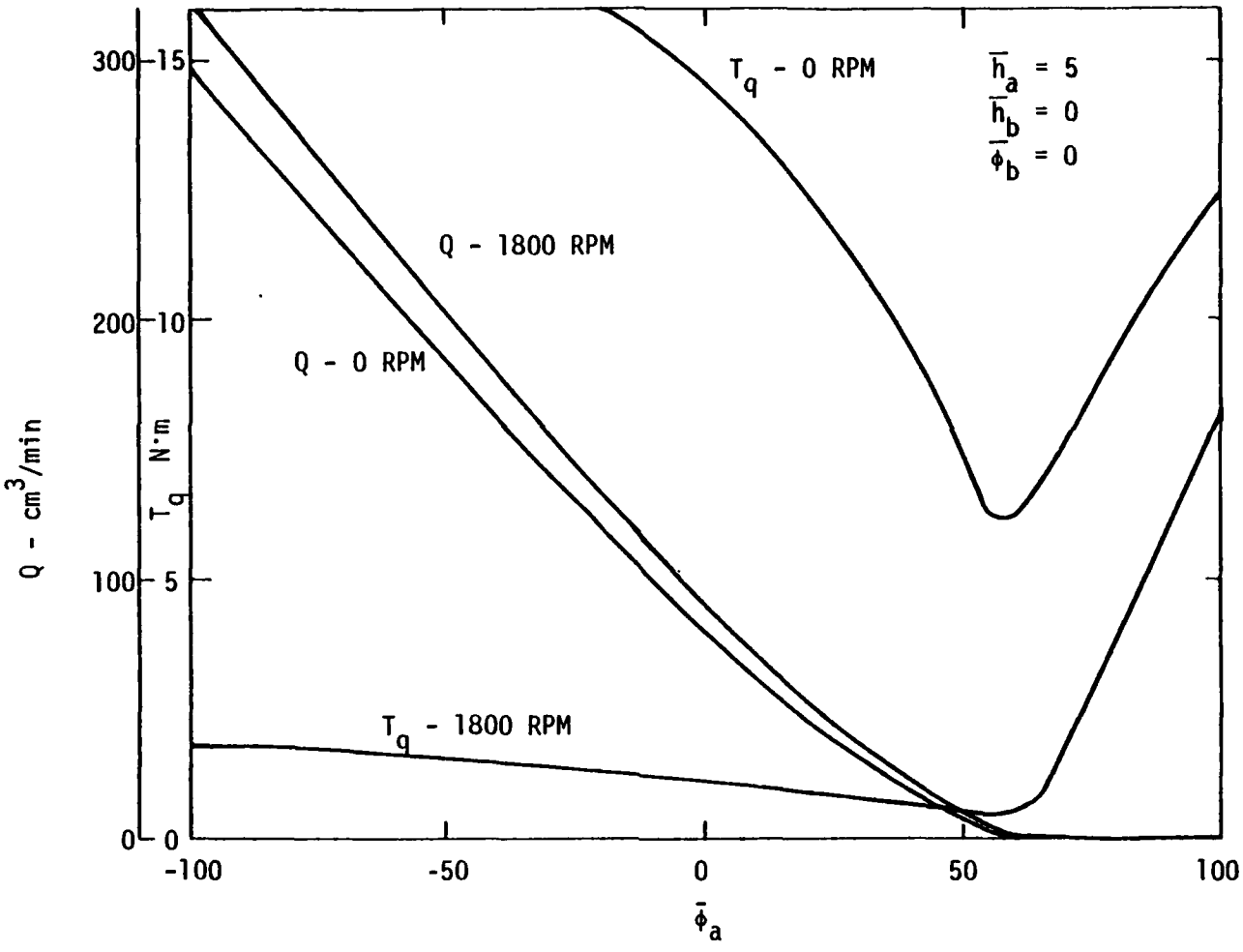

Figure 4-5. Torque and Leakage as Functions of Tilt

$$\bar{\phi}_a = \frac{\bar{h}_a}{\bar{r}_c - \bar{r}_i} \tag{4-36}$$

which is the case where double touching just begins. An illustration of wear profiles for some of the cases shown in Figure 4-5 provides an explanation for the optimum point as well as other behavior. For $\bar{\phi}_a$ = -60, Figure 4-6 shows that the faces are either parallel or divergent. This explains the high torque and leakage for both the static and dynamic cases at negative $\bar{\phi}_a$. When $\bar{\phi}_a$ = 60 (very close to the optimum point), the faces are either parallel or convergent. This convergence explains why friction is so low in both the static and dynamic cases. The seal faces touch at r_i all around the seal. This explains the low leakage, i.e., there is no signficant gap at any point around the seal. As ϕ_a becomes larger, leakage remains low because touching occurs at some point everywhere around the seal. However, the gap becomes divergent for a fraction of the seal face and considerable load support is lost compared to the ϕ_a = 60 case.

From this illustration the principles for operation of a static or dynamic seal utilizing combined waviness and tilt where friction is to be at a minimum and leakage must be small becomes clear. For minimum leakage, touching must occur all around the seal. This does not require, as shown by the middle case of Figure 4-6, that a large radial fraction must contact; a small fraction as shown will suffice. It is only necessary that a touching sealing dam be established everywhere. Concerning friction, where the face departs from the parallel condition it must become convergent rather than divergent. The convergent face causes the fluid pressure to decrease at a lower rate radially across the face than for a divergent face, thus giving much greater load support. In fact, load support is better than for parallel faces even in the hydrodynamic case.

It also becomes clear from this discussion that there is much merit in simply designing a seal face with a converging radial taper uniform around the seal, i.e., no waviness. Indeed, as shown by Snapp and Sasdelli [22] this approach does lead to low friction. However,

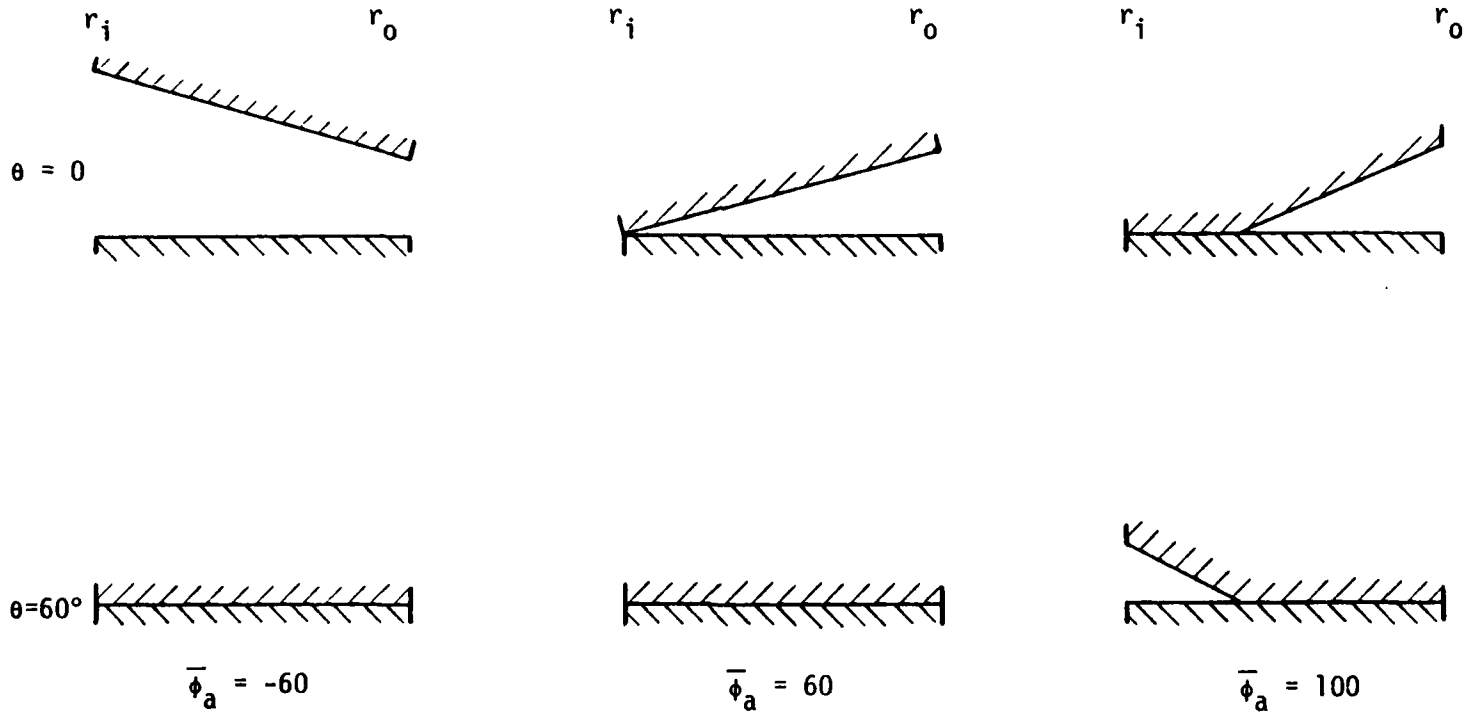

Figure 4-6. Comparisons of Worn Film Shape for Three Angles of Tilt.

there is no mechanism by which to maintain the taper on an indefinite basis as in the case for a wavy seal. Therefore, to minimize wear and degradation of operation, the convergent taper seal must be designed having a large gap and consequently large leakage. The wavy approach eliminates this disadvantage because the gap can be essentially closed and leakage values made quite low.

In Figure 4-5, the waviness and tilt were in phase. Now the effect of a phase shift is considered. For the results shown in Figure 4-7 the following conditions were maintained.

$$\begin{aligned} \bar{h}_a &= 5.0 \\ \bar{h}_b &= 0 \\ \bar{\phi} &= 60 \\ \bar{\phi}_a &= \bar{\phi} \cos \alpha \\ \bar{\phi}_b &= \bar{\phi} \sin \alpha \end{aligned} \qquad (4\text{-}37)$$

This has the effect of moving the tilt an angle α relative to the waviness h_a. The results in Figure 4-7 clearly show that leakage is at a minimum only when the waviness and tilt are in phase for both the static and dynamic cases. Torque for the static case also reaches a minimum under these same conditions. Torque for the dynamic case does reach a relative minimum at $\alpha = \pi$, however, the case where $\alpha = 0$ clearly gives the lowest torque. In conclusion, based on this study, waviness and tilt should be in phase to obtain the lowest leakage and torque.

Optimum Conditions

In Figure 4-8, the results of a study of performance for the base case seal under the optimum condition of equation (4-36) is shown. $\bar{h}_a = 0$ represents a parallel face case. As waviness (and therefore tilt) are increased, torque decreases and leakage increases. In the dynamic case, low values of torque are reached at relatively low leakage values. The selection of an operating point is clearly a trade-off question. If relatively large amounts of leakage can be

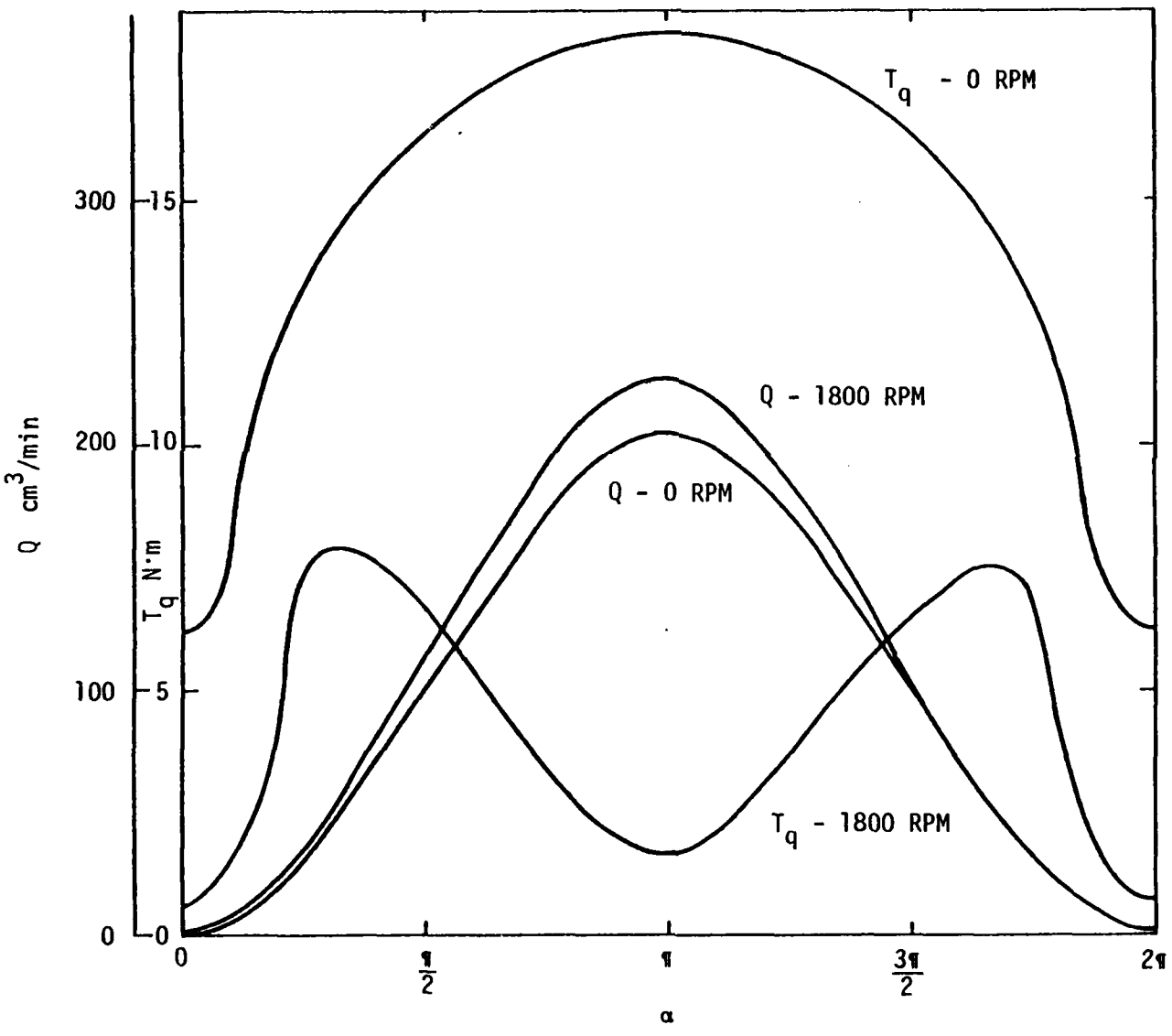

Figure 4-7. Torque and Leakage as Functions of Phase Angle.

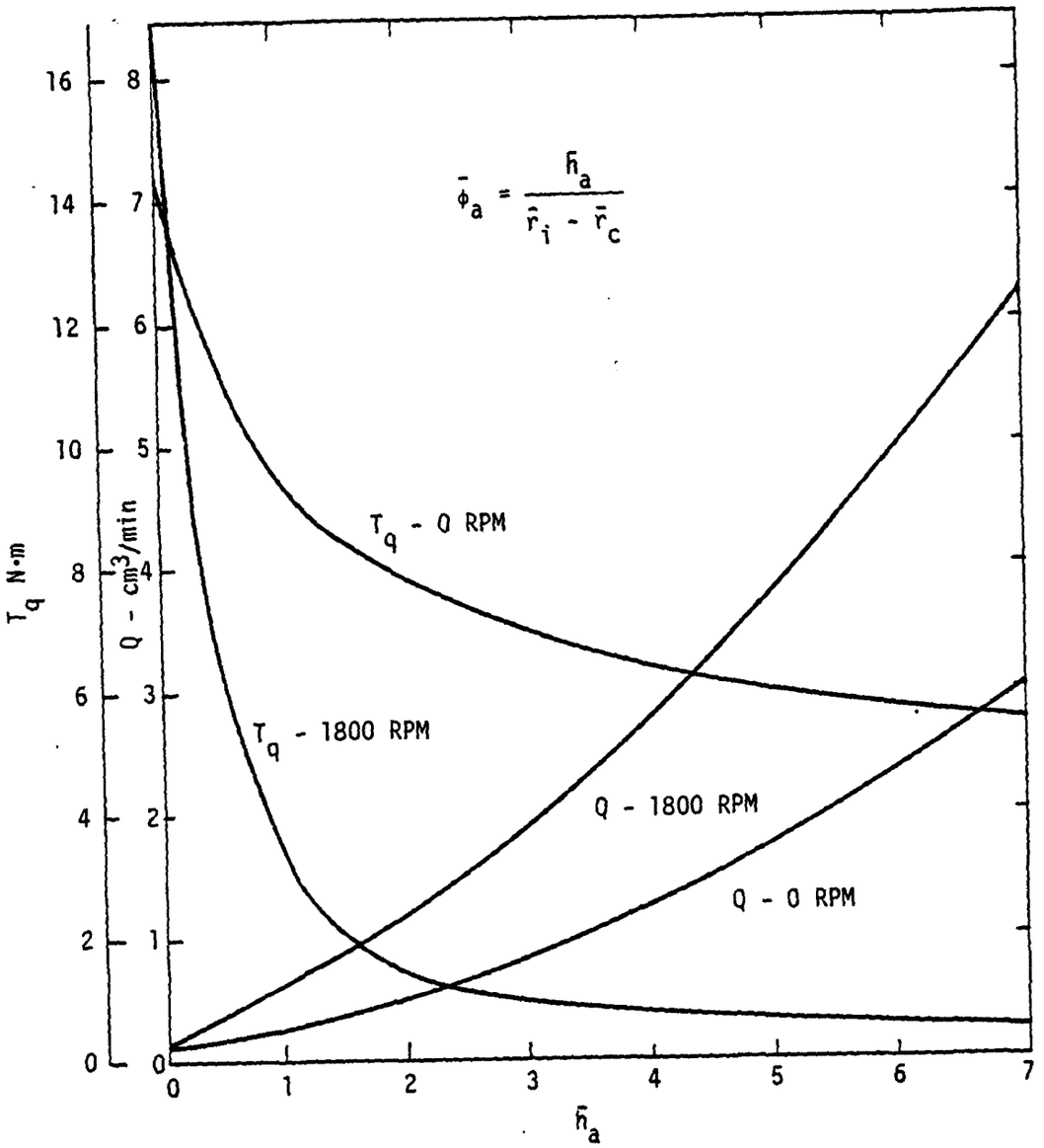

Figure 4-8. Leakage and Torque at Optimum Conditions.

tolerated, then $\bar{h}_a$ should be large. If only a small leakage can be tolerated, then some compromise on torque must be made.

Figure 4-8 shows an additional advantage to this design concept not pointed out previously. The static torque is significantly reduced by the same changes that reduce the dynamic torque. Thus, even at lower operating speeds, the seal will have lower friction than a parallel seal. This feature would minimize wear at low speeds and during start up conditions. Such a seal design is more versatile than a seal that derives its lift purely hydrodynamically.

Ring Deflection

The combined waviness and tilt model just described is applicable to the experimental seal. However, before the model can be used, the waviness in the experimental seal must first be determined. The waviness in the seal occurs due to various deflections. The forces producing these deflections are the waviness producing mechanism, the system of pressures acting on the face, and the drive forces. The resulting deflections are complex, and a thorough analysis must be made.

Loads

As a general approach to calculating deflection, it is first assumed that all loads are distributed such that the load can be represented by a Fourier series. This has the advantage of greatly simplifying the calculations for the simultaneous solutions for deflection needed as the final result, because certain harmonics or terms in the Fourier series become negligible.

A segment of the carbon ring is shown in Figure 4-9. It is assumed that all significant deflections occur in the carbon ring compared to the W-C because of its low Youngs modulus. The loads shown are assumed to be distributed and functions of θ. The distributed force loads are assumed to be acting through the centroid. Given the waviness cylinder arrangement shown in Chapter 2, which applies pressure to the inside surface of the seal ring, and the pressure and friction on the seal face,

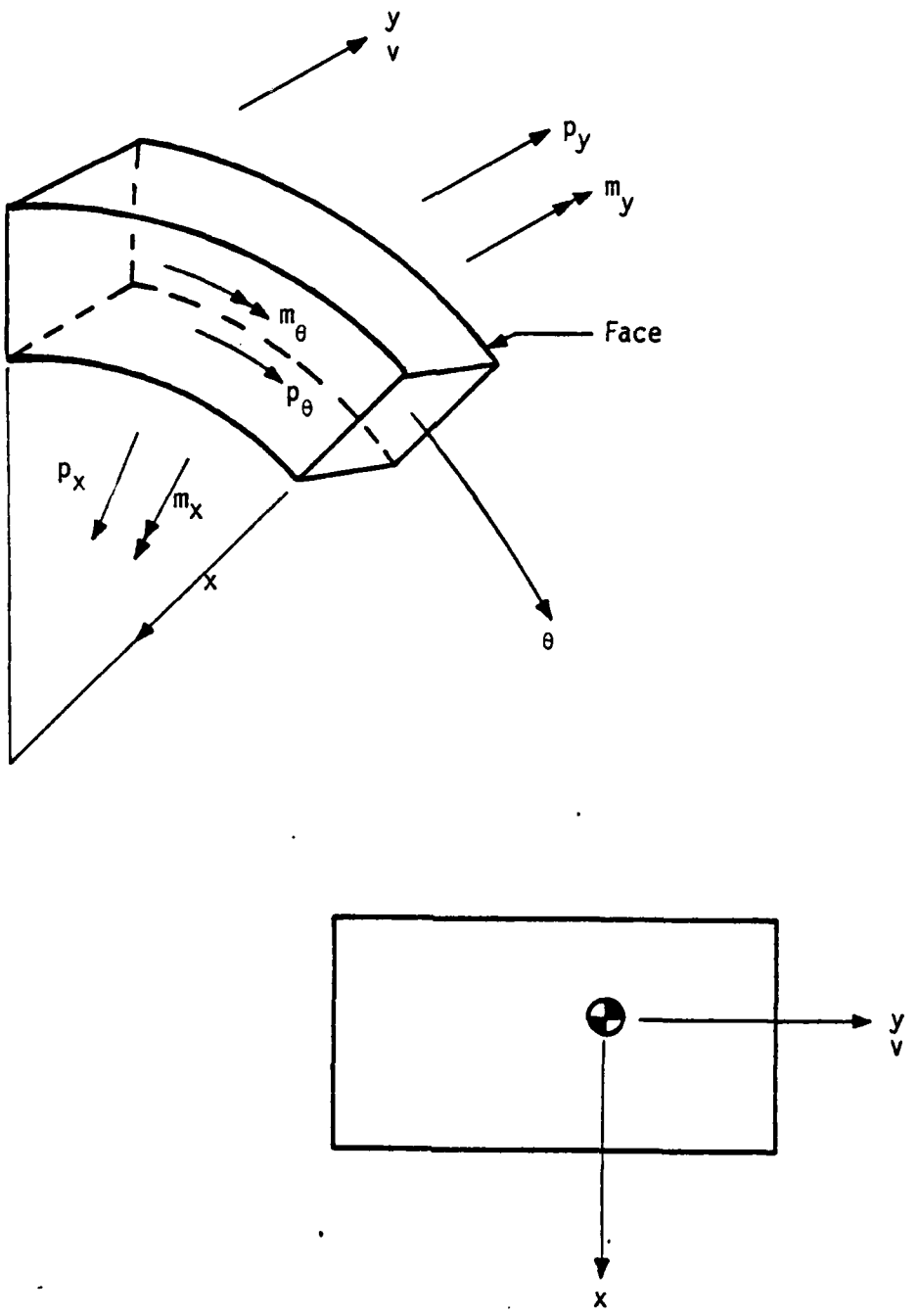

Figure 4-9. Segment of Seal Ring Showing Loading.

the sources of the various loads shown are as follows.

p_x - caused by waviness pressure

p_y - caused by face pressure

p_θ - caused by friction between the O-rings of the waviness cylinder and the inside surface of the ring and by friction at the contact face

m_x - caused by friction of the O-rings and friction at the contact face

m_y - same as m_x

m_θ - caused by the waviness pressure

It can be shown that deflection due to friction forces is small relative to deflection due to the other loads. This is true because friction forces on the face and between the ring and waviness cylinder are relatively small. Therefore, one need only consider p_x, p_y and m_θ.

Now, considering the waviness pressure, Figure 4-10 shows p_x and m_θ caused by the six gas pressure regions acting on the carbon ring. It is assumed that the force distribution can be approximated as a uniform force acting over a distance d, the diameter of the hole, and having a total force equal to that of the gas pressure times the area of the hole. The factor r_i/r_c puts the force and moment in terms of per unit length of centroidal circumference. Moment arm e is the distance in the y direction between the center of the hole and the centroid.

A Fourier analysis for the pressure and moment shown in Figure 3-10 gives

$$p_x \cong p_g \frac{dr_i}{r_c}\left[\frac{1}{2}\sin\frac{3d}{r_i}\cos 6\theta + \frac{1}{4}\sin\frac{6d}{r_i}\cos 12\theta + \cdots\right]$$

$$= p_{xa_6}\cos 6\theta + p_{xa_{12}}\cos 12\theta + \cdots , \qquad (4\text{-}38)$$

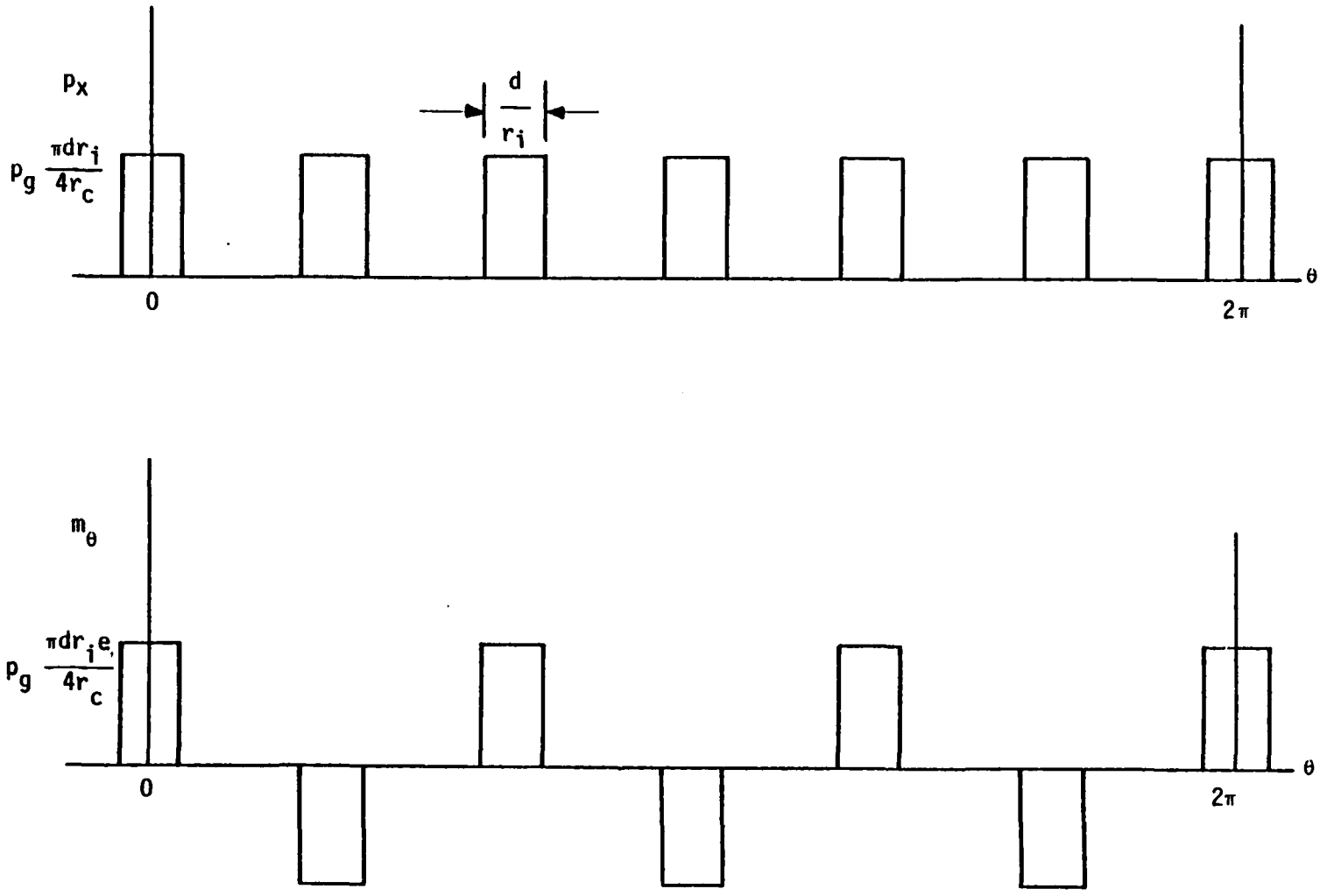

Figure 4-10. p_x and m_θ caused by waviness pressure.

$$m_{\theta g} = p_g \frac{dr_i e}{r_c} \left[\sin \frac{3d}{2r_i} \cos 3\theta + \frac{1}{3} \sin \frac{9d}{2r_i} \cos 9\theta + \cdots \right]$$

$$= m_{\theta g a_3} \cos 3\theta + m_{\theta g a_9} \cos 9\theta + \cdots . \tag{4-39}$$

Now, considering loads applied at the face, assume that the pressure on the seal face is given by $p(r,\theta)$. Then

$$\frac{p_y r_c c^2}{r_o^4 \eta\omega} = -\int_{\bar{r}_i}^{\bar{r}_o} p(r,\theta)\, \bar{r}\, d\bar{r} , \tag{4-40}$$

$$\frac{m_{\theta p} r_c c^2}{r_o^5 \eta\omega} = \int_{\bar{r}_i}^{\bar{r}_o} \bar{p}(r,\theta)\, \bar{r}(\bar{r} - \bar{r}_c)\, d\bar{r} , \tag{4-41}$$

Both p_y and m_θ are functions of θ and may be represented by a Fourier series.

$$p_y \cong p_{ya_3} \cos 3\theta + p_{ya_6} \cos 6\theta + \cdots$$

$$+ p_{yb_3} \sin 3\theta + p_{yb_6} \sin 6\theta + \cdots , \tag{4-42}$$

$$m_{\theta p} \cong m_{\theta p a_3} \cos 3\theta + m_{\theta p a_6} \cos 6\theta + \cdots$$

$$+ m_{\theta p b_3} \sin 3\theta + m_{\theta p b_6} \cos 6\theta + \cdots . \tag{4-43}$$

Only harmonic multiples of three appear because there are three waves. Both sin and cos terms appear because the wave is in general nonsymmetric about the origin.

Loading due to both the waviness pressure and face load appear in series form. Deflection caused by these loadings is now considered.

Deflection

Based upon equation (2-30) of reference [23], one may solve for the deflection of a ring caused by general harmonic loads p_y, p_x and m_θ. For the nth harmonic of deflection the result is

$$\frac{v_{a_n}}{r_c} = -\frac{p_{xa_n} r_c^3}{EJ_x}\frac{J_{xy}}{J_y}\frac{1}{(n^2-1)^2} - \frac{m_{\theta a_n} r_c^2}{EJ_x}\frac{(1+A)}{(n^2-1)^2} + \frac{p_{ya_n} r_c^3}{EJ_x}\frac{A+n^2}{n^2(n^2-1)^2}, \tag{4-44}$$

$$\phi_{a_n} = \frac{p_{xa_n} r_c^3}{EJ_x}\frac{J_{xy}}{J_y}\frac{1}{(n^2-1)^2} + \frac{m_{\theta a_n} r_c^2}{EJ_x}\frac{An^2+1}{(n^2-1)^2} - \frac{p_{ya_n} r_c^3}{EJ_x}\frac{A+1}{(n^2-1)^2}. \tag{4-45}$$

ϕ_{b_n} and v_{b_n} are given by the same expression as above but substituting b's for a's. The symbol A above is given by

$$A = \frac{EJ_x}{GJ_\theta}. \tag{4-46}$$

J_x J_y J_{xy} J_θ are standard section properties for a ring cross section and are given in the list of symbols. The net deflection then becomes

$$v = \sum_n v_{a_n} \cos n\theta + \sum_n v_{b_n} \sin n\theta, \tag{4-47}$$

$$\phi = \sum_n \phi_{a_n} \cos n\theta + \sum_n \phi_{b_n} \sin n\theta. \tag{4-48}$$

Based on the actual seal ring of interest, the ratio J_{xy}/J_y is quite small. Therefore, the effect of p_x is insignificant and this

term will be dropped for the balance of this work. Also note that all deflection terms contain a factor $(n^2 - 1)^2$ in the denominator. This means that deflection of the 6th harmonic will be 5 percent of the magnitude of deflection of the 3rd harmonic assuming comparable loading terms. Therefore, terms of the 6th harmonic and higher will be neglected for the remainder of this work. Since all remaining terms will be for n = 3, the n will be dropped from the symbols.

Now assuming that the reference point ($\theta = 0$) for the system is at the center of one of the waviness gas pressure circles, and with the help of equations (4-25) and (4-26) one can combine equations (4-44) through (4-48) to obtain the following.

$$h = h_o + w(r) + (h_a + (r - r_c)\,\phi_a)\cos 3\theta + (h_b + (r - r_c)\,\phi_b)\sin 3\theta\ , \tag{4-49}$$

where

$$h_a = h_{ma} + h_{ga} + h_{pa}\ , \tag{4-50}$$

$$h_b = h_{mb} + h_{gb} + h_{pb}\ , \tag{4-51}$$

where

$$h_{ma} = m_{\theta pa}\,\frac{r_c^3}{EJ_x}\,\frac{1 + A}{(n^2 - 1)^2}\ , \tag{4-52}$$

$$h_{ga} = m_{\theta ga}\,\frac{r_c^3}{EJ_x}\,\frac{1 + A}{(n^2 - 1)^2}\ , \tag{4-53}$$

$$h_{pa} = -p_{ya}\,\frac{r_c^4}{EJ_x}\,\frac{A + n^2}{n^2(n^2 - 1)^2}\ , \tag{4-54}$$

$$h_{mb} = m_{\theta pb}\,\frac{r_c^3}{EJ_x}\,\frac{1 + A}{(n^2 - 1)^2}\ , \tag{4-55}$$

$$h_{gb} = m_{\theta gb}\,\frac{r_c^3}{EJ_x}\,\frac{1 + A}{(n^2 - 1)^2}\ , \tag{4-56}$$

$$h_{pb} = -p_{yb} \frac{r_c^4}{EJ_x} \frac{A + n^2}{n^2(n^2 - 1)^2} , \tag{4-57}$$

and where

$$\phi_a = \phi_{ma} + \phi_{ga} + \phi_{pa} , \tag{4-58}$$

$$\phi_b = \phi_{mb} + \phi_{gb} + \phi_{pb} , \tag{4-59}$$

where

$$\phi_{ma} = m_{\theta pa} \frac{r_c^2}{EJ_x} \frac{An^2 + 1}{(n^2 - 1)^2} , \tag{4-60}$$

$$\phi_{ga} = m_{\theta ga} \frac{r_c^2}{EJ_x} \frac{An^2 + 1}{(n^2 - 1)^2} , \tag{4-61}$$

$$\phi_{pa} = -p_{ya} \frac{r_c^3}{EJ_x} \frac{A + 1}{(n^2 - 1)^2} , \tag{4-62}$$

$$\phi_{mb} = m_{\theta pb} \frac{r_c^2}{EJ_x} \frac{An^2 + 1}{(n^2 - 1)^2} , \tag{4-63}$$

$$\phi_{gb} = m_{\theta gb} \frac{r_c^2}{EJ_x} \frac{An^2 + 1}{(n^2 - 1)^2} , \tag{4-64}$$

$$\phi_{pb} = -p_{yb} \frac{r_c^3}{EJ_x} \frac{A + 1}{(n^2 - 1)^2} , \tag{4-65}$$

The term $m_{\theta ga}$ is defined by equation (4-39); p_{ya}, p_{yb}, and $m_{\theta pa}$, $m_{\theta pb}$ are derived by making a Fourier analysis of the face pressure as defined by equations (4-40) and (4-41) and (4-42) and (4-43). $m_{\theta gb}$ is zero if the θ coordinate begins at the center of one of the gas pressure holes. The above terms may be thought of as follows.

h_{ma} waviness due to a moment of the face pressure

h_{ga} waviness due to a moment of the gas pressure

h_{pa} waviness due to the force of the face pressure

ϕ_{ma} tilt due to a moment of the face pressure

ϕ_{ga} tilt due to a moment of the gas pressure

ϕ_{pa} tilt due to the force of the gas pressure

The b subscript terms simply represent the sin component of the wave. Rewriting equation (4-49) in the above terms,

$$h = h_o + w(r) + [h_{ma} + h_{ga} + h_{pa} + (r - r_c)(\phi_{ma} + \phi_{ga} + \phi_{pa})] \cos 3\theta + [h_{mb} + h_{gb} + h_{pb} + (r - r_c)(\phi_{mb} + \phi_{gb} + \phi_{pb})] \sin 3\theta \ . \quad (4\text{-}66)$$

Nonparallel Faces

From equations (4-53) and (4-54) and (4-61) and (4-62), deflection ratios are

$$\frac{h_{pa}}{h_{ga}} = - \frac{p_{ya} r_c}{m_{\theta ga}} \frac{A + n^2}{n^2(1 + A)} , \quad (4\text{-}67)$$

$$\frac{\phi_{pa}}{\phi_{ga}} = - \frac{p_{ya} r_c}{m_{\theta ga}} \frac{A + 1}{An^2 + 1} , \quad (4\text{-}68)$$

For A = 7.44 and n = 3 (the test seal values), the above ratios are

$$\frac{h_{pa}}{h_{ga}} = - \frac{p_{ya} r_c}{m_{\theta ga}} (0.22) , \quad (4\text{-}69)$$

$$\frac{\phi_{pa}}{\phi_{ga}} = - \frac{p_{ya} r_c}{m_{\theta ga}} (0.12) . \quad (4\text{-}70)$$

Now for a given ratio of the face pressure harmonic component p_{ya} to the gas pressure moment harmonic component $m_{\theta ga}$, the face pressure

caused waviness h_{pa} is larger than the face pressure caused tilt. This means that when the net waviness component ($h_{pa} + h_{ga}$) is flattened to nearly zero by the face pressure, the net tilt component will not be.

In the original concept of the experimental apparatus, it was assumed that both tilt and waviness would be reduced a proportional amount by the face pressure, thus resulting in relatively small net tilt as well as relatively small net waviness. The above relationship shows that this is not true. Even though waviness flattens to zero, the tilt does not go to zero. Thus in the experimental seal, the film thickness function is quite different than first anticipated [1]. Analysis of the experimental face seal based upon wavy but radially parallel faces led to predictions that totally disagreed with the experiment. After all above effects were included, agreement became much better as will be shown.

After a thorough analysis of the deflection behavior it becomes clear that it is very difficult to deflect a seal face so that the waviness remains radially parallel. Tilt is almost inevitably introduced. However, as the preceeding results show, a combination of waviness and tilt may actually lead to a more improved seal concent than parallel face waviness alone.

Solution for Test Seal

To solve the combined waviness and tilted seal problem for a real case becomes much more difficult than for the hypothetical cases studied previously. The difficulty that arises is that h_{ma} h_{pa} h_{mb} h_{pb} ϕ_{ma} ϕ_{pa} ϕ_{mb} ϕ_{pb} are all unknown and depend on the solution itself. Thus, one must assume a set of values, evaluate the pressure, and then check the resulting deflections against the assumed deflections.

To expedite the solution the following approach was taken. First, since the position of the gas pressure wave can be considered to be arbitrary,

$$m_{\theta pb} = -m_{\theta gb} \, , \tag{4-71}$$

$$m_{\theta pa} + m_{\theta ga} = m_{\theta a} \quad . \tag{4-72}$$

Now $m_{\theta pa}$ is generally much smaller than $m_{\theta ga}$, so if one assumes an $m_{\theta ga}$ based on gas pressure, only a small change in effective pressure results. Conditions (4-71) and (4-72) change equation (4-66) to the following.

$$h = h_o + w(r) + [m_{\theta a}K_1 + h_{pa} + (r - r_c)(m_{\theta a}K_2 + \phi_{pa})] \cos 3\theta$$
$$+ [h_{pb} + (r - r_c)\,\phi_{pb}] \sin 3\theta \quad , \tag{4-73}$$

where K_1 and K_2 are given in equations (4-52) and (4-60). Now since ϕ_{pa} is proportional to h_{pa} and ϕ_{pb} is proportional to h_{pb}, there are only three arbitrary constants remaining in equation (4-73). These are $m_{\theta a}$, h_{pa} and h_{pb}. Given values for these parameters, the solution to the problem then becomes the same as before. Thus, a general solution for an actual seal can be accomplished as follows.

1) Assume a value for $m_{\theta a}$ based on the gas pressure at which the problem is to be solved.
2) Guess values for h_{pa} and h_{pb} calculate ϕ_{pa} and ϕ_{pb} from these.
3) Solve for the pressure distribution and equilibrium h_o based on load as before.
4) Evaluate integrals (4-40) and (4-41) as functions of θ and make a Fourier analysis to obtain p_{ya} p_{yb} $m_{\theta pa}$ $m_{\theta pb}$.
5) Find h_{pa} and h_{pb} using equations (4-54) and (4-57).
6) Compare the calculated values of h_{pa} and h_{pb} to the assumed values. If they agree, then calculated deflection is equal to assumed deflection and the solution is correct. If they do not agree, then new values of h_{pa} and h_{pb} must be assumed and steps 2) through 6) are repeated.

In essence, finding the correct h_{pa} and h_{pb} represents solving two nonlinear equations in two unknowns, where the function to be evaluated each time represents the entire solution to the seal

lubrication problem. This procedure was facilitated by using a non-linear root finding technique based upon fitting approximate planes to the surfaces represented by the two conditions, and solving for the condition where the intersection of the two planes satisfies both conditions. This is equivalent to a two-dimensional version of the secant method for finding a root. The method works quite well if one can guess the correct neighborhood for the solution.

Once the solution above is found, then the actual pressure to which the solution corresponds is determined as follows.

$$m_{\theta gb} = -m_{\theta pb} , \tag{4-74}$$

$$m_{\theta ga} = m_{\theta a} - m_{\theta pa} , \tag{4-75}$$

where $m_{\theta pa}$ and $m_{\theta pb}$ are computed from the pressure as described. The amplitude of $m_{\theta g}$ is

$$m_{\theta g} = \sqrt{m_{\theta gb}^2 + m_{\theta ga}^2} .$$

Since

$$m_{\theta g} = p_g \frac{dr_i e}{r_c} \sin \frac{3d}{2r_i} , \tag{4-77}$$

from equation (4-39), the corresponding gas pressure can be calculated.

It should be pointed out for a static solution all of the subscript b terms vanish because of symmetry, and the solution involves only one unknown.

Partial Wear Conditions

In some of the results to follow, a partial wear condition was used. For a completely worn in seal, the condition given by equation (4-28) for 100 percent wear was used. For an unworn seal, the term w(r) of equation (4-66) was set equal to a constant. Conditions in between these extremes were also evaluated for static cases where the

tilt and waviness were in phase. This was done using the approach shown in Figure 4-11 where the fraction of interference between the faces was calculated for the two extreme deflection positions. When the average height h_o has been adjusted to provide the desired fraction of wear, then the wear function w(r) is defined as the shaded portion in the figure that must be removed to eliminate interference.

Parameter Values for Test Seal

Equations (4-30) and (4-31) show the values of most of the parameters required for the computer solutions for the test seal. Additional parameters and information are given in Figure 4-12. Several of the parameter value selections require some explanation.

The surface roughness used (equation (4-30)) for the computed results is C = 0.51 μm (0.14 μm CLA). The surface finish of the carbon after test was found to vary from 0.2 to 0.5 μm CLA, somewhat larger than the value used in the computed results. It is thought that the 0.14 μm CLA value used is justified as follows.

1) After a running in period no leakage of flat faced seals has ever been measured. Leakage rates lower than 0.1 ml/μin. have been measured so that the measurement of low level leakage rates is known to be possible. Based upon a theoretical analysis using 0.14 μm CLA, the flat face leakage should be 0.1 ml/min. In a parallel face seal the leakage rate is determined primarily by the surface roughness (a cubic relationship). Since no leakage has been measured, it is thought that the effective roughness is even lower than the assumed value.

2) Close examination of a tangential surface profile shows that the surface is characterized by peaks which are quite flat on top and valleys which are quite deep relative to roughness which appears on the flat peaks. The valleys are spaced far enough apart such that most likely they do not connect to each other. Given this situation, flow would be controlled primarily by the roughness magnitude associated with the

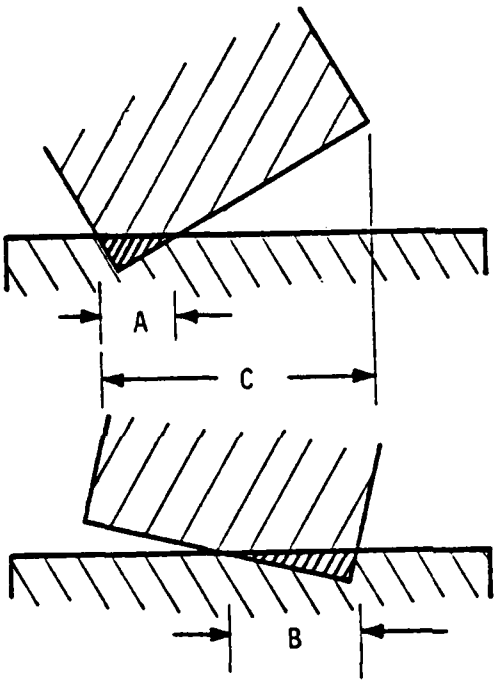

$$\frac{A + B}{C} = \text{Fraction of Wear}$$

Figure 4-11. Fraction of Wear.

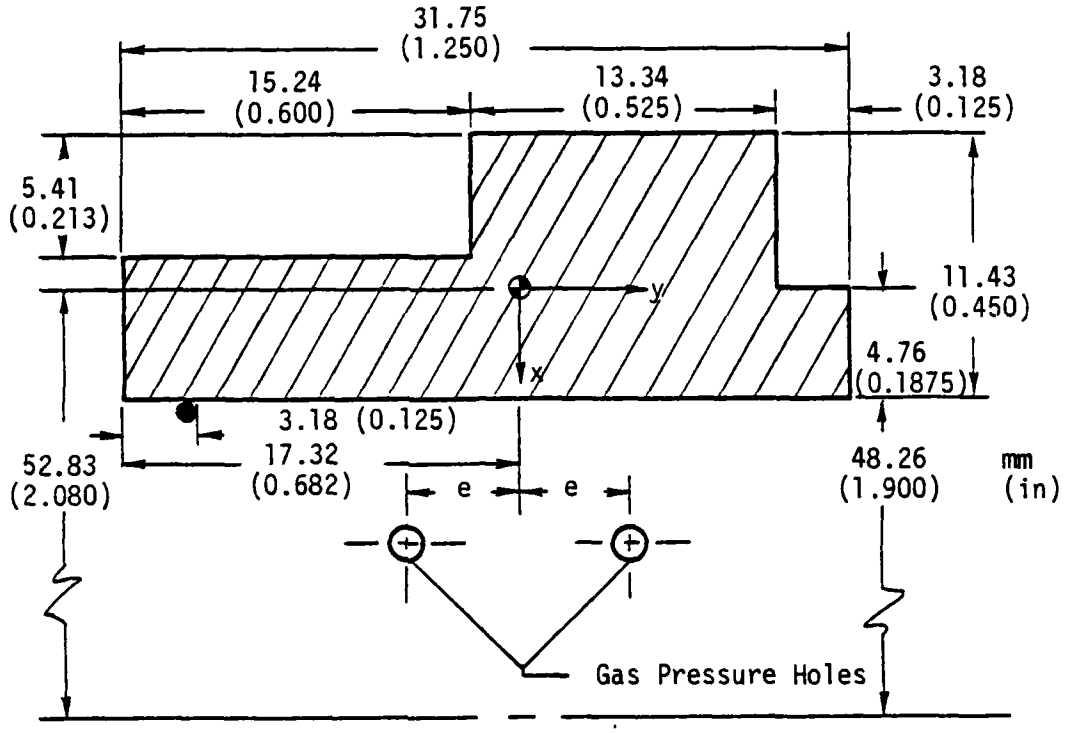

$a = 259\ mm^2\ (0.402\ in^2)$

$J_x^* = 1.840 \cdot 10^4\ mm^4\ (0.0442\ in^4)$

$J_y^* = 2.46 \cdot 10^3\ mm^4\ (0.00591\ in^4)$

$J_{xy}^* = -1.11 \cdot 10^3\ mm^4\ (-0.00267\ in^4)$

$J_\theta^{**} = 5.95 \cdot 10^3\ mm^4\ (0.0143\ in^4)$

$e = 4.85\ mm\ (0.191\ in)$

$E = 20.7\ GPa\ (3.0 \cdot 10^6\ lb/in^2)$

$G = 9.6\ GPa\ (1.25 \cdot 10^6\ lb/in^2)$

$$A = \frac{EJ_x}{GJ_\theta} = 7.44$$

*Calculated assuming $x/r_c << 1$ (creates 2% error).

**Calculated numerically using torsion theory and finite differences.

Figure 4-12. Test Seal Cross Section and Properties.

flat peaks. This value amounts to approximately 0.1 μm CLA, much less than the roughness measured taking the entire surface into account. This value is approximately the roughness value used for the computed results.

The roughness question is very important. Table 4-1 shows the equilibrium operating condition for the test seal at base operating conditions for three roughness values. Torque varies a factor of two, while leakage varies a factor of ten. The effect of roughness on hydrodynamic load support was thoroughly analyzed in reference [1] and shown to be quite significant. Even though a rational basis was used for the effective roughness used in the computed results herein, it is clear that a more thorough analysis of the actual roughness is needed. To this end, investigation of the actual surface using the previously developed flow model [7] is now underway.

Mechanical friction coefficient is taken at 0.1. Based on measurements, this value may be somewhat high as discussed later. However, friction coefficient varies over a wide range depending upon conditions, so a representative value is appropriate. In Figure 4-12 the value of E is taken as the reported value for P658-RC carbon. Deflection tests have been conducted confirming this value to within 10 percent. The value of G is based upon assuming a Poisson's ratio of 0.2 for the carbon.

Comparison of Theory and Experiment

Deflection

Using the method outlined, solutions for deflection and pressure distribution were obtained for the test conditions used for the proximity probe tests outlined in Chapter 2. A zero fraction of wear was assumed. For the zero sealed pressure case, only the spring pressure acted. The tests were conducted under static conditions. Table 4-2 shows the calculated results for the zero pressure case.* Table 4-3, zero wear, shows the computed results for the pressurized case. Deflection at the midpoint of the face (the location of the proximity probes) was calculated using equation (4-66). Figure 4-13 shows a comparison of

*Zero pressure is approximated by 0.007 MPa (1 psi).

Table 4-1

Computed Results - Roughness Effect
p_{H_2O} = 3.45 MPa, p_{gas} = 6.90 MPa, 100% Wear, 1800 RPM

C μm.	CLA μm	$\bar{h}_{pa}$	$\bar{h}_{pa}$ (calc)	$\bar{h}_{pb}$	$\bar{h}_{pb}$ (calc)	$\bar{h}_{a}$ net	$\bar{h}_{b}$ net	ϕ_a net x10^6	ϕ_b net x10^6	$\bar{h}_{ma}$	$\bar{h}_{mb}$	μ	Tq N·m	Q ml/min	%	p_{gas} corrected MPa	$\bar{h}_{o}$
0.25	0.07	-23.41	-23.50	-1.69	-1.70	6.64	-1.69	643	-38	1.21	-1.08	0.0106	2.99	1.51	95.2	6.62	0.724
0.51	0.14	-9.88	-10.00	-1.71	-1.58	5.15	-1.71	724	-76	1.04	0.55	0.0165	4.65	4.45	86.6	6.43	0.650
1.02	0.27	-3.75	-3.71	-0.75	-0.62	3.76	-0.75	830	-67	0.66	-0.03	0.0214	6.03	17.5	80.1	6.29	0.621

Table 4-2

Computed Results - p_{H_2O} = 0.007 MPa, 0 Speed

p_{gas} Mpa	% Wear	$\bar{h}_{pa}$	$\bar{h}_{pa}$ (calc)	$\bar{r}_p$	$\bar{h}_{a_{net}}$	ϕ_{net} x10^6	$\bar{h}_{ma}$	μ	T_q N-m	Q mℓ/min	%	p_{gas} corrected MPa	$\bar{h}_o$
6.90	0	-2	-2.19	.880	13.03	1074	-.027	.098	1.70	1.6	1.4	6.90	-.01
3.45	0	-2	-2.18	.889	5.51	493	-.016	.098	1.70	.12	1.4	3.45	

Table 4-3

Computed Results - p_{H_2O} = 3.45 MPa, 0 Speed

p_{gas} Mpa	% Wear	$\bar{h}_{pa}$	$\bar{h}_{pa}$ (calc)	$\bar{r}_p$	$\bar{h}_{a_{net}}$	ϕ_{net} x10^6	$\bar{h}_{ma}$	μ	T_q N·m	Q mℓ/min	%	p_{gas} corrected MPa	$\bar{h}_o$
6.90	100	-6.21	-6.21	--	8.82	887	1.25	.022	6.08	15.4	78.3	6.32	.57
5.17	100	-5.28	-5.33	.9062	5.99	638	1.16	.022	5.83	3.2	79.1	4.64	.59
3.45	100	-3.81	-4.09	.9102	3.43	400	0.85	.022	6.19	0.80	77.7	3.05	.63
0	100	0	0	--	0	0	0	.051	14.46	0.09	48.6	0.0	.74
6.90	75	-8.08	-8.05	.9135	6.95	804	0.95	.030	8.58	5.8	69.7	6.46	.49
5.17	75												
3.45	75	-4.79	-4.49	.9255	2.72	369	-.03	.032	9.05	0.28	67.8	3.46	.56
6.90	50	-9.74	-10.05	.9269	4.98	717	0.29	.041	11.57	3.95	59.7	6.76	.40
5.17	50												
3.45	50	-5.33	-5.42	.9355	2.18	345	-0.81	.041	11.64	.34	59.1	3.82	.48
6.90	0	-11.7	-12.08	.9467	3.33	643	-1.48	.057	16.09	3.95	45.2	7.57	-.31
5.17	0												
3.45	0	-6.00	-5.92	.9502	1.51	315	-2.38	.055	15.75	.49	46.2	4.54	.04

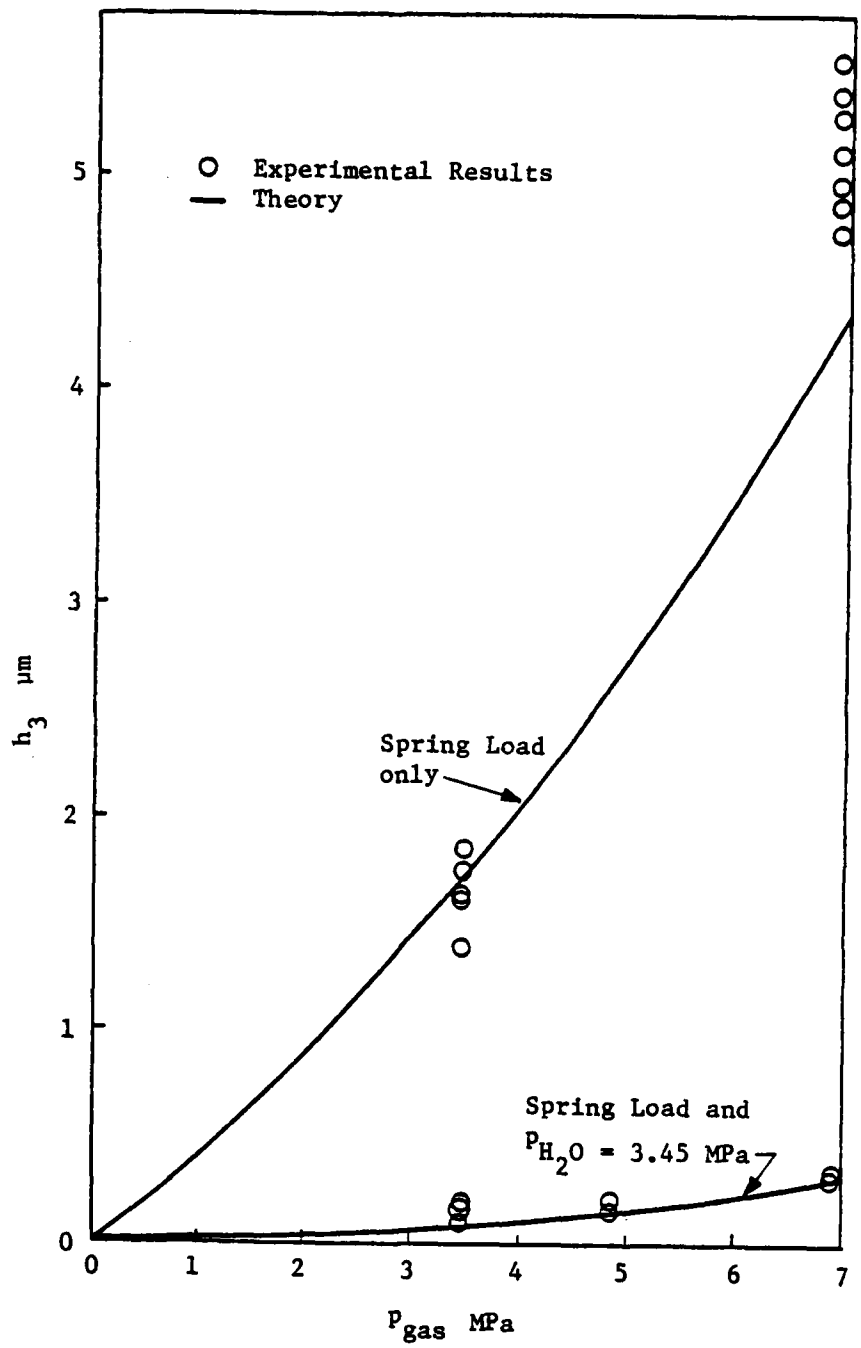

Figure 4-13. Comparison of Measured Face Deflection to Theory.

the theoretical deflection to the measured deflection given in Table 2-7. In the lower curve, where most of the gas pressure caused waviness was flattened out, agreement is quite good. In the upper curve where very little of the wave was flattened, agreement is good at 3.5 MPa but begins to deviate at 7 MPa. Actual error at this level is about 10 percent. Considering the numerous approximations and uncertainties in both theory and experiment, this error appears to be quite acceptable. The results shown in Figure 4-13 show that the deflection theory used is in all probability valid for the purpose of this analysis.

Zero Speed Results

Because of the relatively large gaps that develop in the seal under the combined waviness and tilt conditions, and because no reduction in friction with increasing speed was observed in the tests, it was originally thought that hydrodynamic effects were playing a minimal role in seal performance and that a static analysis might provide an adequate prediction of performance. Thus, the results in Table 4-3 were calculated. Different wear fractions were evaluated to attempt to simulate the type of wear observed and shown in Figure 2-14. The most significant feature of these results indicating disagreement with experiment is that the torque changes very little between 3.5 and 7.0 MPa gas pressure. This is contrary to experimental results which show that torque decreases as gas pressure increases. Also, the calculated leakage is too high at least for the 100 percent wear case. These results do have some use however in that they show how the seal might be expected to behave at low speeds.

Dynamic Results - Gas Pressure Effect

Table 4-4 shows the results for different gas pressures calculated using the model described and assuming 100 percent wear. Note that all of the various deflection terms discussed show up in the table and that the gas pressure is corrected according to the procedures described. The theoretical results of Tables 4-3 and 4-4 are shown compared to experimental results of Table 2-2 in Figures 4-14 and 4-15. Considering first Figure 4-14 for leakage, the 1800 RPM theoretical results

Table 4-4

Computed Results - Waviness Effect at 1800 RPM
p_{H_2O} = 3.45 MPa, 100% Wear

p_{gas} MPa	$\bar{h}_{pa}$	$\bar{h}_{pa}$ (calc)	$\bar{h}_{pb}$	$\bar{h}_{pb}$ (calc)	$\bar{h}_{a_{net}}$	$\bar{h}_{b_{net}}$	$\phi_{a_{net}}$ x10^6	$\phi_{b_{net}}$ x10^6	$\bar{h}_{ma}$	$\bar{h}_{mb}$	ν	T_q N·m	Q mℓ/min	%	p_{gas} corrected MPa	$\bar{h}_o$
6.90	-9.88	-9.98	-1.71	-1.59	5.15	-1.71	724	-76	1.04	0.051	.0161	4.54	4.41	86.5	6.42	.649
5.17	-8.26	-8.13	-0.74	-0.63	3.01	-0.74	506	-33	0.42	-0.46	.0279	7.84	1.19	75.4	4.99	.615
3.45	-5.77	-5.60	-0.33	-0.28	1.74	-0.33	325	-15	-0.21	-0.72	.0364	10.24	0.70	67.7	3.56	.614
0	0	0	0	0	0	0	0	0	0	0	.0593	16.68	0.09	48.8	0	.741

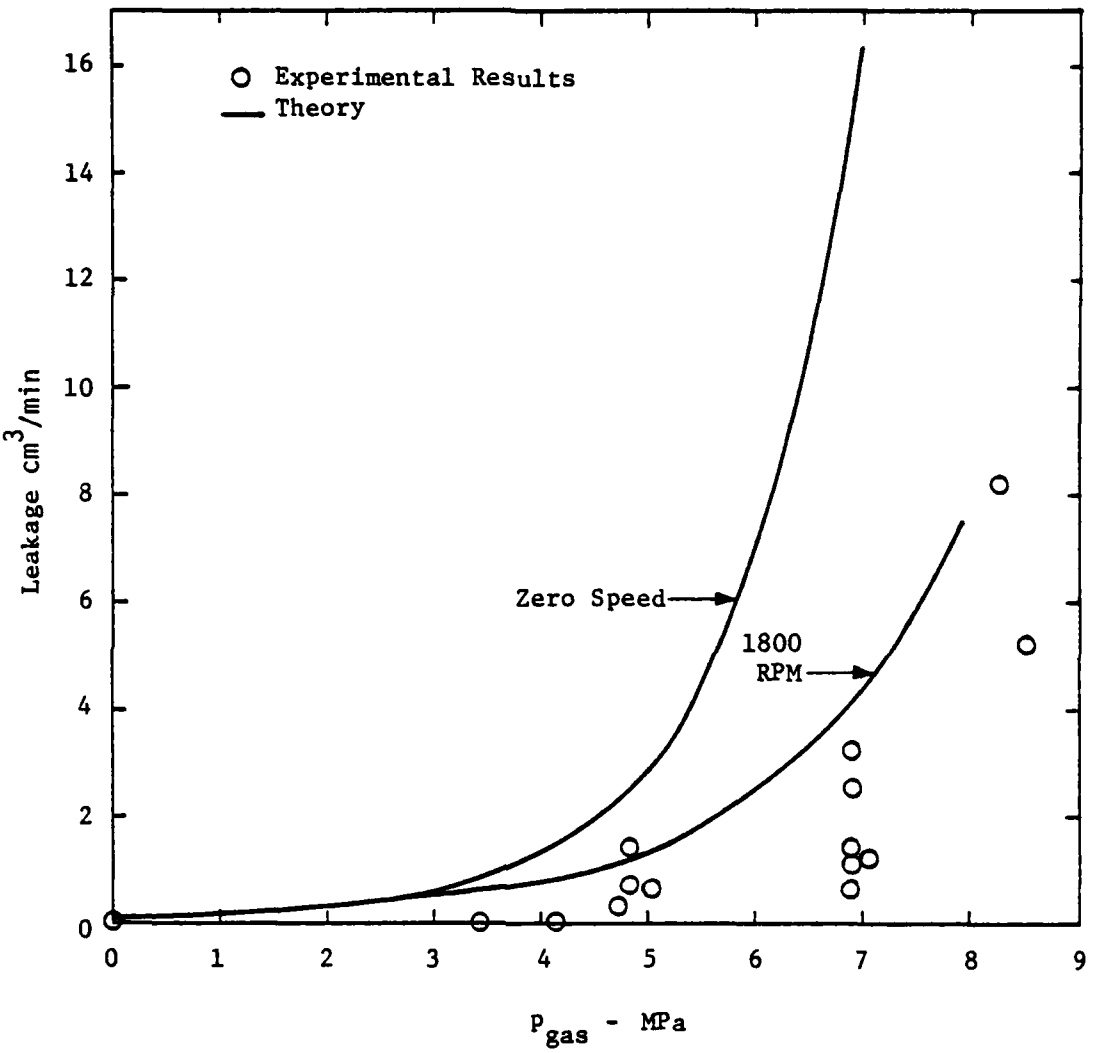

Figure 4-14. Wavy Seal Leakage.

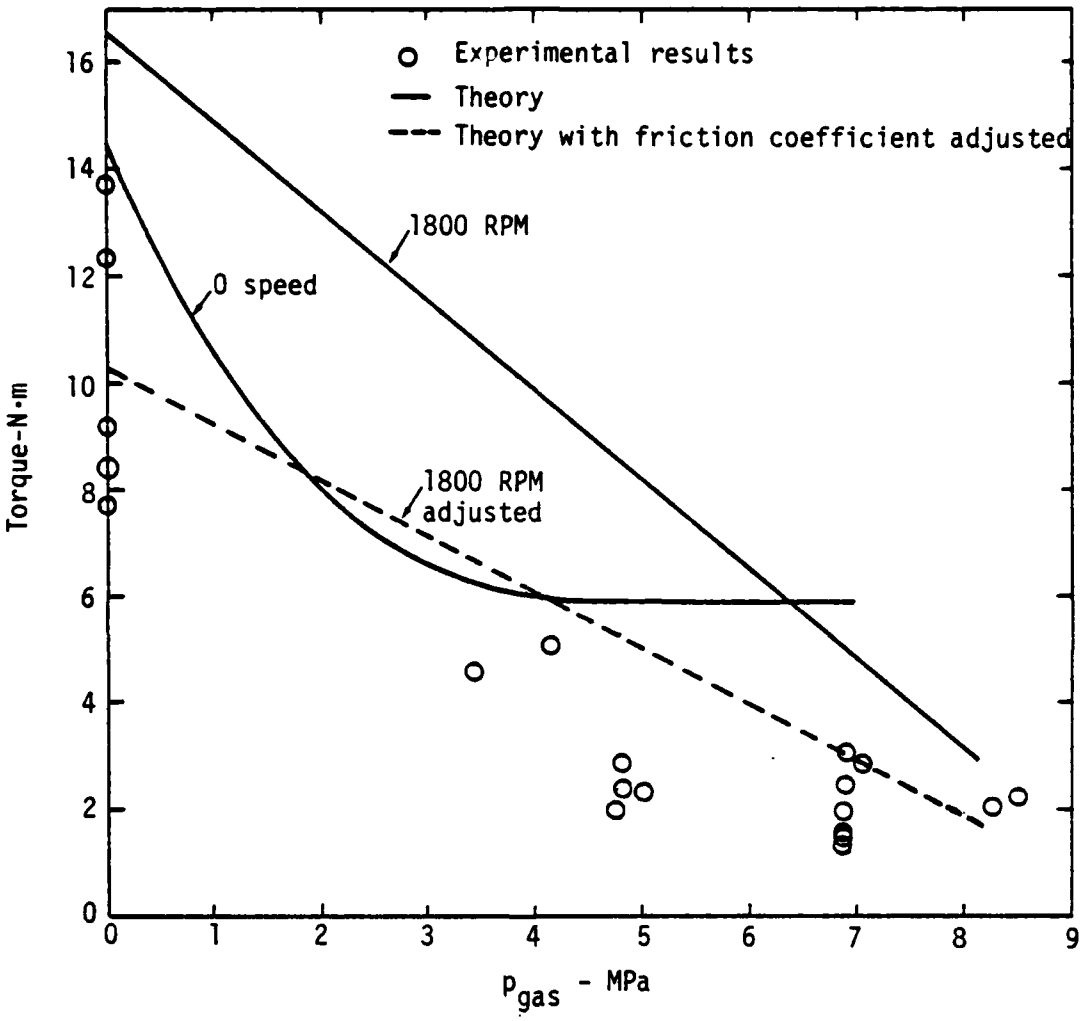

Figure 4-15. Wavy Seal Torque.

clearly follow the experimental trend, and considering the scatter in the leakage results, can be considered to give adequate agreement. The zero speed theoretical result clearly overpredicts leakage. This points out that hydrodynamic effects are significant, even though the seal does not operate in a classically hydrodynamic manner. The added deflection components and load support provided by the effect of hydrodynamic pressure buildup and cavitation clearly alter the seal's behavior relative to the static case. Leakage is smaller in the dynamic case because the net waviness is in fact smaller than in the hydrostatic case.

Now considering Figure 4-15, the 1800 RPM theoretical results clearly predict the trend in torque, that of a gradually decreasing torque with increasing pressure. The static results do not predict this trend as mentioned previously. Since the theoretical prediction of torque requires that the coefficient of friction between carbon and W-C be assumed, and the value assumed in the calculation was not actually measured (since it varies widely depending on conditions), the torque prediction based on a lower coefficient of friction (0.06) is also shown. This theoretical result intersects the experimental results.

Thus, so far, prediction of both leakage and torque by the theoretical model appears to be reasonable and suggests that the model may be satisfactory. However, further verification is desirable and the wear profiles are considered next.

Wear Profiles

Using the test results for 100 h wear tests at 3.45 MPa water pressure and 6.9 MPa gas pressure tabulated in Tables 2-2 and 2-3, average wear slopes were obtained from the surface traces shown in Figure 2-14. These are tabulated in Table 4-5. Based on the theoretical wear profile for 100 percent wear, the theoretical slopes were computed and are also shown in Table 4-5. The comparison for the outside slope is quite good. The inside slope does not compare as well, however, these slopes are rough estimates and good agreement would not be expected.

Perhaps more important than the values of the slopes is the fact that the shape of the theoretical wear surface shown in Figure 4-16 does

Table 4-5

Wear Slope Comparison

p_{gas} = 6.9 MPa p_{H_2O} = 3.45 MPa 1800 RPM

100 h

Test No.	L.H Outside	L.H Inside	R.H Inside	R.H Outside
21	$710^{*} \times 10^{-6}$	390×10^{-6}	400×10^{-6}	875×10^{-6}
34	670×10^{-6}	670×10^{-6}	860×10^{-6}	500×10^{-6}
39	1200×10^{-6}	1300×10^{-6}	--	600×10^{-6}

Slope	Experimental	Theory (1800 RPM case)
Average of Outside Slopes	760×10^{-6}	680×10^{-6}
Average of Inside Slopes	730×10^{-6}	430×10^{-6}

*Data taken from wear profiles in figure 2-14.

match the general shape of the wear profiles shown in Figure 2-14. It is clear that the double-sided touching observable in Figure 2-14 is predicted by the theory in Figure 4-16. Given this theoretical wear shape, it is also probable in Figure 2-14 that in tests 34 and 39, the 100 percent wear condition was not achieved (see also wear test results and compare between tests 21, 34, and 39).

Figure 4-16 illustrates one final limitation of the static analysis. At 100 percent wear, the wear profile is quite different from what is observed. At 50 percent wear however, the profile is similar. However, it is clear that the 1800 RPM case predicts the shape better than the static result.

Speed Effects

Table 4-6 shows the theoretical prediction for 100 percent wear at various speeds. The unexpected result shown here is that torque increases with speed even though it is known that hydrodynamic effects are present. The reason for this is that the lubrication behavior is interactive with deflection. As speed changes the pressure distribution changes and changes the deflection. Given the sensitivity of performance to the deflection or net waviness and tilt described previously, it is quite reasonable to assume that as speed increases for this particular seal, the net waviness and tilt are altered to a less favorable configuration for load support than at the lower speeds. Therefore, what initially appears to be a surprising and contradictory trend is quite explainable in the context of the total interactive mechanism of the seal.

Theoretical seal leakage and torque are compared to experimental results in Table 4-7. The experimental torque shows the same trend as the theoretical torque, an increase with speed beyond a certain speed; agreement for leakage is not good. It is assumed that this poor agreement stems from the fact that the speed tests were short term tests and the seal faces did not approach 100 percent wear.

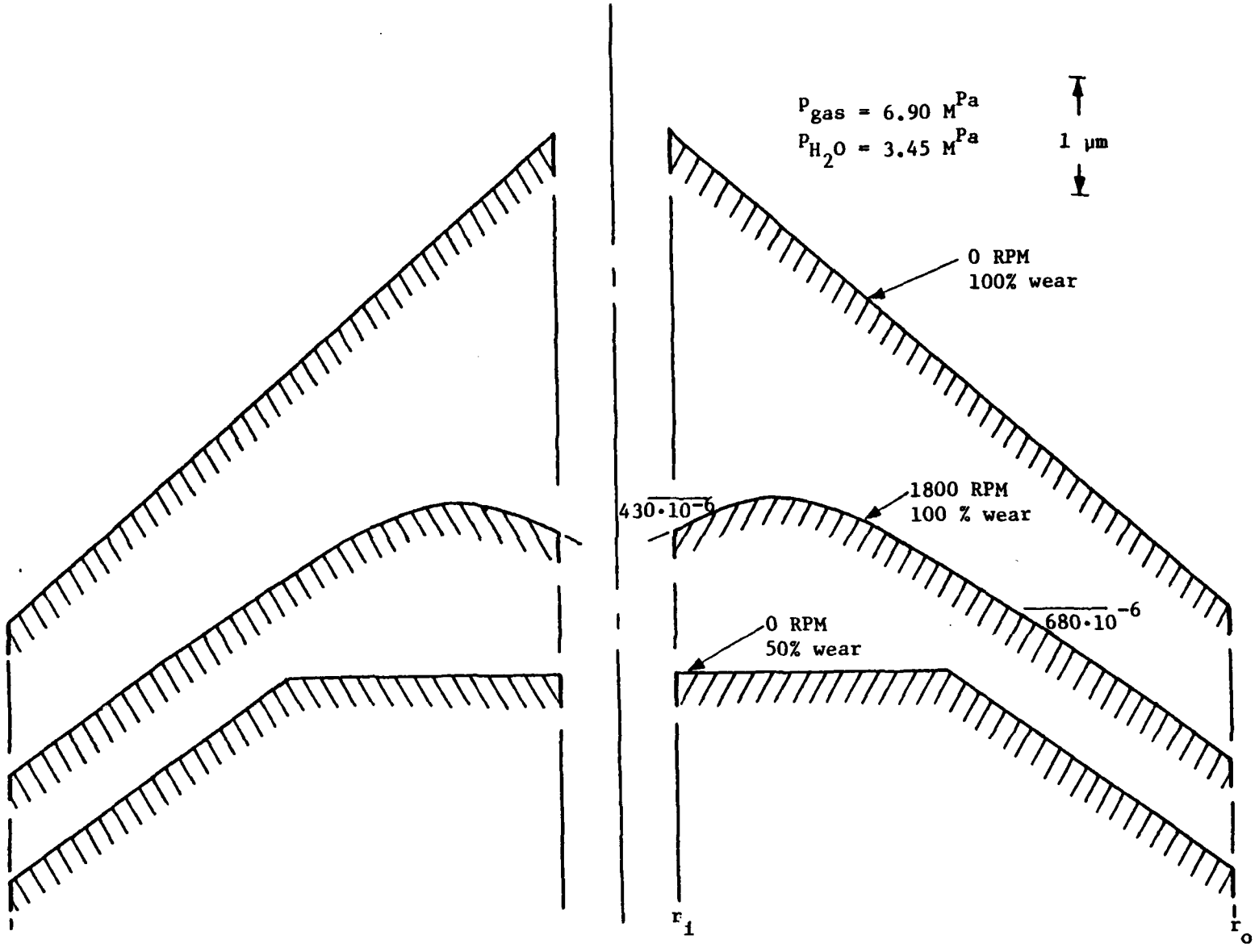

Figure 4-16. Theoretical Carbon Face Wear Profiles. –

Table 4-6

Computed Results - Speed Effect
p_{H_2O} = 3.45 MPa, p_{gas} = 6.90 MPa, 100% Wear

RPM	$\bar{h}_{pa}$	$\bar{h}_{pa}$ (calc)	$\bar{h}_{pb}$	$\bar{h}_{pb}$ (calc)	$\bar{h}_{a_{net}}$	$\bar{h}_{b_{net}}$	$\phi_{a_{net}}$ x10^6	$\phi_{b_{net}}$ x10^6	$\bar{h}_{ma}$	$\bar{h}_{mb}$	μ	T_q N-m	Q mℓ/min	%	p_{gas} corrected MPa	$\bar{h}_o$
0	-6.21	-6.21	0	0	8.82	0	887	0	1.25	0	.022	6.08	15.4	78.3	6.32	.57
900	-7.74	-7.58	-1.78	-1.75	7.29	-1.78	819	-79	1.10	0.17	.0109	3.07	10.4	90.2	6.39	.670
1800	-9.88	-9.98	-1.71	-1.59	5.15	-1.71	724	-76	1.04	0.05	.0161	4.54	4.41	86.5	6.42	.649
2700	-11.01	-11.00	-1.20	-1.21	4.02	-1.20	673	-53	.91	-0.26	.0216	6.07	2.61	83.0	6.52	.639
3600	-11.47	-11.54	-1.02	-0.99	3.56	-1.02	650	-45	0.84	-0.49	.0234	6.60	2.82	83.7	6.52	.644

Table 4-7

Speed Effect
Comparison of Experimental and Theoretical Results
P_{H_2O} = 3.45 MPa, P_{gas} = 6.90 MPa, 100% Wear

	Experimental		Theoretical	
Speed	Tq* N·m	Q* ml/min	Tq N·m	Q ml/min
900	1.8	0.2	3.1	10.4
1800	1.5	1.9	4.5	4.4
2700	3.2	4.5	6.1	2.6
3600	5.0	1.8	6.6	2.8

*Average of values in Table 2-6

Chapter 5

Summary, Conclusions, and Recommendations

In this chapter both specific and general conclusions are drawn.

Experimental Results

1) Test Apparatus - The test apparatus described with the waviness mechanism does provide the capability of measuring the effects of waviness on seal performance. No major operational limitations have been found. While the waviness device works satisfactorily on this experimental apparatus, there is wear on the waviness O-rings which would limit life on commercial applications. Other means of applying waviness must be developed in order to utilize the concept commercially. One aspect that does need improvment is finding the zero torque level. An improvement would incorporate a means of pulling the seal faces apart after the vessel was sealed.

2) Leakage - The use of the leakage measuring device described greatly improves the quality of the leakage data. It does provide leakage measurements over a very wide range of leakage.

3) Computer - The computer data acquisition system greatly improves the quality of data which can be collected and stored for later analysis. The computer also provides the ability to both control the test apparatus and monitor performance from a safety standpoint.

4) Flat Face Results - Torque is high compared to the wavy seal and fluctuates with time. Leakage is zero. Torque does show an initial increase with time indicating that thermal coning causes a converging radial taper which wears off.

5) Wavy Seal Results - Torque level is about one-fifth of that for a flat faced seal. Leakage increases with increasing waviness. Torque level is quite steady except for a pulsing corresponding to the superposition of the third and second harmonic waves.

6) Wear - Wear rates are from four to forty times lower for the wavy seal compared to the flat faced seal. A better method of measuring wear is needed to obtain more consistent results.

7) Radial Taper - A convergent radial taper reduces friction torque as expected. Results show that the radial taper wears away with time as would be expected [8].

8) Sealed Pressure - Tests show that the waviness imposed decreases with increasing sealed pressure. That is, the seal waviness flattens out with increased load.

9) Speed - For the wavy seal torque increases with increasing speed. The reason for this behavior appears to be that the seal deflection changes to a less favorable configuration as the hydrodynamic effects become more significant. These tests need to be repeated to make certain the seal is worn in at each operating condition.

10) Proximity Probe - Tests show that it is possible to measure changes in carbon face displacement relative to the tungsten carbide.

11) Wear Profile - The wear profile on the wavy seal shows that the seal faces tilt as well as wave. This requires a more comprehensive theory to properly analyze behavior than presented previously. The wear profiles for flat face tests clearly show evidence of thermal coning as expected.

12) Surface Roughness - So far, no relationships between seal performance and surface roughness has been found. However, tests where surface roughness has been deliberately altered have not yet been run.

Thermoelastic Instability

1) The model developed shows that ring deflections have a predominant effect over semiinfinite plate deflection at low n and must be considered as a part of a model to describe thermoelastic instability in seal rings.

2) The effect of thermal contact resistance between the faces on critical speed is large. However, the model for heat transfer between the faces used herein requires further investigation. For example, it

was assumed that all heat is generated at the middle of the interface. Also, the effect of tangential mass transfer of the sealed fluid might be significant.

3) The effect of convection losses on ϕ_c is also large. This effect requires further evaluation. Preliminary results suggest that $\phi_c \to \infty$ even with H_∞ small.

4) Although some of the critical speeds and number of waves predicted agree with the experimental observations reported, in view of 2) and 3) above this agreement should be regarded as coincidence. However, the agreement does encourage the refinement of the model.

5) The combined stability curves of Figure 3-6 are only to be considered as first approximations. The curves are based on the sum of two limiting cases. Further refinement will require that elastic and thermal deflection terms be computed using finite element numerical techniques. It is thought that such a refinement would result in a more accurate stability curve, particularly for the nose portion.

6) At this point in the development of thermoelastic theory for rings there is a definite need for further experimental results to determine if the basic shape of the stability curve of Figure 3-6 is correct.

Wavy Seal Analysis

1) Reynolds Equation for Rough Surfaces - Since there is still controvery over how to model the effect of roughness on the Reynolds equation, certain simplifying assumptions were made herein to avoid the problems associated with selecting one model over another model.

2) Waviness Model - A new seal waviness lubrication model was developed. The fact that there is a tilt in addition to the wave necessitated this model. This model is more general but not as accurate because the precise cavity boundary conditions could not be used in conjunction with this more general case. The new model accounts for alteration of the face shape brought about by tilting of the faces and wear.

3) Film Thickness Shape - For the more general case of waviness combined with tilt, it is shown that the film thickness shape becomes complex. Around the circumference of the seal there are in general regions where the faces are radially parallel, converging, and diverging.

4) General Solution - Using the model, a family of solutions was made for various combinations of waviness and tilt. It was found in general that torque and leakage are lowest when waviness and tilt are in phase. The combination of waviness and tilt provides lower torque and leakage than if the faces are simply wavy. This occurs because a favorable hydrostatic pressure distribution results.

5) Optimum Conditions - When tilt is such that seal face contact goes between the extremes of contact at the inside radius in conjunction with a converging taper to flat faced contact, an optimum condition giving minimum torque results. Both hydrodynamic and hydrostatic pressure distributions become favorable to provide maximum load support. Leakage is quite small because there exists a continuous ring of contact around the seal.

6) Ring Deflections - It is shown that the predominant deflection in the seal ring is caused by waviness gas pressure and pressure on the face. Deflection equations are developed. There are twelve significant components of deflection, six sine and six cosine components. Of the six, there is waviness due to gas pressure, moment of the face pressure, and the face pressure itself. Each of these forces also produces corresponding tilt terms.

7) Nonparallel Faces - The tilt term and waviness term are not in general proportional. This means that even though waviness may be completely flattened, tilt will not be flattened. The implications of this is that in general the wavy seal will operate with a large component of tilt in conjunction with waviness.

8) Test Seal Solution - The solution for the test seal requires the simultaneous solution for two deflection terms. This presents some numerical difficulty but a method for doing this was found so

that the performance of the actual seal could be predicted.

9) Surface Roughness - Theoretical results show that surface roughness has a large effect on seal torque and leakage. It is shown how the effective surface roughness is much lower than the measured surface roughness because of the nature of the surface. It is proposed that further theoretical work be done to model the surface roughness effects for the actual surface so that the assumptions made can be supported or rejected.

10) Comparison of Theory and Experiment - Wavy Seals

a) Deflection - Calculated deflection was compared to deflection measured using a proximity probe. Agreement was quite good thus validating the deflection theory.

b) Static Results - Theoretical results based on a static analysis (0 RPM) do not compare well to experiment. This indicates that in spite of the large taper in the seal, hydrodynamic effects must still be significant. While the static analysis is much simpler to use, predictions are inadequate.

c) Dynamic Results - Using the model developed, a comparison of theoretical and experimental results show good agreement for leakage and a good prediction for the trend for torque.

d) Wear Profiles - The model predicts the shape of the wear profile observed.

e) Speed Effects - The model predicts the observed increase in torque with speed.

General

1) The comparison of theoretical to experimental results is generally quite good. While there are known areas where the theoretical model requires improvement, the agreement observed suggests the basis for the model is valid.

2) Hydrodynamic effects do occur in the wavy face seal. This conclusion is supported by the fact that only after hydrodynamic features were included in the model was agreement between theory and

experiment satisfactory.

4) Waviness reduces friction and wear in a face seal. This is now known experimentally as well as theoretically. Given the results herein, it is quite likely that water seals can be designed which have on the order of ten times the life of a comparable flat faced seal.

5) The moving waviness concept does distribute the wear and does preserve the wavy shape as predicted. The moving wave must be used to benefit from waviness in the long term.

6) The discovery of the optimum combinations of waviness and tilt points the way toward designing a moving waviness seal having even better performance (i.e., lower torque and leakage) than those tested herein.

References

1. Lebeck, A. O., Teale, J. L., and Pierce, R. E., "Hydrodynamic Lubrication with Wear and Asperity Contact in Mechanical Face Seals," Annual Report ME-86(78)ONR-414-1, prepared for the Office of Naval Research under Contract No. ONRN-00014-76-C-0071, Bureau of Engineering Research, The University of New Mexico, Albuquerque, New Mexico, January 1978.

2. Findlay, J. A., "Cavitation in Mechanical Face Seals," Transactions of the ASME, Journal of Lubrication Technology, April 1968, pp. 356-364.

3. Pape, J. G., "Fundamental Aspects of Radial Face Seals," Thesis WJHD-17, December 1969 (T. H. Delft, Netherlands), 172 pp.

4. Stanghan-Batch, B., and Iny, E. H., "A Hydrodynamic Theory of Radial Face Seals," Journal of Mechanical Engineering Science, Vol. 15, No. 1, 1973.

5. Lebeck, A. O., Teale, J. L., and Pierce, R. E., "Elastohydrodynamic Lubrication with Wear and Asperity Contact in Mechanical Face Seals," Annual Report ME-76(77)ONR-414-1, ONR Contract N-00014-76-C-0071, Bureau of Engineering Research, The University of New Mexico, Albuquerque, New Mexico, January 1977.

6. Lebeck, A. O., Teale, J. L. and Pierce, R. E., "Hydrodynamic Lubrication with Wear and Asperity Contact in Mechanical Face Seals," Annual Report ME-95(79)ONR-414-1, prepared for the Office of Naval Research under Contract No. ONR-N-00014-76-C-0071, Bureau of Engineering Research, The University of New Mexico, Albuquerque, New Mexico, January 1979.

7. Teale, J. L. and Lebeck, A. O., "An Evaluation of the Average Flow Model [1] for Surface Roughness Effects in Lubrication," ASME Paper 79-Lub-37, presented at the 1979 ASME-ASLE Lubrication Conference, Dayton, Ohio, October 16-18, 1979.

8. Lebeck, A. O., "A Mixed Friction Hydrostatic Face Seal Model with Thermal Rotation and Wear," presented at the 1979 ASLE Annual Meeting, St. Louis, May 1979, ASLE Paper 79-AM-4C-3. To be published in the ASLE Transactions.

9. Burton, R. A., Nerliker, V., and Kilaparti, R., "Thermoelastic Instability in a Seal Like Configuration," Annual Report N00014-67-A-0356-0022 for the Office of Naval Research, Department of Mechanical Engineering, Technological Institute, Northwestern University, September 1, 1973.

10. Dow, T. A. and Burton, R. A., "Thermoelastic Instabilities of Sliding Contact in the Absence of Wear," Wear, Vol. 19, No. 3, March 1972, p. 315.

11. Heckman, S. R. and Burton, R. A., "Effects of Shear and Wear on Instabilities Caused by Frictional Heating in a Seal Like Configuration," ASLE Preprint No. 75-LC-1B-2.

12. Netzel, J., Observations reported at the 1978 NASA Lewis Workshop on Mechanical Seals.

13. Lebeck, A. O., "Theory of Thermoelastic Instability of Rotating Rings in Sliding Contact with Wear," Journal of Lubrication Technology, April 1976.

14. Lebeck, A. O., "Mechanical Loading--A Primary Source of Waviness in Mechanical Face Seals," ASLE Transactions, Vol. 20, No. 3, pp. 195-208.

15. Fenech, H. and Rohsenow, W. M., "Prediction of Thermal Conductance of Metallic Surfaces in Contact," Journal of Heat Transfer, February 1963, pp. 15-24.

16. Lebeck, A. O., "Hydrodynamic Lubrication in Wavy Contacting Face Seals--A Two-dimensional Model," accepted for publication in the ASME Journal of Lubrication Technology, to be presented at the ASME-ASLE Lubrication Conference, San Francisco, August 1980.

17. Lebeck, A. O., Teale, J. L. and Pierce, R. E., "Hydrodynamic Lubrication and Wear in Wavy Contacting Face Seals," presented at the 1977 ASME ASLE Lubrication Conference, Kansas City, October 3-5, 1977, Journal of Lubrication Technology, Vol. 100, January 1978, pp. 81-91.

18. Patir, N. and Cheng, H. S., "An Average Flow Model for Determining Effects of Three-Dimensional Roughness on Partial Hydrodynamic Lubrication," Journal of Lubrication Technology, Trans. ASME, Series F, Vol. 100, January 1978, p. 2.

19. Tonder, K., "Simulation of the Lubrication of Isotropically Rough Surfaces," ASLE Preprint No. 79-AM-6D-4, presented at the 34th Annual Meeting in St. Louis, Missouri, April 30-May 3, 1979.

20. Christensen, H., "Some Aspects of the Functional Influence of Surface Roughness in Lubrication," Wear, 17 (1971), pp. 149-162.

21. Tonder, K., "Lubrication of Surfaces Having Area Distributed Isotropic Roughness," Journal of Lubrication Technology, July 1977, pp. 323-330.

22. Snapp, R. B. and Sasdelli, K. R., "Performance Characteristics of High Pressure Face Seal with Radially Converging Interface Shapes," Paper E4, 6th International Conference on Fluid Sealing, February 27-March 2, 1973, Munich.

23. Lebeck, A. O., "Causes and Effects of Waviness in Mechanical Face Seals," Final Report, Technical Report ME-68(76)NSF-271-1, The University of New Mexico, College of Engineering, Bureau of Engineering Research, Albuquerque, New Mexico, January 1976.

Appendix A

Computer Control and Data Acquisition Program

```
5     ! CONTROL PROGRAM
10    !
15    !
20    STANDARD
25    OPTION BASE 1
30    COM Zero,Inlbmv,Relay,Flag$,Ph2o,Rpm,Tqmax,Tomax,Tfmax,Thmax,Twmax
35    COM T,Timeref,SHORT Thout,Toout,Twout,REAL Lkold,Tlkold,Tlk(200),Thref,Nlk
40    COM I60,I60on,I12,Ngo,SHORT Time,Tfout,Tqout,Lkout,Z11,Z12,Z13,Z14,Vibset,N
vib,Tvib,Days(12)
45    SHORT Timeover,Tqover,Tmpover,Lkover,Filedum
50    DIM Timeover(300),Tqover(300),Tmpover(300),Lkover(300),Da(10)
55    DIM A$(40)
60    READ A$(*)
65    DATA F1,F2,F3,F4,F5,F6,F7,F8,F9,F10
70    DATA F11,F12,F13,F14,F15,F16,F17,F18,F19,F20
75    DATA F21,F22,F23,F24,F25,F26,F27,F28,F29,F30
80    DATA F31,F32,F33,F34,F35,F36,F37,F38,F39,F40
85    READ Days(*)
90    DATA 0,31,60,91,121,152,182,213,244,274,305,335
95     ON ERROR GOSUB 240
100   ! Relay=DECIMAL(20000)
105   OUTPUT 5 WHS USING "#,W";-4000,Relay
110   CONTROL MASK 5;128
115   PLOTTER IS 7,5,"9872A"
120   LIMIT 0,270,0,190
125   ON KEY #0,14 GOSUB I0
130   ON KEY #1,10 GOSUB I1
135   ON KEY #2,10 GOSUB I2
140   ON KEY #3,10 GOSUB I3
145   ON KEY #4,10 GOSUB I4
150   ON KEY #5,10 GOSUB I5
155   ON KEY #6,10 GOSUB I6
160   Ngo=7
165   GOTO 250
170  I1:  Ngo=1   ! RUN
175   RETURN
180  I2:  Ngo=2    ! START
185   RETURN
190  I3:   Ngo=3   ! AXES
195   RETURN
200  I4:  Ngo=4    ! REZERO
205   RETURN
210  I5:  Ngo=5    !CONRUN
215   RETURN
220  I6:  Ngo=6    ! TEST END
225   RETURN
230  I0:  Ngo=7    ! IDLE
235   RETURN
240   PRINT ERRM$
245   RETURN
250   INPUT "Test no?",Testno
255   INPUT "Typetest?",Typetest$
260   INPUT "Date?",Date$
265   INPUT "Ph2o?",Ph2o
270   INPUT "Pgas?",Pgas
275   INPUT "Rpm?",Rpm
280   INPUT "Twmax?",Twmax
285   INPUT "Tqmax?",Tqmax
290   INPUT "Toilmax?",Tomax
295   INPUT "Tfacemax?",Tfmax
```

```
300  INPUT "Thousingmax?",Thmax
305  INPUT "First file for test or current file for continuation?",Nfile
310  ASSIGN A$(Nfile) TO #1
315  GOTO 340
320 File:  Nfile=Nfile+1
325  ASSIGN A$(Nfile) TO #1
330  PRINT "FILE #=";Nfile
335  RETURN
340  INPUT "IS THIS A CONTINUATION?",Y$
345  IF Y$="Y" THEN 360
350  St=0
355  GOTO 475
360  INPUT "REFERENCE TIME=?",St
365  PRINT "* CONTINUATION *"
370  PRINT "REFERENCE TIME=";St
375  INPUT "T1kold?",T1kold
380  INPUT "Lkold?",Lkold
385  Type=TYP(-1)
390  IF Type=2 THEN 465
395  IF (Type=1) OR (Type=6) THEN 405
400  IF (Type=3) OR (Type=4) OR (Type=7) THEN 435
405  READ #1;Value
410  FOR I=1 TO 8
415  Da(I)=Da(I+1)
420  NEXT I
425  Da(9)=Value
430  GOTO 385
435  Na=6
440  IF Da(5)=-2000 THEN Na=1
445  Timeold=Da(Na)
450  Tmpold=Da(Na+1)
455  Tqold=Da(Na+2)
460  GOTO 480
465  READ #1;Value$
470  GOTO 385
475  PRINT #1;Testno,Date$,Typetest$,Ph2o,Pgas,Rpm,Twmax,Tqmax,Tomax,Tfmax,Thmax
,Nfile
480  PRINT "TEST NO =";Testno
485  PRINT "DATE =";Date$
490  PRINT "TYPETEST =";Typetest$
495  PRINT "Ph2o  =";Ph2o
500  PRINT "Pgas  =";Pgas
505  PRINT "Rpm   =";Rpm
510  PRINT "Twmax =";Twmax
515  PRINT "Tqmax =";Tqmax
520  PRINT "Tomax =";Tomax
525  PRINT "Tfmax =";Tfmax
530  PRINT "Thmax =";Thmax
535  PRINT "FIRST FILE =";Nfile
540  FIXED 2
545  ON END #1 GOSUB File
550 INPUT "DO YOU WANT TO CALIBRATE TORQUE?",Y$
555  IF Y$="Y" THEN 2c
560  INPUT "WHAT IS CALIBRATION CONSTANT IN IN-LB/MV",Inlbmv
565  GOTO 2d
570 2c:  CALL Calibrate
575 2d:  PRINT "IN-LB/MV=";Inlbmv
580 INPUT "DO YOU WANT TO FIND ZERO?",Y$
585  IF Y$="N" THEN 2b
590  CALL Zerosub(Thref)
595  GOTO 2a
600 2b: INPUT "WHAT IS ZERO TORQUE IN IN-LB?",Zero
605  INPUT "WHAT IS REF TEMP?",Thref
610 2a: PRINT "Zero  =";Zero
615  PRINT "Thref =";Thref
620  INPUT "CHECK ZERO AGAIN ?",Y$
```

```
625  IF Y$="Y" THEN 590
630  STANDARD
635  INPUT "DO YOU WANT TO DRAW COORDS?",Z$
640  IF Z$="N" THEN Ca
645  Flag$="Idle"
650  CALL Coord(Timemin,Timemax,Trqmin,Trqmax,Lkmax,Tmpmax,Tmpmin)
655  GOTO Cb
660 Ca:  INPUT "Timemin?",Timemin
665  INPUT "Timemax?",Timemax
670  INPUT "Trqmin?",Trqmin
675  INPUT "Trqmax?",Trqmax
680  INPUT "Lkmax?",Lkmax
685  INPUT "Tmpmax?",Tmpmax
690  INPUT "Tmpmin?",Tmpmin
695 Cb:  A=10+120/26*2
700  LOCATE A,130,10,97
705  ON INT #5,14 CALL I6940
710  !
715  !
720 Idle: !
725  D=FNRoff(1)
730  D=FNRoff(2)
735  D=FNRoff(4)
740  Flag$="Idle"
745  !
750 Idleloop:  DISP "CONTROL PROGRAM READY"
755  ON Ngo GOTO Run,Start,Axes,Rezero,Conrun,Testend,Idleloop
760  !
765  !
770 Run:  !
775  Vibset=0
780  Ifirst=0
785  T=0
790  I600=0
795  I60=0
800  I60on=0
805  I12=0
810  Nlk=0
815  IF St<>0 THEN 875
820  CALL Time(Thrs,Time$)
825  Timeref=Thrs
830  PRINT "TEST START TIME=";Time$
835  PRINT "REFERENCE TIME=";Timeref
840  Tlkold=Timemin
845  Tlkplot=Timemin
850  Timeold=Timemin
855  Lkold=0
860  Tqold=0
865  Tmpold=Tmpmin
870  GOTO 890
875  Timeref=St
880  CALL Time(Thrs,Time$)
885  Tlkold=Thrs-Timeref
890  Ndata=0
895  Ioplot=0
900  Ilkrem=0
905  D=FNRon(4)
910  Flag$="Run"
915  Iloop=1
920  Iover=0
925  GOTO Runloop
930  !
935  !
940 Start:  !
945  Vibset=0
```

```
950  D=FNRoff(4)
955  D=FNRon(1)
960  !
965  !
970 Startloop:   Flag$="Start"
975  CALL Tint
980  DISP "Startloop"
985   ON Ngo GOTO Run,Startloop,Axes,Rezero,Conrun,Testend,Idle,Replot
990   !
995   !
1000 Runloop:  ! INFINITE LOOP
1005 DISP "Runloop"
1010 CALL Tint
1015 IF I60<>1 THEN Rloopend
1020 IF I60on<>1 THEN Rloopend
1025 IF Ifirst=0 THEN 1390
1030 ON Iloop GOTO L1,L2,L3,L4,L5,L6,L7,L8
1035 !
1040 L1: PRINT #1;Time,Tfout,Tqout,Lkout
1045 Ndata=Ndata+1
1050 Iloop=Iloop+1
1055 GOTO Rloop
1060 !
1065 L2: SCALE Timemin,Timemax,Trqmin,Trqmax
1070 MOVE Timeold,Tqold
1075 Iloop=Iloop+1
1080 GOTO Rloop
1085 !
1090 L3: IF Time>Timemax THEN M1
1095 IF Tqout>Trqmax THEN Tqout=Trqmax
1100 Hp=Tqout*2*PI*(1/12)*Rpm/33000
1105 IF Hp<5.5 THEN 1125
1110 PRINT "SHUTDOWN - HORSEPOWER IS";Hp
1115 PRINT "TIME=";Time$,"Lkold=";Lkold,"Tlkold=";Tlkold
1120 Ngo=7
1125 IF Tqout<Trqmin THEN Tqout=Trqmin
1130 PLOT Time,Tqout,-1
1135 PENUP
1140 Iloop=Iloop+1
1145 GOTO Rloop
1150 !
1155 L4: SCALE Timemin,Timemax,Tmpmin,Tmpmax
1160 MOVE Timeold,Tmpold
1165 Iloop=Iloop+1
1170 GOTO Rloop
1175 !
1180 L5: IF Tfout>Tmpmax THEN Tfout=Tmpmax
1185 IF Tfout<Tmpmin THEN Tfout=Tmpmin
1190 PLOT Time,Tfout,-1
1195 PENUP
1200 MOVE Timeold,Twold
1205 PLOT Time,Twout,-1
1210 PENUP
1215 Iloop=Iloop+1
1220 GOTO Rloop
1225 !
1230 M1: IF Iover>300 THEN GOTO 1260
1235 Iover=Iover+1
1240 Timeover(Iover)=Time
1245 Tqover(Iover)=Tqout
1250 Tmpover(Iover)=Tfout
1255 Lkover(Iover)=Lkout
1260 I60=0
1265 I600=I600+1
1270 Iloop=1
1275 GOTO Rloop
```

```
1280 !
1285 L6: Iloop=Iloop+1
1290 Noplot=0
1295 SCALE Timemin,Timemax,0,Lkmax
1300 IF T1kplot<Timemin THEN Noplot=1
1305 MOVE T1kplot,Lkold
1310 GOTO Rloop
1315 !
1320 L7: Iloop=Iloop+1
1325 IF Lkout>Lkmax THEN Lkout=Lkmax
1330 IF Lkout=-1000 THEN M2
1335 IF Noplot=1 THEN GOTO 1350
1340 PLOT Time,Lkout,-1
1345 PENUP
1350 T1kplot=Time
1355 Lkold=Lkout
1360 !
1365 M2:MOVE Timemax,Lkmax
1370 Timeold=Time
1375 Tqold=Tqout
1380 Tmpold=Tfout
1385 I600=I600+1
1390 I60=0
1395 IF Ifirst=0 THEN Ifirst=1
1400 Iloop=1
1405 GOTO Rloop
1410 !
1415 L8: !
1420 Filedum=-2000
1425 PRINT #1;Filedum,Time,Twout,Tooout,Thout
1430 I60=0
1435 Iloop=1
1440 GOTO Rloop
1445 !
1450 Rloop: I60on=0
1455 IF I600=10 THEN I60=1
1460 IF I600=10 THEN Iloop=8
1465 IF I600=10 THEN I600=0
1470 !
1475 Rloopend: !
1480 IF I60=1 THEN 1495
1485 IF I60on=0 THEN 1495
1490 IF Ioplot=1 THEN Oplot
1495 ON Ngo GOTO Runloop,Start,Axes,Rezero,Conrun,Testend,Idle
1500 !
1505 !
1510 Axes: Flag$="Start"
1515 D=FNRoff(4)
1520 INPUT "ARE YOU READY TO DRAW COORD.?",Y
1525 CALL Coord(Timemin,Timemax,Trqmin,Trqmax,Lkmax,Tmpmax,Tmpmin)
1530 Ngo=2
1535 GOTO Start
1540 !
1545 !
1550 Conrun:T=0
1555 I600=0
1560 I60=0
1565 I60on=0
1570 I12=0
1575 N1k=0
1580 Ifirst=0
1585 Flag$="Run"
1590 Iloop=1
1595 CALL Time(Thrs,Time$)
1600 T1kold=Thrs-Timeref
1605 D=FNRon(4)
```

```
1610 IF Iover<>0 THEN P1
1615 Ngo=1
1620 Ioplot=0
1625 GOTO Runloop
1630 P1: ! ASSUMES TIMEMMIN HAS BEEN SHIFTED SO DATA FITS
1635 Imax=Iover
1640 Iover=0
1645 Ioplot=1
1650 Ngo=1
1655 Iplot=1
1660 Igo=1
1665 M=1
1670 Timeold=Timeover(Imax)
1675 Tqold=Tqover(Imax)
1680 Tmpold=Tmpover(Imax)
1685 FOR I=Imax TO 1 STEP -1
1690 J=I
1695 IF Lkover(J)<>-1000 THEN M15
1700 NEXT I
1705 GOTO M16
1710 M15: Tlkplot=Timeover(J)
1715 Lkold=Lkover(J)
1720 M16: !
1725 GOTO Runloop
1730 Oplot: ON Igo GOTO S1,S2,S3
1735 S1: SCALE Timemin,Timemax,Trqmin,Trqmax
1740 IF Timeover(M)<Timemin THEN GOTO 1960
1745 !
1750  Tqdum=Tqover(M)
1755 IF Tqdum>Tqmax THEN Tqdum=Tqmax
1760 MOVE Timeover(M),Tqdum
1765     Tqdum=Tqover(M+1)
1770 IF Tqdum>Tqmax THEN Tqdum=Tqmax
1775 PLOT Timeover(M+1),Tqdum,-1
1780 PENUP
1785 Igo=Igo+1
1790 GOTO 1495
1795 S2: SCALE Timemin,Timemax,Tmpmin,Tmpmax
1800 Tmpdum=Tmpover(M)
1805 IF Tmpdum>Tmpmax THEN Tmpdum=Tmpmax
1810 IF Tmpdum<Tmpmin THEN Tmpdum=Tmpmin
1815 MOVE Timeover(M),Tmpdum
1820     Tmpdum=Tmpover(M+1)
1825 IF Tmpdum>Tmpmax THEN Tmpdum=Tmpmax
1830 IF Tmpdum<Tmpmin THEN Tmpdum=Tmpmin
1835 PLOT Timeover(M+1),Tmpdum,-1
1840 PENUP
1845 Igo=Igo+1
1850 GOTO 1495
1855 S3: IF Lkover(M)=-1000 THEN M6
1860 IF Iplot=0 THEN M5
1865 Atover=Timeover(M)
1870 Alkover=Lkover(M)
1875 Iplot=0
1880 !
1885 M5:Lkdum=Alkover
1890 IF Lkdum>Lkmax THEN Lkdum=Lkmax
1895 SCALE Timemin,Timemax,0,Lkmax
1900 MOVE Atover,Lkdum
1905 M6: !
1910     IF Lkover(M)=-1000 THEN M7
1915 Lkdum=Lkover(M)
1920 IF Lkdum>Lkmax THEN Lkdum=Lkmax
1925 PLOT Timeover(M),Lkdum,-1
1930 PENUP
1935 Atover=Timeover(M)
```

```
1940 Alkover=Lkover(M)
1945 M7: MOVE Timemax,Lkmax
1950      IF M+1=Imax THEN M9
1955 IF M=Imax THEN M8
1960 Iqo=1
1965 M=M+1
1970  GOTO 1495
1975 M9: Iqo=3
1980 M=M+1
1985 GOTO 1495
1990 M8: Ioplot=0
1995  GOTO 1495
2000  !
2005  !
2010 Testend: D=FNRoff(4)
2015 Iflag=0
2020 Jflag=0
2025 Kflag=0
2030 Lflag=0
2035 Nn=0
2040 Delt=0
2045 PRINT "LAST FILE FOR TEST =";Nfile
2050 PRINT "NO.OF DATA POINTS ON TAPE =";Ndata
2055 PRINT "T1kold=";T1kold,"Lkold=";Lkold
2060 PRINT "RELATIVE TEST END TIME =";Time
2065 CALL Time(Thrs,Time$)
2070 PRINT "TEST END TIME=",Time$
2075   INPUT "BEGIN SEARCH WITH FILE#=?",Nfile
2080   ASSIGN A$(Nfile) TO #1
2085   ON END #1 GOTO Filechan
2090   Idel=0
2095   IF Time<1 THEN INPUT "TEST END TIME=",Time
2100   INPUT "DELETE ANY DATA ?",Y$
2105   IF Y$="Y" THEN Set
2110   GOTO 2130
2115 Set:   INPUT "START TIME TO DELETE DATA=",Sd
2120   INPUT "END TIME TO DELETE DATA=",Ed
2125   Idel=1
2130   INPUT "PERIOD OF DATA AVERAGING=",Period
2135   PRINT "DATA AVG=";Period;"H"
2140   INPUT "READ TEST#,DATE,Ect. ?",Y$
2145   IF Y$="Y" THEN Read
2150   GOTO If5
2155 Read:   READ #1;A,B$,C$,D,E,F,G,H,J,K,L
2160 GOTO If5
2165 If1:   Iflag=1
2170 Lflag=1
2175 READ #1;A
2180 READ #1;B
2185 READ #1;C
2190 READ #1;D
2195 If5: Iflag=5
2200   READ #1;E
2205   IF E=-2000 THEN If1
2210 READ #1;F
2215 READ #1;G
2220 READ #1;H
2225 IF Time-E>Period THEN If5
2230 IF Idel=1 THEN Delete
2235 GOTO 2245
2240 Delete: IF (E>Sd) AND (E<Ed) THEN If5
2245 IF Jflag=0 THEN E0=E
2250 Jflag=1
2255 IF Lflag=1 THEN Delt=Delt+(F-B)
2260 IF Lflag=1 THEN Nn=Nn+1
2265 IF Lflag=1 THEN Lflag=0
```

```
2270 F1=F1+F
2275 G1=G1+G
2280 IF H<>-1000 THEN 2290
2285 GOTO 2335
2290 IF Kflag=0 THEN 2320
2295 H1=(H+H0)/2*(E-E1)
2300 Hsum=Hsum+H1
2305 H0=H
2310 E1=E
2315 GOTO 2335
2320 E1=E
2325 H0=H
2330 Kflag=1
2335 N=N+1
2340  IF Time-E<.1 THEN 2365
2345 GOTO If5
2350 Filechan: Nfile=Nfile+1
2355 ASSIGN A$(Nfile) TO #1
2360 GOTO If5
2365 FIXED 5
2370 PRINT "Tfavg=";F1/N
2375 PRINT "Tqavg=";G1/N
2380 Havg=Hsum/(E-E0)
2385 PRINT "Lkavg=";Havg
2390 PRINT "Delt T=";Delt/Nn
2395 FIXED 2
2400 IF Idel=1 THEN PRINT "DATA DELETED FROM";Sd;"TO";Ed;"H"
2405 INPUT "INITIAL ZERO VALUE=",Iz
2410 INPUT "INITIAL REF. TEMP. VALUE=",Irt
2415 INPUT "FINAL ZERO VALUE=",Fz
2420 INPUT "FINAL REF. TEMP. VALUE",Frt
2425 PRINT
2430 PRINT "INITIAL          ZERO=";Iz
2435 PRINT
2440 PRINT "INITIAL          REF. TEMP=";Irt
2445 PRINT
2450 PRINT "FINAL            ZERO=";Fz
2455 PRINT
2460 PRINT "FINAL            REF. TEMP.=";Frt
2465 Ct=G1/N-Fz+Iz-.109*(Frt-Irt)
2470 PRINT
2475 PRINT "CORRECTED        TORQUE=";Ct
2480 STANDARD
2485 Ngo=2
2490 GOTO Start
2495 !
2500 !
2505 Rezero: D=FNRoff(1)
2510 D=FNRoff(2)
2515 D=FNRoff(4)
2520 INPUT "ARE YOU READY TO RE-ZERO?",Y$
2525 CALL Zerosub(Thref)
2530 PRINT "Zero = ";Zero
2535 PRINT "Thref = ";Thref
2540 Ngo=7
2545 GOTO Idle
2550 !
2555 !
2560 END
2565 !
2570 !
2575 !
2580 !
2585 !
2590 !
2595 SUB Calibrate
```

```
2600 ON ERROR GOSUB 2610
2605 GOTO 2620
2610 PRINT ERRM$
2615 RETURN
2620 COM Zero,Inlbmv,Relay,Flag$,Ph2o,Rpm,Tqmax,Tomax,Tfmax,Thmax,Twmax
2625 FOR J=1 TO 10
2630 WAIT 50
2635 BEEP
2640 NEXT J
2645 DISP "SET TORQUE AT ZERO"
2650 WAIT 5000
2655 INPUT "READY?",Ready$
2660 Avg1=0
2665 FOR I=1 TO 50
2670 Avg1=Avg1+FNV(1)
2675 NEXT I
2680 FOR J=1 TO 10
2685 WAIT 50
2690 BEEP
2695 NEXT J
2700 DISP "APPLY 50 IN-LB"
2705 WAIT 5000
2710 INPUT "READY?",Ready$
2715 Avg2=0
2720 FOR I=1 TO 50
2725 Avg2=Avg2+FNV(1)
2730 NEXT I
2735 Inlbmv=50*50/(Avg2-Avg1)
2740 SUBEND
2745 !
2750 !
2755 DEF FNTq
2760 ON ERROR GOSUB 2770
2765 GOTO 2780
2770 PRINT ERRM$
2775 RETURN
2780 COM Zero,Inlbmv,Relay,Flag$,Ph2o,Rpm,Tqmax,Tomax,Tfmax,Thmax,Twmax
2785 V=FNV(1)*Inlbmv-Zero
2790 RETURN V
2795 FNEND
2800 !
2805 !
2810 SUB Zerosub(Thref)
2815 ON ERROR GOSUB 2825
2820 GOTO 2840
2825 PRINT ERRM$
2830 RETURN
2835 DIM Th(200),Tl(200)
2840 COM Zero,Inlbmv,Relay,Flag$,Ph2o,Rpm,Tqmax,Tomax,Tfmax,Thmax,Twmax
2845 INPUT "ARE YOU READY?",Ready$
2850 DISP "CRANK C.W. ON BEEP"
2855 WAIT 5000
2860 FOR J=1 TO 10
2865 WAIT 50
2870 BEEP
2875 NEXT J
2880 WAIT 2000
2885 FOR N=1 TO 200
2890 Th(N)=FNV(1)
2895 Thigh=Thigh+Th(N)
2900 NEXT N
2905 Thigh=Thigh/200
2910 FOR J=1 TO 10
2915 BEEP
2920 WAIT 50
2925 NEXT J
```

```
2930 DISP "STOP"
2935 WAIT 5000
2940 DISP "CRANK C.C.W. ON BEEP"
2945 R=FNTref
2950 Thref=FNTemp(4,R)
2955 WAIT 5000
2960 FOR J=1 TO 10
2965 WAIT 50
2970 BEEP
2975 NEXT J
2980 WAIT 2000
2985 FOR N=1 TO 200
2990 Tl(N)=FNV(1)
2995 Tlow=Tlow+Tl(N)
3000 NEXT N
3005 Tlow=Tlow/200
3010 FOR J=1 TO 10
3015 BEEP
3020 WAIT 50
3025 NEXT J
3030 DISP "STOP"
3035 WAIT 5000
3040 FOR N=1 TO 200
3045 Sl=Sl+(Tl(N)-Tlow)^2
3050 Sh=Sh+(Thigh-Th(N))^2
3055 NEXT N
3060 Zero=(Thigh+Tlow)/2*Inlbmv
3065 DISP "ZERO CALCULATED"
3070 Sl=(Sl/200)^.5
3075 Sh=(Sh/200)^.5
3080 PRINT "SDL=";Sl*Inlbmv,"SDH=";Sh*Inlbmv,"Avg.High=";Thigh*Inlbmv,"Avg.Low="
;Tlow*Inlbmv,"N=";N-1
3085 SUBEND
3090 !
3095 !
3100 DEF FNV(Nch)
3105 ON ERROR GOSUB 3115
3110 GOTO 3125
3115 PRINT ERRM$
3120 RETURN
3125 ! A=OCTAL(10010+Nch)
3130 OFF INT #5
3135 WRITE IO 5,5;32
3140 OUTPUT 5 WHS USING "#,W";-3984,A,-3920
3145 WRITE IO 5,4;4096
3150 READ IO 5,4;V
3155 WRITE IO 5,5;128
3160 ON INT #5,14 CALL I6940
3165 OUTPUT 5 WHS USING "#,W";-4064,32767
3170 OUTPUT 5 WHS USING "#,W";-3936,28672,-3792
3175 CARD ENABLE 5
3180 RETURN V*5E-3
3185 FNEND
3190 !
3195 !
3200 DEF FNRoff(N)
3205 ON ERROR GOSUB 3220
3210 COM Zero,Inlbmv,Relay,Flag$,Ph2o,Rpm,Tqmax,Tomax,Tfmax,Thmax,Twmax
3215 GOTO 3230
3220 PRINT ERRM$
3225 RETURN
3230 A=2^(N-1)
3235 Nml=N-1
3240 B=BIT(Relay,Nml)
3245 IF B=0 THEN GOTO 3300
3250 ! A=-OCTAL(A)+OCTAL(Relay)
```

```
3255 ! Relay=DECIMAL(A)
3260 OFF INT #5
3265 WRITE IO 5,5;32
3270 OUTPUT 5 WHS USING "#,W";-4000,Relay
3275 WRITE IO 5,5;128
3280 ON INT #5,14 CALL I6940
3285 OUTPUT 5 WHS USING "#,W";-4064,32767
3290 OUTPUT 5 WHS USING "#,W";-3936,28672,-3792
3295 CARD ENABLE 5
3300 RETURN A
3305 FNEND
3310 !
3315 !
3320 DEF FNRon(N)
3325 ON ERROR GOSUB 3340
3330 COM Zero,Inlbmv,Relay,Flag$,Ph2o,Rpm,Tqmax,Tomax,Tfmax,Thmax,Twmax
3335 GOTO 3350
3340 PRINT ERRM$
3345 RETURN
3350 A=2^(N-1)
3355 Nm1=N-1
3360 B=BIT(Relay,Nm1)
3365 IF B=1 THEN GOTO 3420
3370 ! A=OCTAL(A)+OCTAL(Relay)
3375 ! Relay=DECIMAL(A)
3380 OFF INT #5
3385 WRITE IO 5,5;32
3390 OUTPUT 5 WHS USING "#,W";-4000,Relay
3395 WRITE IO 5,5;128
3400 ON INT #5,14 CALL I6940
3405 OUTPUT 5 WHS USING "#,W";-4064,32767
3410 OUTPUT 5 WHS USING "#,W";-3936,28672,-3792
3415 CARD ENABLE 5
3420 RETURN A
3425 FNEND
3430 !
3435 !
3440 !
3445 !
3450 SUB Tint
3455 ON ERROR GOSUB 3485
3460 OPTION BASE 1
3465 COM Zero,Inlbmv,Relay,Flag$,Ph2o,Rpm,Tqmax,Tomax,Tfmax,Thmax,Twmax
3470 COM T,Timeref,SHORT Thout,Tcout,Twout,REAL Lkold,Tlkold,Tlk(200),Thref,Nlk
3475 COM I60,I60on,I12,Ngo,SHORT Time,Tfout,Tqout,Lkout,Tf,Tq,Th,Z14,Vibset,Nvib
,Tvib,Days(12)
3480 GOTO 3510
3485 PRINT ERRM$
3490 IF ERRN<>160 THEN 3505
3495 Er=Er+1
3500 IF Er=2 THEN 4010
3505 RETURN
3510 IF Flag$="Idle" THEN GOTO Exit
3515 P=fNV(2)*66.66666667
3520 IF P<Ph2o THEN Pulse
3525 GOTO Check
3530 !
3535 Pulse: D=FNRon(7)
3540 WAIT 50
3545 D=FNRoff(7)
3550 Check: IF Flag$="Start" THEN Checkh
3555 Checkl: IF P<.7*Ph2o THEN Down
3560 Checkh: IF P>1.2*Ph2o THEN Down
3565 GOTO Ok
3570 !
3575 Down: PRINT "SHUT DOWN PRESSURE IS ";P
```

```
3580 CALL Time(Thrs,Time$)
3585 PRINT "TIME=";Time$,"Lkold=";Lkold,"Tlkold=";Tlkold
3590 Ngo=7
3595 GOTO Exit
3600 Ok: IF Flag$="Start" THEN Exit
3605 T=T+1
3610 I60on=1
3615 IF T=1 THEN Tme
3620 IF T=2 THEN Rpmm
3625 IF T=3 THEN Lk
3630 IF T=4 THEN Oilwater
3635 IF T=5 THEN Ptgtp
3640 IF T=6 THEN I60=1
3645 IF T=10 THEN Ptgtp
3650 IF T=15 THEN Ptgtp
3655 IF T=20 THEN Ptgtp
3660 IF T=25 THEN Ptgtp
3665 IF T=30 THEN Ptgtp
3670 IF T=35 THEN Ptgtp
3675 IF T=40 THEN Ptgtp
3680 IF T=45 THEN Ptgtp
3685 IF T=50 THEN Ptgtp
3690 IF T=55 THEN Ptgtp
3695 IF T=60 THEN T=0
3700 IF T=0 THEN Ptgtp
3705 GOTO Exit
3710 !
3715 Ptgtp: I60on=0
3720  IF T=5 THEN Zero
3725  IF I12=0 THEN Zero
3730 GOTO Aa
3735 Zero: Tf=0
3740 Th=0
3745 Tq=0
3750 I12=0
3755 Aa: I12=I12+1
3760 R=FNTref
3765 Tff=FNTemp(3,R)
3770 Tf=Tf+Tff
3775 Thh=FNTemp(4,R)
3780 Th=Th+Thh
3785 Tqq=FNTq+.1090*(Thh-Thref)
3790 Tq=Tq+Tqq
3795 ! ASSUMES ZERO AT Thref
3800 IF Tff>Tfmax THEN Ab
3805 GOTO Ac
3810 Ab: PRINT "SHUTDOWN - FACE TEMP IS ",Tff
3815 CALL Time(Thrs,Time$)
3820 PRINT "TIME=";Time$,"Lkold=";Lkold,"Tlkold=";Tlkold
3825 Ngo=7
3830 GOTO Exit
3835 Ac: IF Thh>Thmax THEN Ad
3840 GOTO Ae
3845 Ad: PRINT "SHUTDOWN - HOUSING TEMP IS ";Thh
3850 CALL Time(Thrs,Time$)
3855 PRINT "TIME=";Time$,"Lkold=";Lkold,"Tlkold=";Tlkold
3860 Ngo=7
3865 GOTO Exit
3870 Ae: IF Tqq>Tqmax THEN Af
3875 GOTO Ag
3880 Af: PRINT "SHUTDOWN - TORQUE IS ";Tqq
3885 CALL Time(Thrs,Time$)
3890 PRINT "TIME=";Time$,"Lkold=";Lkold,"Tlkold=";Tlkold
3895 Ngo=7
3900 GOTO Exit
```

```
3905 Ag: IF T=0 THEN Out
3910 IF I12>12 THEN Out
3915 GOTO Exit
3920 Out: Tfout=Tf/I12
3925 Thout=Th/I12
3930 Tqout=Tq/I12
3935 Hp=Tqout*2*PI*(1/12)*Rpm/33000
3940 IF Hp<5.5 THEN 3970
3945 PRINT "SHUTDOWN - HORSEPOWER IS";Hp
3950 CALL Time(Thrs,Time$)
3955 PRINT "TIME=";Time$,"Lkold=";Lkold,"Tlkold=";Tlkold
3960 Ngo=7
3965 GOTO Exit
3970 I12=0
3975 GOTO Exit
3980 Rpmm: I60on=0     !AVAILABLE LATER
3985 GOTO Exit
3990 Oilwater: I60on=0
3995 R=FNTref
4000 Toout=FNTemp(5,R)
4005 Twout=FNTemp(6,R)
4010 IF Toout>Tomax THEN Ba
4015 GOTO Bb
4020 Ba: PRINT "SHUTDOWN - OIL TEMP IS ";Toout
4025 CALL Time(Thrs,Time$)
4030 PRINT "TIME=";Time$,"Lkold=";Lkold,"Tlkold=";Tlkold
4035 Ngo=7
4040 GOTO Exit
4045 Bb: IF Twout>Twmax THEN Bc
4050 GOTO Exit
4055 Bc: PRINT "SHUTDOWN - WATER TEMP IS ";Twout
4060 CALL Time(Thrs,Time$)
4065 PRINT "TIME=";Time$,"Lkold=";Lkold,"Tlkold=";Tlkold
4070 Ngo=7
4075 GOTO Exit
4080 Tme: CALL Time(Thrs,Time$)
4085 Vibset=0
4090 Time=Thrs-Timeref
4095 I60on=0
4100 GOTO Exit
4105 Lk: OFF INT #5
4110 WRITE IO 5,5;32
4115 I60on=0
4120 IF N1k=0 THEN Ea
4125 Lkout=N1k*2/(T1k(N1k)-Tlkold)/60
4130 Tlkold=T1k(N1k)
4135 N1k=0
4140 GOTO Eb
4145 Ea: Lkout=-1000
4150 Eb: WRITE IO 5,5;128
4155 ON INT #5,14 CALL I6940
4160 OUTPUT 5 WHS USING "#,W";-4064,32767
4165 OUTPUT 5 WHS USING "#,W";-3936,28672,-3792
4170 CARD ENABLE 5
4175 GOTO Exit
4180 Exit: !
4185 SUBEXIT
4190 !
4195 !
4200 DEF FNTref
4205 ON ERROR GOSUB 4240
4210 OPTION BASE 1
4215 COM A,B,C,D$,E,F,G,H,I,J,K,L,M
4220 COM A1,A2,SHORT A3,A4,A5,REAL A6,A7,A8(200),A9,A10
4225 COM B1,B2,B3,B4,SHORT B5,B6,B7,B8,B9,B10,B11,Rs
4230 ! SLOT 401, J THERMO 0-400C
```

```
4235 GOTO 4250
4240 PRINT ERRM$
4245 RETURN
4250 OFF INT #5
4255 WRITE IO 5,5;32
4260 OUTPUT 5 WHS USING "#,W";-3984,4103,-3920
4265 WRITE IO 5,4;4096
4270 READ IO 5,4;R1
4275 WRITE IO 5,5;128
4280 ON INT #5,14 CALL I6940
4285 OUTPUT 5 WHS USING "#,W";-4064,32767
4290 OUTPUT 5 WHS USING "#,W";-3936,28672,-3792
4295 CARD ENABLE 5
4300 IF (R1<3900) AND (R1>3600) THEN Rs=R1
4305 R=Rs
4310 R=(R-4096)*10/4352
4315 R=3923.7225/(13.158+LOG(-R))-273.2
4320 R=R*(50.373743+R*(3.0167011E-2-R*7.4293513E-5))*1E-6
4325 RETURN R
4330 FNEND
4335 !
4340 !
4345 DEF FNTemp(N,R)
4350 ON ERROR GOSUB 4365
4355 ! SLOT 401 JTHEMO 0-400C
4360 GOTO 4375
4365 PRINT ERRM$
4370 RETURN
4375 ! A=DECIMAL(10000+N)
4380 OFF INT #5
4385 WRITE IO 5,5;32
4390 OUTPUT 5 WHS USING "#,W";-3984,A,-3920
4395 WRITE IO 5,4;4096
4400 READ IO 5,4;T
4405 WRITE IO 5,5;128
4410 ON INT #5,14 CALL I6940
4415 OUTPUT 5 WHS USING "#,W";-4064,32767
4420 OUTPUT 5 WHS USING "#,W";-3936,28672,-3792
4425 CARD ENABLE 5
4430 T=(T-(T>2047)*4096)*1E-5
4435 T=(R+T)*1E6
4440 T=T*(1.9750953E-2+T*(-1.8542600E-7+T*(8.368395E-12-T*1.3280568E-16)))
4445 T=1.8*T+32
4450 RETURN T
4455 FNEND
4460 !
4465 !
4470 !
4475 !
4480 SUB Coord(Timemin,Timemax,Trqmin,Trqmax,Lkmax,Tmpmax,Tmpmin)
4485 ON ERROR GOSUB 4500
4490 LIMIT 0,270,0,190
4495 GOTO 4510
4500 PRINT ERRM$
4505 RETURN
4510 !
4515 FOR I=1 TO 5
4520 CALL Tint
4525 NEXT I
4530 LOCATE 10,130,10,97
4535 MOVE 70,95
4540 FOR I=1 TO 5
4545 CALL Tint
4550 NEXT I
4555 LORG 5
4560 CSIZE 3,.5
```

```
4565 INPUT "TEST#=?",C
4570 LABEL "TEST#";C
4575 FOR I=1 TO 5
4580 CALL Tint
4585 NEXT I
4590 INPUT "DATE?",A$
4595 LABEL A$
4600 FOR I=1 TO 5
4605 CALL Tint
4610 NEXT I
4615 INPUT "MAX TORQUE=?",Ymax
4620 INPUT "MIN. TORQUE=?",Ymin
4625 Trqmin=Ymin
4630 Trqmax=Ymax
4635 INPUT "MAX TIME=?",Xmax
4640 Timemax=Xmax
4645 INPUT "MIN TIME =?",Timemin
4650 Total=Timemax-Timemin
4655 Q=-(1/12)*Total+Timemin
4660 SCALE Q,Xmax,Ymin,Ymax
4665 INPUT "TORQUE DIV.=?",Yt
4670 INPUT "TIME DIV?",Xt
4675 AXES Xt,Yt,Timemin,Trqmin,1,1
4680 FOR I=1 TO 5
4685 CALL Tint
4690 NEXT I
4695 CSIZE 3,.5
4700 LORG 6
4705 Middle=(Timemax+Timemin)/2
4710 MOVE Middle,Trqmin-2.5/50*(Ymax-Ymin)
4715 LABEL USING "K";"TIME(HRS.)"
4720 FOR I=1 TO 5
4725 CALL Tint
4730 NEXT I
4735 CSIZE 3,.5
4740 LORG 7
4745 Xmin=Timemin
4750 INPUT "TIME STEP=?",T
4755 FOR X1=Xmin TO Xmax STEP T
4760 MOVE X1+.25/24*Total+Timemin/Timemax*(.05/24*Total),Trqmin-1.5/50*(Ymax-Ymi
n)
4765 IF T<1 THEN GOTO 4780
4770 LABEL USING "MDDD";X1
4775 GOTO 4790
4780 !
4785 LABEL USING "MDDD.DD";X1
4790 NEXT X1
4795 FOR I=1 TO 5
4800 CALL Tint
4805 NEXT I
4810 CSIZE 3,.5
4815 LORG 7
4820 INPUT "TORQUE STEP=?",C
4825 FOR Y1=Ymin TO Ymax STEP C
4830  Z=.1/24
4835 Torque=Timemin-Z*Total-Timemin/Timemax*(.1*Total/24)
4840 MOVE Torque,Y1+.3/50*(Ymax-Ymin)
4845 LABEL USING "MDDD";Y1
4850 NEXT Y1
4855 FOR I=1 TO 5
4860 CALL Tint
4865 NEXT I
4870 CSIZE 3,.5
4875 LDIR PI/2
4880 LORG 6
4885 Z=1.5/24
```

```
4890 Torque=Timemin-2*Total-Timemin/Timemax*(.1*Total/24)
4895 MOVE Torque,(Ymax+Ymin)/2
4900 LABEL USING "K";"TORQUE(IN.-LBS.)"
4905 FOR I=1 TO 5
4910 CALL Tint
4915 NEXT I
4920 INPUT "MAX TEMP.=?",Ymax
4925 Tmpmax=Ymax
4930 INPUT "MIN TEMP=?",Ymin
4935 Tmpmin=Ymin
4940 SCALE 0,Xmax,Ymin,Ymax
4945 INPUT "TEMP DIV.=?",Yt
4950 AXES Xt,Yt,Timemin-1/12*Total,0,1,1
4955 FOR I=1 TO 5
4960 CALL Tint
4965 NEXT I
4970 CSIZE 3,.5
4975 LDIR 0
4980 LORG 7
4985 INPUT "TEMP STEP=?",D
4990 FOR Y1=Ymin TO Ymax STEP D
4995 Tem=Timemin-1/12*Total-.1/24*Total-.1/24*Total*Timemin/Timemax
5000 MOVE Tem,Y1+.3/50*(Ymax-Ymin)
5005 LABEL USING "MDDD";Y1
5010 NEXT Y1
5015 FOR I=1 TO 5
5020 CALL Tint
5025 NEXT I
5030 Ymax=Ymax+Ymin
5035 CSIZE 3,.5
5040 LDIR PI/2
5045 LORG 6
5050 Tem=Timemin-1/12*Total-1.0/24*Total-.1/24*Total*Timemin/Timemax
5055 MOVE Tem,Ymax/2
5060 LABEL USING "K";"SEAL TEMPERATURE(F)"
5065 FOR I=1 TO 5
5070 CALL Tint
5075 NEXT I
5080 INPUT "MAX LEAKAGE=?",Ymax
5085 Lkmax=Ymax
5090 Ymin=0
5095 SCALE 0,Xmax,0,Ymax
5100 INPUT "LEAKAGE DIV.=?",Yt
5105 AXES Xmax,Yt,Xmax,0,1,1
5110 FOR I=1 TO 5
5115 CALL Tint
5120 NEXT I
5125 CSIZE 3,.5
5130 LDIR 0
5135 LORG 4
5140 INPUT "LEAKAGE STEP=?",E
5145 FOR Y1=Ymin TO Ymax STEP E
5150 MOVE Timemax+.3/24*Total,Y1+.3/50*Ymax
5155 LABEL USING "MDDD";Y1
5160 NEXT Y1
5165 FOR I=1 TO 5
5170 CALL Tint
5175 NEXT I
5180 CSIZE 3,.5
5185 LDIR PI/2
5190 LORG 6
5195 MOVE Timemax+1.3/24*Total,Ymax/2
5200 LABEL USING "K";"LEAKAGE(ML/MIN.)"
5205 FOR I=1 TO 5
5210 CALL Tint
5215 NEXT I
```

```
5220 MOVE Timemax,Ymax
5225 DRAW Timemin,Ymax
5230 PENUP
5235 LOCATE 10+120/26*2,130,10,97
5240 SUBEXIT
5245 !
5250 !
5255 !
5260 SUB I6940
5265 ON ERROR GOSUB 5295
5270 OPTION BASE 1
5275 COM Zero,Inibmv,Relay,Flag$,Ph2o,Rpm,Tqmax,Tomax,Tfmax,Thmax,Twmax
5280 COM T,Timeref,SHOFT Thout,Tcout,Twout,REAL Lkold,Tlkold,Tlk(200),Thref,Nlk
5285 COM I60,I60cn,I12,Ngo,SHORT Time,Tfout,Tqout,Lkout,Z11,Z12,Z13,Z14,Vibset,N
vib,Tvib
5290 GOTO 5305
5295 PRINT ERRM$
5300 RETURN
5305 OUTPUT 5 WHS USING "#,W";-3936
5310 WRITE IO 5,4;28672
5315 READ IO 5,4;X
5320 X=X+32768
5325 X=4095-X
5330 Y=4
5335 IF X-Y>.5 THEN 5360
5340 Y=2
5345 IF X-Y>-.5 THEN Ch2
5350 Y=1
5355 IF X-Y>-.5 THEN Ch1
5360 PRINT "EVENT SENSE CARD IS RETURNING AN INCORRECT SIGNAL,Y=";Y
5365 SUBEXIT
5370 !
5375 !
5380 Ch1: Nlk=Nlk+1
5385 CALL Time(Thrs,Time$)
5390 Tlk(Nlk)=Thrs-Timeref
5395 WAIT 50
5400 D=FNRoff(4)
5405 WAIT 10
5410 D=FNRon(4)
5415 SUBEXIT
5420 !
5425 !
5430 Ch2:!
5435 IF Vibset=0 THEN Cycle
5440 Nvib=Nvib+1
5445 CALL Time(Thrs,Time$)
5450 Tnew=Thrs-Timeref
5455 IF Tnew-Tvib>10/3600 THEN A1
5460 GOTO Reset
5465 A1: IF Nvib<5 THEN Reset
5470 PRINT "VIBRATION ALARM SHUTDOWN"
5475 PRINT "Nvib= ";Nvib
5480 PRINT "Tnew= ";Tnew
5485 PRINT "Tvib= ";Tvib
5490 Ngo=7
5495 GOTO Reset
5500 Cycle: Nvib=1
5505 CALL Time(Thrs,Time$)
5510 Tvib=Thrs-Timeref
5515 Vibset=1
5520 GOTO Reset
5525 Reset:!
5530 SUBEND
5535 !
```

```
5540 !
5545 SUB Time(Thrs,Time$)
5550 OPTION BASE 1
5555 COM Zero,Inlbmv,Relay,Flag$,Ph2o,Rgm,Tqmax,Tomax,Tfmax,Thmax,Twmax
5560 COM T,Timeref,SHORT Thout,Tcout,Twout,REAL Lkold,Tlkold,Tlk(200),Thref,Nlk
5565 COM I60,I60on,I12,Ngo,SHORT Time,Tfout,Tqout,Lkout,Z11,Z12,Z13,Z14,Vibset,N
vib,Tvib,Days(12)
5570 ! THIS IS TIME FROM BEGINING OF YEAR
5575 ! FEB. IS TAKEN AT 28 DAYS
5580 ON ERROR GOSUB 9b
5585 Er=0
5590 Aa: DISABLE
5595 OUTPUT 10;"R"
5600  ENTER 10;Month,Day,Hour,Minute,Second
5605  ENABLE
5610 IF Er=1 THEN Aa
5615 Er=0
5620 GOTO Cc
5625 Bb: PRINT ERRM$
5630 PRINT Month,Day,Hour,Minute,Second
5635 IF ERRN<>160 THEN Dd
5640 Er=Er+1
5645 Dd: RETURN
5650 Cc: Thrs=(Days(Month)+Day-1)*24+Hour+(Minute+Second/60)/60
5655 M$=VAL$(Month)
5660 D$=VAL$(Day)
5665 H$=VAL$(Hour)
5670 Min$=VAL$(Minute)
5675 Time$=M$&"/"&D$&"/80 "&H$&":"
5680 IF Minute<10 THEN Ee
5685 Time$=Time$&Min$
5690 SUBEXIT
5695 Ee:Time$=Time$&"0"&Min$
5700 SUBEND
```

Appendix B

Test Results

TEST # AND DATE	1 1/11/79	2 1/18/79	3 1/19/79	4 1/26/79	5 1/31/79	6 2/2/79	7 3/7/79	8 3/13/79	9 3/16/79	10 3/21/79	11 3/22/79	12 3/25/79	13 3/28/79
TYPE OF TEST	FLAT FACE	FLAT FACE	FLAT FACE	FLAT FACE	FLAT FACE	FLAT FACE	WAV.	WAV.	WAV.	WAV.	WAV.	WAV.	FLAT FACE
SPEED (RPM)	1800	1800	1800	1800	1800	1800	1800	1800	1800	1800	1800	1800	1800
SEALED PRESSURE (PSI)	250	500	500	500	500	250	250	250	250	500	500	500	500
TEST DURATION (HOURS)	5.0	1.9	2.1	8.08	18.8	8.26	33.0	47.8	24.6	24.0	22.7	24.0	23.6
WAVINESS PRESSURE (PSI)	0.0	0.0	0.0	0.0	0.0	0.0	850	400	1050	1025	1235	730	0.0
COOLING WATER TEMPERATURE (°F)	100.0	100.0	100.0	100.0	100.0	100.0	100.0	100.0	100.0	100.0	100.0	100.0	100.0
LEAKAGE INITIAL / FINAL (ml/min)	/	/ 50.0	/	/ 0.0	/ 0.0	0.0 / 0.0	6.9 / 3.24	.24 / 0.0	50.0 / 11.0	15.88 / 1.22	3.85 / 5.21	.027 / 0.62	0.0 / 0.0
BEARING HOUSING TEMPERATURE (°F)						121.5	121.0	125.0	127.0	124.0	126.3	124.1	124.5
SEAL FACE TEMPERATURE (°F)	111.0	105.0	105.0	114.0	112.0	106.0	107.4	104.3	104.0	104.0	104.3	105.6	115.3
FINAL TORQUE TEMP / ORDER (in-lbs)	32.5 /	2.5 /	14.0 /	62.6 /	61.2 / 67.5	113.6 /	22.6 / 150	46.1 /	19.0 /	29.0 / 25.6	22.7 / 19.6	20.1 /	109.2 /
PRIMARY RING #	1	1	1	2	2	2	2	2	2	2	2	2	2
AVERAGE WEAR (μ in.)	≈0			79.3	30.0	43.3	5.0	→	≈0	→	→	≈0	→
RADIAL CLR. INITIAL / FINAL (μ in.)	2.0 / 11.2	/	/	18.0 / 8.4	17.2 / 7.6	18.3 / 6.0	19.0 / 14.0	16.4 →	/ 15.4	18.2 →	→	/ 7.6	20.0 →
TANGENTIAL CLR. INITIAL / FINAL (μ in.)	10.0 / 7.8	/	/	26.0 / 24.4	20.0 / 20.6	18.8 / 13.0	23.0 / 20.0	19.6 →	/ 16.0	24.2 →	→	/ 13.0	24.0 →
RADIAL TAPER INITIAL / FINAL (μ in./in.)	/	/	/	/	D / 517.5	D / 204.5	D / 106.0	→	D / 15.9	→	→	D / 36.6	→
SECONDARY RING #	0	0	0	0	0	0	0	0	0	0	0	0	0
RADIAL CLR. INITIAL / FINAL (μ in.)	/	/	/	/	/	/	/	/	/	/	/	/	/
TANGENTIAL CLR. INITIAL / FINAL (μ in.)	/	/	/	/	/	/	/	/	/	/	/	/	/
RADIAL TAPER INITIAL / FINAL (μ in./in.)	/	/	/	/	/	C / 36.8	26.8 / C	/	/	/	/	/	/
AVERAGE WEAR (μ in.)													

TEST # AND DATE	14 3/30/79	15 4/3/79	16 4/4/79	17 4/5/79	18 4/10/79	19 4/11/79	20 4/13/79	21 4/20/79	22 4/25/79	23 5/1/79	24 5/16/79	25 5/22/79	26 5/24/79
TYPE OF TEST	FLAT FACE	WAV.	WAV.	WAV.	WAV.	WAV.	WAV.	WAV.	FLAT FACE	WAV.	TAPERED SEAL	WAV.	WAV.
SPEED (RPM)	1800	1800	1800	1800	1800	2700	2700	1800	1800	1800	1800	1800	500
SEALED PRESSURE (PSI)	750	750	750	750	750	500	500	500	500	500	500	500	500
TEST DURATION (HOURS)	6.3	20.5	24.0	32.3	22.6	24.4	516	100.0	100.0	100.0	116.0	48.0	4.0
WAVINESS PRESSURE (PSI)	0.0	500	790	1100	1550	800	1100	1000	0.0	690	0.0	1000	1000
COOLING WATER TEMPERATURE (°F)	100.0	100.0	100.0	100.0	100.0	100.0	100.0	100.0	100.0	100.0	100.0	100.0	100.0
LEAKAGE INITIAL / FINAL (ml/min)	0.0 / 0.0	0.0 / 0.0	0.0 / 0.0	2.34 / 2.26	11.36 / 6.4	1.06 / 0.88	3.39 / 6.05	1.21 / 1.05	0.0 / 0.0	0.0 / .29	0.0 / 0.0	6.76 / .57	/ .25
BEARING HOUSING TEMPERATURE (°F)	130.7	128.5	132.9	130.7	128.5	145.6	140.0	125.0	126.5	126.5	120.58	123.22	98.22
SEAL FACE TEMPERATURE (°F)	115.3	116.2	108.7	106.5	106.6	104.7	104.5	103.8	120.0	104.6	102.5	104.3	103.4
FINAL TORQUE, TEMP / COEFF (INCLES.)	124.9 / 121.2	82.2 /	52.4 /	48.9 /	20.9 /	25.5 /	20.3 / 22.0	8.0 / 12.5	135.7 / 121.4	12.0 / 17.5	55.1 / 34.46	24.05 / 21.83	19.2 / 14.04
PRIMARY RING #	2	2	2	2	2	2	2	3	4	5	2	3	3
AVERAGE WEAR (μ in.)	29.2	→	→	→	→	→	46.7	98.3	3706.0	358.0		→	10.33
RADIAL C.L.A. INITIAL / FINAL (μ in.)	/ 8.8	25.0 →	→	→	→	→	/ 9.8	7.0 / 3.5	8.0 / 7.5	7.5 / 6.0	/	15.0 →	/ 3.3
TANGENTIAL C.L.A. INITIAL / FINAL (μ in.)	/ 7.2	23.0 →	→	→	→	→	/ 8.2	11.0 / 4.0	11.0 / 5.3	8.0 / 6.0	/	9.0 →	/ 3.5
RADIAL TAPER INITIAL / FINAL (μ in./in.)	D / 529.0	→	→	→	→	→	C / 5.6	19.5 C /	3.1 D / 1176.0	2.4 D /	1058 C / C	53.3 D /	D / 164.0
SECONDARY RING #	0	0	0	0	0	0	0	2 SIDE A	3 SIDE A	1 SIDE A	3 SIDE A	2 SIDE A	2 SIDE A
RADIAL C.L.A. INITIAL / FINAL (μ in.)	/	/	/	/	/	/	/	1.2	1.5	1.6	2.0	1.2 →	/ 2.52
TANGENTIAL C.L.A. INITIAL / FINAL (μ in.)	/	/	/	/	/	/	/	2.08	1.8	2.4	2.0	2.08 →	/ 2.36
RADIAL TAPER INITIAL / FINAL (μ in./in.)	/	/	/	/	/	/	/	C / 104	C / 63.2	C / 100.5	C / 10.7	104.4 C /	C / 120.0
AVERAGE WEAR (μ in.)												→	≈0

TEST # AND DATE	27 5/24/79	28 5/25/79	29 5/30/79	30 6/11/79	31 6/13/79	32 6/13/79	33 6/14/79	34 6/15/79	35 6/15/79	36 6/22/79	37 6/26/79	38 8/15/79	39 8/20/79
TYPE OF TEST	WAV.	WAV.	WAV	WAV.	WAV.	WAV.	WAV.	WAV.	FLAT FACE	WAV.	WAV. (HYDRO-DYNAMIC EFFECTS)	WAV.	WAV.
SPEED (RPM)	1800	900	1800	2700	3600	1800	900	1800	1800	1800	2700	1800	1800
SEALED PRESSURE (PSI)	500	500	500	500	500	500	500	500	500	500	250	500	500
TEST DURATION (HOURS)	20.5	4.83	24.9	45.5	5.5	17.6	20.3	100.0	100.0	100.0	72.0	41.5	100
WAVINESS PRESSURE (PSI)	700	700	600	1000	1000	1000	1000	1000	0.0	700	500	1000	1000
COOLING WATER TEMPERATURE (°F)	100.0	100.0	100.0	100.0	100.0	100.0	100.0	100.0	100.0	100.0	100.0	100.0	100.0
LEAKAGE INITIAL / FINAL (ml/min)	- / .65	.23 / .38	1.0 / 0.0	1.01 / 4.5	1.9 / 1.8	.67 / .74	.46 / .19	2.11 / 1.43	0.0 / 0.0	2.58 / 1.35	2.0 / ~0	2.0 / 2.5	/ 2.23
BEARING HOUSING TEMPERATURE (°F)	122.18	99.90	116.2	138.6	150.5	117.0	102.1	121.9	125.0	120.6	115.0	116.0	120.7
SEAL FACE TEMPERATURE (°F)	104.3	104.3	108.7	106.6	108.7	104.3	102.1	103.4	110.9	103.8	104.3	103	102.5
FINAL TORQUE TEMP. / COOLER (INCLUDED)	25.30 / 26.42	30.30 / 30.11	42.6 / 44.7	38.1 / 28.75	44.3 /	27.15 /	21.0 / 15.83	18.7 / 11.79	78.0 / 73.8	22.0 / 20.71	13.1 / 18.7	18.0 / 17.75	12.3 / 14.16
PRIMARY RING #	4	4	5	2	2	2	2	3	3	5	4	4	5
AVERAGE WEAR (μ in.)	→ ~0.0		10.0	→	→	→	10.0	-45	456	-52	→	147	- 42
RADIAL C.L.A. INITIAL / FINAL (μ in.)	14.9 → 13.4		9.6 / 13.0	19.2 →	→	→	11.0	21.0 / 19.0	19.0 / 15.8	24.0 / 22.0	22.0 →	18.0	/ 25.4
TANGENTIAL C.L.A. INITIAL / FINAL (μ in.)	16.5 → 16.4		22.0 / 9.6	21.0 →	→	→	12.3	20.0 / 16.0	12.0 / 16.2	25.0 / 25.0	23.0 →	17.4	/ 28
RADIAL WAVE INITIAL / FINAL (μ in./rev.)	<11.5 → C 79.4		<11.5 / D -300	<11.5 →	→	→	D 154.1	<11.5 / <11.5	22.7 D / D 1502	<11.5 / C 105	<11.5 →	F 108	158 / 47
SECONDARY RING #	0 SIDE A	0 SIDE A	3 SIDE A	2 SIDE A	2 SIDE A	2 SIDE A	2 SIDE A	2 SIDE B	3 SIDE B	0 SIDE A	1 SIDE A	1 SIDE A	0 SIDE B
RADIAL C.L.A. INITIAL / FINAL (μ in.)	2.0 → 4.48		1.5 / 3.6	2.52 →	→	→	2.8	3.76 / 2.2	2.2 / 2.2	4.48 / 2.72	1.6 →	2.0	2.5 / 1.6
TANGENTIAL C.L.A. INITIAL / FINAL (μ in.)	2.0 → 4.60		1.8 / 4.25	2.36 →	→	→	2.2	3.8 / 2.36	2.36 / 2.44	4.6 / 2.6	2.4 →	2.5	3.8 / 2.9
RADIAL WAVE INITIAL / FINAL (μ in./rev.)	-2.0 C → C -2.0		63.2 C / C -45	-100.0 C →	→	→	C -82.0	22.8 C / C 35.7	35.7 C / C 63.6	-2.0 C / C 8.93	100.5 C →	C -30	<115 / <11.5
AVERAGE WEAR (μ in.)	→ -0.0		~3.0	→	→	→	~0	~0	~6.0	~0	→	~0	~0

TEST # AND DATE	40 8/30/79	41 9/5/79	42 9/19/79	43 10/4/79	44 10/6/79	45 12/17/79	46 2/7/80	47 2/13/80	48 2/14/80	49 2/19/80	50 2/20/80	51 2/21/80	52 2/22/80
TYPE OF TEST	FLAT FACE	WAV.	RADIAL TAPER	RADIAL TAPER	WAV.	WAV.	HOT	HOT	HOT	HOT	HOT	HOT	HOT
SPEED (RPM)	1800	1800	1800	1800	1800	1800	1800	1800	1800	1800	1800	1800	1800
SEALED PRESSURE (PSI)	500	500	500	500	500	500	238	238	238	238	238	238	238
TEST DURATION (HOURS)	110.9	102.0	355.6	164.3	27	500	29.7	24.9	29.4	32.7	15.3	23.9	41.2
WAVINESS PRESSURE (PSI)	0.0	500	0.0	0.0	1200	1000							
COOLING WATER TEMPERATURE (°F)	100.0	100.0	100.0	100.0	100.0	100.0	200	250	300	250	300	200	150
LEAKAGE INITIAL / FINAL (ML/MIN)	0.0 / 0.0	~3 / 0.0	~2.5 / 0.0	0.0 / 0.0	~26 / 8.23	~8.5 / 6.8	/ 0.0	/ 0.0	/ 0.0	/ 0.0	/ 0.0	/ 0.0	/ 0.0
BEARING HOUSING TEMPERATURE (°F)	—	—	119.5	119.5	—	? 91.98	100.14	112.35	116.50	115.29	116.13	111.08	103.31
SEAL FACE TEMPERATURE (°F)	108.6	108.8	103.6	103.0	101.4	102.6	209.38	257.35	309.37	258.32	307.18	212.63	164.22
FINAL TORQUE TEMP. OSSIC (INCHES)	81.2 / 81.2	40.9 / 40.9	24.7 / 22.15	27.1 / 26.3	18.99 / 18.99	20.11 / 11.17	65.48 / 60.5	89.78 / 80.9	80.93 / 78.9	84.35 / 72.6	76.80 / 76.0	113.59 / 113.9	107.21 / 98.9
PRIMARY RING #	6	2	5	7	8	8	5	5	5	5	5	5	5
AVERAGE WEAR (μm)	641	—			—	12							
RADIAL C.L.A. INITIAL / FINAL (μm)	29 / 14	/ 16.1	/	/	/	25.4 / 13	/	/	/	/	/	/	/
TANGENTIAL C.L.A. INITIAL / FINAL (μm)	28 / 12.7	/ 11.9	/	/	/	25 / 18	/	/	/	/	/	/	/
RADIAL TAPER INITIAL / FINAL (μm/in)	74 / 1203	/	/	/	/	<115 /	/	/	/	/	/	/	/
SECONDARY RING #	2 SIDE B	3 SIDE B	2 SIDE A	3 SIDE A		3 SIDE A							
RADIAL C.L.A. INITIAL / FINAL (μm)	2.3 / —	1.6 /	—	/	/	/	/	/	/	/	/	/	/
TANGENTIAL C.L.A. INITIAL / FINAL (μm)	3.8 / —	2.9 /	—	/	/	/	/	/	/	/	/	/	/
RADIAL TAPER INITIAL / FINAL (μm/in)	101 C / —	<11.5 /	—	/	/	/	/	/	/	/	/	/	/
AVERAGE WEAR (μm)			—										

$ NO FINAL ZEED MEASUREMENT MADE

TEST # AND DATE	53 2/24/80	54 3/5/80											
TYPE OF TEST	HOT	HOT											
SPEED (RPM)	1800	1800											
SEALED PRESSURE (PSI)	238	238											
TEST DURATION (HOURS)	46.5	72.0											
WAVINESS PRESSURE (PSI)													
COOLING WATER TEMPERATURE (°F)	100	200											
LEAKAGE INITIAL / FINAL (CC/MIN)	0.0	0.0											
BEARING HOUSING TEMPERATURE (°F)	110.64	109.03											
SEAL FACE TEMPERATURE (°F)	114.27	209.57											
FINAL FORWARD TEMP / OUTBD (INCLUDE)	119.95 / 100.8	81.3 / 80.3											
PRIMARY RING #	5	7											
AVERAGE WEAR (MILS)													
RADIAL C.L.A. INITIAL / FINAL (MICRO IN.)													
TANGENTIAL C.L.A. INITIAL / FINAL (MICRO IN.)													
RADIAL TAPER INITIAL / FINAL (MICRO IN./IN.)													
SECONDARY RING #													
RADIAL C.L.A. INITIAL / FINAL (MICRO IN.)													
TANGENTIAL C.L.A. INITIAL / FINAL (MICRO IN.)													
RADIAL TAPER INITIAL / FINAL (MICRO IN./IN.)													
AVERAGE WEAR (MILS)													

Appendix C

Performance Curves

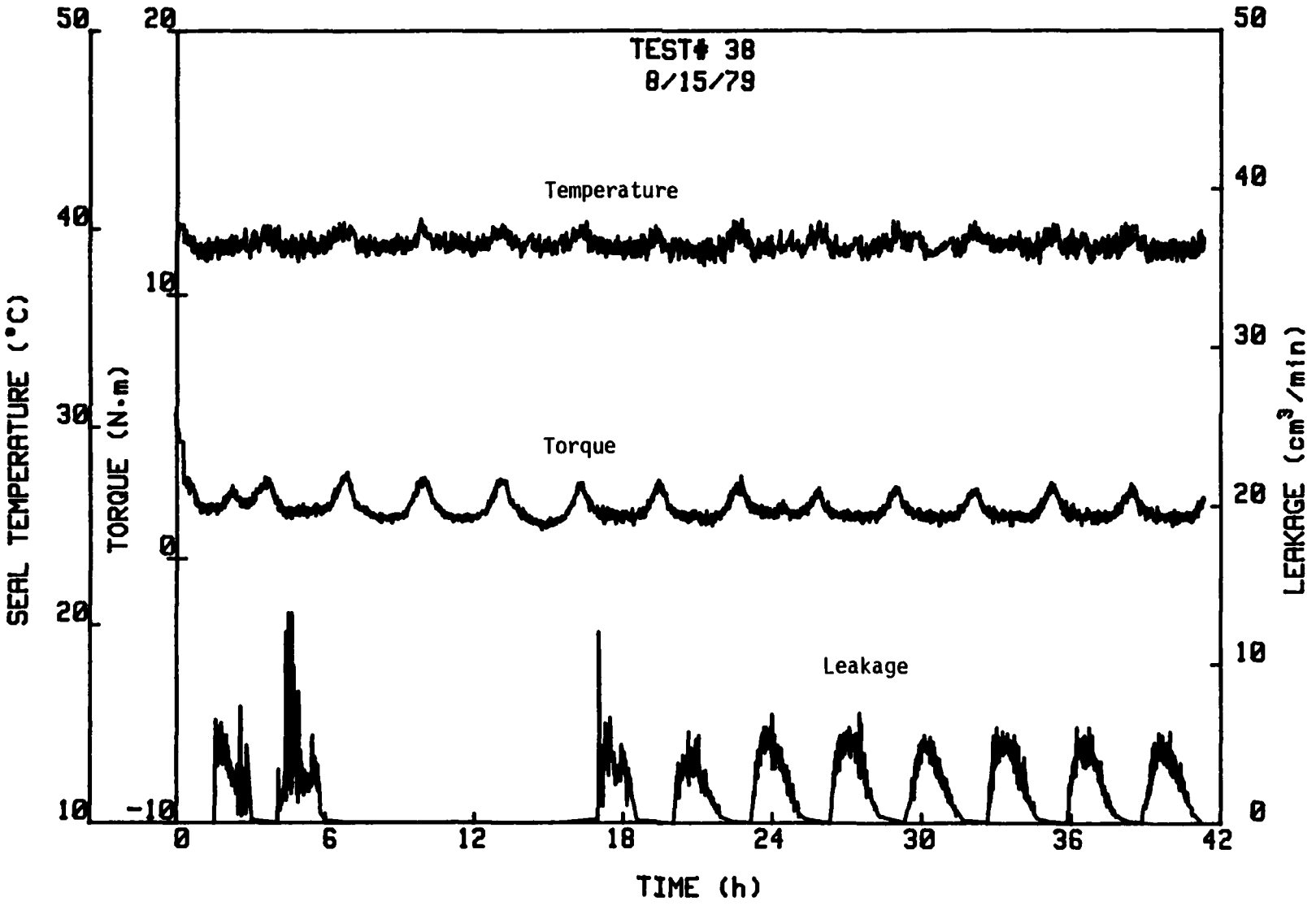

Figure C-1. Test #38, 1800 RPM, p_{H_2O} = 3.45 MPa, p_g = 6.9 MPa.

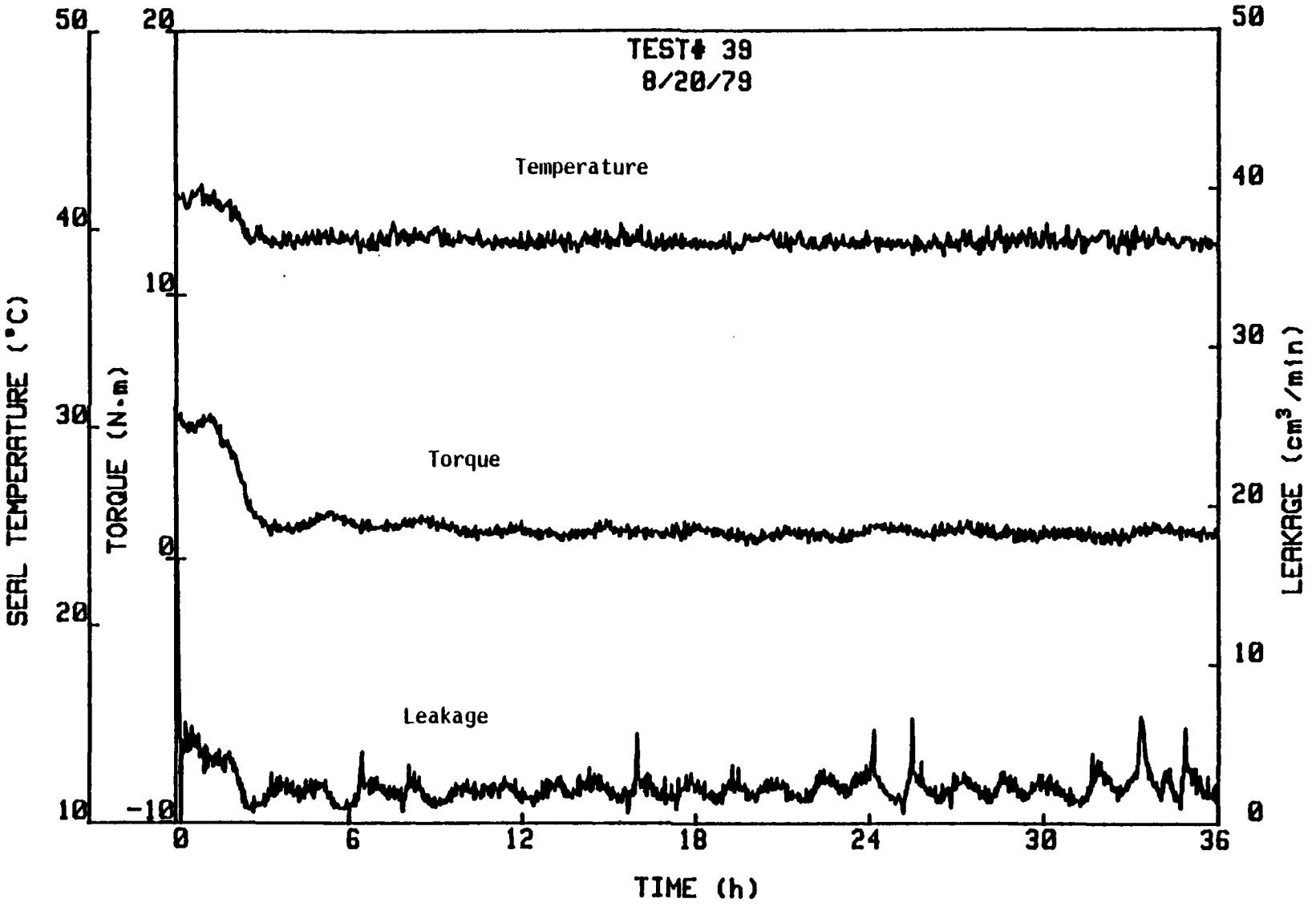

Figure C-2. Test #39, 1800 RPM, p_{H_2O} = 3.45 MPa, p_g = MPa.

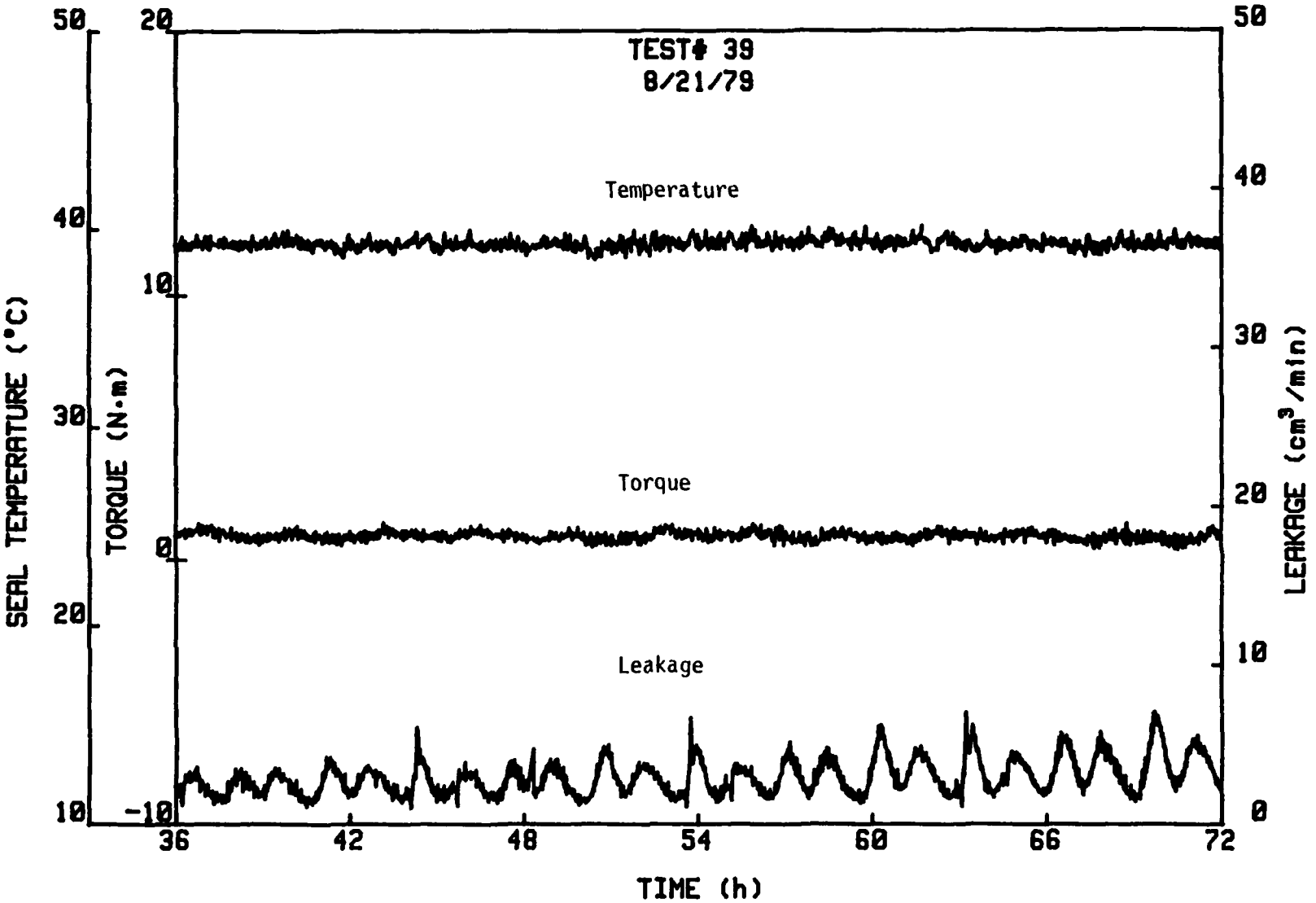

Figure C-2, cont.

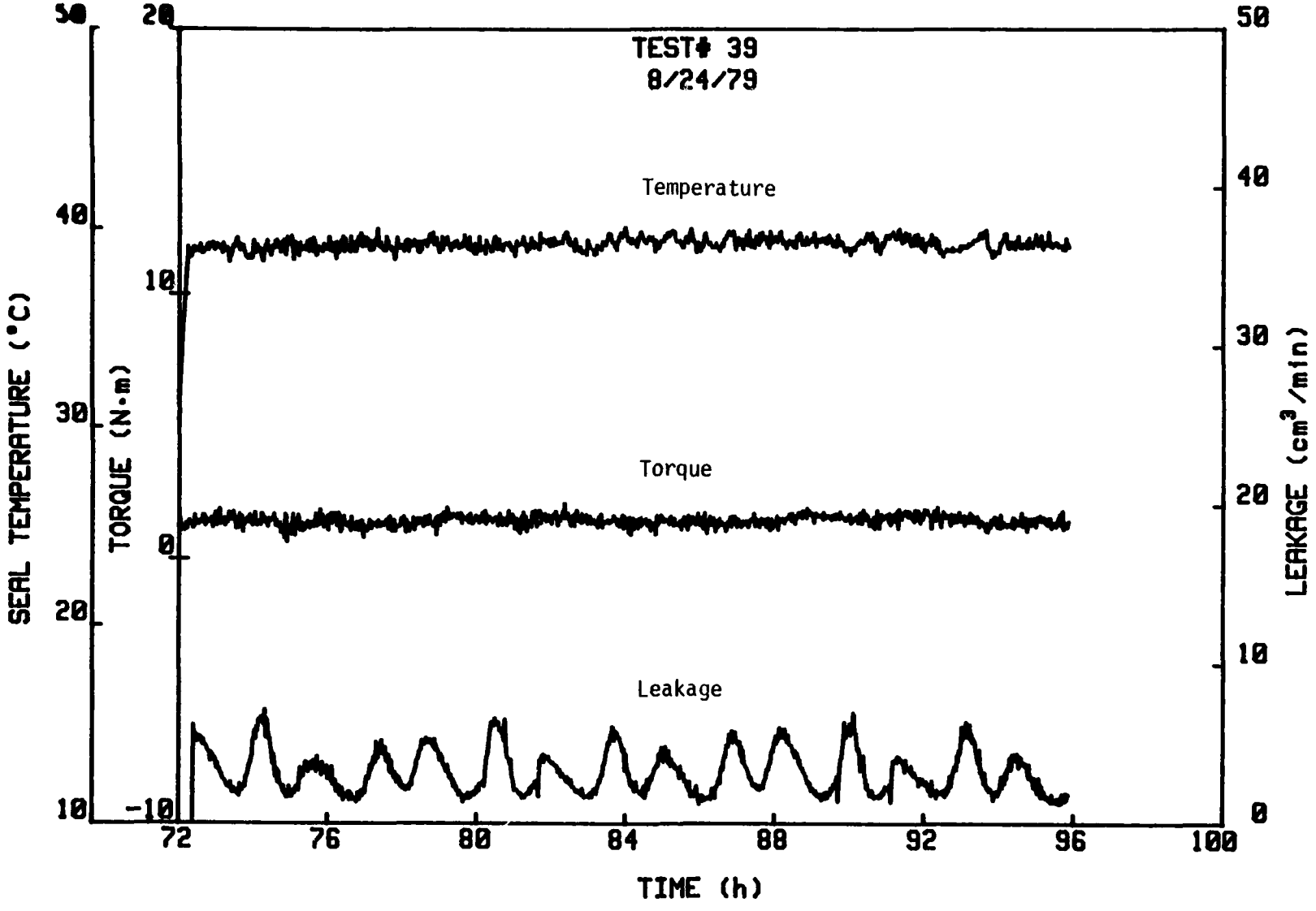

Figure C-2, cont.

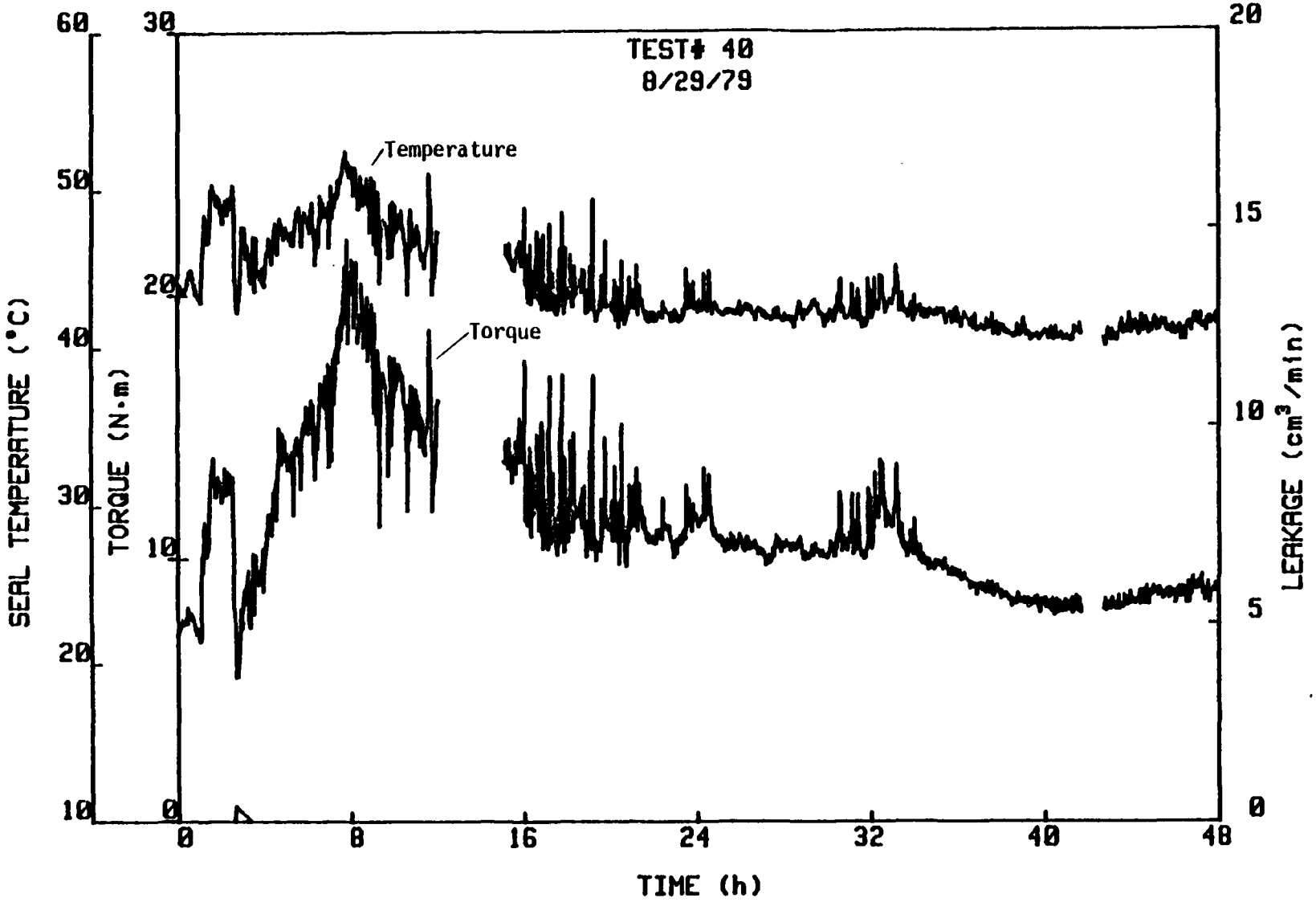

Figure C-3. Test #40, 1800 RPM, p_{H_2O} = 3.45 MPa, p_g = 0.

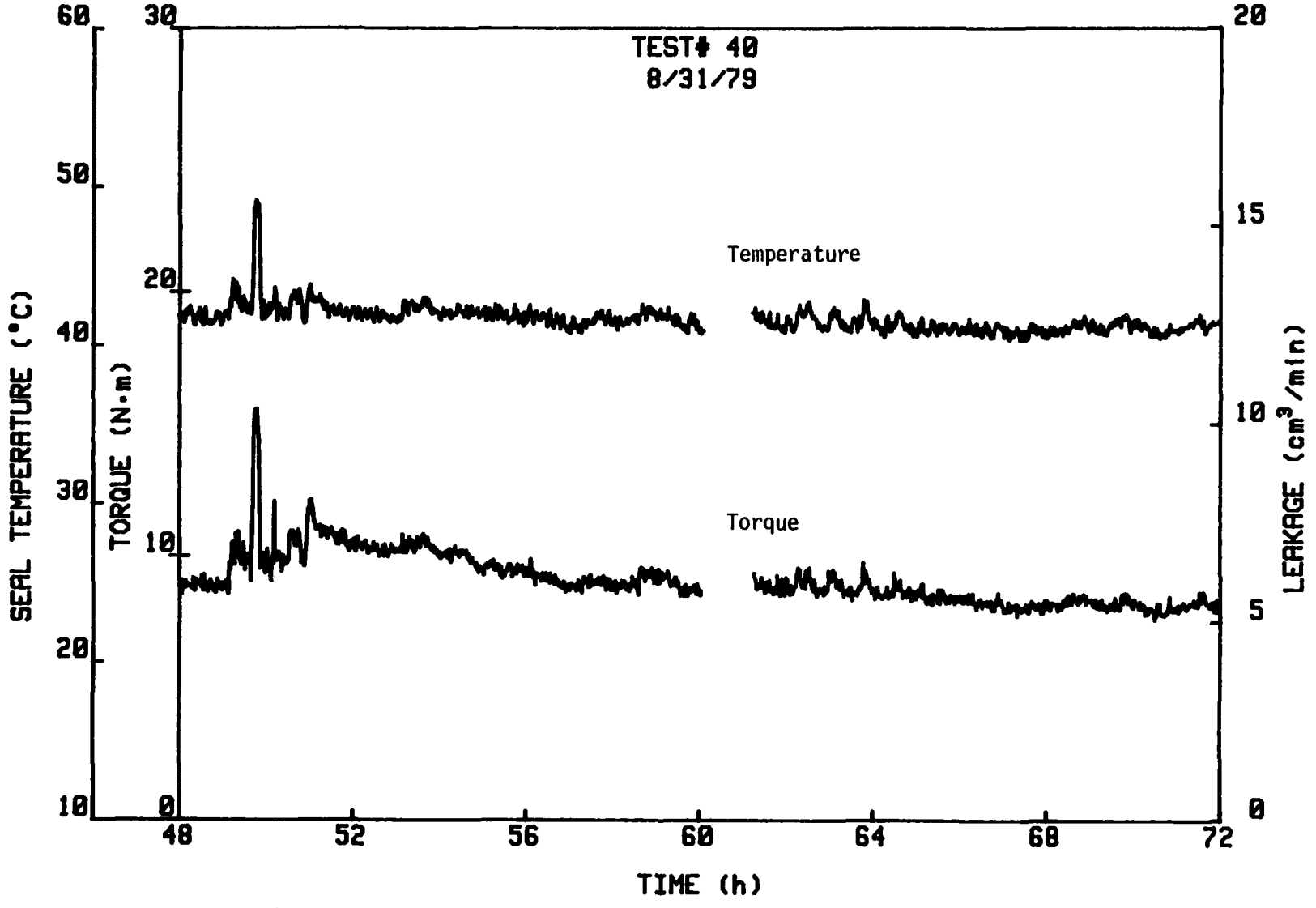

Figure C-3, cont.

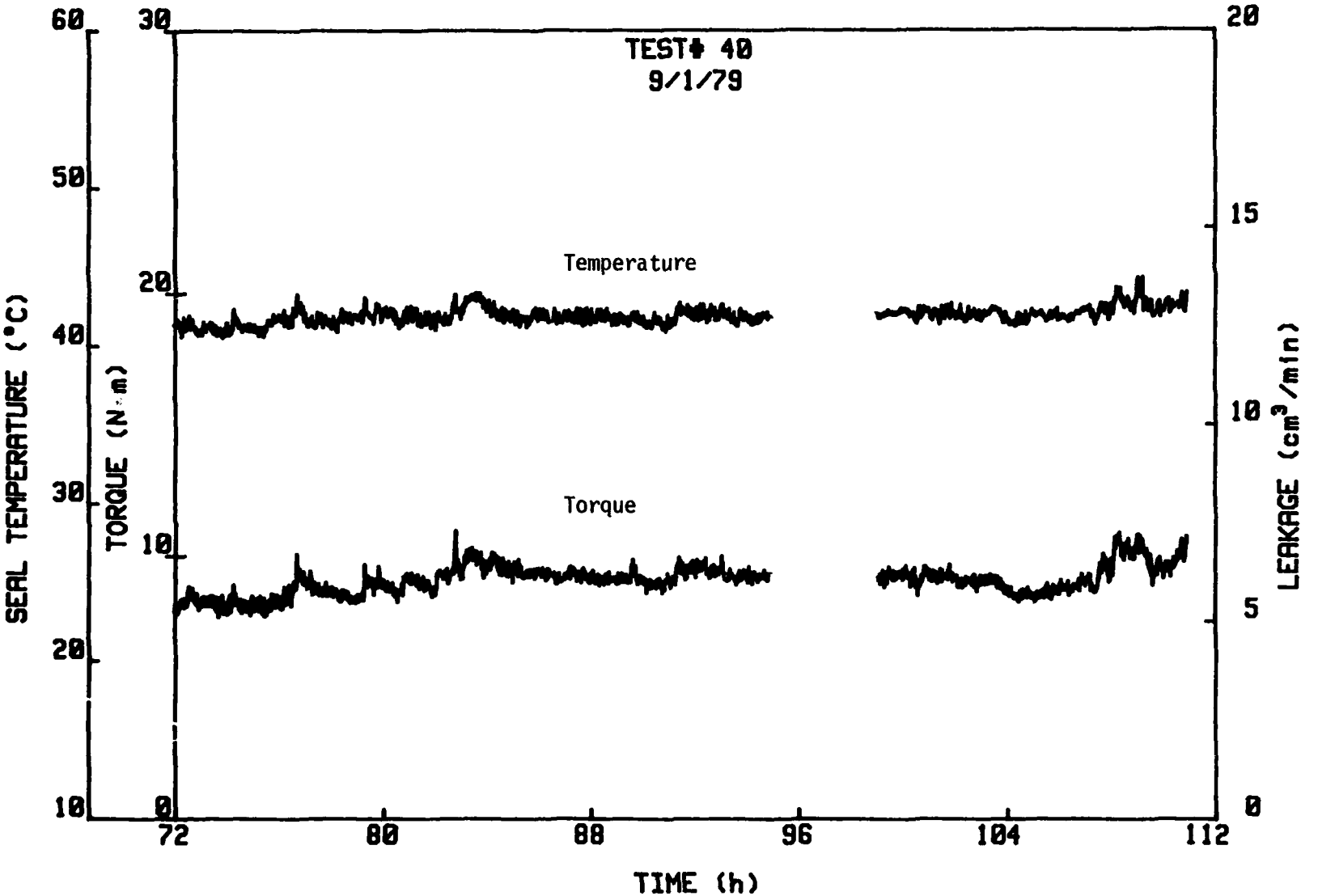

Figure C-3, cont.

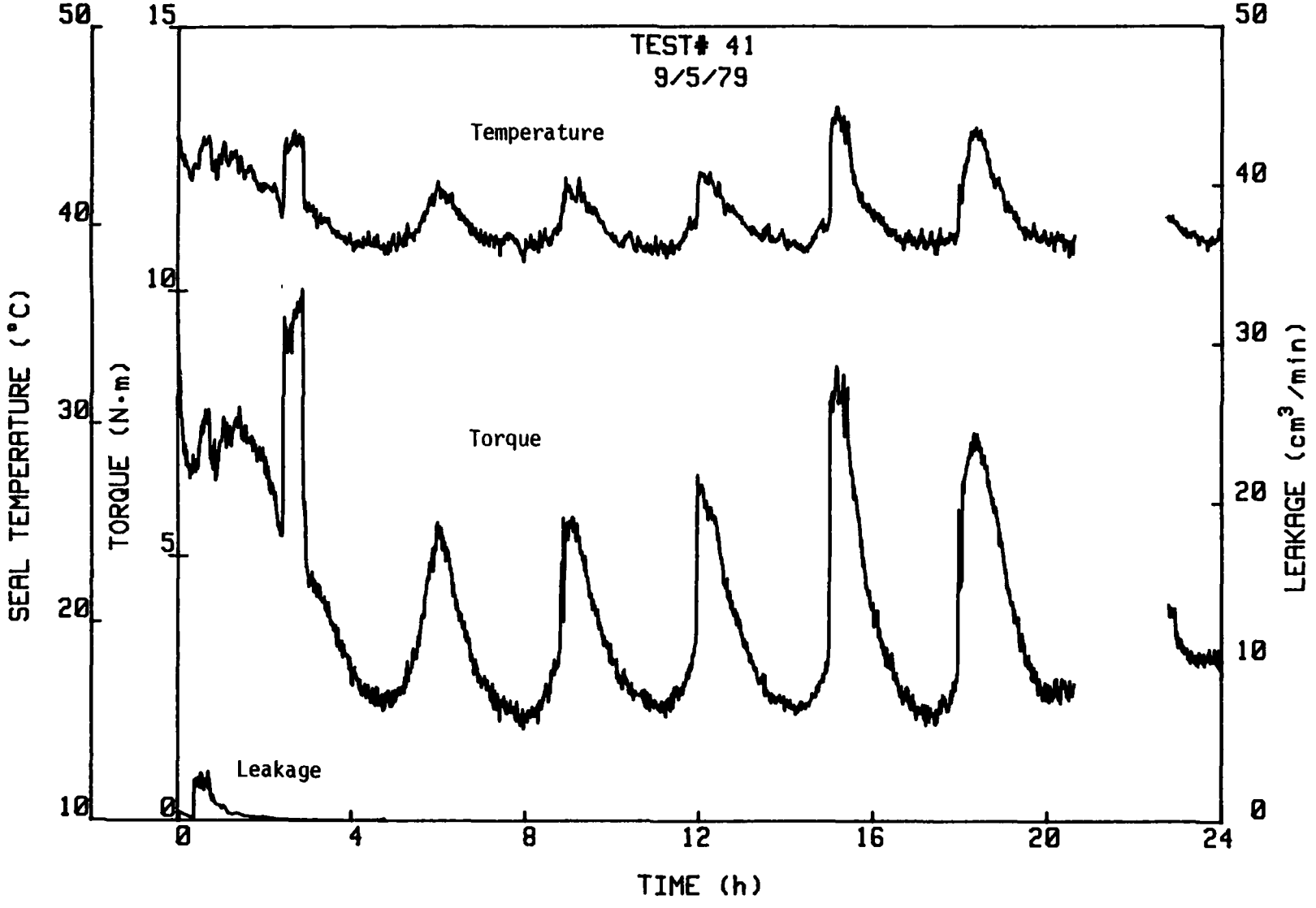

Figure C-4. Test #41, 1800 RPM, p_{H_2O} = 3.45 MPa, p_g = 3.45 MPa.

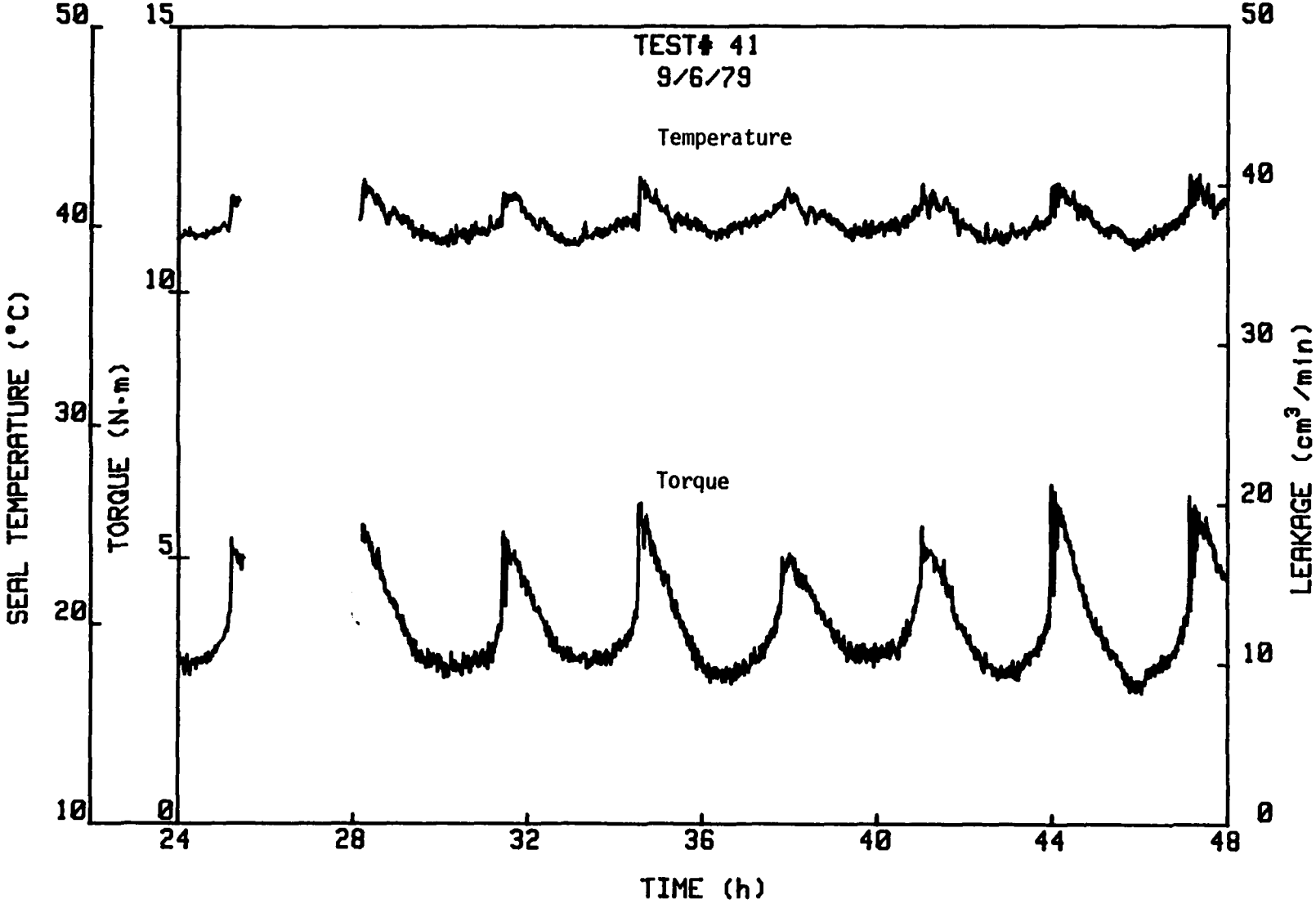

Figure C-4, cont.

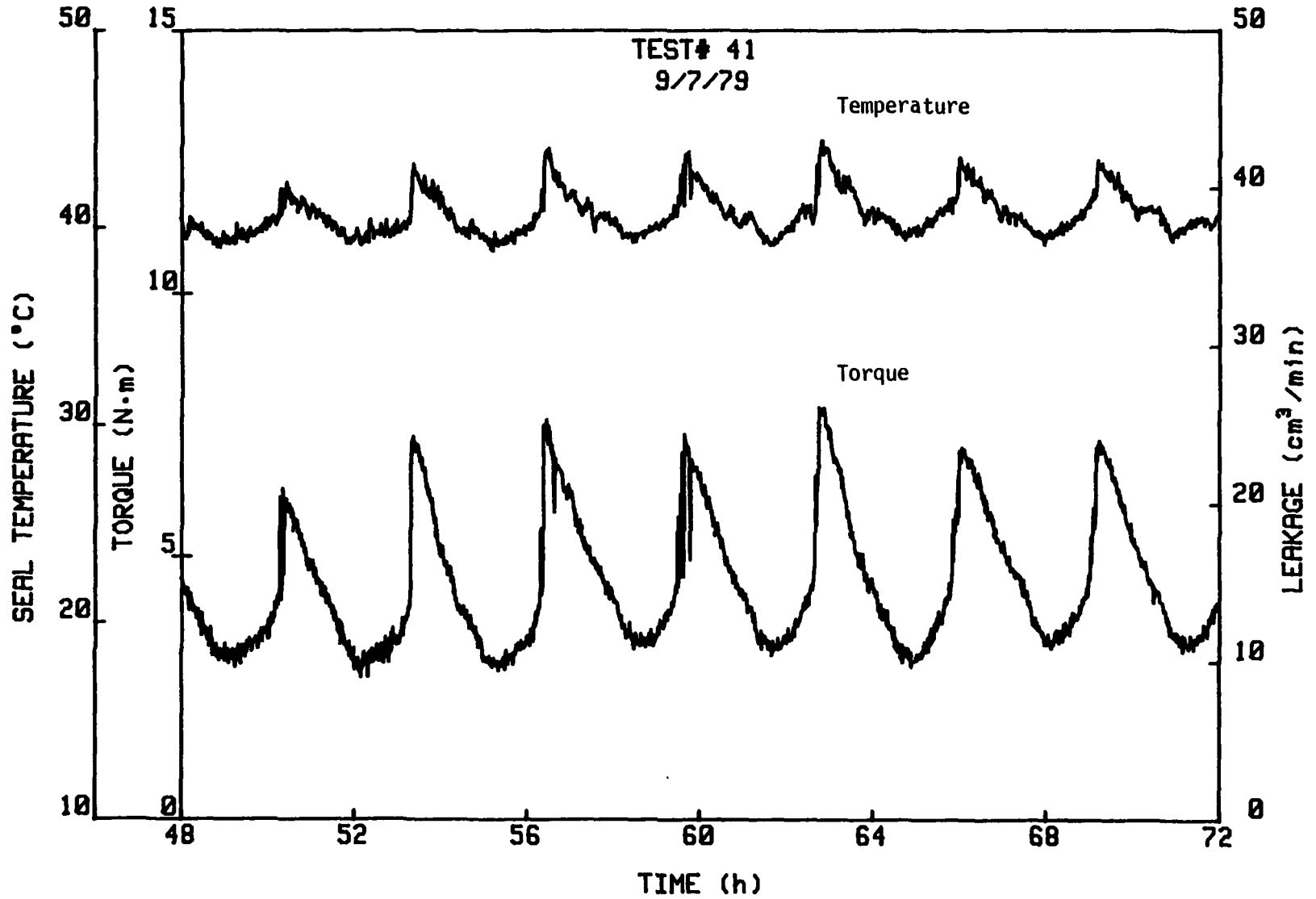

Figure C-4, cont.

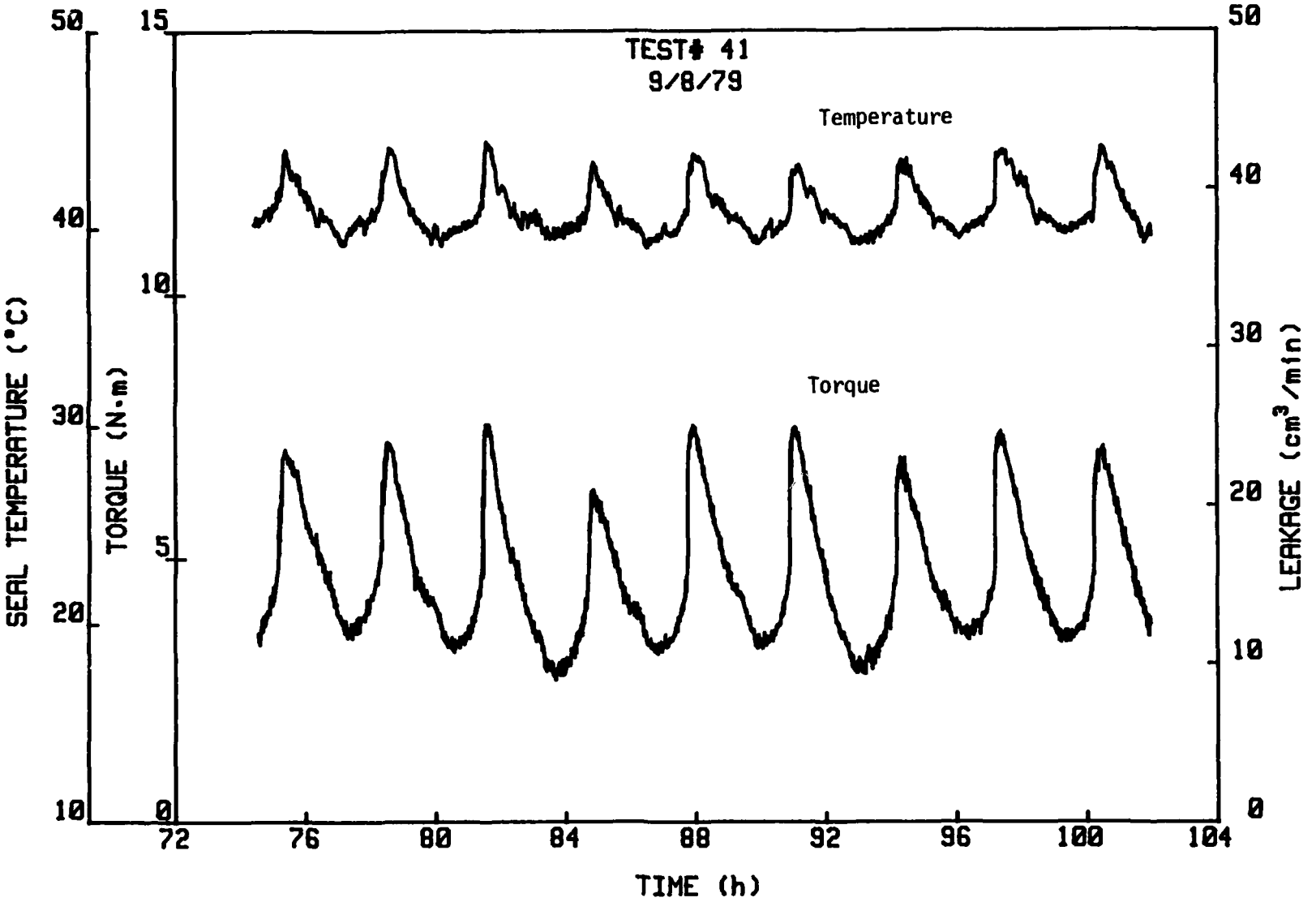

Figure C-4, cont.

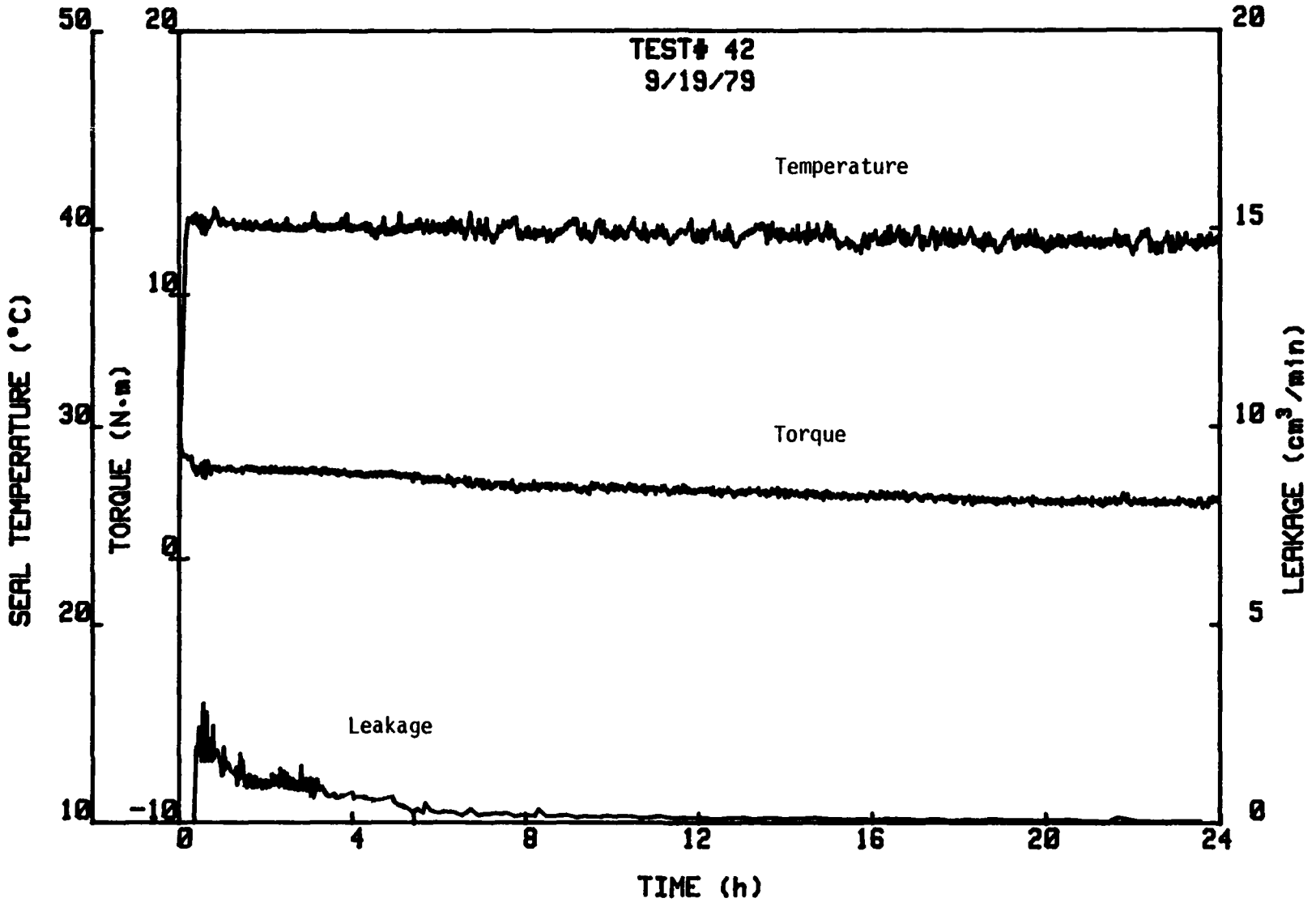

Figure C-5. Test #42, Radial Taper, 1800 RPM, p_{H_2O} = 3.45 MPa.

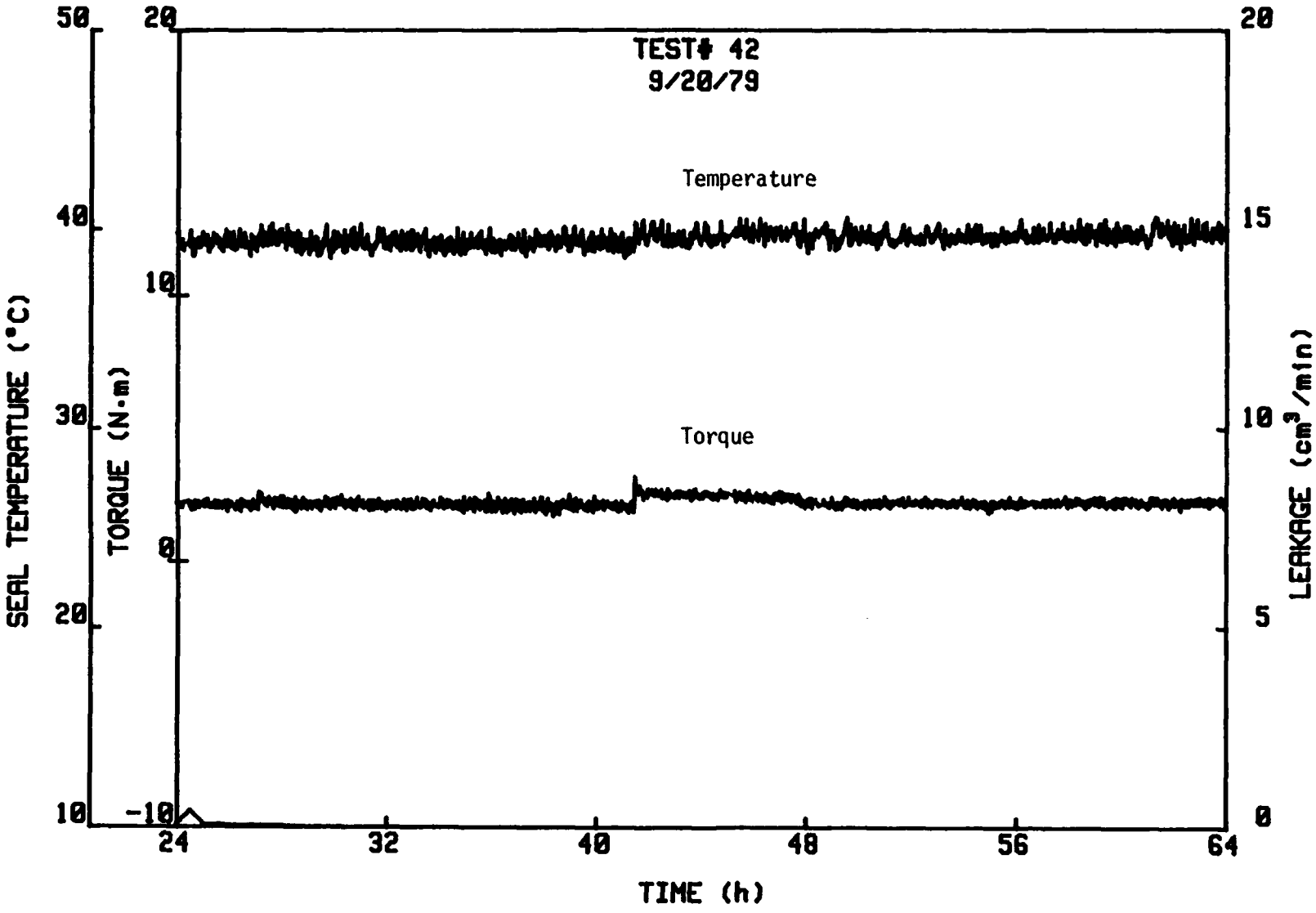

Figure C-5, cont.

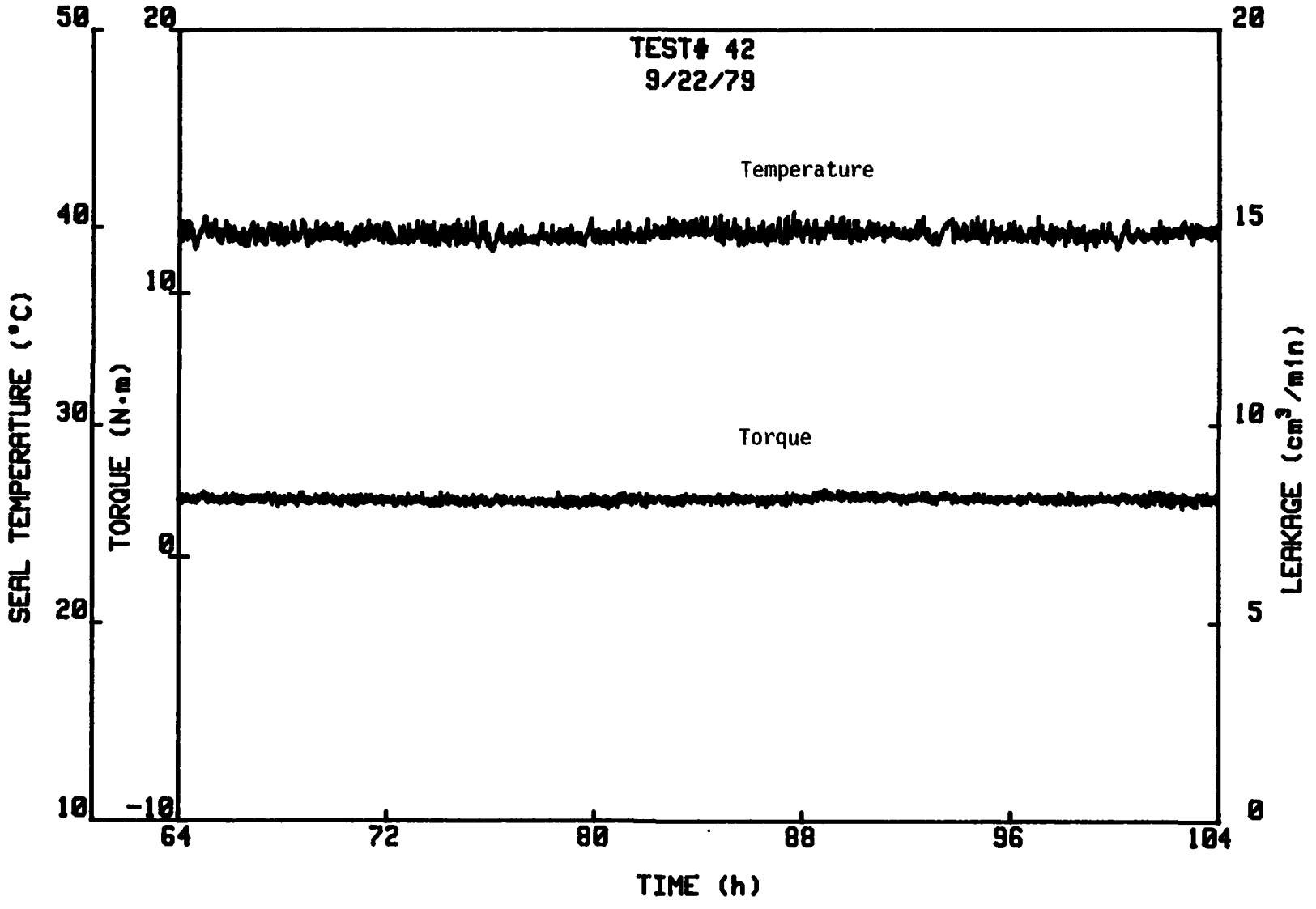

Figure C-5, cont.

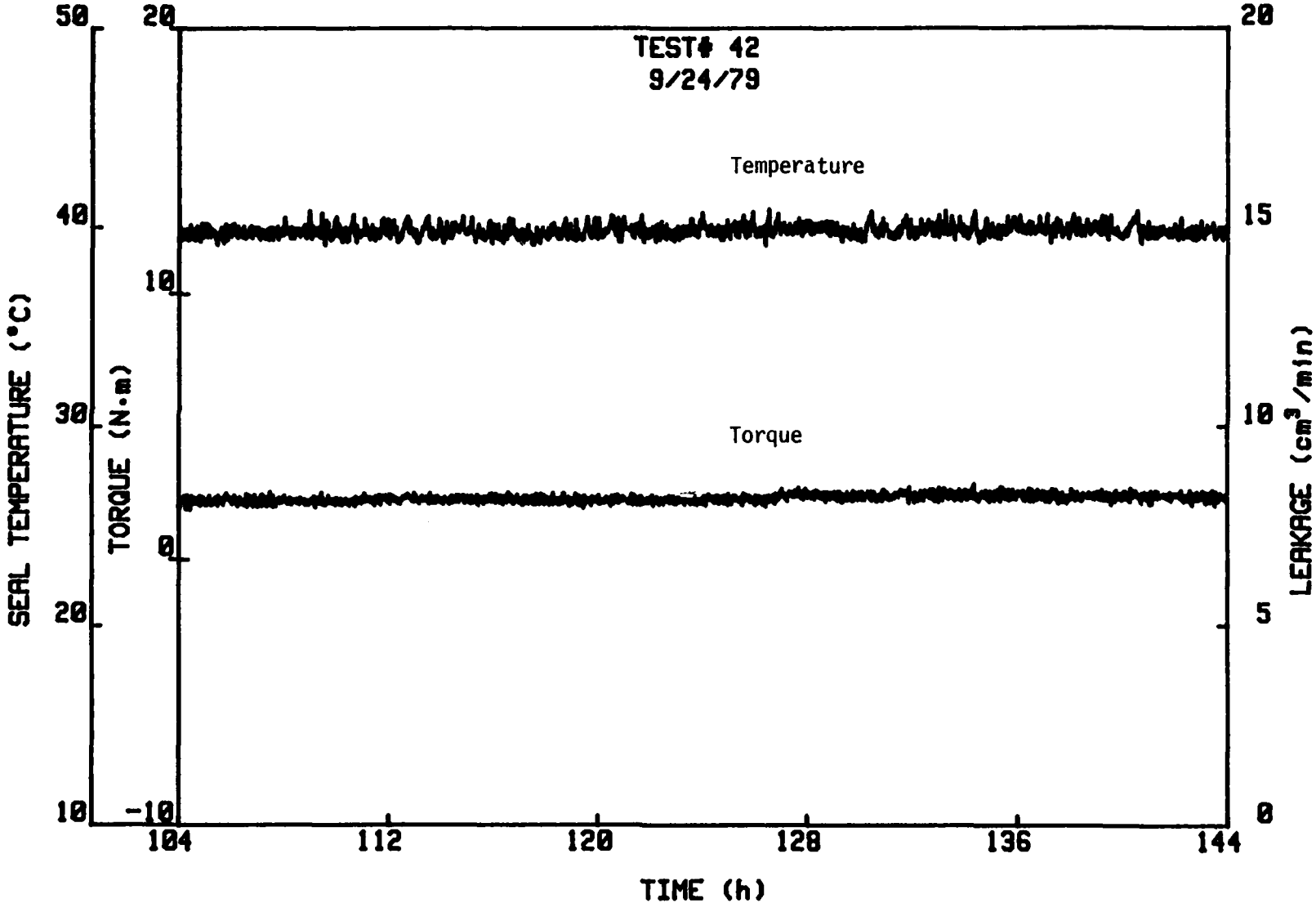

Figure C-5, cont.

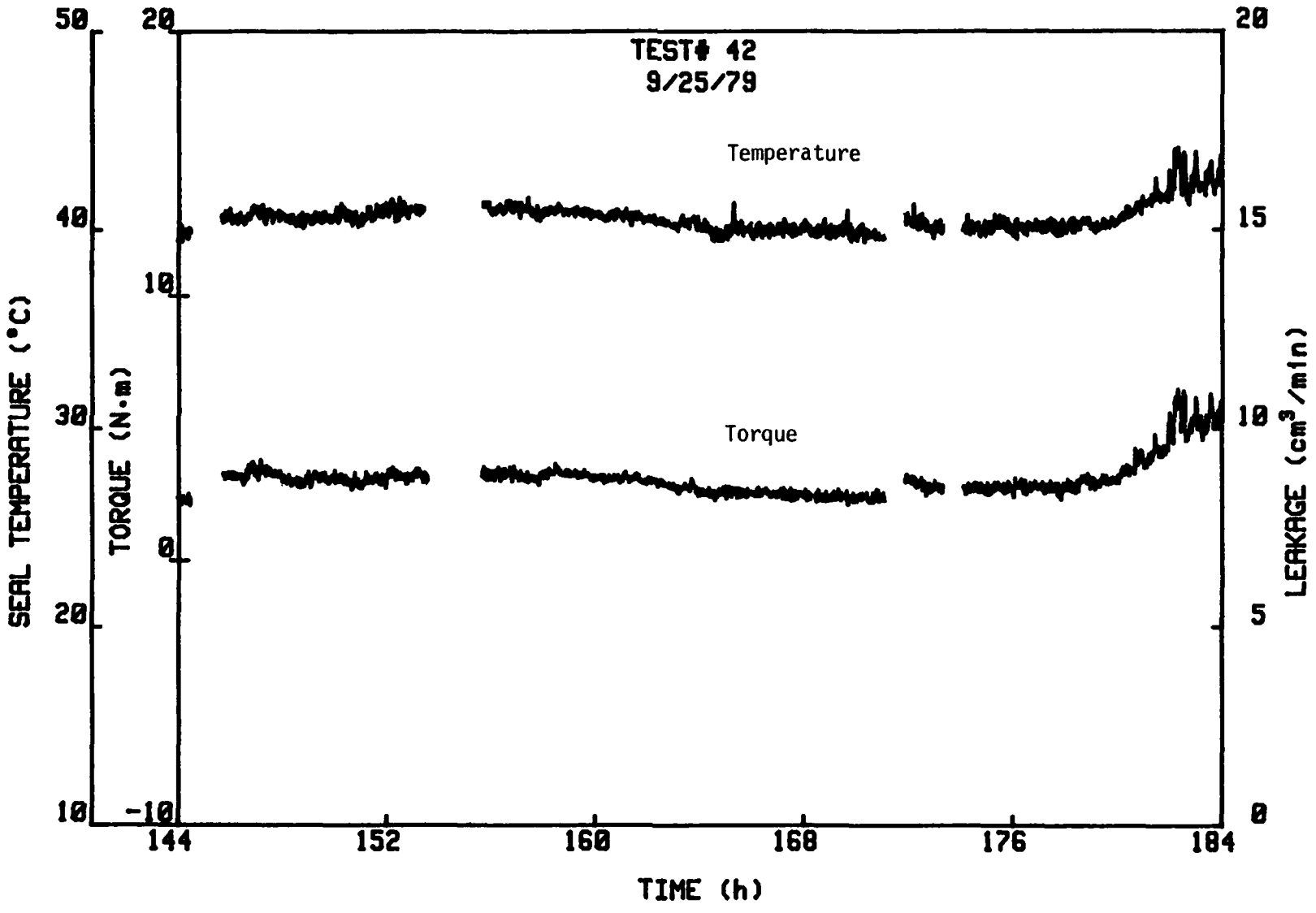

Figure C-5, cont.

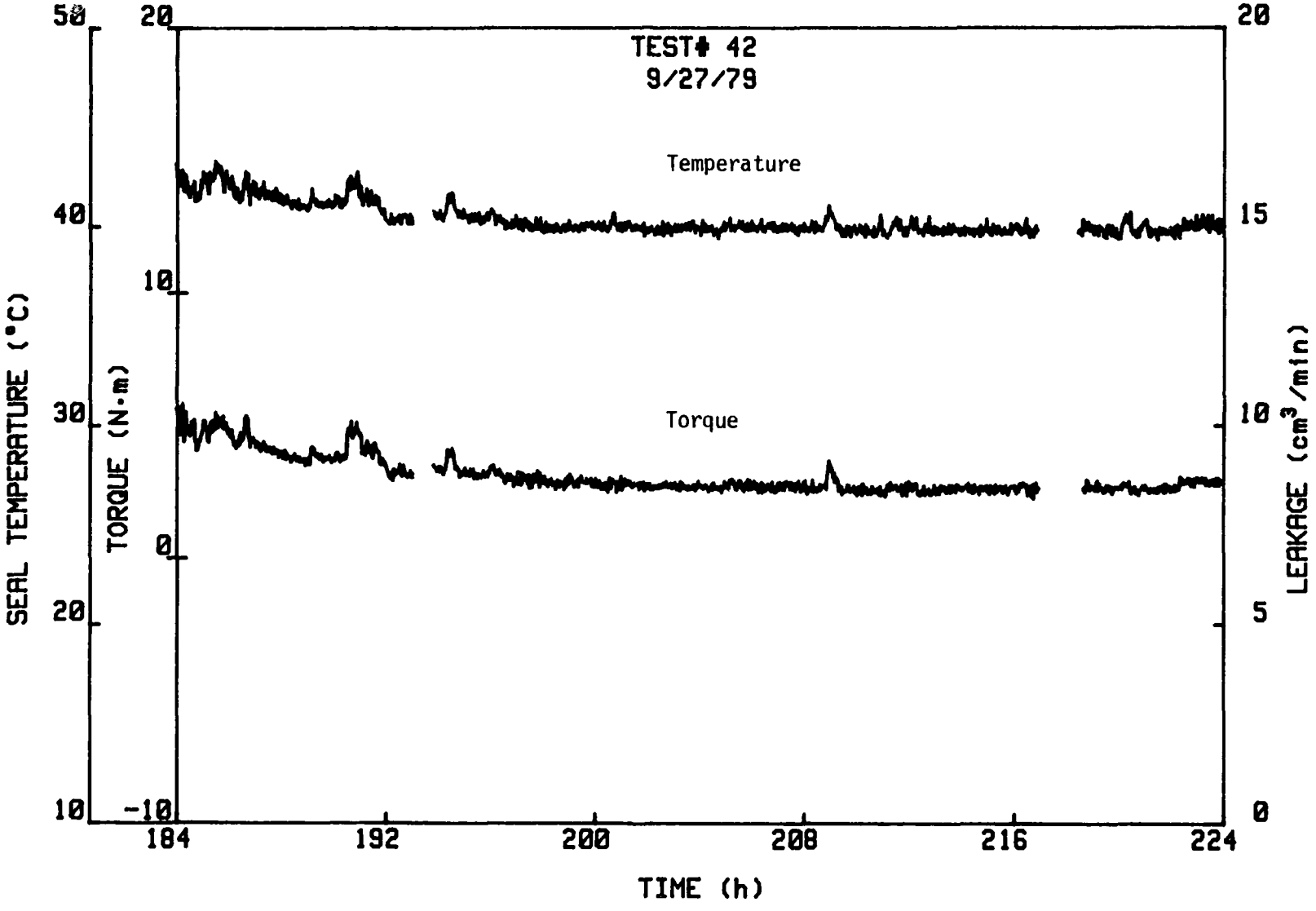

Figure C-5, cont.

AD-A083 933 NEW MEXICO UNIV ALBUQUERQUE DEPT OF MECHANICAL ENGI--ETC F/G 11/1
THE WAVY MECHANICAL FACE SEAL - THEORETICAL AND EXPERIMENTAL RE--ETC(U)
JAN 80 A O LEBECK, L A YOUNG N00014-76-C-0071
UNCLASSIFIED ME-105(80)ONR-414-1 NL

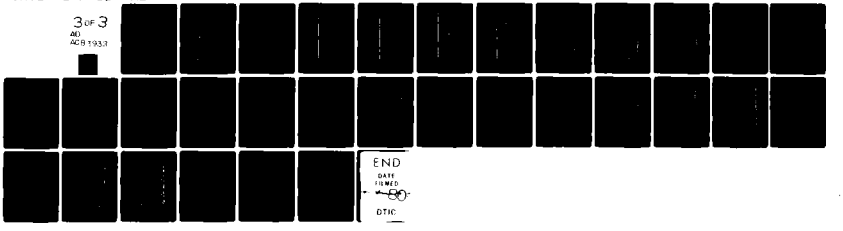

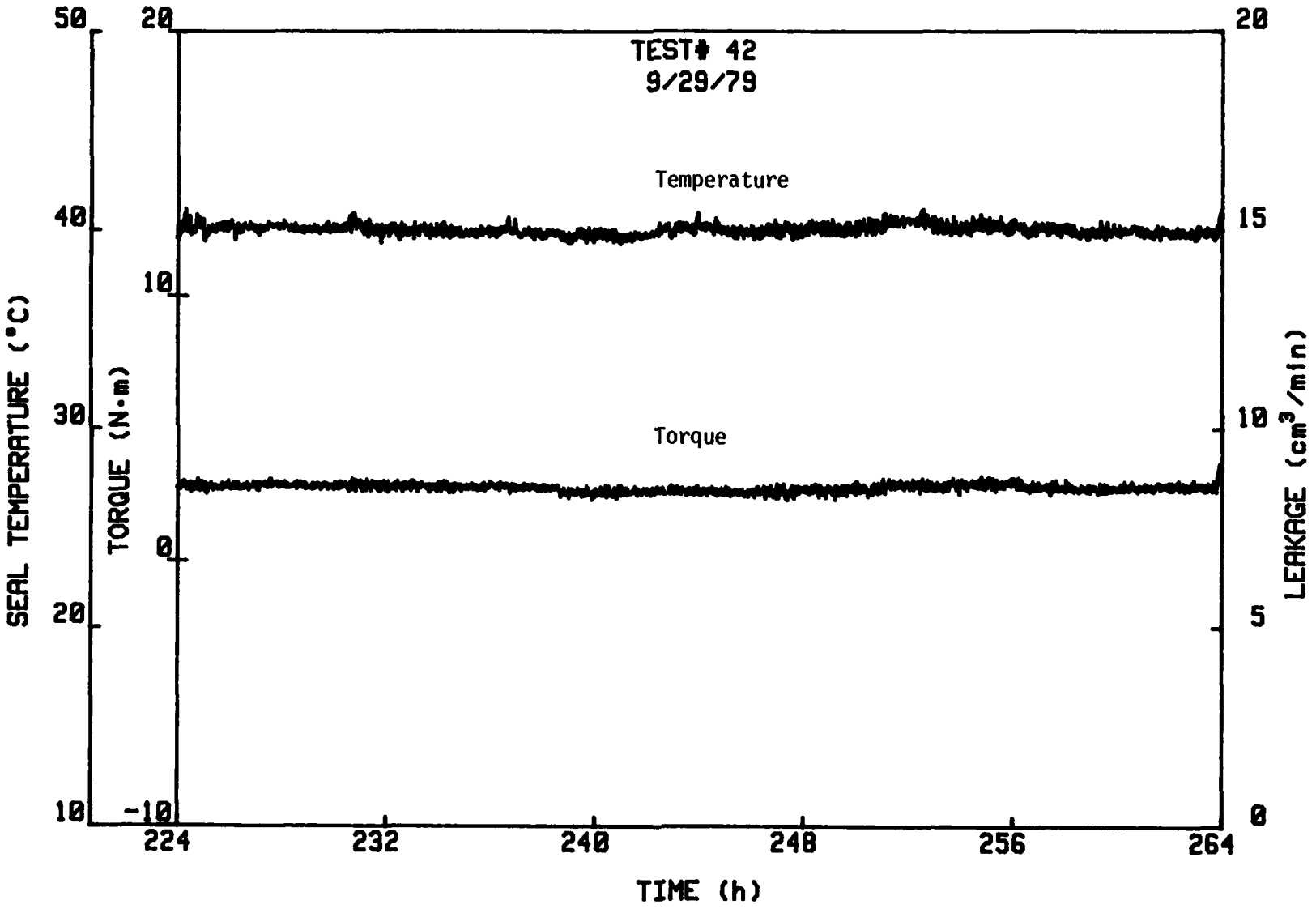

Figure C-5, cont.

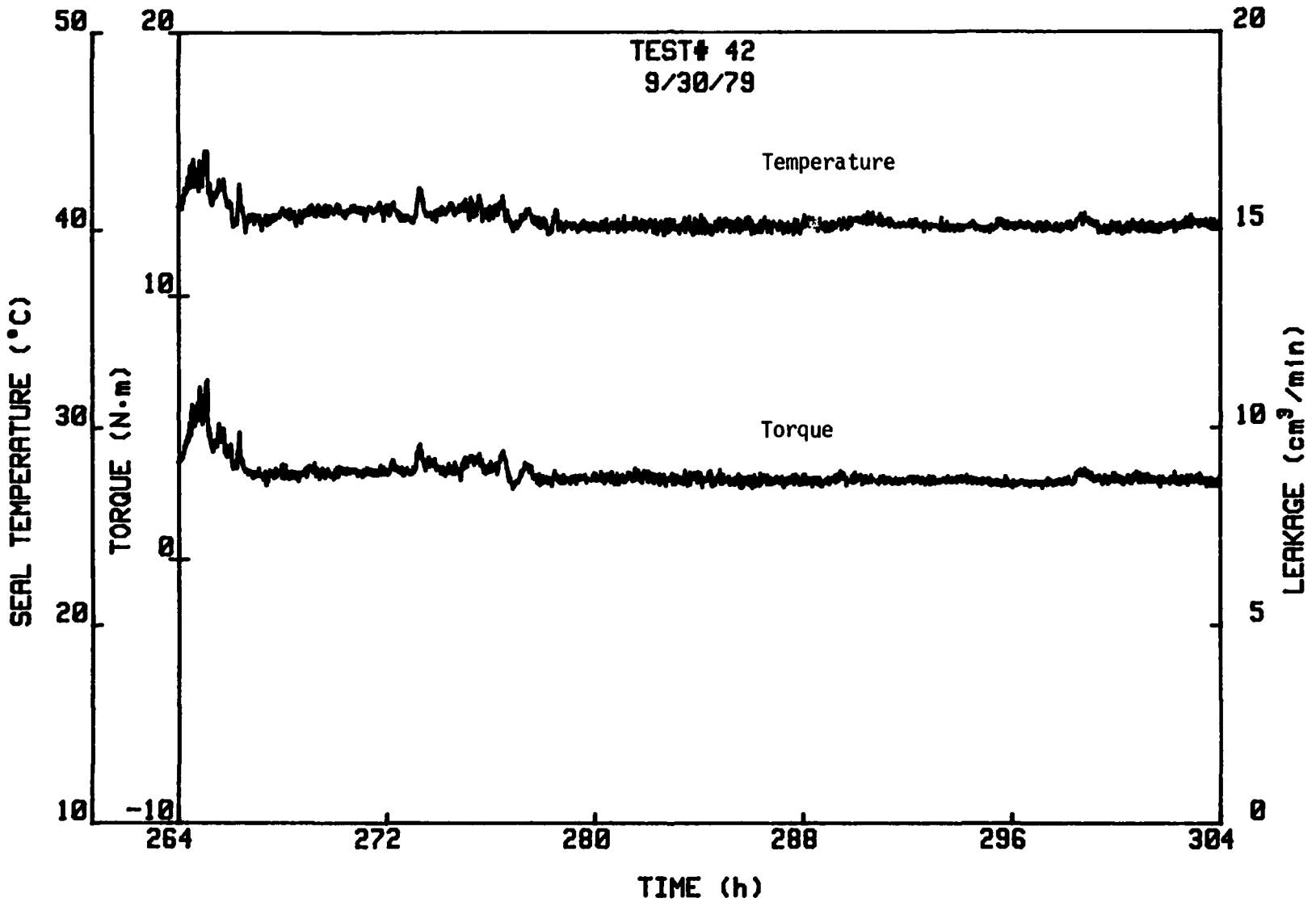

Figure C-5, cont.

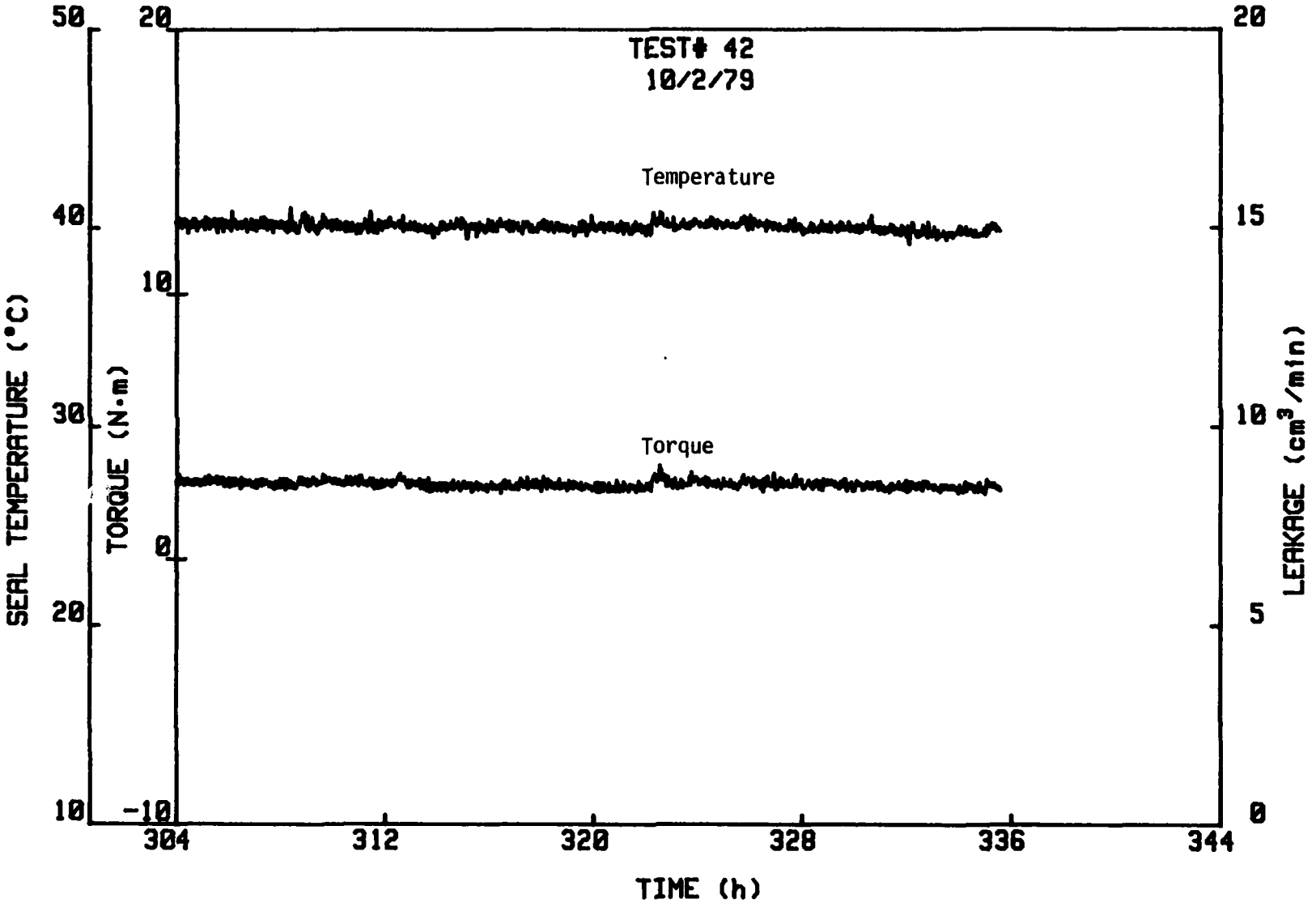

Figure C-5,cont.

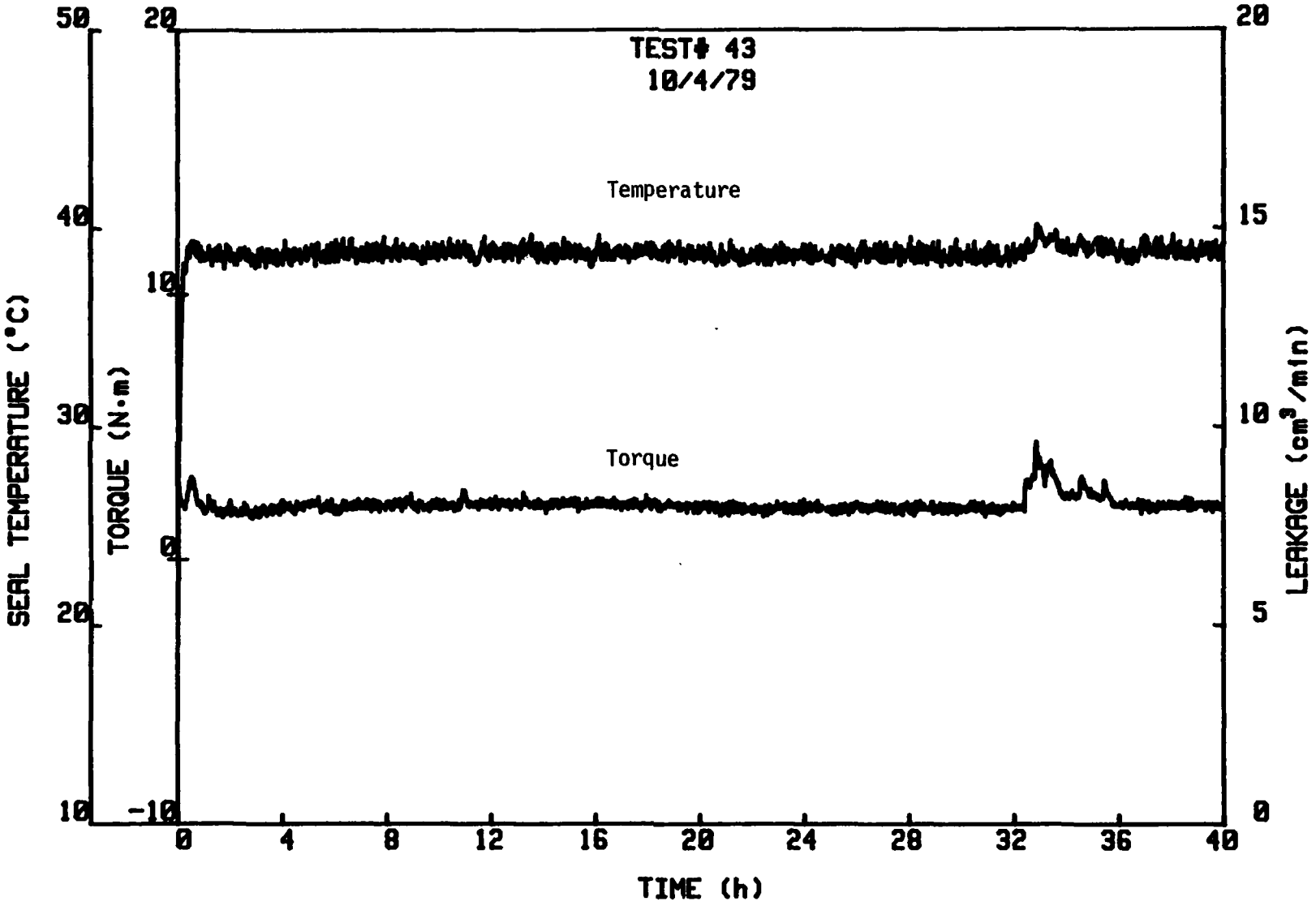

Figure C-6. Test # 43, Radial Taper, 1800 RPM, p_{H_2O} = 3.45 MPa.

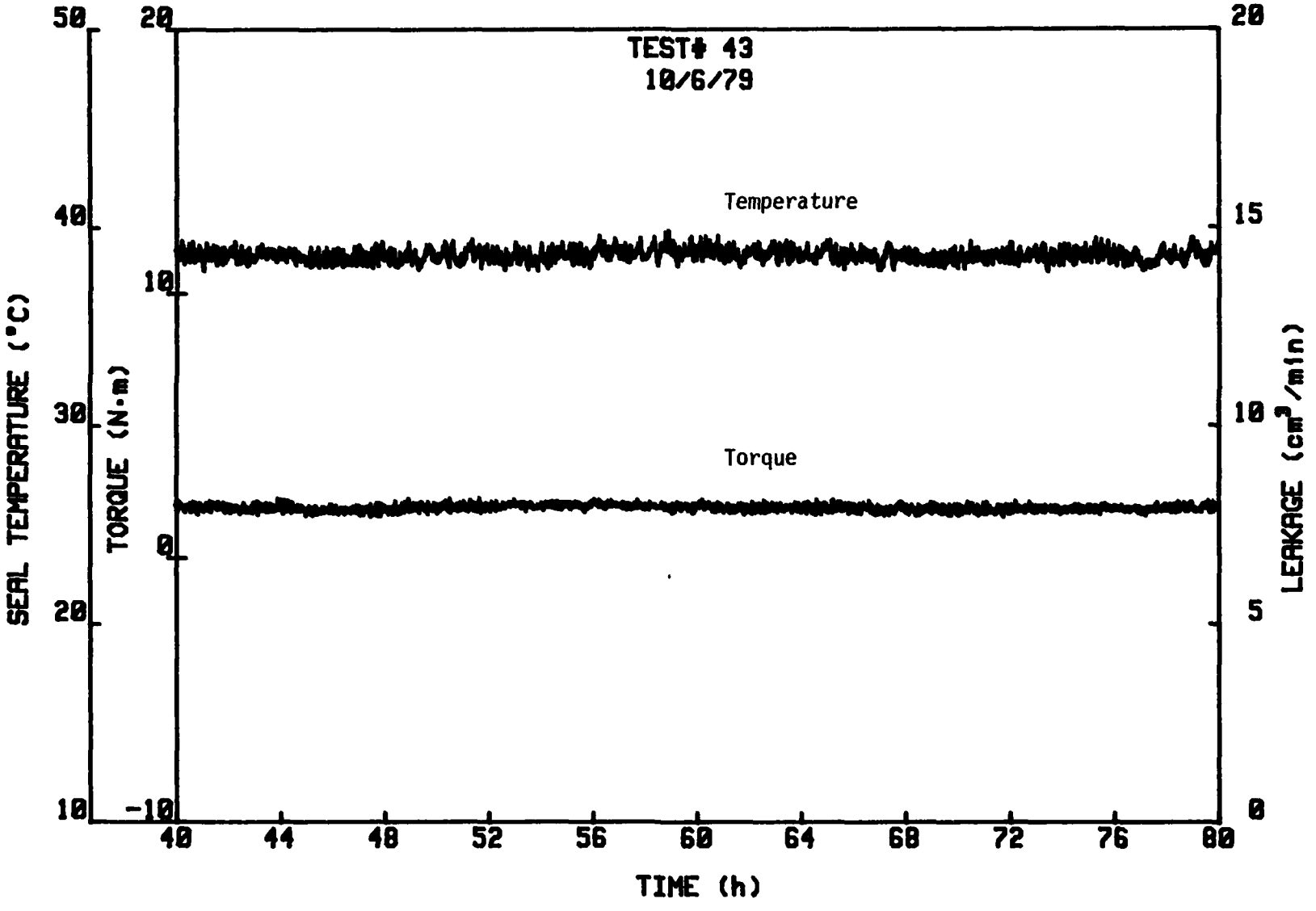

Figure C-6, cont.

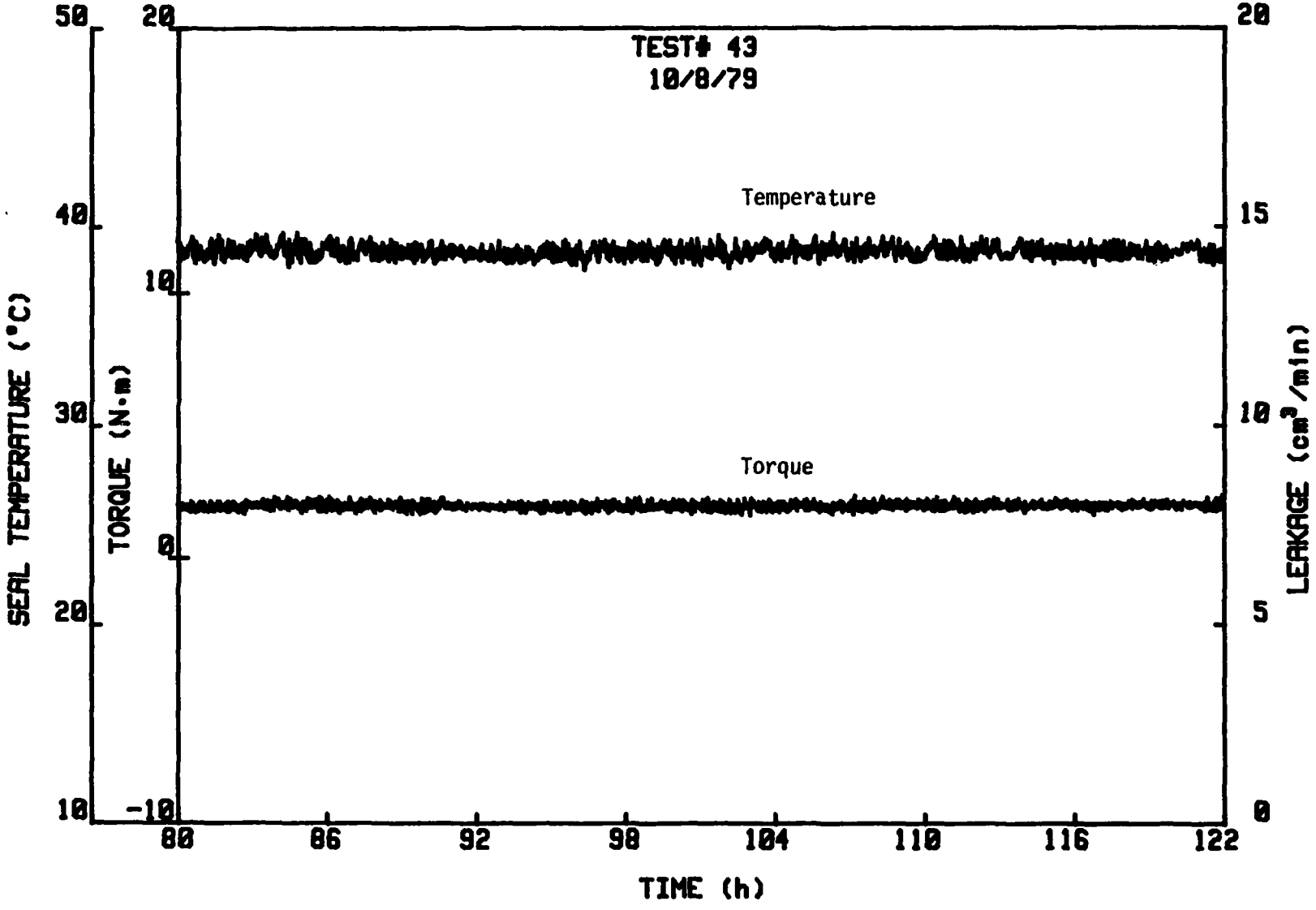

Figure C-6, cont.

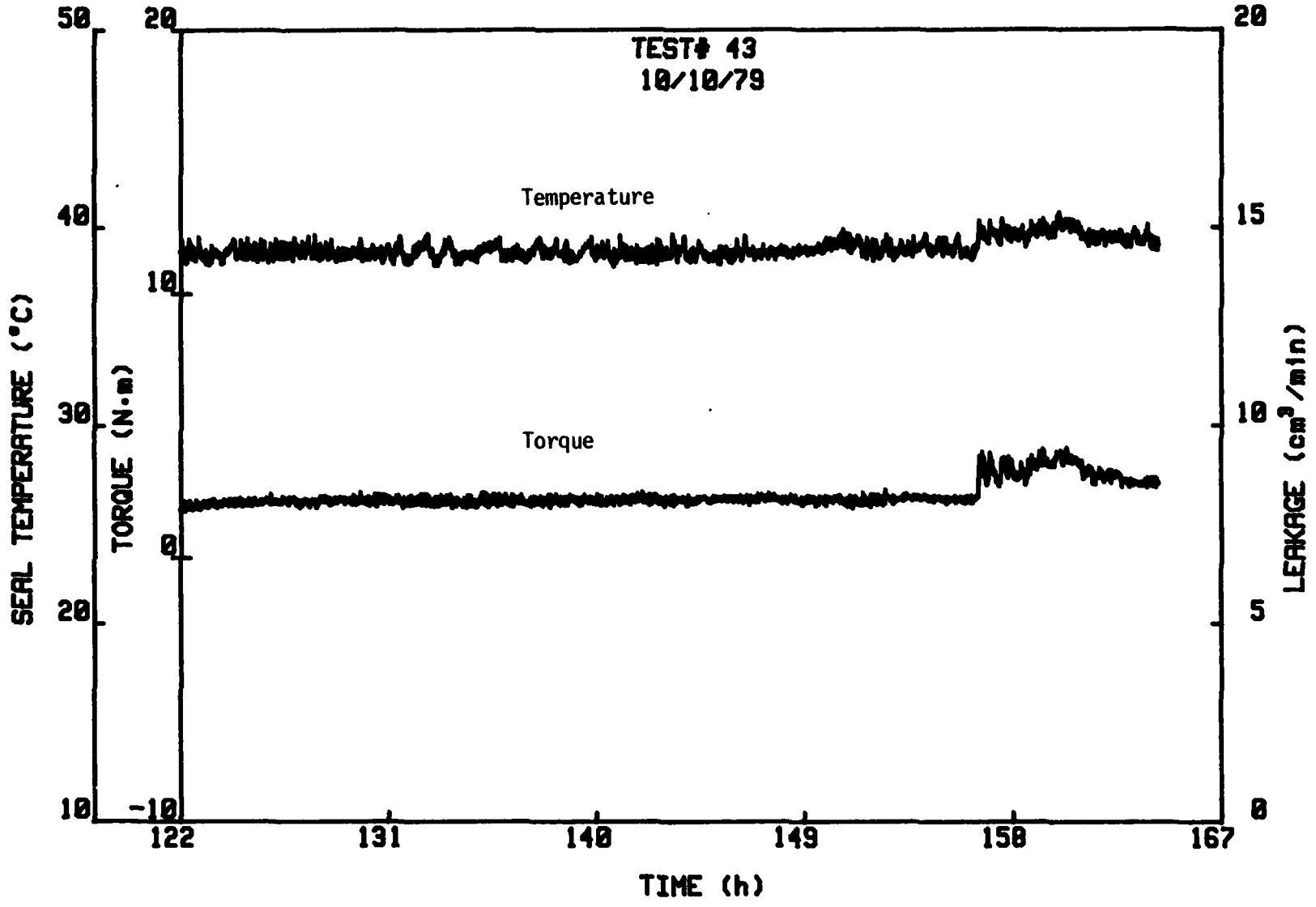

Figure C-6,cont.

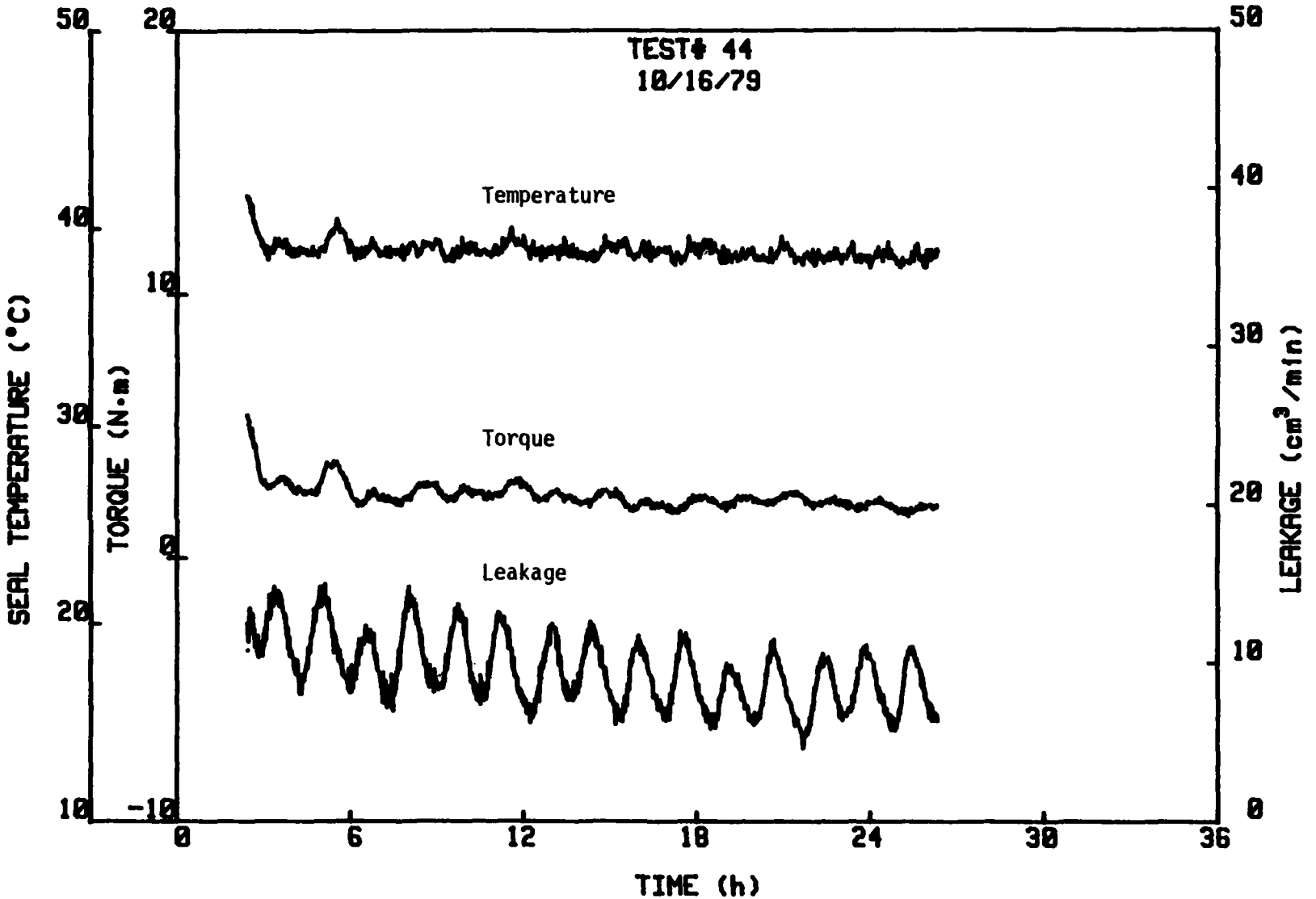

Figure C-7. Test #44, 1800 RPM, p_{H_2O} = 3.45 MPa, p_g = 8.3 MPa.

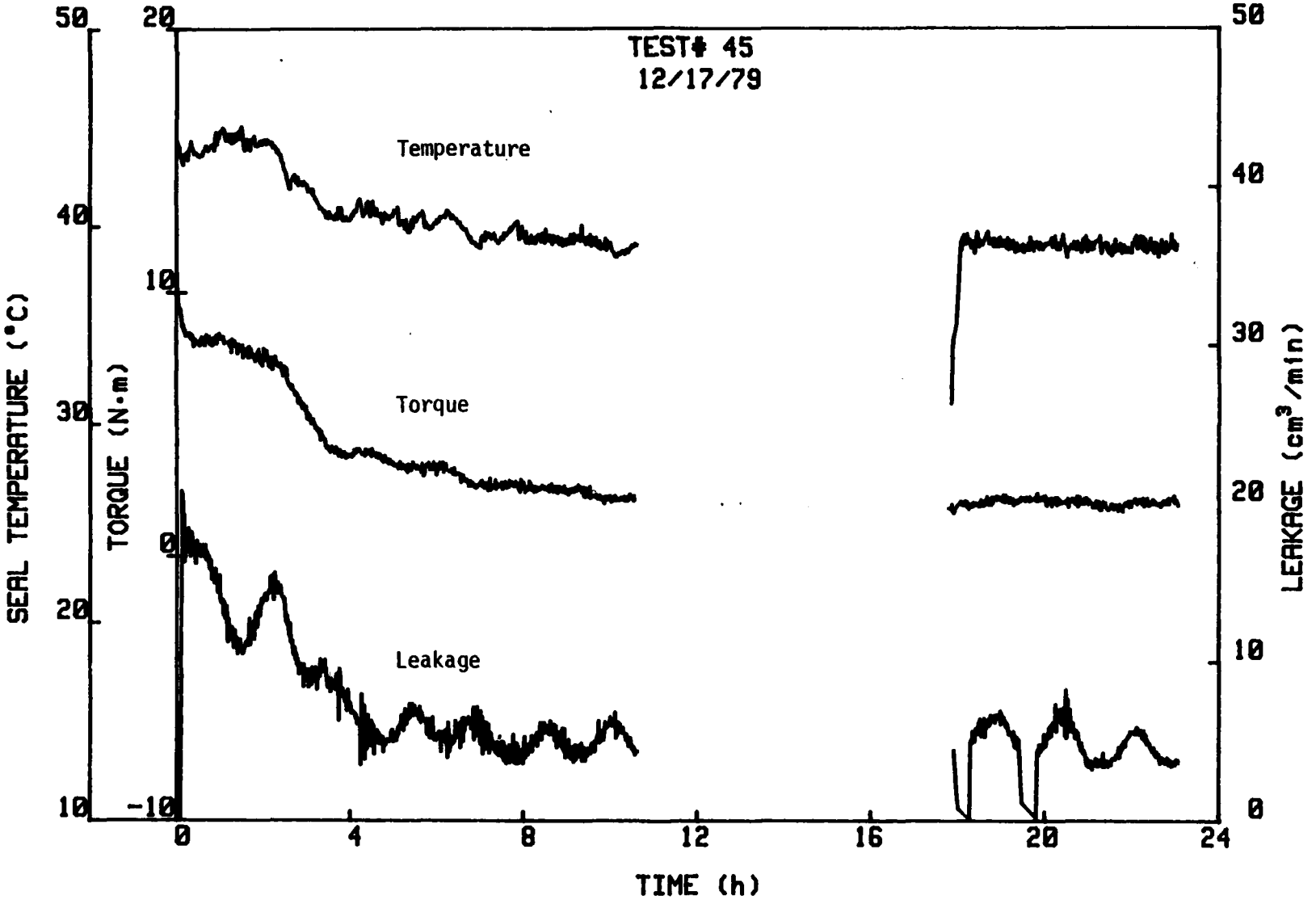

Figure C-8. Test #45, 1800 RPM, P_{H_2O} = 3.45 MPa, P_g = 6.9 MPa.

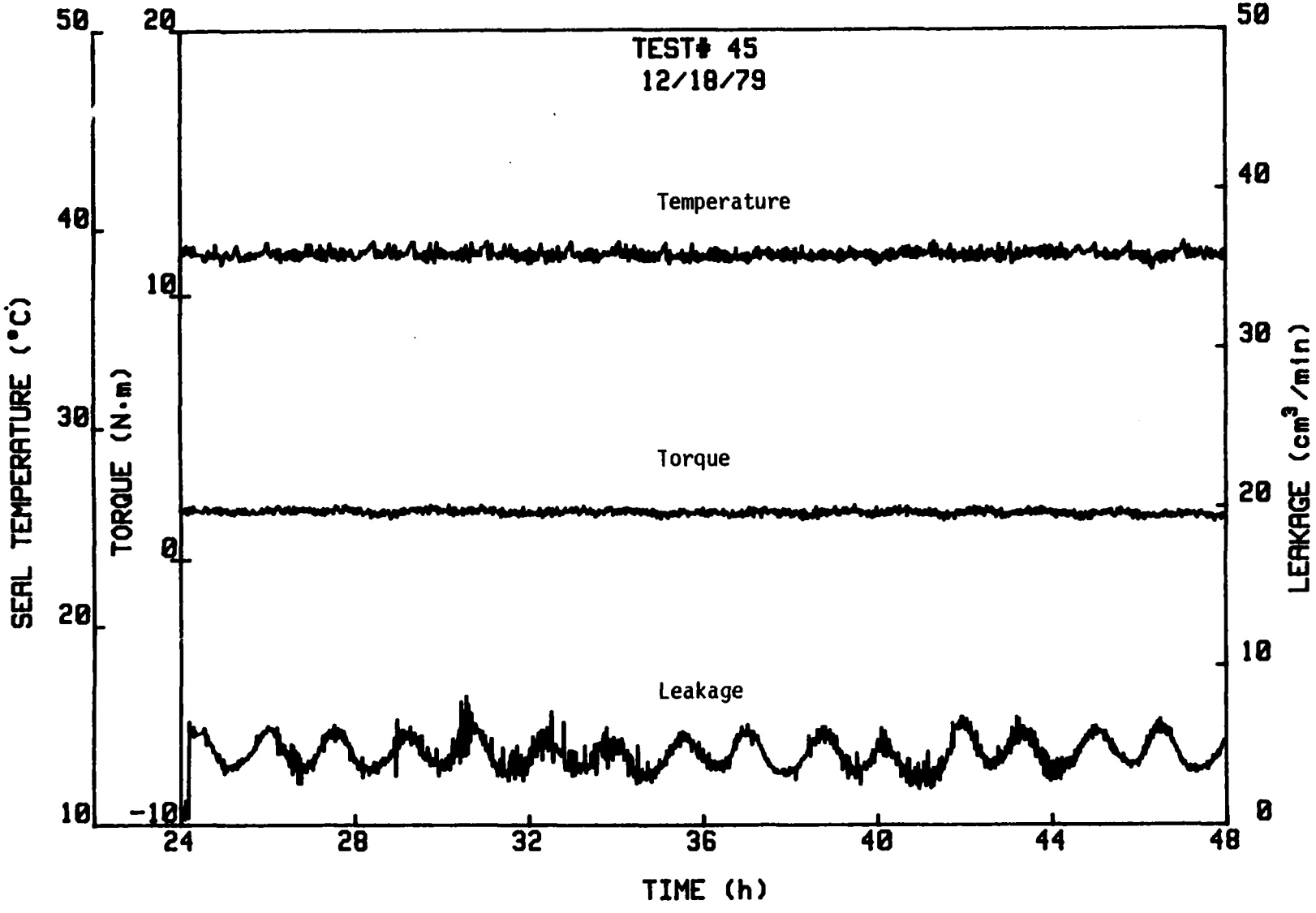

Figure C-8, cont.

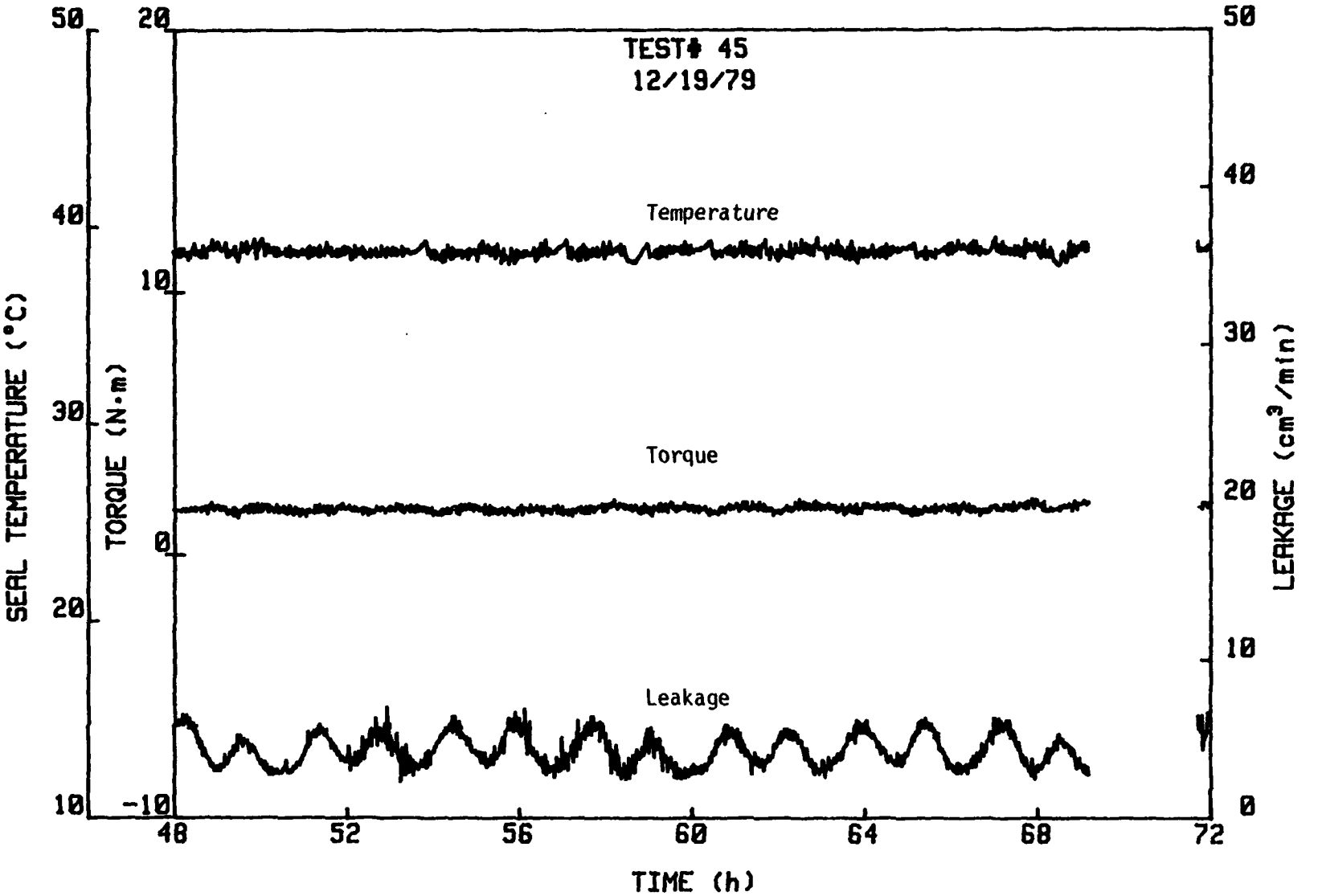

Figure C-8, cont.

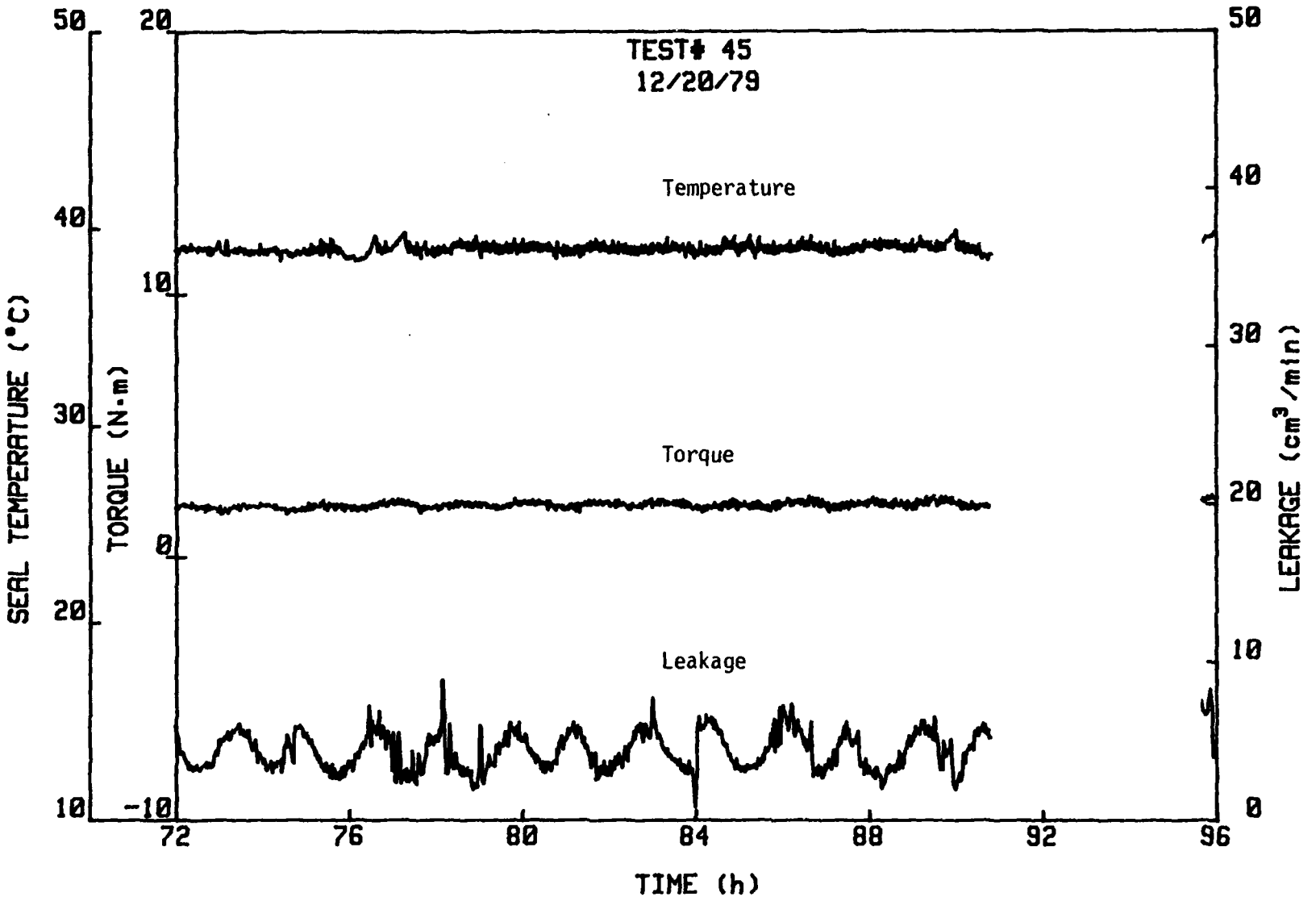

Figure C-8, cont.

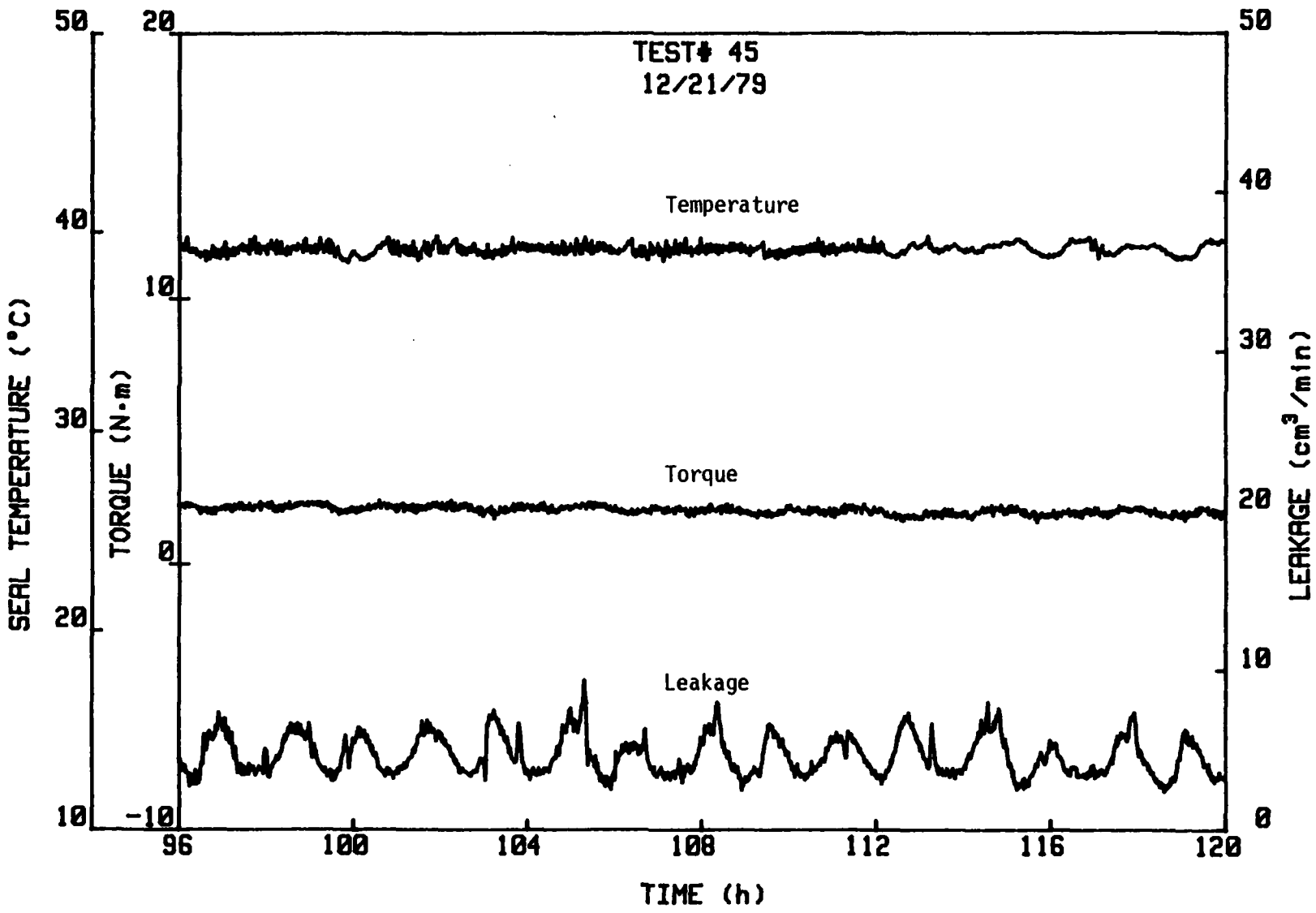

Figure C-8, cont.

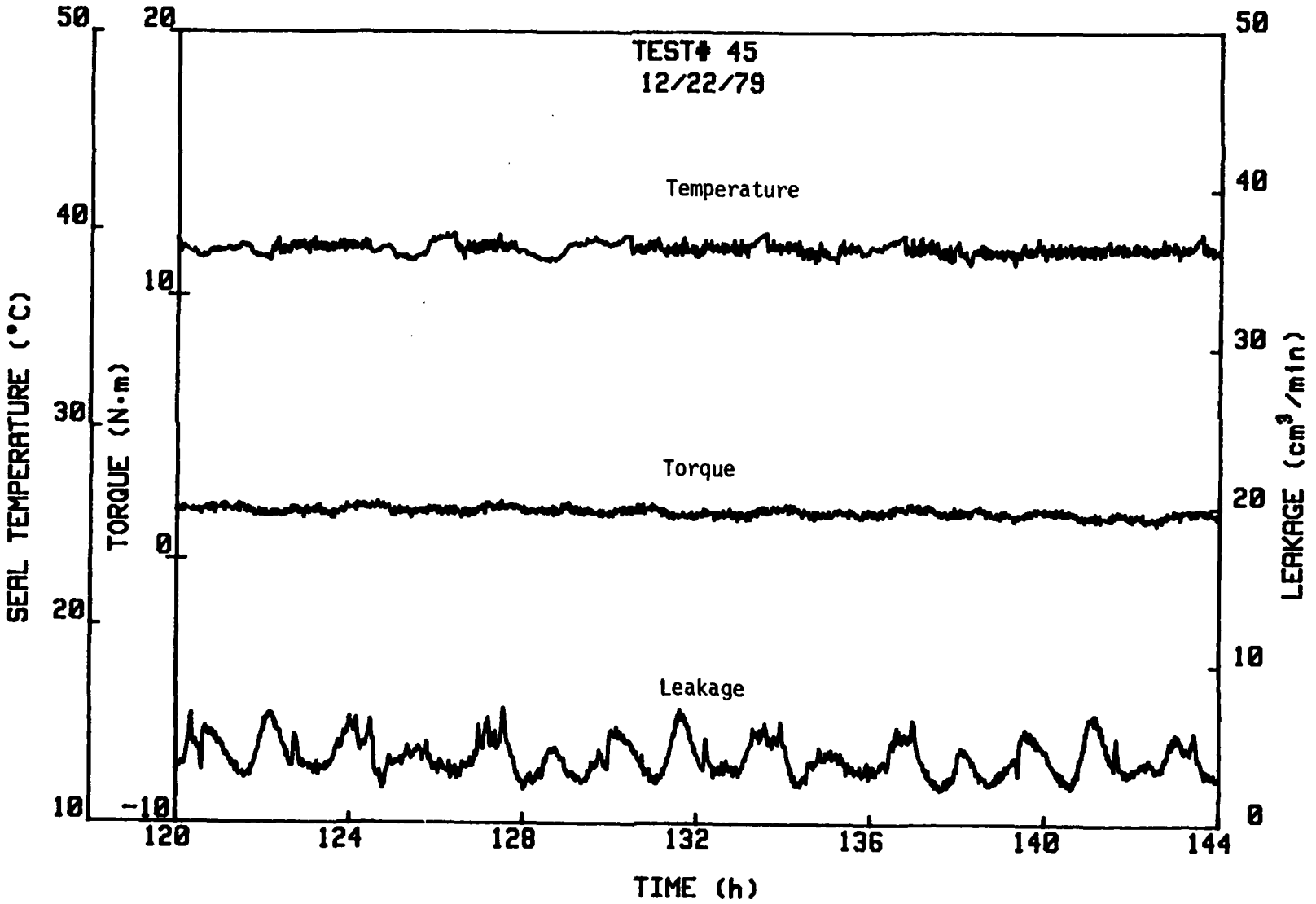

Figure C-8, cont.

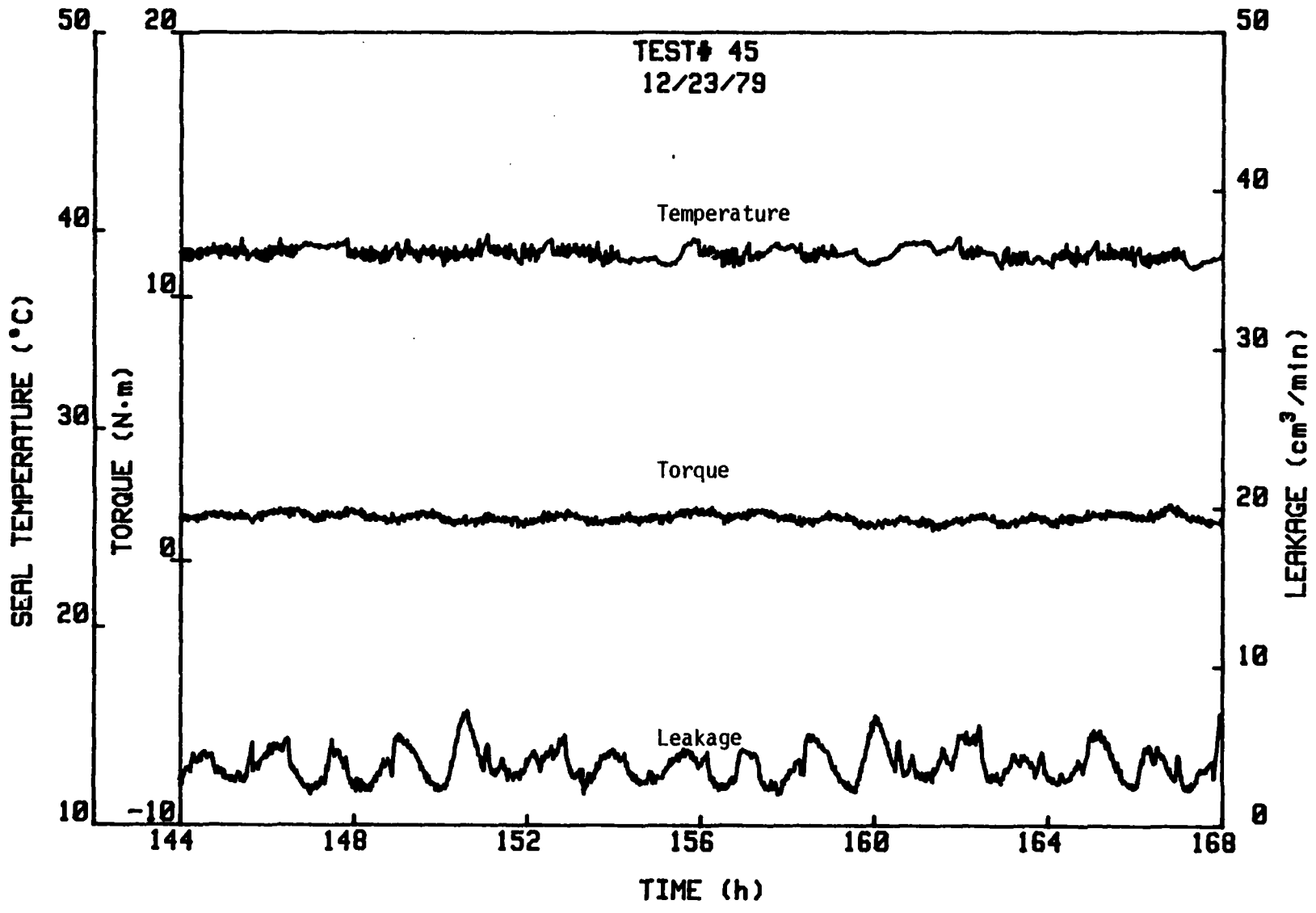

Figure C-8, cont.

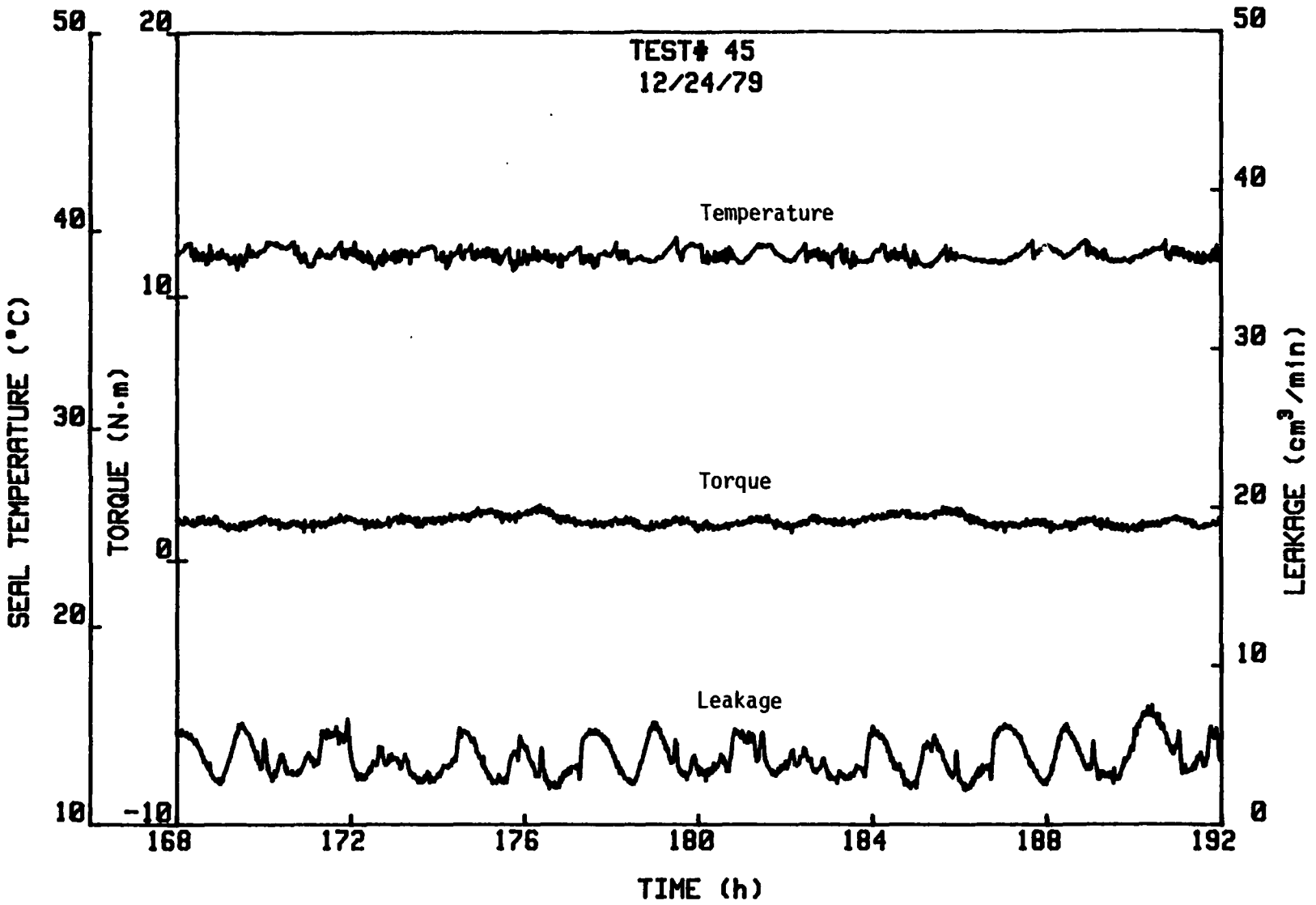

Figure C-8, cont.

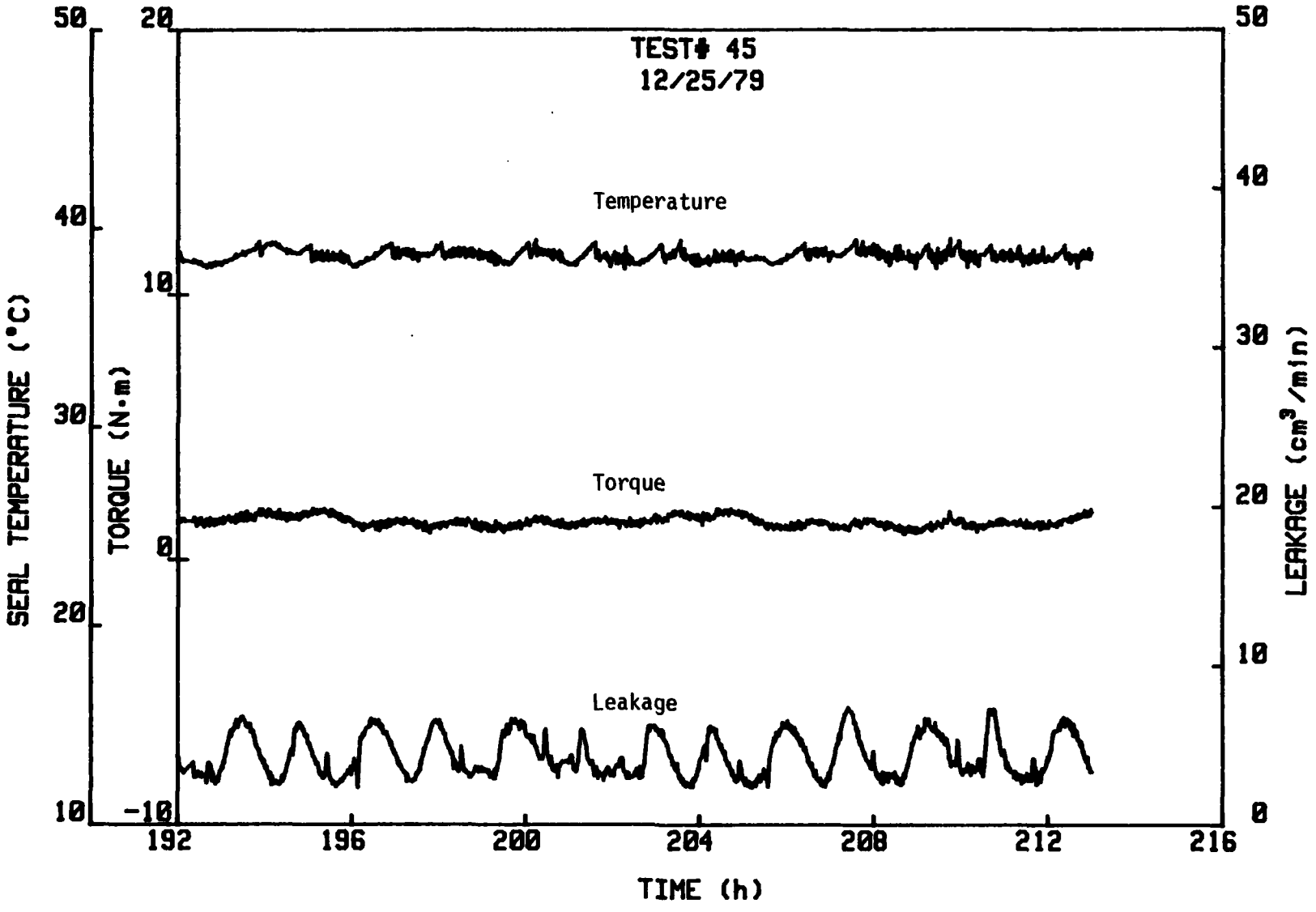

Figure C-8, cont.

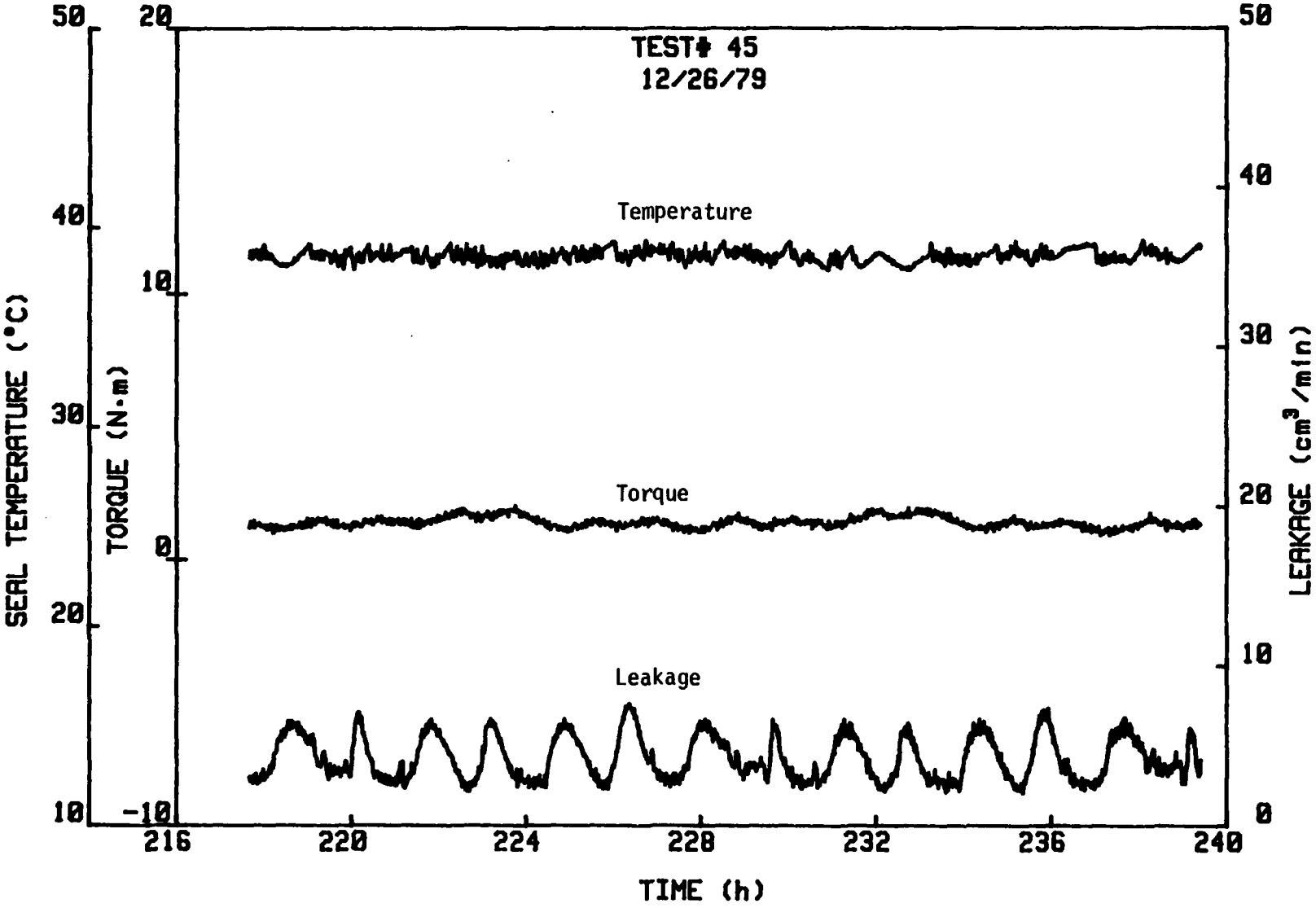

Figure C-8, cont.

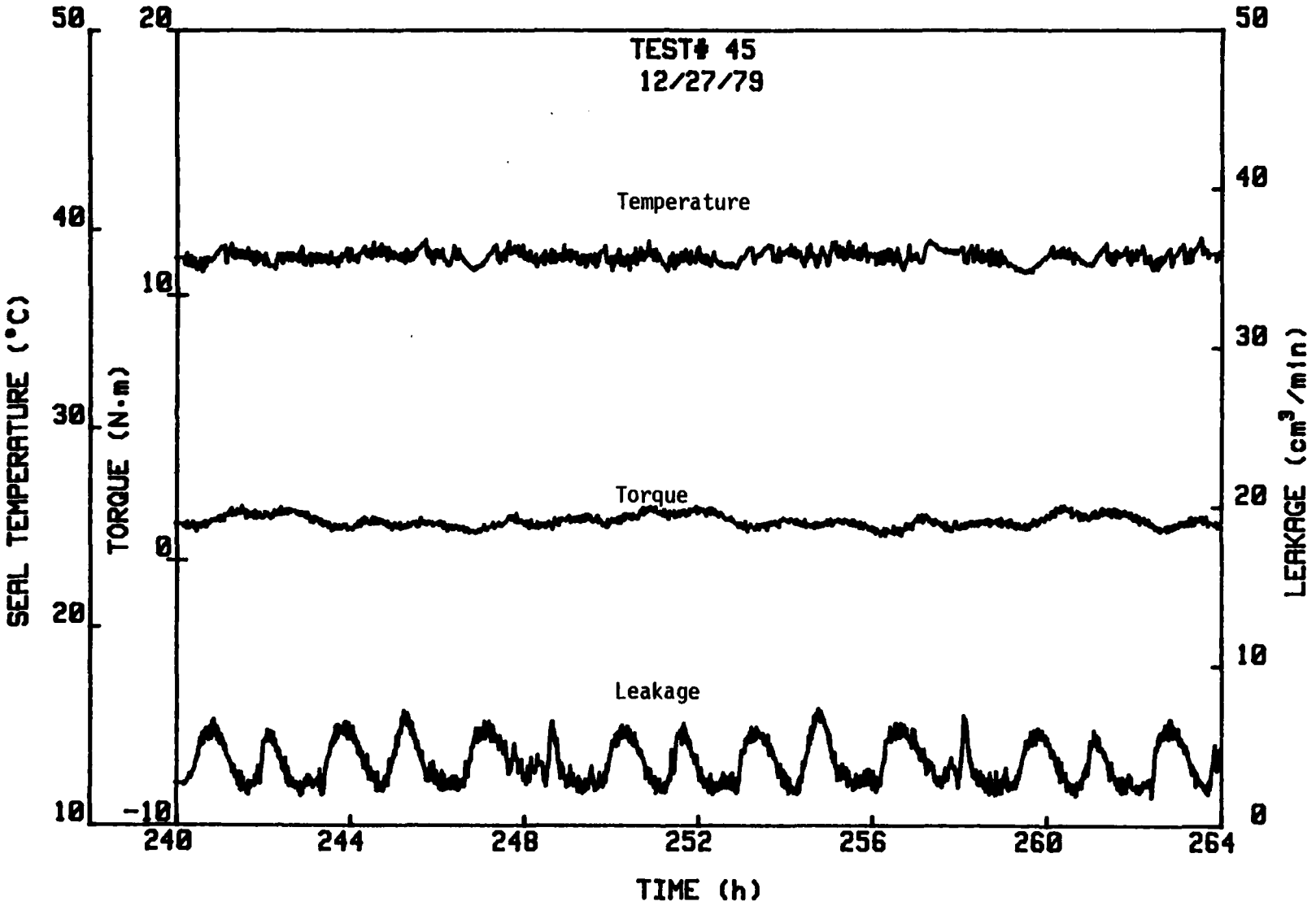

Figure C-8, cont.

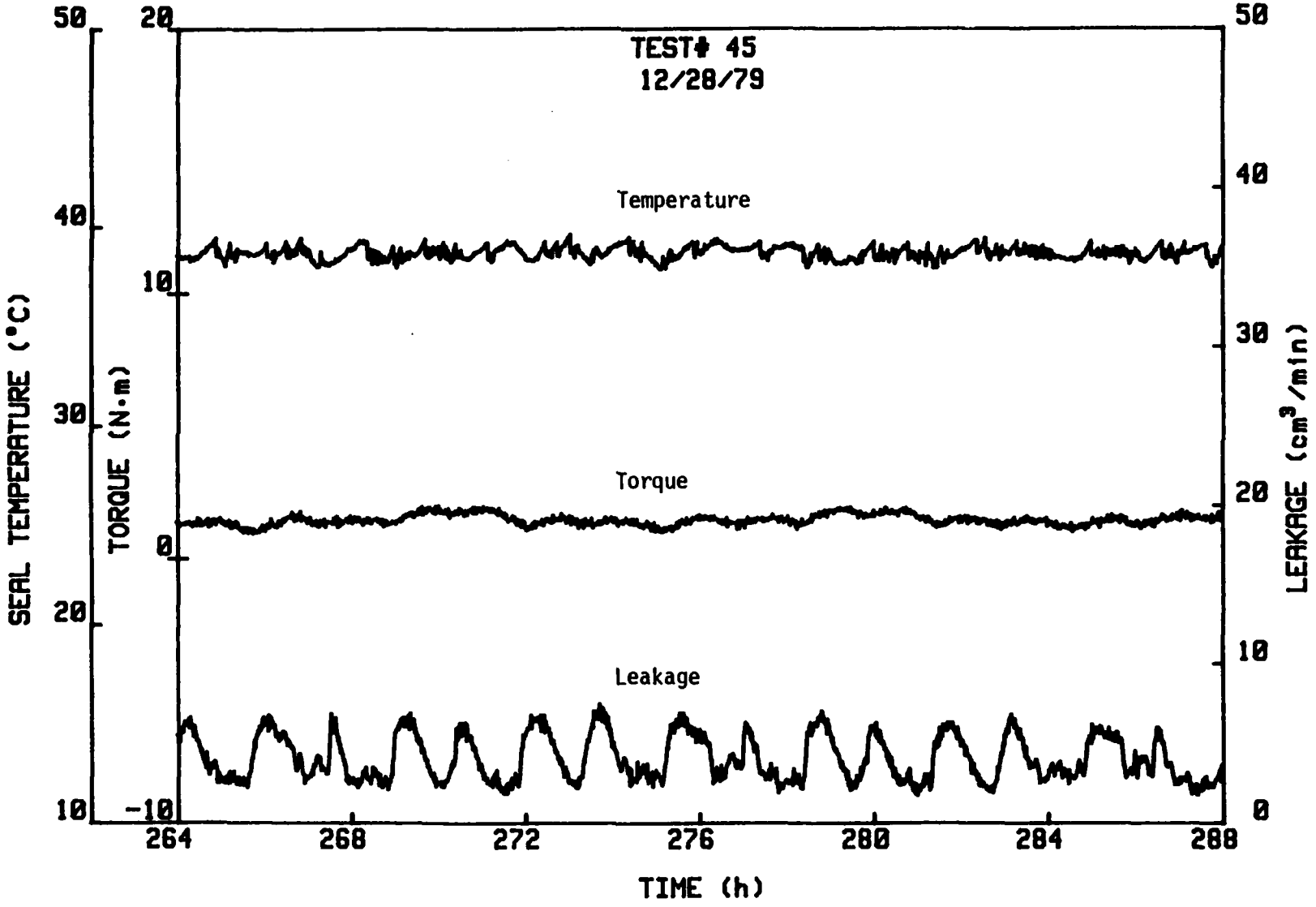

Figure C-8, cont.

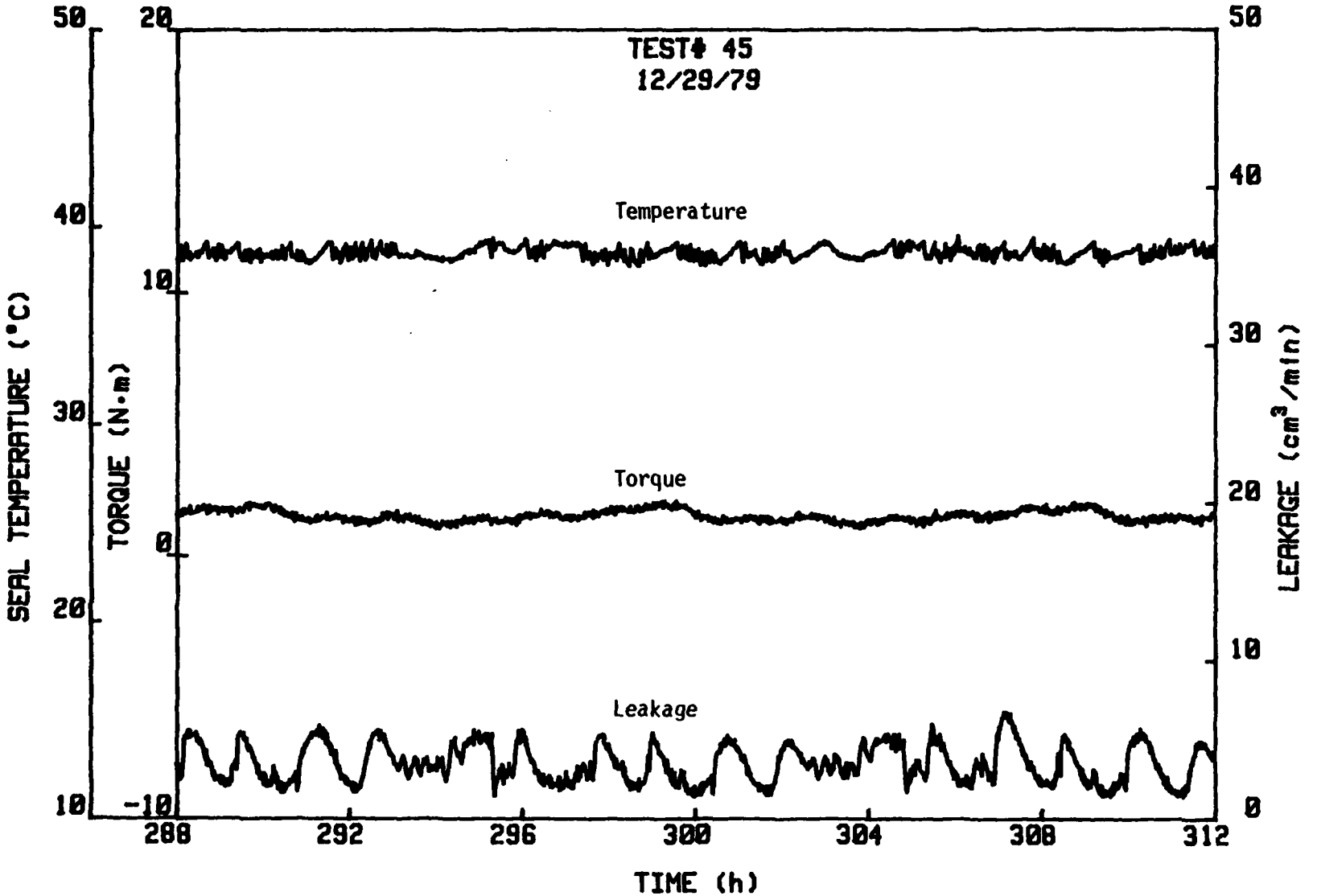

Figure C-8, cont.

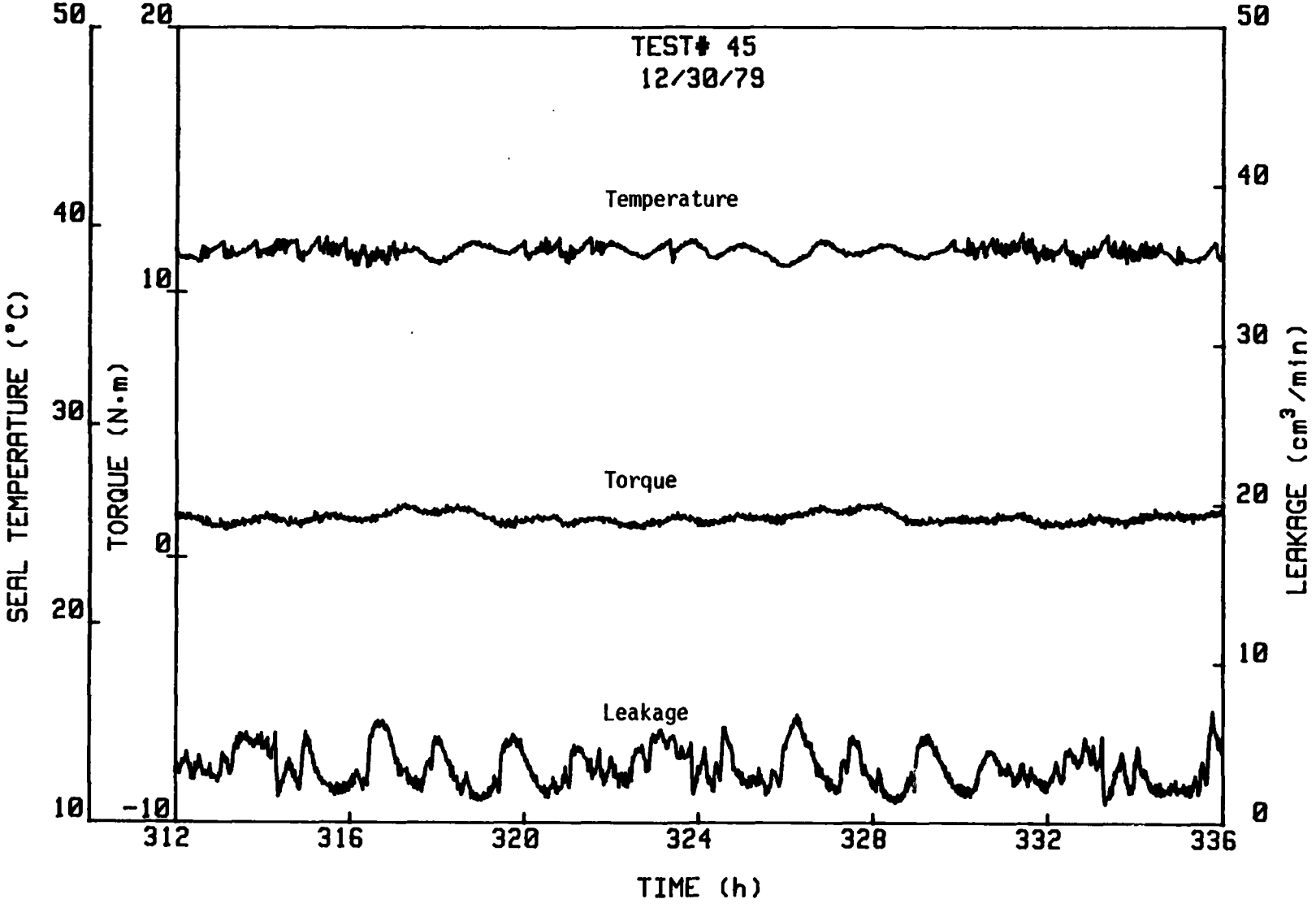

Figure C-8, cont.

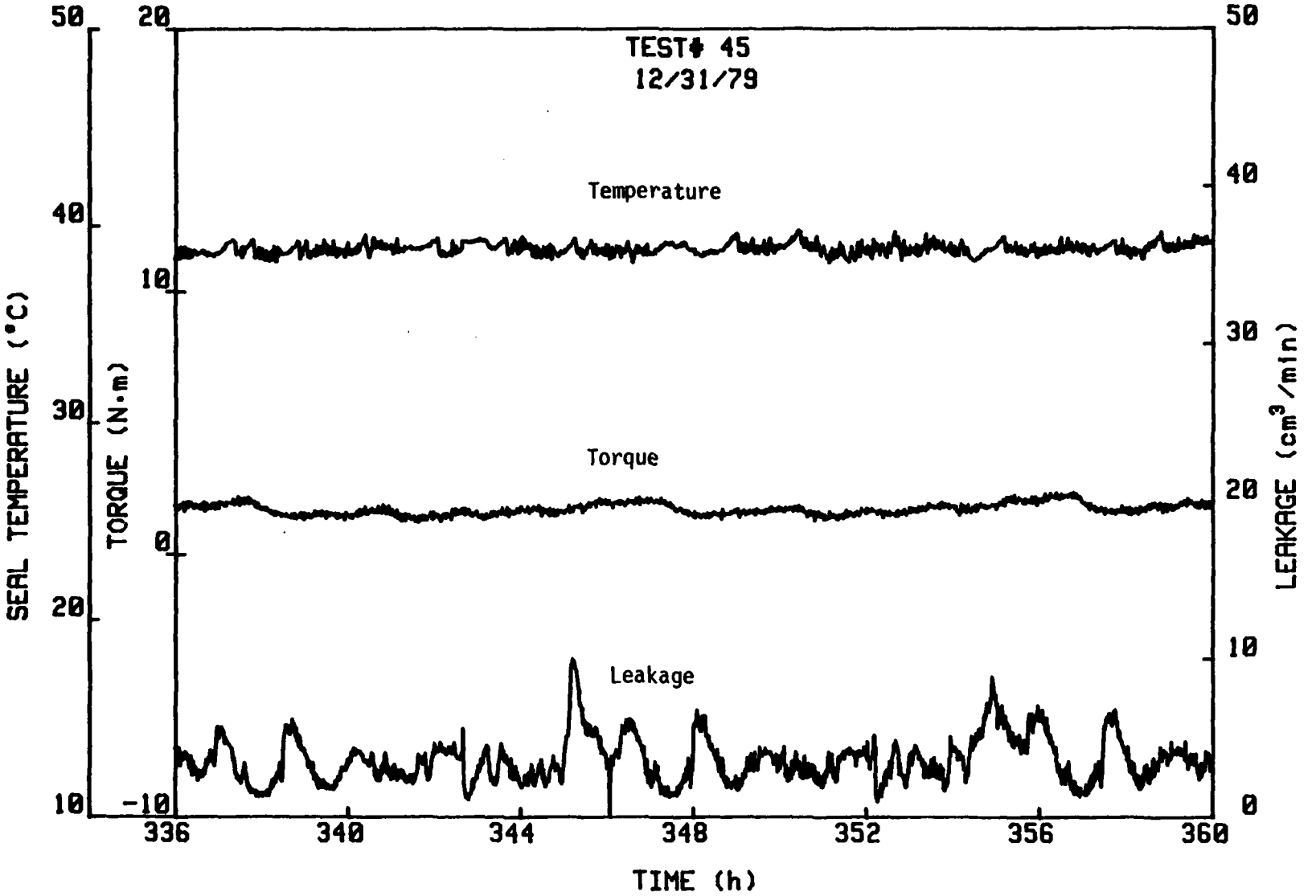

Figure C-8, cont.

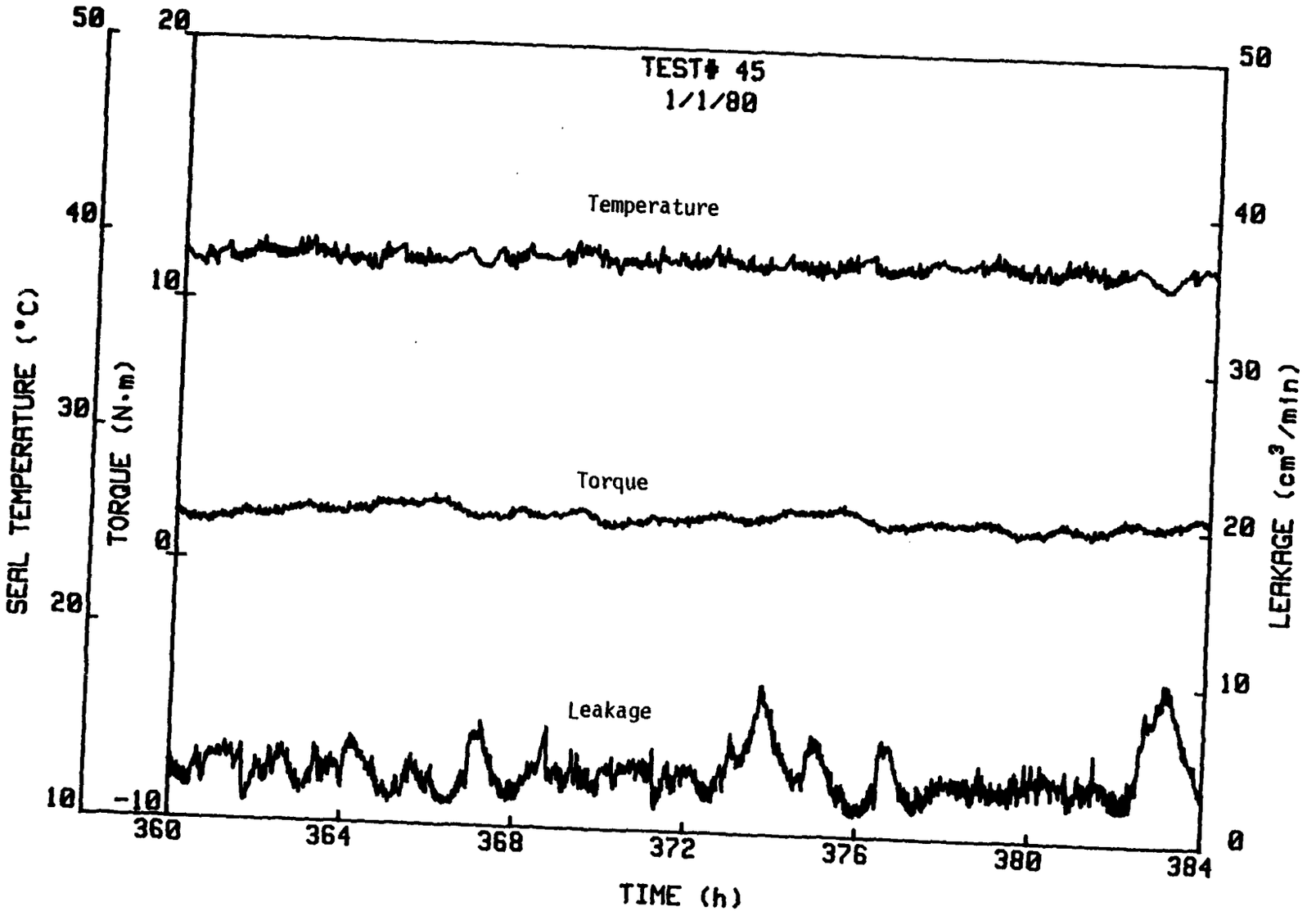

Figure C-8, cont.

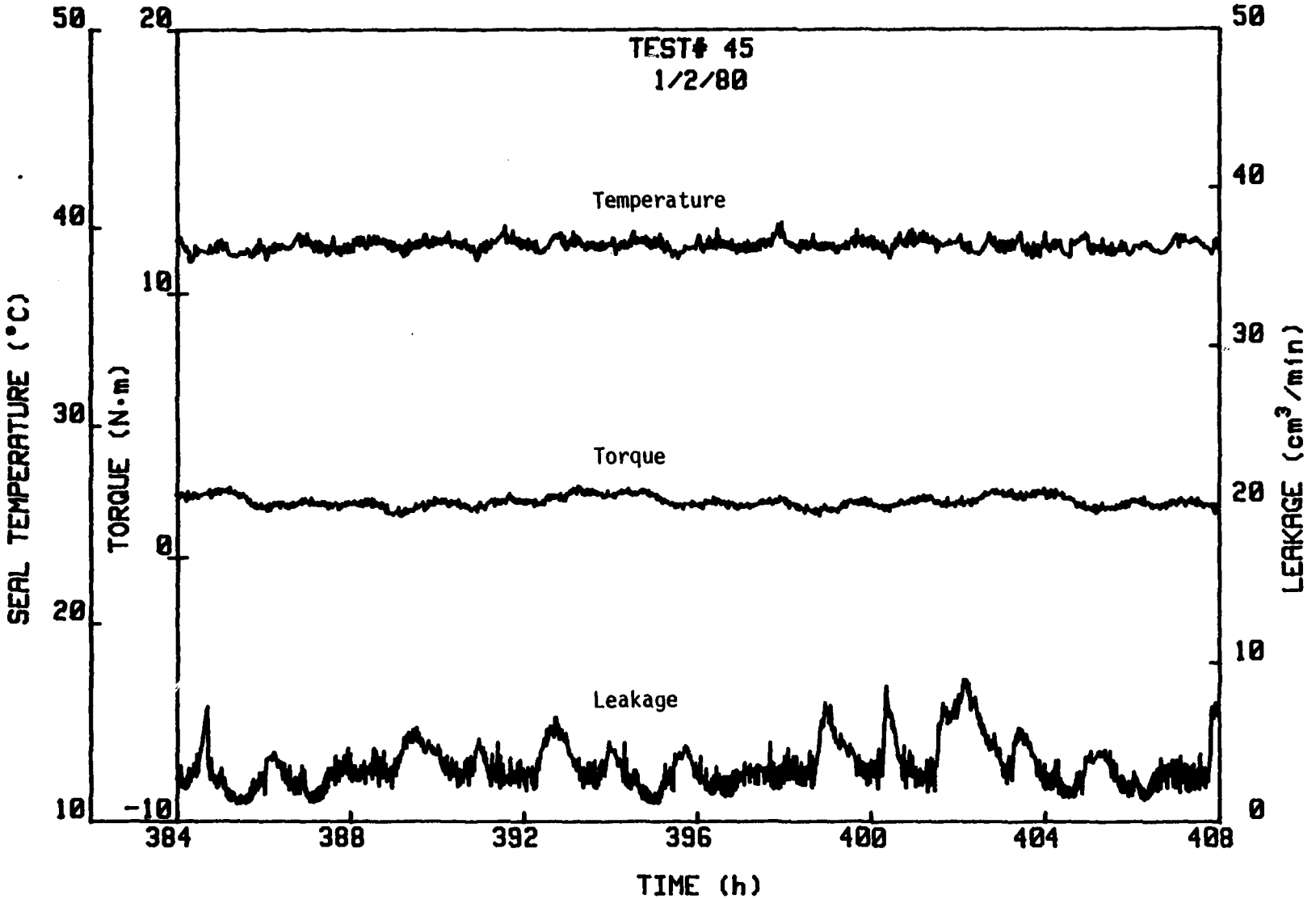

Figure C-8, cont.

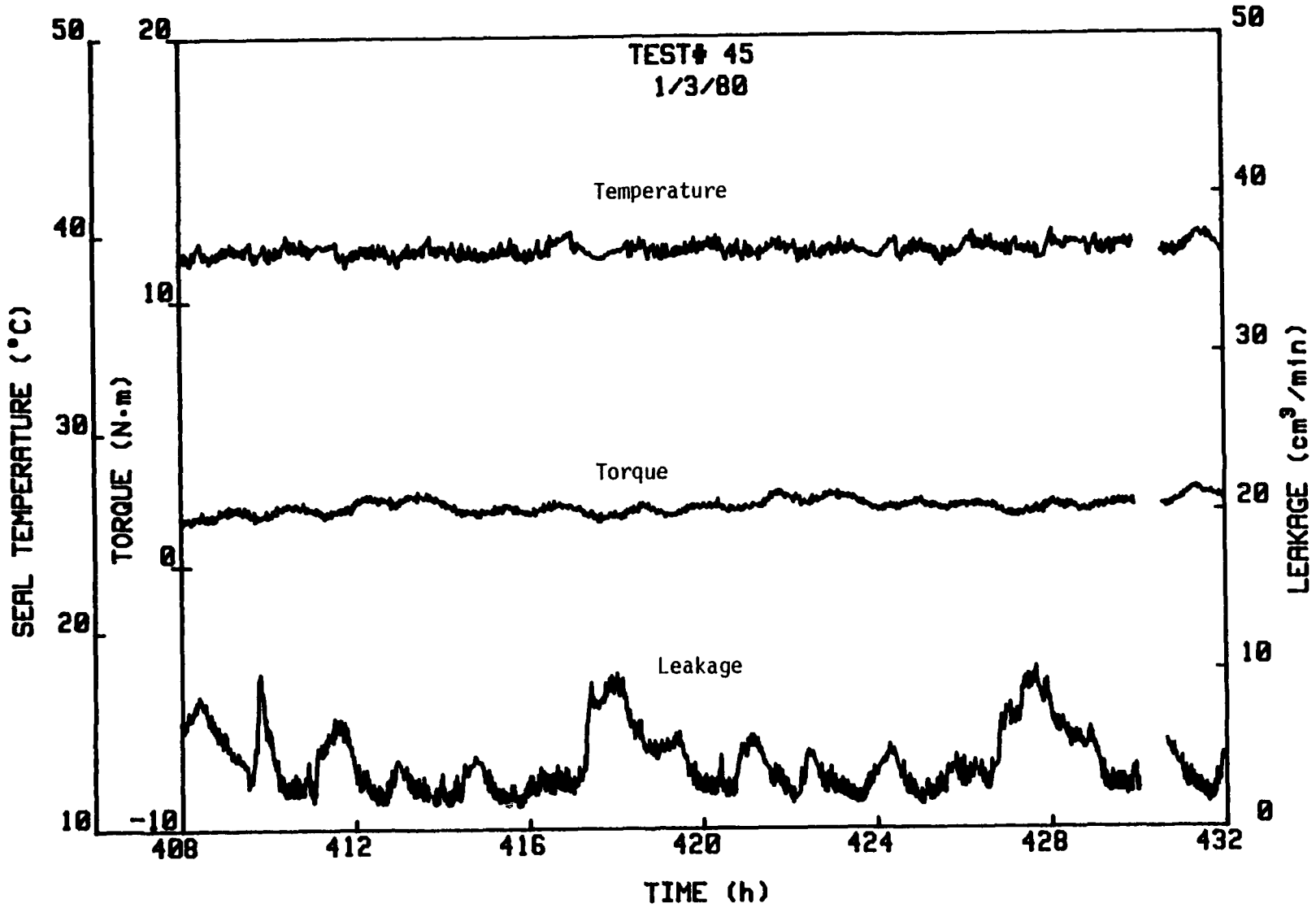

Figure C-8, cont.

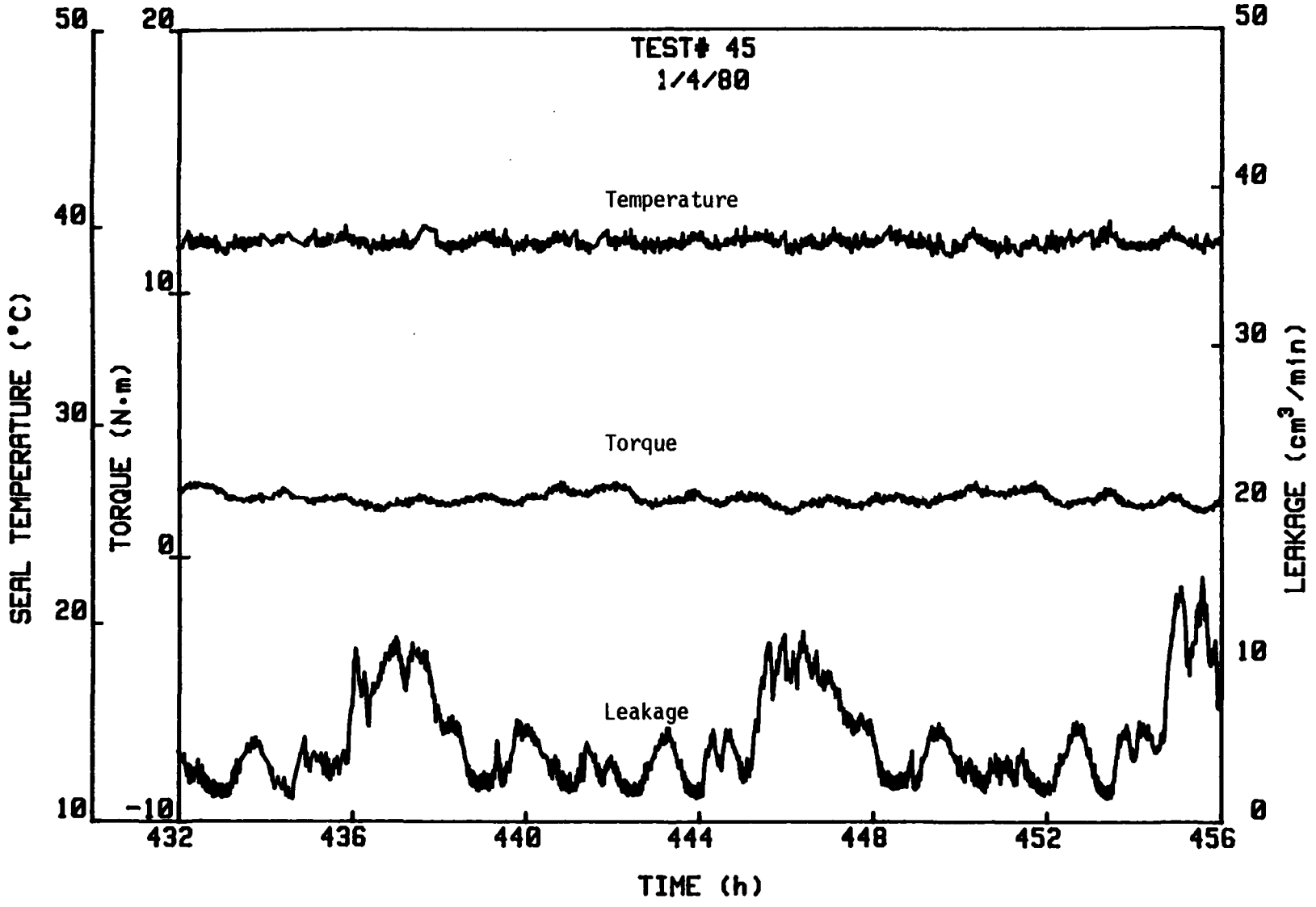

Figure C-8, cont.

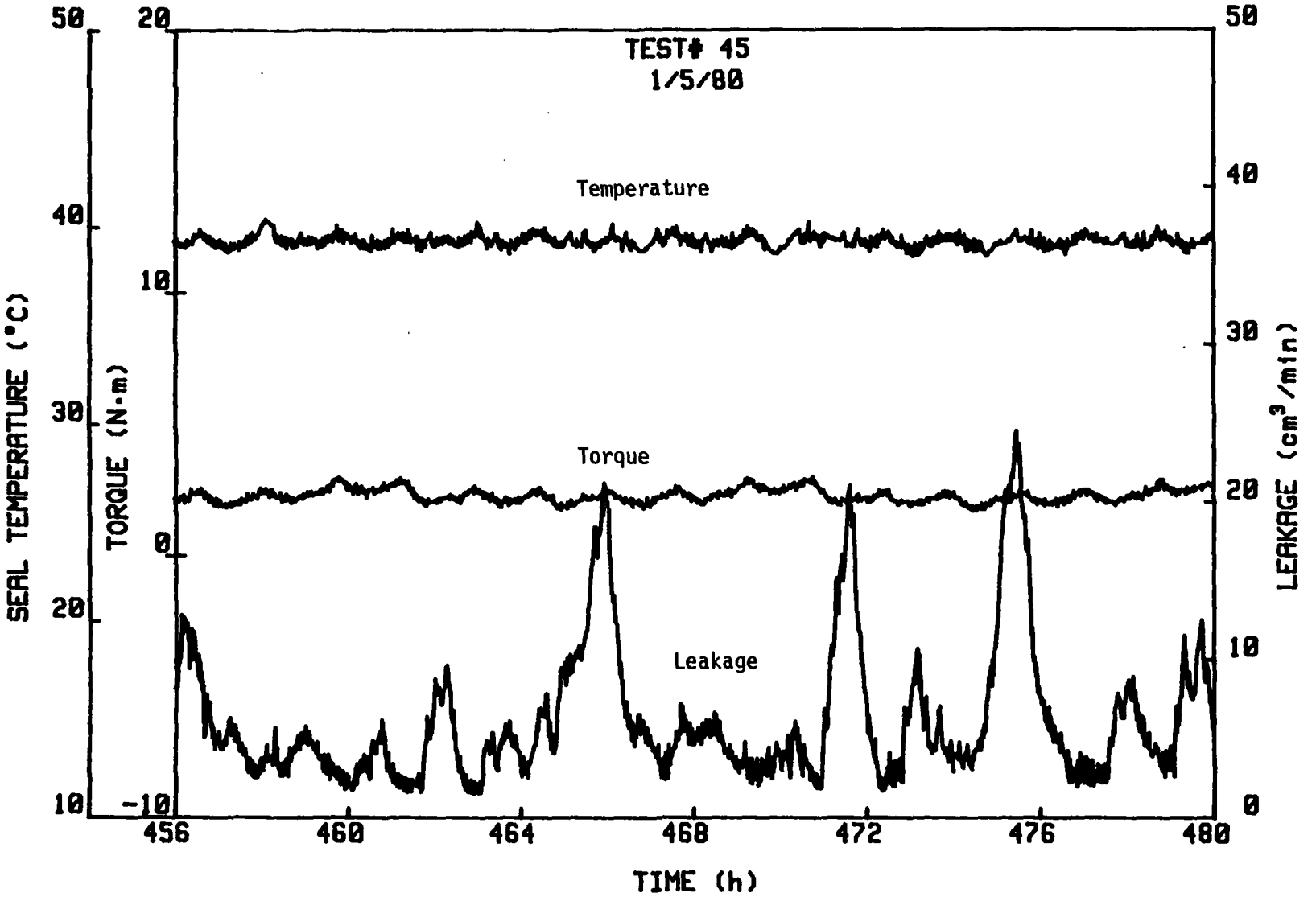

Figure C-8, cont.

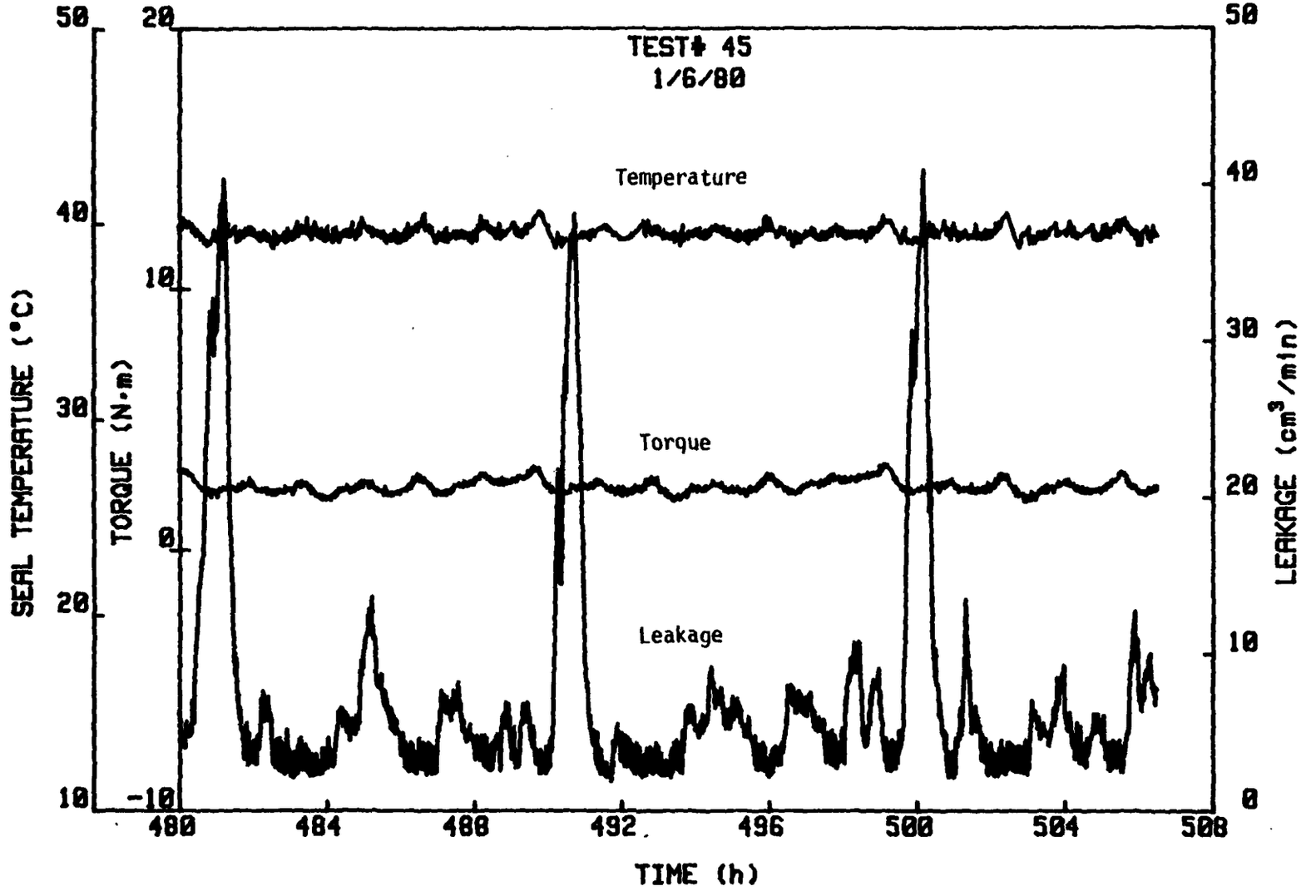

Figure C-8, cont.

Distribution List

Recipient	Number of Copies
Office of Naval Research 800 N. Quincy Street Arlington, Virginia 22217 Attn: M. Keith Ellingsworth, Code 473	(3)
Defense Documentation Center Building 5 Cameron Station Alexandria, Virginia 22314	(12)
Naval Research Laboratory 4555 Overlook Avenue Washington, DC 20390 Attn: Technical Information Division Code 2627 Dr. Ravner, Code 6170	 (6) (1)
U.S. Naval Postgraduate School Monterey, California 93940 Attn: Dept. of Mechanical Engineering	(1)
U.S. Naval Academy Annapolis, Maryland 21402 Attn: Dept. of Mechanical Engineering	(1)
Naval Air Systems Command Jefferson Plaza Washington, DC 20360 Attn: B. Poppert, Code 240E	(1)
Naval Sea Systems Command Crystal City, National Center #3 Washington, DC 20360 Attn: Frank Ventriglio, Code OSR14	(1)
Naval Ships R&D Center Annapolis, Maryland 21402 Attn: Friction and Wear Branch J. F. Dray	(1)
Naval Air Engineering Center Lakehurst, New Jersey 08733 Attn: Mr. P. Senholzi	(1)
Naval Air Propulsion Test Center Trenton, New Jersey 08628 Attn: Mr. R. Valori	(1)

Distribution List (continued)

Recipient	Number of Copies
Naval Air Development Center Warminster, Pennsylvania 18974 Attn: Mr. A. Conte	(1)
National Science Foundation 1800 G Street, NW Washington, DC 20550 Attn: Dr. C. J. Astill	(1)
National Bureau of Standards Washington, DC 20234 Attn: Dr. W. Ruff	(1)
NASA Lewis Research Center 21000 Brookpark Road Cleveland, Ohio 44135 Attn: R. L. Johnson	(1)
Air Force Office of Scientific Research Washington, DC 20333 Attn: Directorate of Engineering Sciences	(1)
Air Force Aeropropulsion Laboratory Wright-Patterson Air Force Base, Ohio 45433 Attn: AFAPL/POD-1, Dick Quigley, Jr.	(1)
Army Research Office Durham, North Carolina 27706 Attn: Dr. E. A. Saibel	(1)
Office of Naval Research Branch Office 1030 East Green Street Pasadena, California 91106	(1)
Assistant Chief for Technology Office of Naval Research, Code 200 Arlington, Virginia	(1)
Prof. H. S. Cheng Department of Mechanical Engineering Northwestern University Evanston, Illinois	(1)
Crane Packing Company 6400 Oakton Street Morton Grove, Illinois 60053 Attn: Art Zobens	(1)

Distribution List - continued

Recipient	Number of Copies
Sealol, Inc. Box 2158 Providence, Rhode Island 02905 Attn: H. F. Greiner	(1)
Pure Carbon Company St. Marys, Pennsylvania 15857 Attn: R. R. Paxton	(1)
Franklin Research Institute 20th and Race Streets Philadelphia, Pennsylvania 19103 Attn: Harry C. Rippel	(1)
Naval Sea Systems Command Crystal City, National Center #3 Washington, DC 20360 Attn: Code 524, Dick Graham	(1)
Naval Ships R&D Center Annapolis, Maryland 21402 Attn: Al Harbaugh	(1)